AUS DEM LEHRSTUHL FÜR DERMATOLOGIE

PROF. DR. DR. H.C. M. LANDTHALER

DER FAKULTÄT FÜR MEDIZIN

DER UNIVERSITÄT REGENSBURG

STUDY OF POTENTIAL PHOTOSENSITIZERS FOR SELF-DISINFECTING SURFACES USING THE METHOD OF ANTIMICROBIAL PHOTODYNAMIC ACTION

INAUGURAL – DISSERTATION

ZUR ERLANGUNG DES DOKTORGRADES

DER BIOMEDIZINISCHEN WISSENSCHAFTEN

DER

FAKULTÄT FÜR MEDIZIN

DER UNIVERSITÄT REGENSBURG

VORGELEGT VON

ARIANE FELGENTRÄGER

AUS KÖTHEN

2013

Dekan:	*Prof. Dr. Dr. Torsten E. Reichert*
Betreuer:	*Prof. Dr. Wolfgang Bäumler*
Tag der mündlichen Prüfung:	01.07.2013

Meinen Lieben:

Il mio caro Andrea und meiner Familie.

„Das tiefste und erhabenste Gefühl, dessen wir fähig sind, ist das Erlebnis des Mystischen. Aus ihm allein keimt wahre Wissenschaft. Wem dieses Gefühl fremd ist, wer sich nicht mehr wundern und in Ehrfurcht verlieren kann, der ist seelisch bereits tot."

Albert Einstein

„In der Wissenschaft gleichen wir alle nur den Kindern, die am Rande des Wissens hier und da einen Kiesel aufheben, während sich der weite Ozean des Unbekannten vor unseren Augen erstreckt."

Isaac Newton

ACKNOWLEDGEMENTS

Zu danken habe ich natürlich weitaus mehr Personen, als ich hier je aufzählen könnte, aber besonders herausheben möchte ich folgende Kollegen, Wegbegleiter und Freunde:

Ein großes Dankeschön geht an meinen Betreuer ***Prof. Dr. Wolfgang Bäumler*** für die Annahme als Doktorandin und die Begleitung in den letzten Jahren. Seine fachlichen Diskussionen schätzte ich sehr. Wolfgang ermöglichte mir Freiheiten in der Schwerpunktsetzung meiner Projekte, die Teilnahme an internationalen Konferenzen, auf denen ich mich wissenschaftlich austauschen konnte und unterstützte mich bei all meinen Vorhaben stets unvoreingenommen und uneingeschränkt.

Darüber hinaus danke ich meinem Mentor ***PD Dr. Tim Maisch*** für seine wertvollen Tipps im Doktorandenalltag, speziell in Bezug auf Konferenzen und für seine fachliche Unterstützung insbesondere in mikrobiologischen Angelegenheiten.

Danken will ich ausdrücklich…

…*Anita*, für ihre überlegte und ausgleichende Art, ihre fachlichen Ratschläge und dafür, einfach eine tolle Freundin zu sein!

…*Andy*, für die Kooperationsmöglichkeiten mit dem Institut für Organische Chemie an der Uni Regensburg und die aus seinen Synthesen resultierenden Phenothiazinium-Derivate und Photosensibilisatoren für die PU-Oberflächen, die dann in meinem Messaufbau landeten. Mit der Hilfe bei den NMR-Messungen stand er mir in chemischen Angelegenheiten immer beratend zur Seite.

…*Johannes*, für die seinerseits jederzeit zur Verfügung gestellt Hilfe bei allen technischen Fragen am Experimentalaufbau.

…*Anja*, für die Antworten auf meine biologischen Fragen und die gute Zeit zusammen im Büro – in allen Lebenslagen.

…*Fernanda*, für die Herstellung der Biofilme und planktonischen Suspensionen von *C. albicans*.

…*Lisa*, für die Herstellung der Zelluloseazetat-Oberflächen und der guten Kooperation bei diesem Projekt.

…*Micaela*, für die helfende Hand bei den Phototoxizitätstests auf den PU-Oberflächen während ihres Praktikums bei mir.

…***Friederike***, für die auf meinen Voruntersuchungen zu Phenothiazinen basierenden, aufbauenden Untersuchungen während ihrer Masterarbeit.

…und allen weiteren Doktoranden, technischen Assistenten, Masterstudenten und H4-Belegschaft für die gute Arbeitsatmosphäre und auch für den einen oder anderen Witz zwischen Tür und Angel und der positiven Grundeinstellung im Laboralltag: dazu gehören ***Alena, Andi, Christoph***, ***Eva***, ***Ewa***, ***Fabian***, ***Francesco, Freddy, Judith***, ***Laura***, ***Manni, Manu, Michl***, ***Petra***, ***Tatjana***, ***Sebastian*** und alle anderen ***H4'lern***…

…der ***Sensorik Bayern GmbH*** für die finanzielle Unterstützung zu Beginn meiner Doktorarbeit, die möglichen Firmenkooperationen, um einige Untersuchungen aus dieser Dissertation in der Praxis zu erproben, und dem ganzen Sensorik-Team für die freundschaftliche Aufnahme und köstliche Versorgung bei den Veranstaltungen im Biopark.

…all meinen ***Freunden***, nah und fern, die ich gerade in der Endphase der Dissertation viel zu selten sehen konnte.

Special thanks to all of my ***favourite musicians***, who know that playing music is much more than only a distraction… it's essential ♪

Aber zuletzt – doch sicher an erster Stelle – gilt mein besonderer Dank …

…meiner ***Familie*** für ihre Unterstützung, ihre Zuversicht in schwierigeren Zeiten, ihr Vertrauen in meine Entscheidungen,

…und ***Andrea***, für seine Liebe, und dafür, dass er mir durch sein Wesen vermittelt, dass es gut ist, nicht alles messen und in Einheiten ausdrücken zu können und müssen. Unsere Ausdauer die letzten Jahre, sowie der Konsens über die wichtigen Dinge im Leben sind etwas ganz besonderes.

SUMMARY

This thesis addresses the principle of antimicrobial photodynamic inactivation (PDI) as a complementary method to antibiotics or disinfection in order to deactivate pathogenic microorganisms. Herein, the prevention of settlement and growth of microorganisms on surfaces using the PDI method is a main issue with focus on the development and improvement of such surfaces. Therefore, different photosensitizers were investigated first in solution in regard to their ability to generate singlet oxygen and their phototoxic effect. Some of these photosensitizers were polymerized into different surface structures, their physical properties were clarified with spectroscopic methods and the phototoxic efficacy on the surfaces was determined.

Chapter 3: In literature a rather high dark toxicity component of the photosensitizer class of phenothiazines was described and the systematics of the toxic processes were controversially discussed. Due to their wide use in PDI, the phenothiazine Methylene blue (MB) and common derivatives of this photosensitizer class were investigated in solution of H_2O with direct spectroscopic methods in regard to their singlet oxygen generation and thus to clarify the singlet oxygen quantum yield. For all photosensitizers substantially smaller quantum yields as compared to values in literature were obtained *via* direct monitoring of singlet oxygen. This is considered as a probable effect of dimerisation or the use of indirect methods to monitor singlet oxygen without the explicit exclusion of the participation of other reactive species. Further, the attachment to Gram(+) and Gram(-) bacteria was determined quantitatively. In a second study, newly synthesized derivatives of MB were investigated in order to systemize the influence of side chains on the spectroscopic characteristics, especially the ability to generate singlet oxygen, the photostability and the phototoxic effectivity. In contrast to the commercially available dimerisation could be suppressed in some derivatives and achieving a higher photostability whilst comparable phototoxicity.

Chapter 4: The phototoxic properties of the porphyrin XF73 were reported to be rather high due to good cell attachment or penetration abilities with allowing a therapeutic window. Therefore, the photophysical characteristics of this photosensitizer were investigated in H_2O and in cell physiological solution with regard to aggregation and singlet oxygen generation. The results were compared to findings with TMPyP. Aggregation was enhanced in XF73, most probably due to the flexible side chains, and a stacking was further

driven by the presence of Cl^-, which is found to a high extent in cell physiological solution like PBS. The singlet oxygen generation was dramatically influenced by this stacking effect.

Chapter 5: The porphyrin TMPyP was incubated in *C. albicans* planktonic and biofilm growing samples. Thereafter, the singlet oxygen luminescence was directly detected at 1270 nm being the first report of the involvement of singlet oxygen in these cell types with this highly sensitive, non-invasive monitoring technique. Biofilm samples were considered as complex surfaces, exhibiting different decay kinetics for singlet oxygen than their planktonic counterparts. Different experimental laser setups were used for the measurements, thus allowing irradiation of the Soret- or Q-band of the photosensitizer with different irradiation power. With an enhanced sensitivity when irradiating at 420 nm, very low photosensitizer concentrations were necessary to monitor the singlet oxygen luminescence with a good signal-to-noise ratio. A dependency of the rise and decay times of the singlet oxygen luminescence on the photosensitizer concentration used for incubation was detected. Based on these findings a model was proposed, suggesting different surroundings for TMPyP within or adherent to the cell.

Chapter 6: Cellulose acetate surfaces and polyurethane-coated PMMA surfaces doped with different photosensitizers were produced and compared with regard to singlet oxygen generation and phototoxic efficacy. The generation of singlet oxygen by irradiation of the photosensitizer was proven within direct spectrally and time-resolved single-photon counting. The assignment of the rise and decay time was challenging, because the bi-exponential fit model was not sufficient for the complex surface system, which showed a multi-exponential decay manner. The presence of singlet oxygen was also monitored *via* an indirect method using the reaction with potassium iodide. Nevertheless, the PU-surfaces showed an effect without photosensitizer inherent, which indicates ROS generation of the material itself. The phototoxic efficacy against *S. aureus* was dependent on the irradiation time and the photosensitizer concentration in the material. Also, a difference in the phototoxic efficacy of the porphyrin-based and phenalenone-based photosensitizer doped in the surface material was detected, resulting in $> 2\ log_{10}$ reduction (> 99%) with the first and $> 3\ log_{10}$ reduction (> 99.9%) with the latter sample ($P = 50\ mW cm^{-2}$, irradiation time 30 min).

ZUSAMMENFASSUNG

Die vorliegende Doktorarbeit behandelt die antimikrobielle photodynamische Inaktivierung (PDI) als eine ergänzende Methode zur Verwendung von Antibiotika oder Desinfektionsmitteln, um pathogene Mikroorganismen zu deaktivieren. Prävention von Ansiedlung und Wachstum dieser Mikroorganismen auf Oberflächen mit Hilfe der PDI ist dabei das Hauptthema; dabei liegt der besondere Fokus auf der Herstellung und Verbesserung solcher Oberflächen. Dafür wurden verschiedene photoaktive Substanzen (Photosensibilisatoren) erst in Lösung in Hinblick auf ihre Fähigkeit zur Singulett-Sauerstoff-Generierung untersucht. Einige dieser Photosensibilisatoren wurden anschließend in verschiedene Oberflächenstrukturen einpolymerisiert und im Anschluss mit Hilfe spektroskopischer Methoden hinsichtlich ihrer physikalischen Eigenschaften und ihrer phototoxischen Effektivität untersucht.

Kapitel 3: In der Literatur ist eine Dunkeltoxizität der Photosensibilisatorklasse der Phenothiazine beschrieben und die Systematik des toxischen Prozesses wird kontrovers diskutiert. Aufgrund ihres breiten Anwendungsspektrums im Bereich PDI, wurden die Phenothiazine Methylen blau (MB) und gebräuchliche Derivate dieser Photosensibilisator-klasse in wässriger Lösung mit spektroskopischen Methoden untersucht und dabei die Singulett-Sauerstoff Generierung durch Bestimmung der Quantenausbeute für Singulett-Sauerstoff ermittelt. Für alle Photosensibilisatoren wurden mit direktem Monitoring von Singulett-Sauerstoff deutlich niedrigere Quantenausbeuten bestimmt, als in der Literatur angegeben. Als Grund dafür werden ein Dimerisierungseffekt oder die in der Literatur verwendeten indirekten Messmethoden für Singulett-Sauerstoff, welche nicht explizit die Beteiligung anderer reaktiver Spezies ausschließen, verantwortlich gemacht. Desweiteren wurde die Anlagerung oder Aufnahme der Photosensibilisatoren in Gram(+) und Gram(-) Bakterien quantitativ bestimmt. In einer zweiten Studie wurden neu synthetisierte MB-Derivate hinsichtlich des Einflusses der Seitenketten am jeweiligen Molekül auf die spektroskopische Charakteristik hin untersucht, insbesondere bezüglich der Fähigkeit zur Singulett-Sauerstoff Generierung, der Photostabilität und der phototoxischen Effektivität. Im Gegensatz zu den käuflich erhältlichen Derivaten aus dem ersten Teil konnte Dimerisierungsverhalten bei einigen Exemplaren unterdrückt werden, bei gleichzeitig hoher Photostabilität und mit MB vergleichbarer Phototoxizität.

Kapitel 4: Die phototoxischen Eigenschaften des Porphyrins XF73 wurden als effektiv eingestuft aufgrund einer guten Anlagerung bzw. Aufnahme in Zellen, unter gleichzeitigem Vorhandensein eines therapeutischen Fensters. Deswegen wurden die photophysikalischen Eigenschaften dieses Photosensibilisators in H_2O und in zellphysiologischer Lösung hinsichtlich Aggregationsverhalten und Singulett-Sauerstoff Generierung untersucht. Die Ergebnisse wurden mit denen des Referenzphotosensibilisators TMPyP verglichen. Aggregation war mit XF73 sehr wahrscheinlich durch dessen flexible Seitenketten erhöht und wurde zusätzlich konzentrationsabhängig getrieben in Gegenwart von Cl^-, welches in zellphysiologischer Lösung wie PBS zu finden ist. Aggregation von XF73 beeinflusst deutlich negativ die Generierung von Singulett-Sauerstoff.

Kapitel 5: Das Porphyrin TMPyP wurde in *C. albicans* inkubiert, welche sowohl planktonisch als auch als Biofilm wuchsen. Anschließend wurde die Lumineszenz von Singulett-Sauerstoff direkt bei $1270\,nm$ detektiert und in dieser Arbeit erstmalig als beteiligtes toxisches Agens in diesem Mikroorganismus mit Hilfe der hochsensitiven und nicht-invasiven Monitoring-Technik beschrieben. Die Biofilm-Proben werden als komplexe Oberflächen angesehen, die unterschiedliche Abklingkinetik für Singulett-Sauerstoff aufweisen, im Vergleich zu ihren planktonischen Entsprechungen. Verschiedene Laseraufbauten wurden für die Messungen verwendet und ermöglichten Bestrahlung in der Soret- oder Q-Bande von TMPyP mit unterschiedlicher Leistung. Mit der erzielten erhöhten Sensitivität für die Bestrahlung bei $420\,nm$ (Soret) waren nur sehr niedrige Photosensibilisatorkonzentrationen nötig, um die Singulett-Sauerstoff-Lumineszenz mit einem guten Signal-Rausch-Verhältnis zu aufzunehmen. Eine Abhängigkeit der Anstiegs- und Abklingzeiten der Singulett-Sauerstoff-Lumineszenz von der Konzentration des Photosensibilisators wurde bestimmt. Basierend auf diesen Ergebnissen wird hier ein Modell vorgeschlagen, welches verschiedene Umgebungen für TMPyP innerhalb oder anhaftend an die Zelle vorschlägt.

Kapitel 6: Oberflächen aus Zelluloseazetat oder mit Polyurethan überzogenes PMMA wurden mit unterschiedlichen Photosensibilisatoren dotiert und miteinander verglichen hinsichtlich Generierung von Singulett-Sauerstoff und phototoxischer Effektivität. Die Generierung von Singulett-Sauerstoff konnte mit Hilfe von spektral- und zeitaufgelöster Einzelphotonenzählung nachgewiesen werden. Die Zuordnung von Anstiegs- und Abklingzeiten war eine Herausforderung, weil das bi-exponentielle Fitmodell nicht ausreichte, um das komplexe Oberflächensystem zu beschreiben, welches ein multi-exponentielles Verhalten an den Tag legte. Das Vorhandensein von Singulett-Sauerstoff wurde zudem mit einer indirekten Methode überprüft, die sich die Reaktion von

Kaliumiodid mit Singulett-Sauerstoff zu Triiodid zunutze macht. Nichtsdestotrotz zeigte mit dieser Methode auch das PU-Material ohne inhärenten Photosensibilisator die Ausbildung reaktiver Spezies. Die Phototoxizität gegen *S. aureus* war abhängig von der Bestrahlungszeit und der Konzentration des Photosensibilisators im Material. Zudem wurde ein Unterschied zwischen der phototoxischen Effektivität der Oberfläche mit einpolymerisiertem Photosensibilisator auf Porphyrin-Basis und Phenalenone-Basis festgestellt. Ersterer führte zu einer Reduktion von $> 2\ log_{10}$-Schritten (> 99%), letzterer zu einer Reduktion von $> 3\ log_{10}$-Schritten (> 99.9%) mit einer Bestrahlungsleistung von $P = 50\ mW cm^{-2}$ und einer Bestrahlungszeit von 30 min.

LIST OF ABBREVIATIONS

aPDT	antimicrobial photodynamic treatment
CA	cellulose acetate
C. albicans	*Candida albicans*
CFU	colony forming units
DMMB	Di-methyl methylene blue
DNA	deoxyribonucleic acid
E. coli	*Escherichia coli*
EM	electromagnetic
F	fluorescence
H_2O	water
H_2O_2	hydrogen peroxide
IC	internal conversion
IR	infrared
ISC	intersystem crossing
k_q	quenching rate constant
LPS	lipopolysaccharides
μ	micro
MH	Müller-Hinton
MB	3,7-Bis(dimethylamino)-phenothiaziniumchlorid, Methylene blue
MB-1	3-[(2-Ammoniumethyl)(methyl)amino]-7-(dimethylamino) phenothiazin-5-ium dichloride
MB-2	3-{methyl[2-(methylammonio)ethyl]amino}-7-(dimethylamino) phenothiazin-5-ium dichloride
MB-3	3-(piperazin-4-ium-1-yl)-7-(dimethylamino)phenothiazin-5-ium dichloride
MB-4	3-[(2-Hydroxyethyl)(methyl)amino]-7-(dimethylamino) phenothiazin-5-ium chloride
MB-5	3-(morpholin-4-yl)-7-(dimethylamino)phenothiazin-5-ium chloride

MB-6	3-(4-methylpiperazin-4-ium-1-yl)-7-(dimethylamino)phenothiazin-5-ium dichloride
mL	millilitre
MRSA	Methicillin-resistant *Staphylococcus aureus*
MW	molecular weight
NaN_3	sodium azide
NIR	near infrared
NMB	New methylene blue N
O_2	molecular oxygen
$^1O_2$, $O_2(a^1\Delta_g)$	singlet molecular oxygen, singlet oxygen
$O_2^{\cdot-}$	superoxide radical
OPO	optical parametric oscillator
P	phosphorescence
PACT	photodynamic antimicrobial chemotherapy
PBS	phosphate buffered saline
PDI	photodynamic inactivation
PDT	photodynamic therapy
PIB	photodynamic inactivation of bacteria
PMMA	*poly*-methylmethacrylate
PMT	photomultiplier tube
PN	Phenalenone
PN-O-A	N,N-Dimethyl-N-(2-hydroxyethyl)-2-ammoniummethyl-phenalen-1-one chloride
PN-O-B	N-(3-Hydroxypropyl)-N-(2-methylen-phenalen-1-one)acetamid
PNS	1h-Phenalen-1-One-2-Sulfonic Acid
PS	photosensitizer
PU	polyurethane
PUR	polyurethane containing no photosensitizer
ROS	reactive oxygen species
S. aureus	*Staphylococcus aureus*

T_1	lowest occupied photosensitizer triplet state
τ_Δ	singlet oxygen decay time
TBO	Toluidine blue O
TCSPC	time-correlated single photon counting
TMPyP	5,10,15,20-Tetrakis(1-methyl-4-pyridinio)-porphyrin tetra(p-toluenesulfonate)
TPP	5,10,15,20-Tetraphenyl-21H,23H-porphine, *meso*-Tetraphenylporphyrin
TPP-O-A	5-(4-Hydroxyphenyl)-10,15,20-triphenylporphyrin
TPP-O-B	5-[4-(6-Hydroxyhexoxy)-phenyl]-10,15,20-triphenylporphyrin
TRPD	time-resolved phosphorescence detection
τ_{T_1}	photosensitizer triplet state decay time
UV	ultraviolet
VIS	visible
VR	vibrational relaxation
XF73	5,15-bis-[4-(3-Trimethylammonio-propyloxy)-phenyl]-porphyrin

INDEX

Chapter 1

Introduction

In this chapter a short introduction to the overall topic of this doctoral thesis is given, ranging from the complex of problems of antibiotics to efficiently kill pathogen microorganisms to describing antimicrobial photodynamic inactivation as an alternative treatment modality. The historical development is described in short, as well as the basic physical principles of photosensitizer and singlet oxygen. The development and studies on surfaces is outlined in regard to effective photosensitizing efficacy and their photophysical properties, and the objectives of the thesis are presented.

1.1 PROBLEMATICS OF ANTIBIOTICS and ESCAPING MICRO-ORGANISMS

The widespread and inappropriate use of antibiotics in health system for diseases of man and the over-use in food industry for maintaining a low infection level and a fast animal growth in industrial livestock farming has provoked resistance patterns of both fungal and bacterial pathogens against these [1-6]. It might be no exaggeration to call it one of the main challenges for health care in the 21st century. Darwin's theory of selection pressure, in form of antibiotics having highly specific mechanisms of antimicrobial action, again gives credit to this genetic flexibility of these human pathogenic microorganisms [7, 8]. The World Economic Forum (WEF) concluded in their report on global risks that "arguably the greatest risk ... to human health comes in the form of antibiotic-resistant bacteria. We live in a bacterial world where we will never be able to stay ahead of the mutation curve" [9].

The most serious infections are caused by a group of microorganisms which are merged under the acronym "ESKAPE", because this group of microorganisms has the ability to escape the effects of antimicrobial agents. These important pathogens are *Enterococcus faecium, Staphylococcus aureus, Klebsiella pneumoniae, Acinetobacter baumannii, Pseudomonas aeruginosa*, and *Enterobacter* species [10]. This group of superbugs was extended by Peterson including *Clostridium difficile* as one of the most common hospital-acquired infections [11] and especially pointing out that infections by *Enterobacter E. coli* currently account for ≈ 20% of all cases of bacteraemia in the United Kingdom [12]. Not only methicillin-resistant *S. aureus* (MRSA), but also the *Enterobacter* species have developed a broad-spectrum resistance against many classes of antibiotics. The eukaryotic fungus *Candida albicans* as the main agent for superficial skin mycosis has of course to be added to that list of 'escaping' microorganisms, since also within this pathogen resistance patterns became an increasing problem, especially in patients with immune deficiency [13].

The production and admission of new classes of antibiotics is a slow process outdistanced at the moment by the faster resistance development. Therefore, new alternative treatments are developed amongst which photodynamic treatment is one approach that has become important and prevalent within the past years [14-19].

1.2 ANTIBACTERIAL PHOTODYNAMIC TREATMENT and BASIC PRINCIPLES

As an alternative treatment against microorganisms photodynamic inactivation (PDI) is described in this work. The pathogen is treated with a photoactive dye or photosensitizer in combination with light and in the presence of oxygen, which results in the formation of reactive oxygen species (ROS), such as singlet oxygen. Singlet oxygen is described to be one of the key agents in PDI [20-25] and in contrast to antibiotics, which act toxically specific as a single drug, in PDI not the photosensitizer drug, but singlet oxygen or other ROS react by oxidising the surrounding unspecifically.

In the 1970's first treatments against cancer cells were reported with this method, but reports of the photodynamic action go back more than 100 years to the laboratories of Raab and Tappeiner, who discovered PDI by staining *Paramecium caudatum* with the photosensitizer Acridine orange and detected their death upon light exposure under involvement of oxygen [26, 27]. The physical background of photosensitizer activation with light and deactivation in the presence of oxygen was offered by Kautsky *et al.* [28, 29].

Overviews of the basic PDI principle in regard to historical development and physical, chemical and biological aspects can be found to a great extent in literature [30] and Denis *et al.* give an outline of its development by additionally describing the main problems that PDI still has - despite its use as an anti-cancer agent - of gaining ground as a medical treatment against microorganisms [31]. The treatment or prevention of infectious diseases caused by microorganisms with PDI uses different acronyms, mainly aPDT for antimicrobial photodynamic therapy, PDI for photodynamic inactivation or PACT for photodynamic antimicrobial chemotherapy. The treatment is applied so far in dentistry as treatment of oral cancer, bacterial and fungal infections, or for the photodynamic diagnosis (PDD) of the malignant transformation of oral lesions [32-34]. PDI also represents a novel therapeutic approach in the controlling of biofilms, which are able to grow on variable surfaces, organic or non-organic [35-37].

The usage of PDI in general might be split in therapy and prevention of infection with pathogens. As a therapeutic method for the decolonisation of infected wounds PDI might be a powerful medical treatment, if the structure of the photosensitizers is chosen selective enough to distinguish between human cells and pathogen with unique chemical binding features and therefore offer a therapeutic window.

In contrast to that, the preventive character of PDI gets increasingly in the focus of research, helpful against hospital-acquired infections but also in food industry [38-41]. The prevention of microorganisms from settling and growing on surfaces is a matter of great concern, since disinfection as such might then be obsolete. Therefore, a photosensitizer is linked or doped into a polymer and with the condition of sufficient oxygen permeability of the material singlet oxygen will be generated under light irradiation, can diffuse from the surface and induce the death of adherent microorganisms [37, 42-48].

1.2.1 Generation and mode of action of molecular singlet oxygen

The ground state of di-oxygen, O_2, is a triplet state, with two unpaired electrons with parallel spins in a non-binding orbital. Thus, oxygen has paramagnetic properties and is a bi-radical. The bi-radical character and the double bond of the two oxygen atoms are illustrated best with $\langle O \div O \rangle$ according to and extending the Lewis formulae [49]. Since the ground state is a triplet state the radical properties of oxygen are limited due to the spin-conservation for chemical reactions. Singlet molecular oxygen, $^1O_2$, which is molecular oxygen in its lowest excited singlet state, therefore is highly reactive. This state has two electrons with antiparallel spin in one of its non-binding orbital. The existence of $^1O_2$ was experimentally confirmed with its emission band $\approx 1270\ nm$ in the earth atmosphere and with oxygen in the liquid phase 5 years after the theoretical description by Mulliken [50]. The first direct spectroscopic detection of the decay of dissolved singlet molecular oxygen into its ground state in a solution of CCl_4 was done by Krasnovsky *et al.* [51]. The detection of the decay of singlet oxygen is still challenging for low quantum yields and in some liquids due to the low signal-to-noise ratio of the luminescence signal at $1270\ nm$. According to Kasha the relaxation from singlet to triplet molecular oxygen is quantum mechanically forbidden, due to a violation of the conservation of the spin, the symmetry and the orbital angular momentum, which results in a metastable state and a relatively long lifetime of singlet oxygen on a typical time scale for chemical reactions [49, 52]. In solution a shorter lifetime of singlet oxygen is yielded due to perturbation.

After the photoactivation of a photosensitizer with a light source with photons of an appropriate wavelength and thus energy ($h\nu$), the photosensitizer is promoted in an electronically excited state S_n. The photosensitizer can then release the additional energy via radiative or non-radiative processes, which are indicated in figure 1.1.

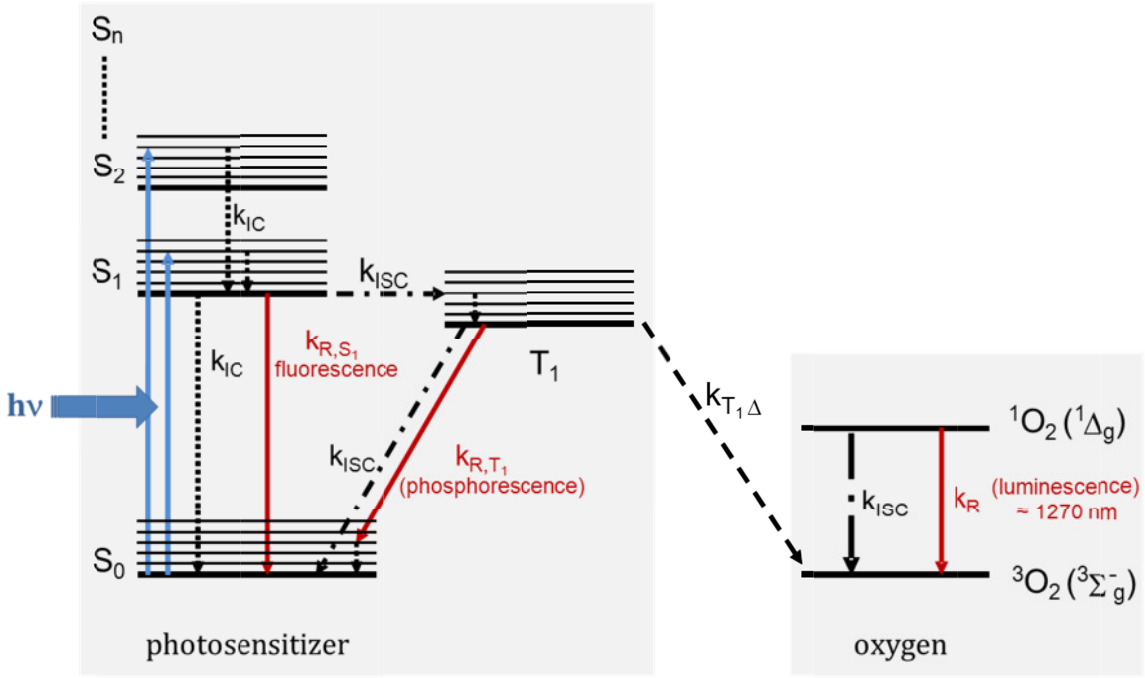

Fig. 1.1: Jablonski diagram showing the process of the generation of singlet oxygen via direct energy transfer from photosensitizer to oxygen; energy levels of the photosensitizer, PS (left) and energy levels of molecular oxygen, O_2 (right) are shown. S_0 is the ground state of the PS, S_1 the first excited singlet state, S_n higher excited singlet states; T_1 is the first excited triplet state of the PS; O_2 and $^1O_2$ are the ground state and the first excited singlet state of molecular oxygen, respectively. Possible relaxation rates of the excited PS are internal conversion (k_{IC}), fluorescence ($k_{R,S1}$), intersystem crossing (k_{ISC}), phosphorescence ($k_{R,T1}$) and energy transfer from the excited T_1-state of the PS to molecular oxygen ($k_{T1\Delta}$). The energy transfer yields the generation of singlet oxygen $^1O_2$.

After relaxation into the first excited singlet state S_1, the excited state can spontaneously relax into the S_0 ground state via non-radiative mechanisms like vibrational relaxation, internal conversion (IC); when energy is transferred to a different electronic state, a long-lived triplet-T_1-state, distinguished from the S_1 state by its spin multiplicity another vibrational relaxation named intersystem crossing (ISC) can occur. Energy loss might also occur via radiative relaxation resulting in fluorescence ($S_n \rightarrow S_1$, conservation of spin multiplicity) or phosphorescence ($T_1 \rightarrow S_1$, changing spin multiplicity). Energy can be transferred from the triplet-T_1-state to adjacent molecular oxygen in its triplet ground state resulting in the formation of singlet oxygen [30].

After formation of the T_1-state other photochemical reactions might occur, leading to a relaxation to the ground state. In general, two different types of reaction pathways are distinguished: in the type-I-reaction the photosensitizer reacts in its excited singlet or triplet state with other molecules by electron transfer or hydrogen abstraction, which leads to the generation of free radicals. In the type-II-reaction singlet oxygen is generated by

direct energy transfer from the excited triplet-state of the photosensitizer to molecular oxygen in its triplet ground state. Type-I and type-II can occur simultaneously and their probability depends mainly on the photosensitizer properties, the substrate, or the properties of the surrounding medium, such as the oxygen concentration.

The direct microbicidal efficacy of singlet oxygen was proven by an experiment in the late 1980s by Dahl *et al*. who exposed bacteria to pure singlet oxygen under exclusion of any kind of other ROS. In this case, a possible type-I-mechanism due to direct contact of photosensitizer and microorganism was excluded by increasing the distance between the origin of singlet oxygen and the microorganisms [53].

1.2.2 Photosensitizers

Effective photosensitizers should generate singlet oxygen to a high extent, *i.e.* have a high quantum yield of singlet oxygen formation. In regard to differences in the outer cell membrane of microorganisms and thus different uptake features of neutral, anionic or cationic photosensitizers in comparison to human eukaryotic cells furthermore a therapeutic window should possible. Especially Gram(-) bacteria responded poorly to PDI with the first discovered photosensitizers, but it was found that positive charges in the photosensitizer enhance the antibacterial efficacy [54].

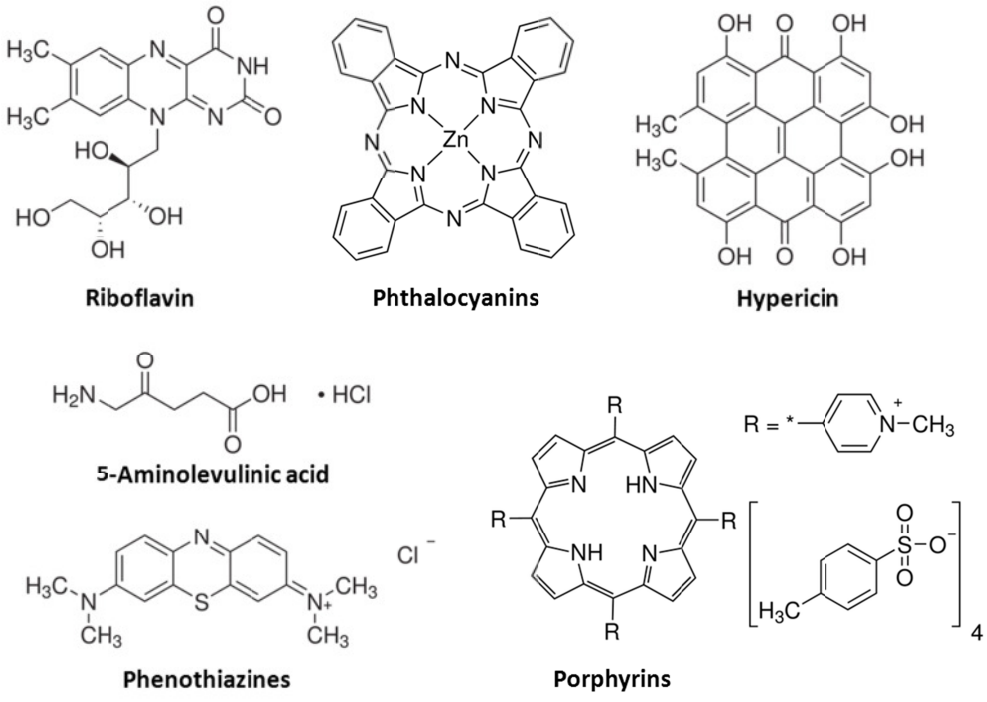

Fig. 1.2: Chemical structures of frequently used classes of photosensitizers.

A lot of different photosensitizer types, occurring naturally or having been synthesized, were investigated in the last decades in regard to the generation of singlet oxygen and to a phototoxic effect against pathogen microorganisms. Some examples, frequently tested in PDI, are displayed in figure 1.2. Many of these photoactive dyes exhibit de-localised electrons in their binding π-orbitals. In these orbitals the spins typically are antiparallel; a change of the spin multiplicity from singlet to triplet excited state (see 1.2.1) is quantum mechanically forbidden, but the probability therefore is enhanced if electronic ring currents due to spin-orbit-coupling are possible, due to collisions with the solvent or due to heavy atom effects [49].

1.2.3 Cells

In this work both, prokaryotic and eukaryotic, microorganisms were used, which are facultative pathogens and can cause severe illness. The risk of infection is enhanced due to their settlement and growth on surfaces, and thus a distribution through humans.

Candida albicans is a eukaryotic cell symbiotically present in healthy individuals and is considered to be the most common fungal pathogen. This yeast organism causes infections in both immunocompromised and immunocompetent humans and may affect the mucosal epithelia, in severe cases also followed by dissemination *via* the bloodstream and infection of internal organs [55-58]. The cytoplasm of *C. albicans* is separated from the exterior by a cell wall and contains for eukaryotes typical organelles like a nucleus, capsules, vacuoles, mitochondria, and several cytoplasmic inclusion bodies [59]. The cell type is polyphenic and thus grows vegetatively in either ovoid yeast, pseudohyphae or hyphae (filamentous) form.

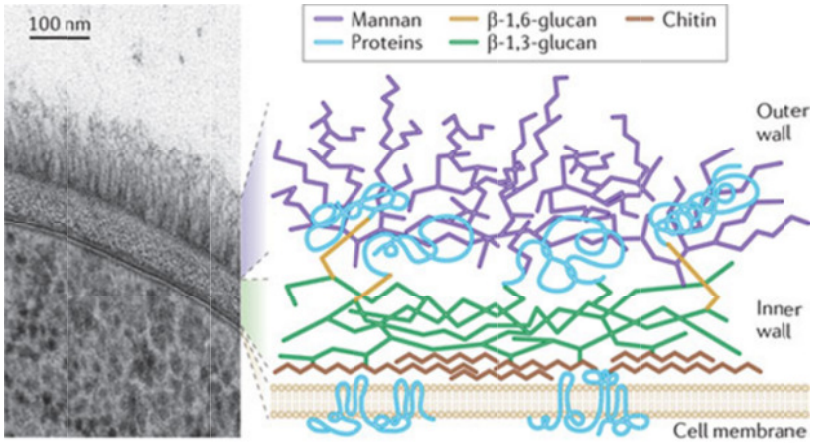

Fig. 1.3: C. albicans cell wall structure [60].

The *C. albicans* cell wall can be separated into two layers of which the outer layer contains mannose polymers, responsible for the formation of glycoproteins, and the inner layer consists of the polysaccharides chitin and β-1,3-glucan, responsible for the cell shape (fig. 1.3). Both layers are linked by β-1,6-glucan [60]. Polysaccharides, specifically β-1,3 glucan, have been described to be the main component of the *C. albicans* biofilm matrix while containing less carbohydrate compared to the planktonic counterparts [61, 62]. In the biofilm state *C. albicans* infections can be up to 2000 times more resistant to antimicrobial agents than in their planktonic form and causes frequently infections that can evolve to deep-seated mycoses [63-69].

Staphylococcus aureus and *Escherichia coli* are prokaryotes, which represent Gram(+) or Gram(-) strains, respectively, divided by the differences of their cell wall structure, thus leading to different staining behaviour (Gram staining). The cytoplasm of Gram(−) bacteria is separated from the outside by an inner wall, which is a peptidoglycan ($2-3\,nm$), followed by a periplasmic space and an outer lipid bilayer ($\approx 7\,nm$). The lipid bilayer contains phospholipids, lipoproteins, lipopolysaccharides (LPS) and proteins like porins (fig. 1.4, A). The outer cell wall of Gram(-) bacteria can be an additional permeability barrier for photosensitizer molecules. Gram(+) bacteria do not form this outer cell wall, but a cell wall containing peptidoglycan layers with an enhanced thickness between $15-80\,nm$, containing teichoic or lipoteichoic acids, as well as proteins (fig. 1.4, B) [70].

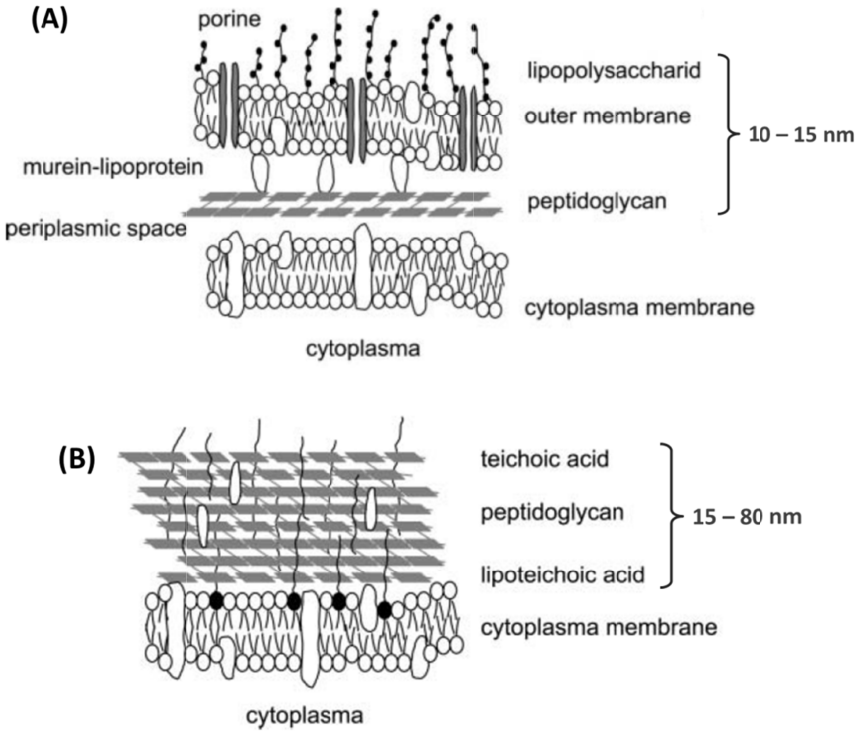

Fig. 1.4: Cell wall structures of (A) Gram(-) and (B) Gram(+) bacteria [70].

1.3 SELF-DISINFECTING SURFACES and CURRENT STATE OF RESEARCH

In order to stop or slow down transmission of microorganisms to new hosts, which results in the spread of infectious diseases, self-disinfecting surfaces using the PDI mechanism are in the focus of interest since several years and some reports are summarized in the following. The main methods to avoid contamination are cleaning or using disinfectants. With PDI-based surfaces, a photosensitizer is embedded in a transparent surface, thus can be activated by light and transfer its energy to oxygen to form ROS. Optimally, mainly singlet oxygen should be generated, because its gaseous properties lead to diffusion into the air surrounding the surface. An overview of examples of antimicrobial surfaces in the light of hospital-acquired infections is given by Page *et al.* [44]. There, different surfaces with the ability to kill microorganisms are presented like structures with embedded photosensitizers or release mechanisms or materials which kill pathogens upon direct contact [44]. In general, studies of polymer surfaces with embedded photosensitizers aim to answer the questions about

- the duration of microorganism survival on surfaces,
- the appropriate photosensitizer and irradiation lamp,
- the ideal light doses and photosensitizer concentrations,
- the photostability of surface and photosensitizer,
- the exact mechanism of generation and decay of singlet oxygen and the involvement of other ROS
- or the active photokilling or growth hindrance (phototoxic efficacy).

Reports of bacterial cell number on surface hospitals reveal a rather low number of colony forming units (CFU) per area. Ruatala *et al.* report bacterial densities between $4-7\ CFU\ cm^{-2}$ encountered on hospital surfaces of rooms occupied by patients with *Staphylococcus aureus* infections [71]. Therefore, it has to be defined what is considered as 'effective photokill'.

1.3.1 Reported phototoxic efficacy of some PDI-surfaces

Wilson *et al.* and Decraene *et al.* investigated cellulose acetate polymer films containing TBO ($0.005\ mg\ mL^{-1}$) for their efficacy to kill bacteria in several studies [42, 43, 72, 73]. After

24 h irradiation with white light (60 W domestic light bulb, 778 lux) and under exclusion of leaking effects of the photosensitizer from the material, a killing efficacy of 94% for EMRSA-16 ($10^5\ CFU\ mL^{-1} \triangleq 0.4 \cdot 10^5\ CFU\ cm^{-2}$) and 99.9% for *Pseudomonas aeruginosa* ($2 \cdot 10^5\ CFU\ mL^{-1} \triangleq 0.99 \cdot 10^5\ CFU\ cm^{-2}$) was obtained [42]. The group furthermore investigated *Staphylococcus aureus*, *Escherichia coli*, *Clostridium difficile*, and *Candida albicans* and concluded that different irradiation times lead to different killing activity; also a difference in the susceptibility of these microorganism strains was detected and killing efficacies of up to 6 log_{10}-steps were reported for an irradiation time of 16 h [73]. A test of these surface coating in a hospital for 24 h led to a killing percentage of organisms per hour of 63.8% for aerobic and 81.8% for anaerobic microorganisms [43].

Disinfection of water is one of the aims to reach with PDI-surfaces. Bonnet *et al.* describe a polymeric membrane which can be used for water disinfection [74]. There, the immobilized zinc phthalocyanine attached to a reinforced chitosan polymer membrane *via* a sulfonamide linkage provides a photomicrobicidal system using PDI. At contamination levels of up to $10^5\ CFU\ mL^{-1}$ a kill of *E. coli* of more than 2 log_{10}-steps (99%) was detected.

Funes *et al.* investigated the photodynamic properties of a polymeric film containing 5,10,15,20-tetra(4-N,N-diphenylaminophenyl)porphyrin and its complex with Pd(II) that were polymerized electrochemically. Singlet oxygen generation was determined with indirect measurements using 9,10-dimethylanthracene. The irradiation of the surfaces 30 min yielded a reduction of 2.5 and 3 log_{10}-steps for *C. albicans* and *E. coli*, respectively, *in vitro* in aqueous cell suspensions [75].

A basic question will remain, to which extent the phototoxicity is considered as 'effective', since the self-disinfecting surfaces are not disinfecting already existing microorganism colonies, but rather prevent the settling and growing of these pathogens.

1.3.2 Singlet oxygen detection and decay of photosensitizer triplet state in polymer materials

The assignment of the decay times of the excited photosensitizer triplet state and singlet oxygen from the directly detected singlet oxygen luminescence signals is still challenging due to complex deactivation mechanisms of photosensitizer and singlet oxygen. Early investigations of singlet oxygen decay and photosensitizer quenching in polymers were performed by Clough *et al.* following the oxidising properties of molecular oxygen on these

materials. They used direct IR-spectroscopy to detect singlet oxygen within the material but reported difficulties multi-exponential decay manner. A model was proposed to clarify photosensitizer triplet-state decay and decay of singlet oxygen stating an intrinsic single-exponential decay of singlet oxygen and a multi-exponential decay of the excited photosensitizer triplet state [76].

Poulsen *et al.* investigated the time dependence of oxygen transport of a bilayer of two polymers. Therefore, the oxygen transport through poly(ethylene-co-norbornene) into a polystyrene polymer film was determined by the phosphorescence of singlet oxygen. This experiment showed the possibility to quantify the diffusion of oxygen [77].

Chirvony *et al.* studied the photophysical properties of matrices of nano-porous silicon impregnated with TMPyP as cationic or TPPS as anionic porphyrins. There, the ability of the material itself to transfer its energy directly to molecular oxygen to form singlet oxygen was reported as well. They described difficulties in detecting singlet oxygen directly by its luminescence, which was only possible for TMPyP. The fluorescence decay of the photosensitizers was reported to be non-exponential. They assume that singlet oxygen is effectively quenched on the surface due to electronic energy transfer to the high-frequency OH stretching vibrations of the SiOH surface groups [78].

Jesenska *et al.* investigated different polymeric nanofiber materials doped each with the photosensitizer 5,10,15,20-tetraphenylporphyrin (TPP) in regard to their property to generate singlet oxygen as well as their antibacterial activity against *E. coli*. They determined a dependency of the photokilling effect on the oxygen permeability or diffusion coefficients and reported a post-irradiation effect due to the presence of H_2O_2, which was besides $^1O_2$ another ROS being photogenerated [46].

These examples show in short the complexity of the matter of self-disinfecting surfaces and were used as basis and guidelines throughout this thesis.

1.4 OBJECTIVES

The main aim of this thesis was to clarify the photophysical and photobiological effects of different photosensitizers that are potential candidates for PDI. Therefore, the photosensitizers were investigated in regard to their ability to generate singlet oxygen and singlet oxygen was detected by an indirect method of the formation of tri-iodide upon contact of potassium iodide with singlet oxygen and direct NIR-spectroscopy at 1270 nm.

By changing the properties of the surrounding of the photosensitizer and singlet oxygen such as a change of the oxygen, photosensitizer or quencher concentration, by investigation of photosensitizer and singlet oxygen in aqueous surrounding with and without cell physiological additives, incubated into microorganisms in suspension or formed as a biofilm-layer and doped into different types of polymer surfaces new insights into the photophysics of the different photosensitizers and the behaviour of singlet oxygen in these complex systems should be gained. The following main questions were addressed:

- Which photosensitizers are suitable to be doped into surfaces?
- To which extent are the photophysical properties of photosensitizers changed by the additives in cell physiological solution, such as phosphate buffered saline (PBS)?
- Can the singlet oxygen signal generated by photosensitizers in or attached to cells give insight to the localisation of the photosensitizer?
- Do the photosensitizers maintain their ability to generate singlet oxygen when doped into surfaces and can the singlet oxygen luminescence signals be interpreted in regard to oxygen concentration or diffusion behaviour and quenching kinetics of the photosensitizer?
- To which extent are the created surfaces effective against microorganisms?

To answer these questions, different techniques were applied like absorption spectroscopy, direct detection of singlet oxygen and the characterisation of its luminescence. These techniques were used furthermore to investigate the uptake of photosensitizers into microorganisms and the effect on the singlet oxygen generation within cells. Microbiological experiments included irradiation of photosensitizers in solution or linked to surfaces with different light sources to clarify the phototoxicity against both, Gram(-) and Gram(+) bacteria.

1.5 REFERENCES

1. Bisdorff, B., et al., *MRSA-ST398 in livestock farmers and neighbouring residents in a rural area in Germany.* Epidemiol Infect, 2012. **140**(10): p. 1800-8.
2. Kuehn, B., *MRSA may move from livestock to humans.* JAMA, 2012. **308**(17): p. 1726.
3. Bos, M.E., et al., *Livestock-associated MRSA prevalence in veal calf production is associated with farm hygiene, use of antimicrobials, and age of the calves.* Prev Vet Med, 2012. **105**(1-2): p. 155-9.
4. Appelbaum, P.C., *MRSA - the tip of the iceberg.* Clinical Microbiology and Infection, 2006. **12**: p. 3-10.
5. Bower, C.K. and M.A. Daeschel, *Resistance responses of microorganisms in food environments.* International Journal of Food Microbiology, 1999. **50**(1-2): p. 33-44.
6. Ang, J.Y., E. Ezike, and B.I. Asmar, *Antibacterial resistance.* Indian J Pediatr, 2004. **71**(3): p. 229-39.
7. Darwin, C., *On the Origin of Species by Means of Natural Selection, or the Preservation of Favoured Races in the Struggle for Life.* 1859.
8. Baquero, F., et al., *Antibiotic-selective environments.* Clinical Infectious Diseases, 1998. **27**: p. S5-S11.
9. Howell, L.*e.a.*, *Global Risks 2013.* World Economic Forum, 2013: p. 80.
10. Boucher, H.W., et al., *Bad bugs, no drugs: no ESKAPE! An update from the Infectious Diseases Society of America.* Clin Infect Dis, 2009. **48**(1): p. 1-12.
11. Peterson, L.R., *Bad bugs, no drugs: no ESCAPE revisited.* Clin Infect Dis, 2009. **49**(6): p. 992-3.
12. Livermore, D.M., et al., *Non-susceptibility trends among Enterobacteriaceae from bacteraemias in the UK and Ireland, 2001-06.* J Antimicrob Chemother, 2008. **62 Suppl 2**: p. ii41-54.
13. Gonzales, F.P. and T. Maisch, *Photodynamic inactivation for controlling Candida albicans infections.* Fungal Biology, 2012. **116**(1): p. 1-10.
14. Maisch, T., et al., *Photodynamic inactivation of multi-resistant bacteria (PIB) - a new approach to treat superficial infections in the 21st century.* J Dtsch Dermatol Ges, 2011. **9**(5): p. 360-6.
15. Pereira Gonzales, F. and T. Maisch, *Photodynamic inactivation of microorganisms as an innovative approach to kill mucocutaneous and skin microorganisms.* G Ital Dermatol Venereol, 2010. **145**(4): p. 477-89.
16. Donnelly, R.F., P.A. McCarron, and M.M. Tunney, *Antifungal photodynamic therapy.* Microbiol Res, 2008. **163**(1): p. 1-12.
17. Hamblin, M.R. and T. Hasan, *Photodynamic therapy: a new antimicrobial approach to infectious disease?* Photochem Photobiol Sci, 2004. **3**(5): p. 436-50.
18. Hamblin, M.R., *Antimicrobial photodynamic therapy and photodynamic inactivation, or killing bugs with dyes and light--a symposium-in-print.* Photochem Photobiol, 2012. **88**(3): p. 496-8.
19. Ferro, S., et al., *Efficient photoinactivation of methicillin-resistant Staphylococcus aureus by a novel porphyrin incorporated into a poly-cationic liposome.* Int J Biochem Cell Biol, 2007. **39**(5): p. 1026-34.
20. Baier, J., et al., *Time-resolved investigations of singlet oxygen luminescence in water, in phosphatidylcholine, and in aqueous suspensions of phosphatidylcholine or HT29 cells.* J Phys Chem B, 2005. **109**(7): p. 3041-6.
21. Snyder, J.W., et al., *Subcellular, time-resolved studies of singlet oxygen in single cells.* J Am Chem Soc, 2005. **127**(42): p. 14558-9.
22. Redmond, R.W. and I.E. Kochevar, *Spatially resolved cellular responses to singlet oxygen.* Photochem Photobiol, 2006. **82**(5): p. 1178-86.
23. Ragas, X., M. Agut, and S. Nonell, *Singlet oxygen in Escherichia coli: New insights for antimicrobial photodynamic therapy.* Free Radic Biol Med, 2010. **49**(5): p. 770-6.
24. Niedre, M.J., et al., *In vitro tests of the validity of singlet oxygen luminescence measurements as a dose metric in photodynamic therapy.* Cancer Res, 2003. **63**(22): p. 7986-94.
25. Maisch, T., et al., *The role of singlet oxygen and oxygen concentration in photodynamic inactivation of bacteria.* Proc Natl Acad Sci U S A, 2007. **104**(17): p. 7223-8.
26. Raab, O., *Ueber die Wirkung Fluorescierenden Stoffe auf Infusorien.* Z. Biol., 1904. **39**: p. 23.
27. Tappeiner, H.v.J., A., *Uber die Wirkung der photodynamischen (fluorescierenden) Stoffe auf Protozoen und Enzyme.* Dtsch. Arch. Klin. Med., 1904 **80**: p. 61.

28. Kautsky, H.H., A., *Wechselwirkung zwischen angeregten Farbstoff-Molekülen und Sauerstoff.* Berichte der deutschen chemischen Gesellschaft, 1931. **64**: p. 7.
29. Kautsky, A.d.B., H.; Neuwirth, R.; Baumeister, W., *Photo-sensibilisierte Oxydation als Wirkung eines aktiven, metastabilen Zustandes des Sauerstoff-Moleküls.* Berichte der deutschen chemischen Gesellschaft, 1933. **66**(10): p. 13.
30. Krasnovsky, A.A., Jr., *Primary mechanisms of photoactivation of molecular oxygen. History of development and the modern status of research.* Biochemistry (Mosc), 2007. **72**(10): p. 1065-80.
31. Denis, T.G.S., et al., *All you need is light Antimicrobial photoinactivation as an evolving and emerging discovery strategy against infectious disease.* Virulence, 2011. **2**(6): p. 509-520.
32. Konopka, K. and T. Goslinski, *Photodynamic therapy in dentistry.* J Dent Res, 2007. **86**(8): p. 694-707.
33. Spratt, D.A., et al., *An in vitro evaluation of the antimicrobial efficacy of irrigants on biofilms of root canal isolates.* Int Endod J, 2001. **34**(4): p. 300-7.
34. Wilson, M., *Susceptibility of oral bacterial biofilms to antimicrobial agents.* Journal of Medical Microbiology, 1996. **44**(2): p. 79-87.
35. Biel, M.A., *Photodynamic therapy of bacterial and fungal biofilm infections.* Methods Mol Biol, 2010. **635**: p. 175-94.
36. Wilson, M., T. Burns, and J. Pratten, *Killing of Streptococcus sanguis in biofilms using a light-activated antimicrobial agent.* J Antimicrob Chemother, 1996. **37**(2): p. 377-81.
37. Taraszkiewicz, A., et al., *Innovative Strategies to Overcome Biofilm Resistance.* Biomed Research International, 2013.
38. Maisch, T., et al., *Fast and effective: intense pulse light photodynamic inactivation of bacteria.* J Ind Microbiol Biotechnol, 2012. **39**(7): p. 1013-21.
39. Buchovec, I., E. Paskeviciute, and Z. Luksiene, *Photodynamic Inactivation of Food Pathogen Listeria monocytogenes.* Food Technology and Biotechnology, 2010. **48**(2): p. 207-213.
40. Brovko, L.Y., et al., *Photodynamic Treatment: A Novel Method for Sanitation of Food Handling and Food Processing Surfaces.* Journal of Food Protection, 2009. **72**(5): p. 1020-1024.
41. Brovko, L., *Photodynamic treatment: a new efficient alternative for surface sanitation.* Adv Food Nutr Res, 2010. **61**: p. 119-47.
42. Wilson, M., *Light-activated antimicrobial coating for the continuous disinfection of surfaces.* Infect Control Hosp Epidemiol, 2003. **24**(10): p. 782-4.
43. Decraene, V., J. Pratten, and M. Wilson, *An assessment of the activity of a novel light-activated antimicrobial coating in a clinical environment.* Infect Control Hosp Epidemiol, 2008. **29**(12): p. 1181-4.
44. Page, K., M. Wilson, and I.P. Parkin, *Antimicrobial surfaces and their potential in reducing the role of the inanimate environment in the incidence of hospital-acquired infections.* Journal of Materials Chemistry, 2009. **19**(23): p. 3819-3831.
45. Perni, S., et al., *The antimicrobial properties of light-activated polymers containing methylene blue and gold nanoparticles.* Biomaterials, 2009. **30**(1): p. 89-93.
46. Jesenska, S., et al., *Antibacterial nanofiber materials activated by light.* J Biomed Mater Res A, 2011. **99**(4): p. 676-83.
47. Perni, S., et al., *Antimicrobial properties of light-activated polyurethane containing indocyanine green.* J Biomater Appl, 2011. **25**(5): p. 387-400.
48. Perni, S., et al., *Prevention of biofilm accumulation on a light-activated antimicrobial catheter material.* Journal of Materials Chemistry, 2010. **20**(39): p. 8668-8673.
49. Regensburger, J., *Spektroskopische Untersuchungen zur Singulett-Sauerstoff-Lumineszenz in Biomolekülen, Bakterien und Zellen.* Dissertation, 2010: p. 202.
50. Mulliken, R.S., *Interpretation of the Atmospheric Oxygen Bands; Electronic Levels of the Oxygen Molecule.* Nature, 1928. **122**: p. 1.
51. Krasnovsky, A.A., *Quantum Yield of Photosensitized Luminescence and Radiative Lifetime of Singlet (1-Delta-G) Molecular-Oxygen in Solutions.* Chemical Physics Letters, 1981. **81**(3): p. 443-445.
52. Kasha, M., *Singlet O2, volume 1.* CRC Press, Boca Raton, Florida, 1985.
53. Dahl, T.A., W.R. Midden, and P.E. Hartman, *Pure singlet oxygen cytotoxicity for bacteria.* Photochem Photobiol, 1987. **46**(3): p. 345-52.
54. Jori, G., et al., *Photodynamic therapy in the treatment of microbial infections: basic principles and perspective applications.* Lasers Surg Med, 2006. **38**(5): p. 468-81.

55. Kothavade, R.J., et al., *Candida tropicalis: its prevalence, pathogenicity and increasing resistance to fluconazole.* Journal of Medical Microbiology, 2010. **59**(8): p. 873-880.
56. Singh, N., *Trends in the epidemiology of opportunistic fungal infections: predisposing factors and the impact of antimicrobial use practices.* Clin Infect Dis, 2001. **33**(10): p. 1692-6.
57. Gudlaugsson, O., et al., *Attributable mortality of nosocomial candidemia, revisited.* Clin Infect Dis, 2003. **37**(9): p. 1172-7.
58. Larriba, G., et al., *Candida albicans molecular biology reaches its maturity.* Int Microbiol, 2000. **3**(4): p. 247-52.
59. Osumi, M., *The ultrastructure of yeast: Cell wall structure and formation.* Micron, 1998. **29**(6): p. 207-233.
60. Gow, N.A.R., et al., *Candida albicans morphogenesis and host defence: discriminating invasion from colonization.* Nature Reviews Microbiology, 2012. **10**(2): p. 112-122.
61. Baillie, G.S. and L.J. Douglas, *Matrix polymers of Candida biofilms and their possible role in biofilm resistance to antifungal agents.* Journal of Antimicrobial Chemotherapy, 2000. **46**(3): p. 397-403.
62. Al-Fattani, M.A. and L.J. Douglas, *Biofilm matrix of Candida albicans and Candida tropicalis: chemical composition and role in drug resistance.* Journal of Medical Microbiology, 2006. **55**(8): p. 999-1008.
63. Douglas, L.J., *Candida biofilms and their role in infection.* Trends Microbiol, 2003. **11**(1): p. 30-6.
64. Chandra, J., et al., *Biofilm formation by the fungal pathogen Candida albicans: development, architecture, and drug resistance.* J Bacteriol, 2001. **183**(18): p. 5385-94.
65. Ramage, G., et al., *Characteristics of biofilm formation by Candida albicans.* Rev Iberoam Micol, 2001. **18**(4): p. 163-70.
66. Ramage, G., B.L. Wickes, and J.L. Lopez-Ribot, *Biofilms of Candida albicans and their associated resistance to antifungal agents.* Am Clin Lab, 2001. **20**(7): p. 42-4.
67. Ramage, G., et al., *Candida biofilms: an update.* Eukaryotic Cell, 2005. **4**(4): p. 633-638.
68. Chandra, J., P.K. Mukherjee, and M.A. Ghannoum, *Candida biofilms associated with CVC and medical devices.* Mycoses, 2012. **55**: p. 46-57.
69. Pereira Gonzales, F.F., A.; Maisch, T., *Fungicidal photodynamic effect of a two-fold positively charged porphyrin against Candida albicans planktonic and biofilm cells.* 2013. **in revision**.
70. Maisch, T., et al., *Antibacterial photodynamic therapy in dermatology.* Photochem Photobiol Sci, 2004. **3**(10): p. 907-17.
71. Rutala, W.A., et al., *Environmental study of a methicillin-resistant Staphylococcus aureus epidemic in a burn unit.* J Clin Microbiol, 1983. **18**(3): p. 683-8.
72. Decraene, V., J. Pratten, and M. Wilson, *Novel light-activated antimicrobial coatings are effective against surface-deposited Staphylococcus aureus.* Curr Microbiol, 2008. **57**(4): p. 269-73.
73. Decraene, V., J. Pratten, and M. Wilson, *Cellulose acetate containing toluidine blue and rose bengal is an effective antimicrobial coating when exposed to white light.* Appl Environ Microbiol, 2006. **72**(6): p. 4436-9.
74. Bonnett, R., et al., *Water disinfection using photosensitizers immobilized on chitosan.* Water Res, 2006. **40**(6): p. 1269-75.
75. Funes, M.D., et al., *Photodynamic Properties and Photoantimicrobial Action of Electrochemically Generated Porphyrin Polymeric Films.* Environ Sci Technol, 2009. **43**(3): p. 902-908.
76. Clough, R.L., et al., *Behavior of Singlet Molecular-Oxygen (1-Delta-G02) in a Polymer Matrix - Effects of Temperature, Matrix Rigidity, and Molecular Composition.* Macromolecules, 1989. **22**(9): p. 3620-3628.
77. Poulsen, L., et al., *Oxygen diffusion in bilayer polymer films.* Journal of Physical Chemistry B, 2003. **107**(50): p. 13885-13891.
78. Chirvony, V., et al., *Fluorescence and O-1(2) generation properties of porphyrin molecules immobilized in oxidized nano-porous silicon matrix.* Journal of Photochemistry and Photobiology a-Chemistry, 2006. **181**(1): p. 106-113.

Chapter 2

Material and Methods

The chapter describes the experimental setups and techniques used in order to investigate the light-induced photophysical behaviour of the photosensitizers in different surroundings and their phototoxic efficacy against microorganisms. Details of the spectroscopic analysis of the biologically relevant dyes in solution with water, incubated in cells, or doted into surface materials are described specifically.

2.1 CHEMICALS: PHOTOSENSITIZERS, SOLVENTS, QUENCHER, AND SUBSTANCES FOR CHEMICAL ANALYSES

2.1.1 Photosensitizers

2.1.1.1 Porphyrins

XF 73

The water-soluble di-cationic 5,15-bis-[4-(3-Trimethylammonio-propyloxy)-phenyl]-porphyrin (XF73) with a molar mass of $MW = 765.81\ g\ mol^{-1}$ (including the counter ion) was synthesized by Xiangdong Feng (Solvias Company, Basel, Switzerland) and kindly provided by Destiny Pharma Ltd. (Brighton, United Kingdom). XF73 is used in clinical trials for the decolonisation of *S. aureus* in the nasal region using its high dark toxicity by Destiny Pharma Ltd. Due to its very good uptake properties and phototoxicity it had been investigated spectroscopically in H_2O already with regard to singlet oxygen generation and a quantum yield for singlet oxygen formation of 0.57 was determined [1].

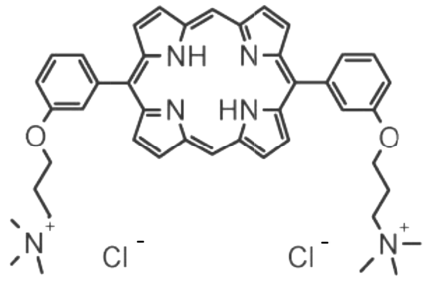

XF73

TMPyP

5,10,15,20-Tetrakis(1-methyl-4-pyridinio)-porphyrin tetra(p-toluenesulfonate) (TMPyP) with a molar mass of $MW = 1363.63\ g\ mol^{-1}$ (including the counter ion), purity ≥ 97%, was purchased by Sigma Aldrich (Taufkirchen, Germany). TMPyP is a commonly used dye in the field of aPDT due to different properties: TMPyP has a high photostability, shows also thermal stability up to $200°C$, which was shown previously in our group. It has a sufficient

quantum yield of 0.74 [2] which was confirmed by Frederikson *et al. with* 0.77 ± 0.04 [3] and Angeli *et al.* with 0.75 in H_2O [4]. Recently, Eichner *et al.* showed the photodynamic effectiveness of TMPyP against microorganisms within few seconds [5].

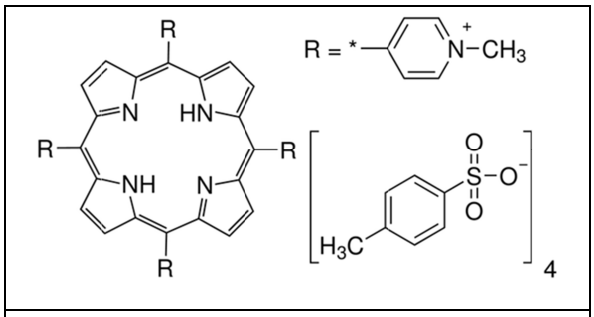

TMPyP

TPP

The hydrophobic 5,10,15,20-Tetraphenyl-21H,23H-porphine, (*meso*-Tetraphenylporphyrin, TPP) with a molar mass of $MW = 614.74\ g\ mol^{-1}$, purity ≥ 99%, was received from Sigma Aldrich. It was dissolved in benzene for the preparation of the cellulose acetate surfaces, whereas in literature many spectroscopic investigations were reported in acetone. TPP has a sufficient quantum yield of 0.65 [6] which was confirmed by Redmond *et al.* with 0.62 in CCl_4 [2].

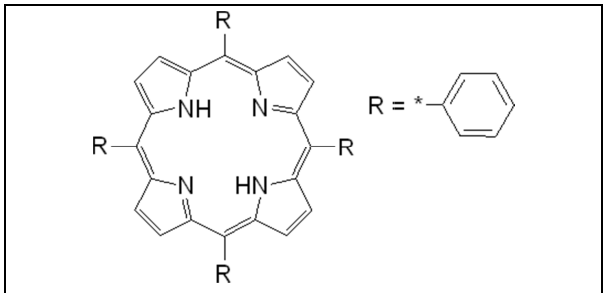

TPP

2.1.1.2 Perinaphthenons

Perinaphthenone derivatives are photosensitizers that have been described photochemically and physically by Oliveros *et al.* [7] and Nonell *et al.* [8]. The polar sulfonised 1h-Phenalen-1-One-2-Sulfonic Acid (PNS, $MW = 260.27\ g\ mol^{-1}$) was used for

reference measurement since it has a quantum yield ≈ 1 and is therefore a very effective water-soluble singlet oxygen generator [8, 9].

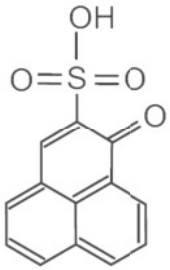
PNS

2.1.1.3 Phenothiaziniums

Methylene blue (MB, $MW = 319.86\ g\ mol^{-1}$), New Methylene blue N (NMB, $MW = 347.91\ g\ mol^{-1}$), Dimethyl Methylene blue (DMMB, $MW = 416.05\ g\ mol^{-1}$) and Toluidine Blue O (TBO, $MW = 305.83\ g\ mol^{-1}$) were purchased from Sigma Aldrich and thereafter purified by flash chromatography with silica gel using dichloromethane/ethanol 10:1 as the eluent mixture resulting in an overall purity of > 99% (HPLC-MS). The purification was performed by Dr. Andreas Späth, Institute of Organic Chemistry (University of Regensburg, Germany). MB and its derivatives were diluted in H_2O and kept in the dark at 4°C until use.

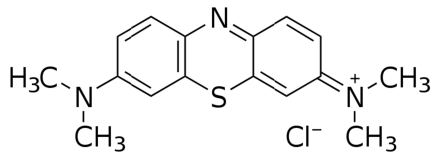	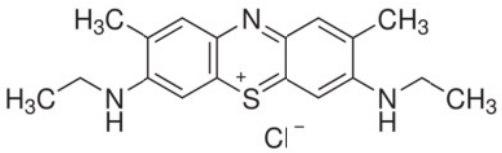
MB	NMB
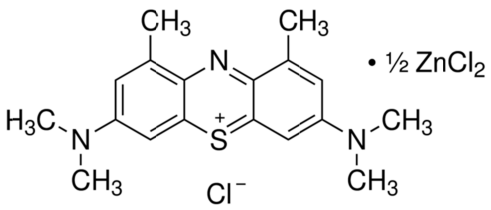	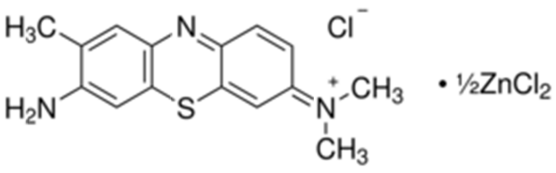
DMMB	TBO

The quantum yields (Φ_Δ) of the new derivatives of MB were compared to the Φ_Δ of MB which is reported in literature being $\Phi_\Delta = 0.52$ in aqueous solution [10].

Except simple substituents like alkyl or hydroxyalkyl residues, nearly no modifications of the phenothiazinium derivatives were pursued at the auxochromic sites. A set of six mainly novel MB derivatives were prepared with the ability of additional hydrogen bonding and/or additional cationic charges to study the effect of the substituents on their activity, *e.g.* toxicity profiles, cell attachment and photophysical properties [11].

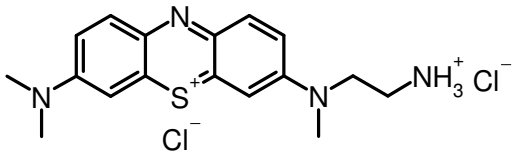	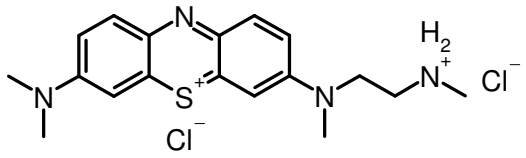
(MB-1)	(MB-2)
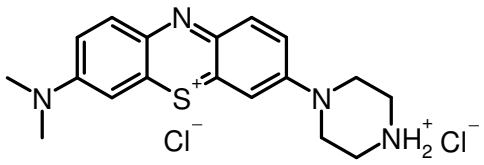	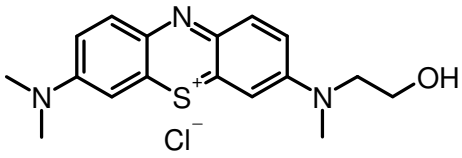
(MB-3)	(MB-4)
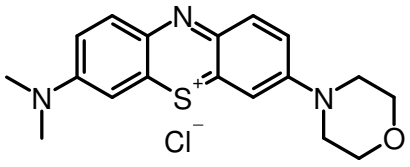	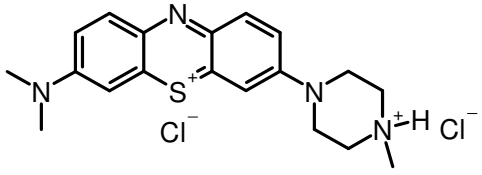
(MB-5)	(MB-6)

Short name	Chemical name	Molecular formula	Molecular weight [$g\ mol^{-1}$]
MB-1	3-[(2-Ammoniumethyl)(methyl)amino]-7-(dimethylamino)phenothiazin-5-ium dichloride	$C_{17}H_{22}N_4SCl_2$	314.46 (+2× 35.45)
MB-2	3-{methyl[2-(methylammonio)ethyl]amino}-7-(dimethylamino)phenothiazin-5-ium dichloride	$C_{18}H_{24}N_4SCl_2$	328.48 (+2× 35.45)
MB-3	3-(piperazin-4-ium-1-yl)-7-(dimethylamino)phenothiazin-5-ium dichloride	$C_{18}H_{22}N_4SCl_2$	326.47 (+2× 35.45)
MB-4	3-[(2-Hydroxyethyl)(methyl)amino]-7-(dimethylamino)phenothiazin-5-ium chloride	$C_{17}H_{20}N_3SOCl_2$	314.43 (+1× 35.45)
MB-5	3-(morpholin-4-yl)-7-(dimethylamino)phenothiazin-5-ium chloride	$C_{18}H_{20}N_3SOCl$	326.44 (+1× 35.45)
MB-6	3-(4-methylpiperazin-4-ium-1-yl)-7-(dimethylamino)phenothiazin-5-ium dichloride	$C_{19}H_{24}N_4SCl_2$	340.49 (+2× 35.45)

2.1.1.4 Photosensitizers doped into polyurethane

The porphyrin- and the phenalenone-derivatives (synthesized by Dr. Andreas Späth, Institute of Organic Chemistry, University of Regensburg, Germany) were mixed with the coating material (PU) and applied to the substrate (PMMA) by the company Warnecke & Böhm. The aim was to polymerize the PSs irreversibly into a polymer by changes of the side chains and with keeping the basic photophysical properties of the dyes. TPP is not water-soluble, a premise for surfaces that will be in contact to H_2O due to incubation with bacteria. Side chains were added to the basic chemical structures of the photosensitizers (PN, TPP) that linked to the basic polymer surface material Polyurethane (PU). *Per se* PN-O-A and –B are water-soluble but modified side chains to link with PU should prevent leakage.

The following figures show the chemical structure formulas for the photosensitizers that were doped into PU. In the case of TPP-O-A the side chain of the ring system of TPP is an additional hydroxyl-group ($-OH$). To enhance the solubility in PU further, TPP-O-B has a hexyl-spacer between the chromophore and the hydroxyl-group. At both PN-O-A and –B a hydroxyl-group was added in order to link the photosensitizers to PU.

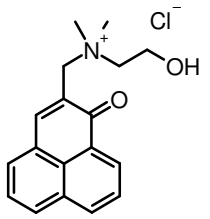	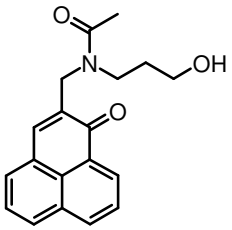
(PN-O-A)	(PN-O-B)
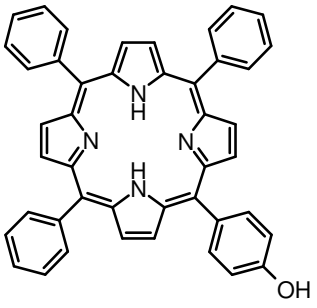	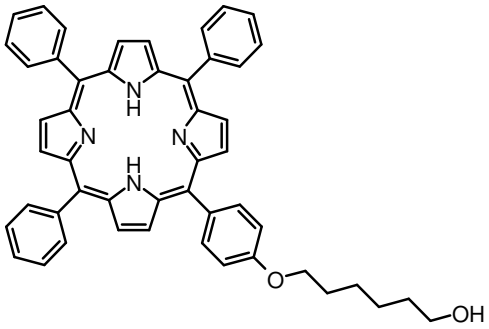
(TPP-O-A)	(TPP-O-B)

Short name	**Chemical name**	**Molecular formula**	**Molecular weight [$g\ mol^{-1}$]**
TPP-O-A	5-(4-Hydroxyphenyl)-10,15,20-triphenylporphyrin	$C_{44}H_{20}N_4O$	630.76
TPP-O-B	5-[4-(6-Hydroxyhexoxy)-phenyl]-10,15,20-triphenylporphyrin	$C_{50}H_{42}N_4O_2$	730.92
PN-O-A	N,N-Dimethyl-N-(2-hydroxyethyl)-2-ammoniummethyl-phenalen-1-one chloride	$C_{18}H_{20}NO_2Cl$	282.37 (+1× 35.45)
PN-O-B	N-(3-Hydroxypropyl)-N-(2-methylen-phenalen-1-one)acetamid	$C_{19}H_{19}NO_3$	309.37

TPP-O-A

A solution of 4-hydroxybenzaldehyde (8.79 g; 71.9 $mmol$) and benzaldehyde (24.0 mL, 24.7 $mmol$) in propionic acid (700 mL) was heated to nearly reflux. To the yellow solution was added dropwise a solution of pyrrole (18.0 mL, 26.0 $mmol$) in propionic acid (20 mL). The reaction mixture was stirred under reflux for 1.5 h. After cooling, propionic acid was evaporated *in vacuo*. The dark residue was filtered through a silica column with CH_2Cl_2 (DCM, R_f = 0.2) as eluent. The solvent was again evaporated under reduced pressure. Next,

the dark solid was recrystallized from EtOH, followed by another column purification with CH_2Cl_2 as eluent, to yield a violet solid (1.8 g, 29.0 $mmol$, 4% relating to 4-hydroxybenzaldehyde).

M = 630.74 g/mol; - **^{1}H-NMR** (400 MHz; $CDCl_3$): δ [ppm] = 8.88 (d, *J* = 4.8 Hz, 2H); 8.85 (d, *J* = 6.2 Hz, 6H) 8.22 (dd, *J* = 1.6 Hz, *J* = 7.8 Hz, 6H), 8.08 (m, 2H), 7.76 (m, 9H), 7.20 (d, *J*= 8.4 Hz, 2H); - **^{13}C-NMR** (75 MHz, $CDCl_3$): δ [ppm] = 155.4 (1C), 142.2 (3C), 135.7 (2C), 134.6 (6C), 131.1 (1C), 127.7 (2C), 126.7 (9C), 120.1 (8C), 113.7 (8C); - **MS** (ES-MS): e/z (%) = 631.3 (100, MH^+);

TPP-O-B

To a solution containing HO-TPP (730 mg, 1.15 $mmol$) and 6-hydroxyhexyl 4-methylbenzenesulfonate (468 mg, 1.72 $mmol$) in 14 mL of DMF, 480 mg K_2CO_3 (3.34 $mmol$) and 285 mg KI (1.72 $mmol$) were added. The reaction mixture was heated to 80°C and was stirred for 2 h. After cooling to room temperature, the reaction mixture was diluted with $EtOAc$ and washed with water and brine. The organic layer was dried over $MgSO_4$ and concentrated under reduced pressure. The purple residue was purified by column chromatography (DCM/PE, 2/1; R_f DCM/PE, 2/1 = 0.2) to give the product as a purple glimmering solid (674 mg, 0.92 $mmol$, 80%).

M = 732.91 g/mol; - **^{1}H-NMR** (400 MHz; $CDCl_3$): δ [ppm] = 8.87 (d, *J* = 4.8 Hz, 2H); 8.84 (d, *J* = 6.2 Hz, 6H) 8.23 (dd, *J* = 1.6 Hz, *J* = 7.8 Hz, 6H), 8.11 (m, 2H), 7.77 (m, 9H), 7.23 (d, *J* = 8.4 Hz, 2H), 4.22 (t, *J* = 6.5, 2H), 2.01 (t, *J* = 6.6, 2H), 1.68 (s, 1H), 1.2 – 1.56 (m, 6H); - **^{13}C-NMR** (75 MHz, $CDCl_3$): δ [ppm] = 159.2 (1C), 142.3 (3C), 135.6 (2C), 134.6 (6C), 134.3 (1C), 127.7 (2C), 126.7 (9C), 120.1 (8C), 113.7 (8C), 68.4 (1C), 32.0 (1C), 29.8 (1C), 29.7 (1C), 26.3 (1C), 22.7 (1C); - **IR**: ν [cm^{-1}] = 3579 (w), 3317 (w), 3027 (w), 2920 (m), 2858 (m), 1596 (w), 1471 (s), 1243 (s), 1174 (s), 964 (s), 798 (s), 731 (s), 701 (s); - **UV-vis** (DCM): λ_{max} (Soret) = 418 nm; λ_{max} (Q) = 514 nm, 551 nm, 590 nm, 648 nm; - **EI-MS** m/z (%): 732.91 [MH^+];

PN-O-A

2-Chlormethyl-1H-phenalen-1-one (230 mg, 1 $mmol$) in N,N-dimethylaminoethanol (1.78 g, 2.0 mL, 20 $mmol$) was stirred for 48 h. Diethylether (30 mL) was added, the precipitate was allowed to settle and the solvent was decanted off. The product was dissolved in ethanol

(1 mL) and precipitated with diethylether (30 mL). It was allowed to settle and the solvents were decanted off. The residue was dried under reduced pressure to give 248 mg of pure yellow solid.

M = 311.2 g/mol; - **^{1}H-NMR** (300 MHz, $CDCl_3$): δ [ppm] = 8.67 (dd, *J* = 1.2 Hz, *J* = 7.4 Hz, 1H), 8.24 (dd, *J* = 1.0 Hz, *J* = 8.1 Hz, 1H), 8.06 (dd, *J* = 0.6 Hz, *J* = 8.2 Hz, 2H), 7.80 (dd, *J* = 7.0 Hz; *J* = 1.2 Hz, 1H), 7.64 (dd, *J* = 7.0 Hz; *J* = 1.2 Hz, 1H), 7.18 (s, 1H), 4.76 (s, 2H), 4.12 (m, 2H), 3.66 (m, 2H), 3.21 (s, 6H), 2.31 (bs, 1H), 1.1 – 1.3 (m, 2H); - **^{13}C-NMR** (75 MHz, $CDCl_3$): δ [ppm] = 183.3 (1C), 149.3 (1C), 134.2 (1C), 133.7 (1C), 130.9 (1C), 128.3 (1C), 127.6 (1C), 127.3 (1C), 126.8 (1C), 126.0 (1C), 65.7 (1C), 61.6 (1C), 55.0 (1C), 50.4 (2C); - **IR**: ν [cm^{-1}] = 3310 (bs), 3030 (m), 2957 (w), 1622 (s), 1618 (s), 1566 (s), 1511 (m), 1477 (m), 1437 (m), 1406 (m), 1362 (m), 1257 (m), 1191 (m), 1127 (w), 1078 (m), 985 (m), 937 (m), 903 (m), 841 (w), 791 (s), 771 (m); **MS (ESI)**: m/z = 282.1 (M+);

PN-O-B

2-Chlormethyl-1H-phenalen-1-one (230 mg, 1.0 $mmol$) in acetonitril (20 mL) was added dropwise to a solution of 3-aminopropanol (1.5 mL, 20 $mmol$) in acetonitril (50 mL) over a period of 30 min. After stiring at room temperature overnight, triethylamine (2.02 g, 2.66 mL, 20 $mmol$) was added and the solution was cooled in an ice bath. Acetic anhydride (3.06 g, 2.83 mL, 30 $mmol$) was added dropwise at 0°C. The mixture was stirred for two hours at room temperature, then heated to 50°C for 1 h. All volatiles were evaporated in vacuo. The product was purified by column chromatography with dichloromethane / ethanol 20:1 to give 261 mg of yellow syrup. This material was dissolved in methanol (2 mL). Aqueous sodium hydroxide (1 M, 0.5 mL) was added and the solution was stirred overnight at room temperature. The alcohol was evaporated, the residual solution was diluted with water (10 mL) and the product was extracted with dichloromethane (2 × 10 mL). The organic solution was dried over $MgSO_4$, filtered and evaporated to dryness to give the product as yellow oil (215 mg, 69 %, 0.69 $mmol$).

M = 311.2 g/mol; - **^{1}H-NMR** (300 MHz, $CDCl_3$): δ [ppm] = 8.69 (dd, *J* = 1.2 Hz, *J* = 7.4 Hz, 1H), 8.26 (dd, *J* = 1.0 Hz, *J* = 8.1 Hz, 1H), 8.08 (dd, *J* = 0.6 Hz, *J* = 8.2 Hz, 1H), 7.78 – 7.90 (m, 2H), 7.62 (dd, *J* = 7.0 Hz; *J* = 1.2 Hz; 1H), 7.51 (s, 1H), 4.65 (s, 2H), 3.83 (bs, 1H), 3.66 (t, *J* = 5.6 Hz, 2H), 3.59 (t, *J* = 5.6 Hz, 2H), 2.16 (s, 3H), 1.78 (m, 2H); - **^{13}C-NMR** (75 MHz, $CDCl_3$): δ [ppm] = 184.7 (1C), 173.2 (1C), 140.2 (1C), 136.6 (1C), 135.6 (1C), 134.1 (1C), 132.2 (1C), 132.0 (1C), 131.9 (1C), 130.8 (1C), 128.9 (1C), 127.1 (1C), 127.0 (1C), 126.8 (1C), 58.2 (1C), 47.6 (1C),

42.1 (1C), 30.1 (1C), 21.4 (1C); - **IR**: ν [cm^{-1}] = 3397 (bs), 2930 (w), 2877 (w), 1620 (s), 1570 (s), 1476 (w), 1426 (m), 1406 (m), 1362 (m), 1245 (m), 1183 (m), 1057 (m), 986 (m), 910 (m), 846 (w), 781 (s), 731 (m); **MS (ESI)**: m/z = 310.1 (MH+);

2.1.2 Solvents and salts

For all experiments H_2O (Millipore water, bidistilled water) or EtOH (Ethanol Absolute, J.T. Baker, Deventer, Netherlands, purity 99.9%) was used as the respective solvent. Phosphate buffered saline (PBS; PAA Laboratories GmbH, Pasching, Austria) with a pH value between 7.0 and 7.5 has been used for experiments with microorganisms to guarantee their vitality and in order to investigate effects on the spectroscopic properties of the photosensitizer XF73. The constituents of PBS, the salts and phosphates $NaCl$ (0.14 M), KCl ($2.7 \cdot 10^{-3}$ M), Na_2HPO_4 ($1.0 \cdot 10^{-2}$ M), KH_2PO_4 ($1.8 \cdot 10^{-3}$ M) have been purchased by Sigma Aldrich.

2.1.3 Quencher

Quenchers are molecules that deactivate the excited states of excited molecules during collision by different mechanisms such as energy transfer or chemical reaction of collision partners. In case one molecule is the photosensitizer, oxygen may quench the triplet-T_1-state of the excited PS yielding singlet oxygen. The excitation energy of a singlet oxygen molecule can be transferred to another quencher such as sodium azide (NaN_3), which quenches specifically singlet oxygen with a high quenching rate constant close to a diffusion controlled limit value. The action of a singlet oxygen quencher yields an enhancement of the deactivation rate constant and thus a shorter lifetime τ_Δ of singlet oxygen. Nevertheless NaN_3 is also able to quench the excited singlet and triplet states of the photosensitizer to some extent, however, the quenching rate constant is usually smaller than for singlet oxygen [12]. In H_2O NaN_3 dissociates into a sodium cation Na^+ and the functional singlet oxygen quenching part, the azide N_3^-.

In contrast to sodium azide, the quencher D-Mannitol specifically quenches the hydroxyl radical. The quencher sodium azide (NaN_3, $M = 65.01\ g\ mol^{-1}$, purity > 99%) and D-Mannitol ($C_6H_{14}O_6$, $M = 182.17\ g\ mol^{-1}$, purity > 98%) were purchased from Sigma Aldrich.

2.1.4 Potassium iodide

Indirect detection of singlet oxygen was performed with potassium iodide (KI). This substance reacts with singlet oxygen via the following mechanism, which was described by Mosinger *et al.* [13, 14].

$$^1O_2 + I^- + H_2O \xrightarrow{-OH^-} IOOH \xrightarrow{+I^-} HOOI_2^- \rightarrow I_2 + HO_2^-$$

$$\xrightarrow{+I^-,+H_2O} I_3^- + H_2O_2 + OH^-$$

In slightly acid buffered solution, the reaction might follow the step below:

$$H_2O_2 + 2I^- + 2H^+ \xrightarrow{-2H_2O} I_2 \xrightarrow{I^-} I_3^-$$

Sc. 2.1: Chemical schemes of the reaction pathway of iodine with singlet oxygen.

In water the reaction of singlet oxygen and the iodine anion results in the formation of tri-iodide I_3^-. During this process hydrogen peroxide, H_2O_2, is generated which can react further with I^-. Therefore, it is important to notice that in principle also H_2O_2 can react with I^- in order to form tri-iodide. For all investigations KI was dissolved in H_2O with a concentration of 0.12 M. The characteristic absorption maxima for the formation of tri-iodide were detected in the ultraviolet EM-spectrum at 287 nm and 350.5 nm.

2.2 SURFACES AND THEIR MANUFACTURING

The main part of the PhD thesis was to produce different surfaces in order to investigate their photodynamic effectiveness against microorganisms and to use spectral methods to clarify the photophysical properties of each surface. Prior to its use in surfaces, the dyes were investigated in solution that represents a simple approach for a better understanding of the photophysical properties and the change after the polymerisation process.

2.2.1 PS in Cellulose acetate (CA)

Cellulose acetate surfaces were doped with the photosensitizers MB, TMPyP or TPP using the preparation scheme similar to the procedure presented in Decraene *et al.* [15]. 360 mg of powdered cellulose acetate (Sigma Aldrich) and 7 mL acetone were added to a flat-bottom glass petri dish with a diameter of 5 cm, resulting in a concentration of approximately 50 $mg\ mL^{-1}$. The photosensitizers MB and TMPyP were dissolved in *acqua dist.*, TPP was dissolved in benzene, each with the appropriate concentration in order to have a final concentration of 250, 100, 50, 25, or 10 µM before the drying process of the surface. For a homogeneous distribution of the photosensitizer in the surface the glass petri dishes were under constant movement of an orbital shaker for 24 h and were covered with a glassy cover plate to slow down the evaporation process. After 48 h the polymeric films were finally hardened and carefully unhinged from the petri dish.

2.2.2 PS in Polyurethane (PU) covering *poly*-methylmethacrylate (PMMA)

Polyurethane components are based on the linking of hydroxy groups ($-OH$) with isocyanates ($-CNO$) as illustrated in the following scheme 2.2. In the varnish, branching alcohols with at least three hydroxyl groups are used in order to create 3-dimensional networks. A photosensitizer with at least one hydroxyl group therefore can be linked and – in the optimal case – irreversibly immobilized into this network.

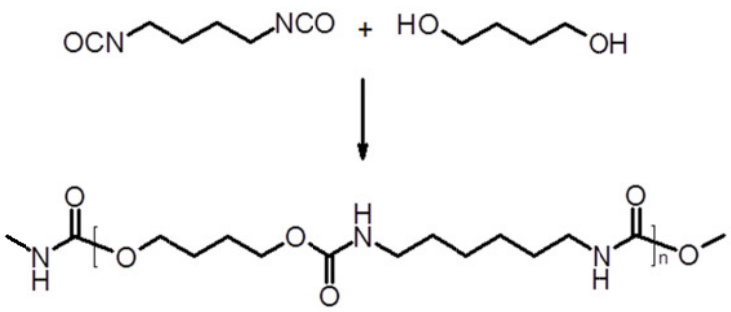

Sc. 2.2: Scheme of the linking of hydroxy groups with isocyanates

A mix of pure Polyurethane (varnish raw material) and Hexyldiisocyanate in the ratio of 5:1 was appropriate for the polymerisation procedure. An airbrush-system was used in order to spray the PU varnish onto the PMMA surface and to guarantee a homogeneous distribution of PU with a constant thickness. The PU layer was produced with different thicknesses between 20– 70 μm.

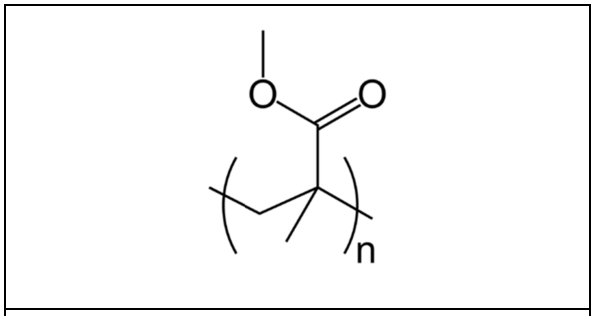

PMMA

PMMA shows different properties that are versatile for the use as basic layer. First PMMA is a common and cheap material and is inured to scratches or similar mechanical influences. Furthermore it is transparent in the visible part of the electromagnetic spectrum (transparent for light, 400– 700 nm) and shows the first absorption band bellow 380 nm.

The specific properties of the monolayer samples (PU-layer on PMMA) and sandwich structures (PU-layer between two PMMA polymer plates) are summarized in table 2.1.

number	Monolayer/ sandwich	Photosensitizer	concentration [M]	thickness [µm]
PUR	m	---	---	30
1A	m	TPP-O-A	$1 \cdot 10^{-4}$	50
	s		$1 \cdot 10^{-4}$	50
1B	m		$2 \cdot 10^{-4}$	45
	s		$2 \cdot 10^{-4}$	45
1C	m		$1 \cdot 10^{-5}$	30
	s		$1 \cdot 10^{-5}$	30
1D	m		$5 \cdot 10^{-5}$	35
	s		$5 \cdot 10^{-5}$	35
2A	m	TPP-O-B	$1 \cdot 10^{-4}$	35
	s		$1 \cdot 10^{-4}$	35
2B	m		$2 \cdot 10^{-4}$	30
	s		$2 \cdot 10^{-4}$	30
2C	m		$1 \cdot 10^{-5}$	35
	s		$1 \cdot 10^{-5}$	35
2D	m		$5 \cdot 10^{-5}$	45
	s		$5 \cdot 10^{-5}$	45
3A	m	PN-O-A	$1 \cdot 10^{-4}$	40
	s		$1 \cdot 10^{-4}$	40
3B	m		$2 \cdot 10^{-4}$	45
	s		$2 \cdot 10^{-4}$	45
3C	m		$1 \cdot 10^{-5}$	35
	s		$1 \cdot 10^{-5}$	35
3D	m		$5 \cdot 10^{-5}$	35
	s		$5 \cdot 10^{-5}$	35
4A	m	PN-O-B	$1 \cdot 10^{-4}$	35
	s		$1 \cdot 10^{-4}$	35
4B	m		$2 \cdot 10^{-4}$	40
	s		$2 \cdot 10^{-4}$	40
4C	m		$1 \cdot 10^{-5}$	40
	s		$1 \cdot 10^{-5}$	40
4D	m		$5 \cdot 10^{-5}$	45
	s		$5 \cdot 10^{-5}$	45

Tab. 2.1: Summary of the PU polymer plates samples with different concentrations of the photosensitizers TPP-O-A/B and PN-O-A/B.

2.3 BASIC TECHNIQUES

2.3.1 Absorption spectroscopy

Absorption spectra were recorded at room temperature with a spectrophotometer (DU640, Beckman Instruments GmbH, Munich, Germany). The percentaged transmission has been measured and the absorption cross section σ $[cm^2]$ was calculated according to the following equation

Eq. 2.1

$$\sigma = -\frac{\ln\left(\frac{T}{100}\right)}{c \cdot l \cdot N_A}$$

where c the concentration of PS, l the length of light path through the solution, T the transmission in %, and N_A the Avogadro constant. The function and measurement techniques of the spectrometer can be found in detail in [1].

2.3.2 NMR spectroscopy

The NMR spectra were recorded on a Bruker Avance 600 (^{1}H: 600.1 MHz, ^{13}C: 150.1 MHz, $T = 300\,K$), Bruker Avance 400 (^{1}H: 400.1 MHz, ^{13}C: 100.6 MHz, $T = 300\,K$) or Bruker Avance 300 (^{1}H: 300.1 MHz, ^{13}C: 75.5 MHz, $T = 300\,K$) relative to external standards. NMR spectra were recorded in $CDCl_3$ at 300 MHz (^{1}H) or 75 MHz (^{13}C) unless stated otherwise.

Integration was determined as the relative number of atoms and the coupling constants are given in Hertz $[Hz]$. The multiplicity of the carbon atoms is given as (+] = CH_3 or CH, (-] = CH_2 and (C_{quat}) for quaternary carbon atoms. Structural assignments are based on DEPT and COSY experiments where applicable. The errors of the reported values are given the chemical shift as 0.01 ppm for ^{1}H-NMR, as 0.1 ppm for ^{13}C-NMR and as 0.1 Hz for coupling constants. The solvent used is reported for each spectrum.

2.4 TIME-RESOLVED OPTICAL TECHNIQUES

2.4.1 Time-correlated single photon counting

Time-correlated single photon counting is a common technique that is used to determine the decay time or the lifetime of excited singlet or triplet states. Therefore, single photons emerging from a sample are collected after excitation of molecules (photosensitizers) by periodically pulsed light at a high repetition pulse rate. The photons are collected with a photomultiplier tube (PMT) and give a time-resolved histogram of single events.

2.4.2 Time-resolved NIR phosphorescence detection

In order to detect the formation and decay of singlet oxygen, the technique of time-resolved near-infrared phosphorescence (NIR) detection was used, which is based on time-correlated single photon counting. With this method the decay time τ_Δ of singlet oxygen and the excited triplet state of the photosensitizer (τ_T) can be detected, as well as the singlet oxygen quantum yield Φ_Δ which describes the effectivity of the generation of singlet oxygen.

Two types of lasers were used for excitation of the photosensitizers:

(1) a diode-pumped solid-state Q-switched Nd:YAG laser (Photon Energy AWL GmbH, Ottensoos, Deutschland), which works at a 2 kHz or 5 kHz repetition rate, producing laser pulses of 60 ns pulse width at either 355 nm or 532 nm and variable power output between 0– 100 mW and

(2) a tunable laser system (EKSPLA, Lithuania), which works at a 1 kHz repetition rate with laser pulses of $4-7$ ns pulse width at different wavelengths. At each wavelength the laser power was different and will be mentioned for each experimental section.

Figure 2.2 shows the experimental setup for the direct detection of the singlet oxygen luminescence at 1270 nm.

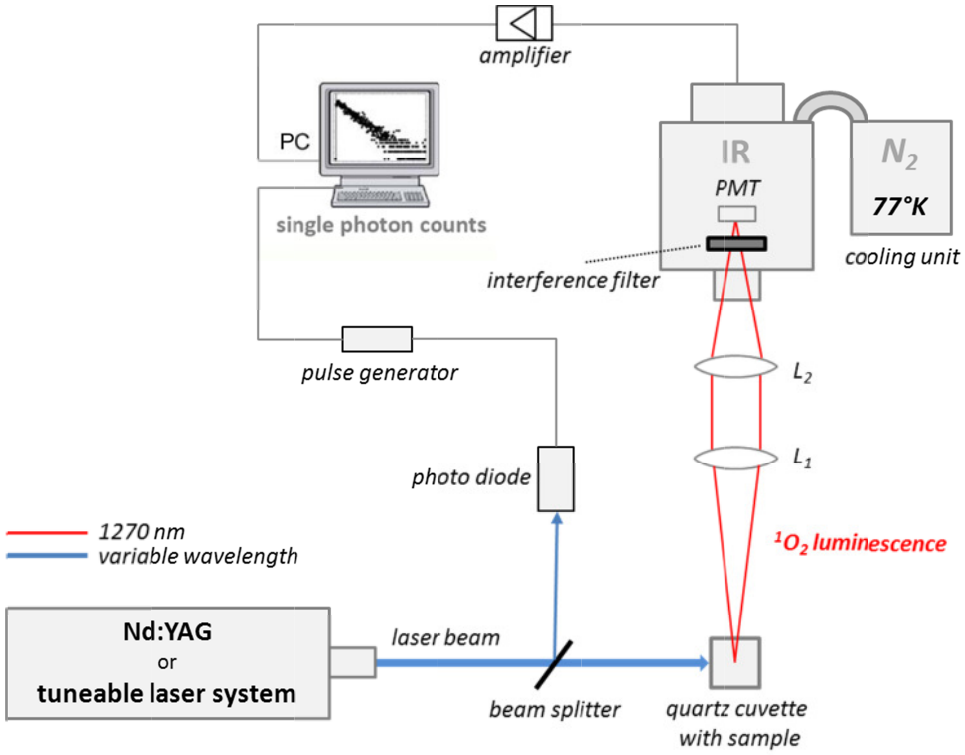

Fig. 2.2: Experimental setup of the direct detection of the singlet oxygen luminescence; light pulses of a Nd:YAG laser or tuneable laser system irradiates (blue line) the sample that is either placed into a quartz cuvette or irradiated directly in air; singlet oxygen luminescence (red line) is detected by a photomultiplier tube (PMT) after it passes lenses and an interference filter system; the signal of the PMT is amplified and sent to a PC in parallel to a signal from the pulse generator giving a start position in time for the measurement.

Direct detection of the weak singlet oxygen luminescence as described in [16, 17] was done by time-resolved measurements at 1270 nm (10 nm or 30 nm FWHM filter) with an additional 950 nm cut-off-filter in near-backward direction with respect to the exciting beam (the angle does not fit with the angle in the graphic) using a liquid nitrogen cooled infrared-sensitive photomultiplier tube (PMT, R5509-42, Hamamatsu Photonics Deutschland GmbH, Herrsching, Germany).

Considering no energy back-transfer from singlet oxygen to the photosensitizer, the luminescence intensity is then given by

Eq. 2.2

$$I(t) = \frac{C}{t_R^{-1} - t_D^{-1}}\left[\exp\left(-\frac{t}{t_D}\right) - \exp\left(-\frac{t}{t_R}\right)\right]$$

where $C = [T_1]_{t=0} k_{T_1\Delta}[O_2]$ was used to fit the singlet oxygen luminescence signal, and t_R and t_D are the rise and decay times that are assigned to either the decay time of the excited triplet state of the photosensitizer τ_T or the decay time of singlet oxygen τ_Δ. The meaning of

the rise and decay time can change depending on the oxygen concentration [17]. For the optimisation of the fit, the Levenberg-Marquardt-algorithm of Mathematica (V. 5.2, Wolfram Research, Champaign, USA) was used. The exact mathematical descriptions and deviation of the formula for the luminescence intensity using the rate and rate constants can be found in Baier *et al.* [17].

When changing the oxygen concentration the quenching rate k_q for the excited triplet state τ_T by oxygen can be calculated with a Stern-Volmer-plot:

Eq. 2.3

$$\frac{1}{\tau_T} = \frac{1}{\tau_0} + k_q \cdot [O_2]$$

The integral of the luminescence intensity $\int I(t)dt$ is proportional to the luminescence energy and has been used to estimate the singlet oxygen quantum yield. This integral is compared to the integral of the luminescence generated by a photosensitizer with known quantum yield at the same conditions (reference photosensitizer), *i.e.* the same irradiation wavelength, irradiation power, irradiated volume, and percentaged absorption. Then the quantum yield of the sample can be calculated as follows, when the sample and the reference photosensitizer absorb the same amount of energy:

Eq. 2.4

$$\Phi_\Delta^{sample} = \Phi_\Delta^{comparison} \cdot \frac{\int I^{sample}(t)dt}{\int I^{comparison}(t)dt}$$

Nevertheless the molar concentration, possibly resulting in a dimerisation processes or shielding effect, are not taken into account, which might influence as well the ability to generate singlet oxygen. Since with the tuneable laser the photosensitizer can be irradiated at its absorption maximum the molar concentration can be adjusted to small values ($\approx$ 1 μM) and therefore a dimerisation process might not occur yet.

The luminescence signal was spectrally resolved using interference filters in front of the photomultiplier tube at different wavelengths ranging from 1150– 1400 nm. The values in each plot show the integrated luminescence signals detected at a certain wavelength and are normalized to the maximal value. A Lorentz-shaped curve has been fitted through the measured values yielding a maximum in the wavelength range of $1270 - 1276\ nm$.

The samples of photosensitizers in solution were irradiated in quartz cuvettes (QS-101, Hellma Optik, Jena, Germany) applying magnetic stirring of the solution. The oxygen

concentration in the solution was determined with a needle sensor (MICROX TX3, Microsensor Oxygen Meter, PreSens GmbH, Regensburg, Germany).

For experiments with different oxygen concentrations, the polymeric samples containing the photosensitizers were positioned in the quartz cuvettes, for all other experiments, the samples were fixed with a holder in front of the PMT with an angle of ≈ 45°. The surfaces were investigated in air at a room temperature of 25°C and pressure of 1013 hPa. It was not possible to measure the oxygen concentration in the polymeric samples.

The bacteria or fungi cells were investigated in either acryl cuvettes or polystyrene Petri dishes, which both did not show singlet oxygen generation at the respective conditions.

2.5 MICROSCOPY TECHNIQUES

2.5.1 Fluorescence microscopy

The localisation of photosensitizers in cells or their distribution in the surfaces was examined by fluorescence microscopy (Zeiss Vario-AxioTech, Goettingen, Germany) with an appropriate dual-band filter set for excitation and emission (Omega® Optical Inc., Brattleboro, USA) and different magnification ranging from 10 × to 63 × (fig. 2.3). The resolution of the microscope is not high enough to study structures within bacteria cells, but the uptake of the fluorescent dye can be clarified. For the investigation of the fluorescence of XF73 and TPP-O-A the excitation filter 405 DF 40, the dichroic mirror 415 DRLP and the emission filter 600 EFLP were used.

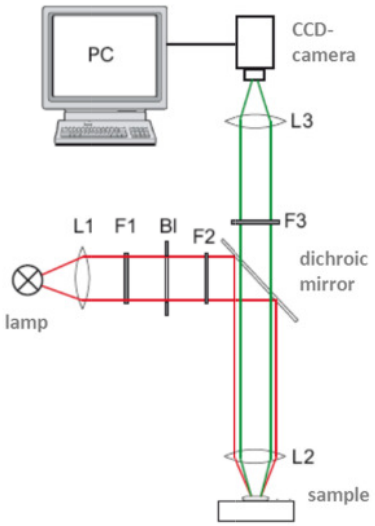

Fig. 2.3: Scheme of the Zeiss Vario-AxioTech fluorescence microscope [18].

2.5.2 Transmission electron microscopy

The roughness of the PU surfaces was investigated by transmission electron microscopy (TEM, LEO 912AB, Zeiss, Oberkochen, Germany) at 100 kV in cooperation with the Central EM Lab at the University Hospital Regensburg. Thin probes were cut with an ultra-microtome accompanied by light microscopy. The polymer layers had a thickness around 50 nm and were placed on the TEM-microscopy grids. The documentation was performed by a CCD-camera with the OSIS-Software iTEM (Olympus Soft Imaging Solutions, Münster, Germany).

2.6 EMISSION SPECTRA OF THE LAMPS

Different light sources were used during the investigation of the photostability of the PS or the phototoxic effects on microorganisms to match the different absorption spectra of the different photosensitizers.

2.6.1 Waldmann UV236: Irradiation of XF73 and TMPyP with *C. albicans*

TMPyP and XF73 were illuminated with an incoherent light source UV236 (broadband lamp; spectral radiation distribution emission $\lambda = 380 - 480\ nm$) provided by Waldmann Medizintechnik (Villingen-Schwenningen, Germany). The maximal light intensity was $P = 15.2\ mW\,cm^{-2}$ at the level of the illuminated samples. The samples were illuminated for either $15\ min$ ($13.7\ J\,cm^{-2}$) or $60\ min$ ($54.8\ J\,cm^{-2}$). The emission spectrum of the Waldmann UV lamp was normalized to its maximum between 400– 450 nm.

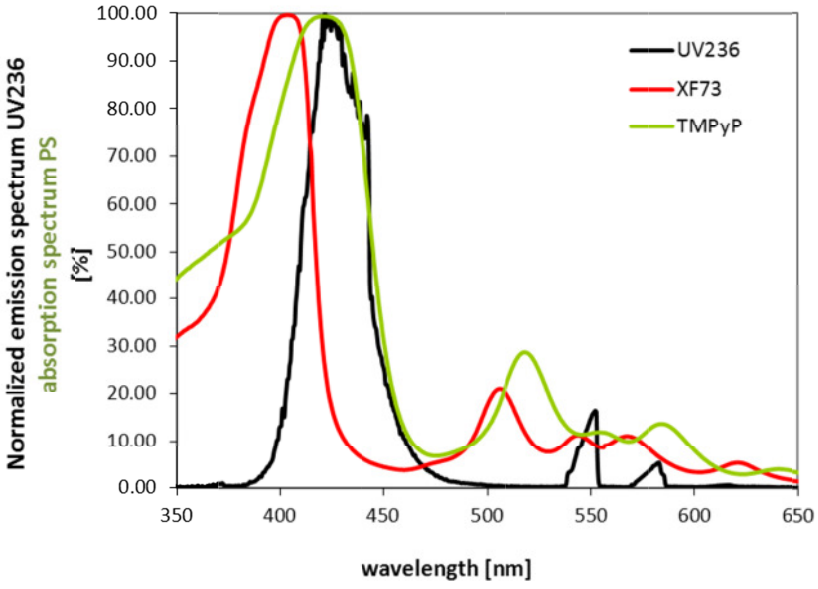

Fig.2.4: Emission spectrum of the Waldmann UV236 broadband light source (black line); emission values are normalized to 100%. Absorption spectra of XF73 and TMPyP in H_2O at a concentration of 10 µM are shown in red and green, the absorption values are given between 0% - 100%.

2.6.2 Waldmann PDT1200: Irradiation of MB derivatives with *S. aureus* and *E. coli*

MB and its derivatives were illuminated with the incoherent light source PDT1200 (broadband lamp; spectral radiation distribution: emission $\lambda = 600 - 720\,nm$, emission maximum: $615 - 680\,nm$). The lamp and the data were provided by Waldmann Medizintechnik. The maximal light intensity was $P = 50\,mW\,cm^{-2}$ at the level of the illuminated samples.

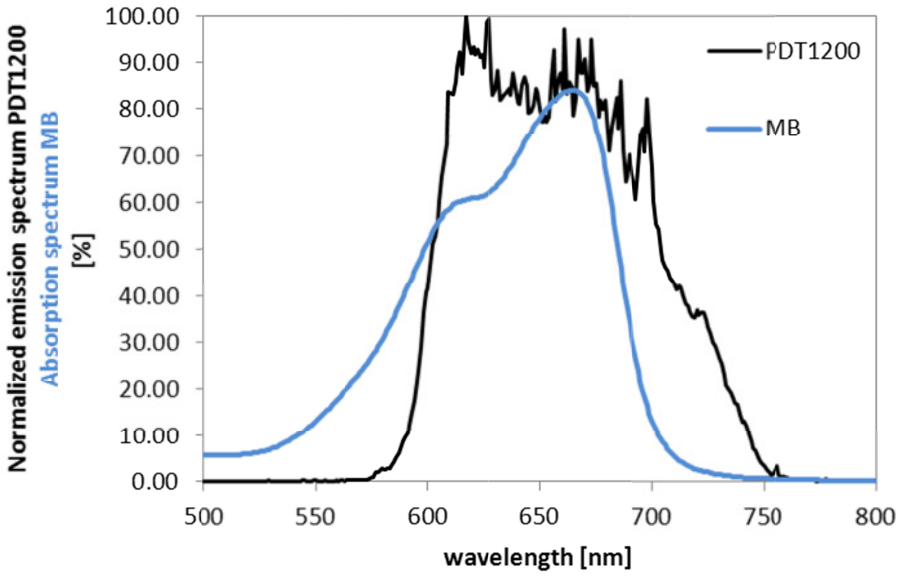

Fig. 2.5: Emission spectrum of the Waldmann PDT1200 broadband light source (black line); emission values are normalized to 100%.The values for the absolute absorption of MB are given between 0 and 100%; MB had a concentration of 10 µM in H_2O.

2.6.3 Waldmann PIB 3000 (full spectrum > 400 nm): Toxicity tests on PU-surfaces

The PU-surfaces with doped with TPP-O-A, -B and PN-O-A, -B were illuminated with the incoherent light source PIB 3000 (broadband lamp; spectral radiation distribution: emission $\lambda > 400\,nm$, Waldmann Medizintechnik). The maximal light intensity was $P = 50\,mW\,cm^{-2}$ at the level of the illuminated samples with the full lamp spectrum at wavelengths $> 400\,nm$. The emission spectrum of the light source was kindly provided by Waldmann; the emission spectrum was normalized to its maximum.

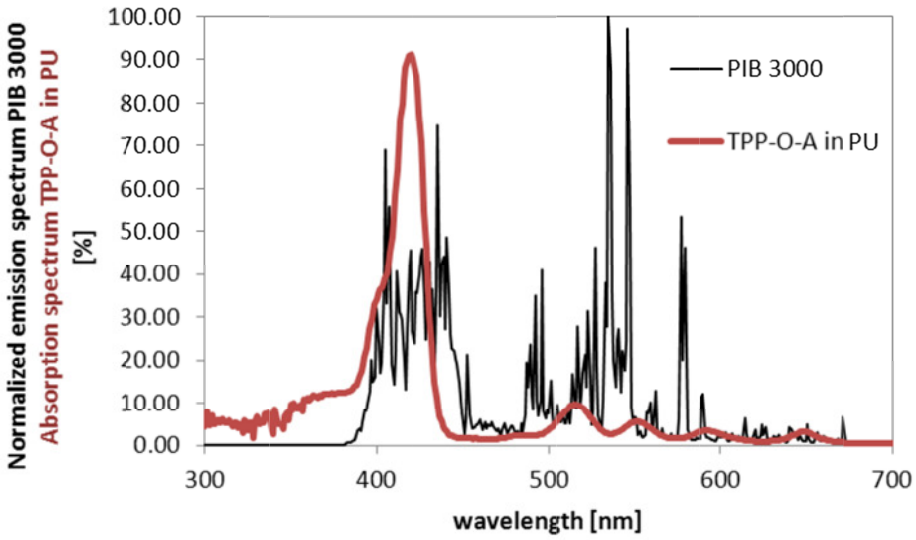

Fig.2.6: Emission spectrum of the Waldmann PIB 3000 broadband light source (black line); emission values are normalized to 100%. The absorption spectrum of TPP-O-A doped into PU (TPP-O-A concentration of 10^{-4} M; PU thickness of 55 µm) is shown in red.

2.7 MICROBIOLOGICAL TECHNIQUES

2.7.1 Microbial strains

Three different microorganisms were used for the investigation of photosensitizers in cells or the phototoxic efficacy of PS in solution or on surfaces. Bacteria are assigned to Gram(+) and Gram(-) species reflecting the differences in the cell wall structure. The very common bacteria strains, the Gram(+) *Staphylococcus aureus* (ATCC 25923) and the Gram(-) *Escherichia coli* (ATCC 25922), were received by the Institute of Microbiology und Hygiene of the University Hospital Regensburg.

Candida albicans is a fungal pathogen, which already showed resistances against commonly used fungicides. *C. albicans* strain (ATCC-MYA-273) was received by the Institute of Microbiology und Hygiene of the University Hospital Regensburg.

2.7.2 Culture conditions

The bacterial strains *S. aureus* (ATCC 25923) and *E. coli* (ATCC 25922) were grown aerobically at $37°C$ for $16\,h$ overnight in $5\,mL$ Mueller-Hinton broth (Gibco Life Technologies GmbH, Eggenstein, Germany). When the cultures reached the stationary phase of growth the bacteria were harvested by centrifugation (200g, $10\,min$), washed with phosphate-buffered saline (PBS; Biochrom, Berlin, Germany) at pH 7.4, and suspended in PBS at an optical density of $OD = 0.6$ at $600\,nm$, which corresponded to $\approx 10^8$– $10^9\ CFU\ mL^{-1}$. Cell suspensions were incubated in the dark with the desired amount of PS for a given period of time. The cells were then washed two times with PBS and re-suspended in PBS or non-washed.

The *C. albicans* strain ATCC-MYA-273 was grown overnight in Sabouraud Dextrose Broth medium (SDB, Sigma Chemical Co., St. Louis, Mo) at $37°C$. When the cultures reached the stationary phase of growth, the cells were harvested by centrifugation (3100 rpm, $5\,min$) and washed once with PBS.

For biofilm formation, *C. albicans* cells were diluted in 25% of fetal bovine serum (FBS) to $10^6\ CFU\ mL^{-1}$. The cells were transferred to cell culture dishes (Petri dish, $35 \times 10\,mm^2$, Cellstar, Frickenhausen, Germany) and incubated for $24\,h$ at $37°C$ to allow biofilm formation. The cells were washed twice with PBS to remove nonadherent cells and

incubation with different concentrations of the PS was done for 1 h. The biofilm cells were washed once, or non-washed. To gain visible dryness, the biofilms were left for 1 h under the laminar flow of a sterile workbench [19].

2.7.3 Spectroscopic measurements with cells

$^1O_2$ luminescence experiments in cells were immediately done after incubation and washing steps in acrylic cuvettes in case of planktonic solutions and in polystyrene Petri dishes in case of biofilms. Both materials did not show $^1O_2$-generation when irradiated at 532 nm or 420 nm. Cell numbers are given separately for each experiment in the respect chapter.

Fig.2.7: (left) biofilm in polystyrene Petri dish; (right) polystyrene Petri dish without biofilm [20]

The biofilm in polystyrene Petri dishes showed inhomogeneous growth and therefore the errors for the luminescence signals, which depend on the geometry of the irradiation, have to be considered to be rather high, resulting in part wise non-reproductive results.

2.7.4 aPDT phototoxicity experiments *in vitro* and on surfaces

In vitro experiments

A bacterial cell number of $10^8 - 10^9\ CFU\ mL^{-1}$, corresponding to an optical density of $OD = 0.6$, was incubated for a defined time in the dark with different concentrations of photosensitizers. At the end of the incubation period the cells were transferred into a 96-well microtitre plate (200 µl per well) and illuminated for a certain time period applying different energy doses (energy E per area A) to the samples, which were calculated by multiplication of the emitted power P of the light source and the illumination period t.

Eq. 2.5

$$Energy\ dose = \frac{E(t)}{A} = \frac{P \cdot t}{A}$$

Controls were neither sensitized with a photosensitizer nor exposed to the light source, or were incubated with the photosensitizer only. After illumination, the survival of the bacteria was determined by standardized CFU assay according to Eichner *et al.* [5]. Serially diluted aliquots of treated and untreated (no photosensitizer, no light) cells were plated on Mueller-Hinton agar and the $CFU\ mL^{-1}$ were determined after 24 h of incubation at 37°C.

Experiments on surfaces

50 µl of the bacteria suspension with an optical density of $OD = 0.6$ corresponding to $5 \cdot 10^6$– $5 \cdot 10^7\ CFU$ was dropped on the surface and drying 1.5 h under a laminar flow. Each drop had a radius of about 0.5 cm and therefore covered an area of $A \approx 0.79\ cm^2$. The cell number per area is then between $6.3 \cdot 10^6 - 6.3 \cdot 10^7\ CFU\ cm^{-2}$. Afterwards the probes were illuminated with the incoherent light source Waldmann PIB 3000 (emission $\lambda > 400\ nm$) with a maximal light intensity of 50 $mW cm^{-2}$ at the level of the illuminated samples. The samples were illuminated for either 10 min (30 $J cm^{-2}$), 30 min (90 $J cm^{-2}$) or 60 min (180 $J cm^{-2}$).

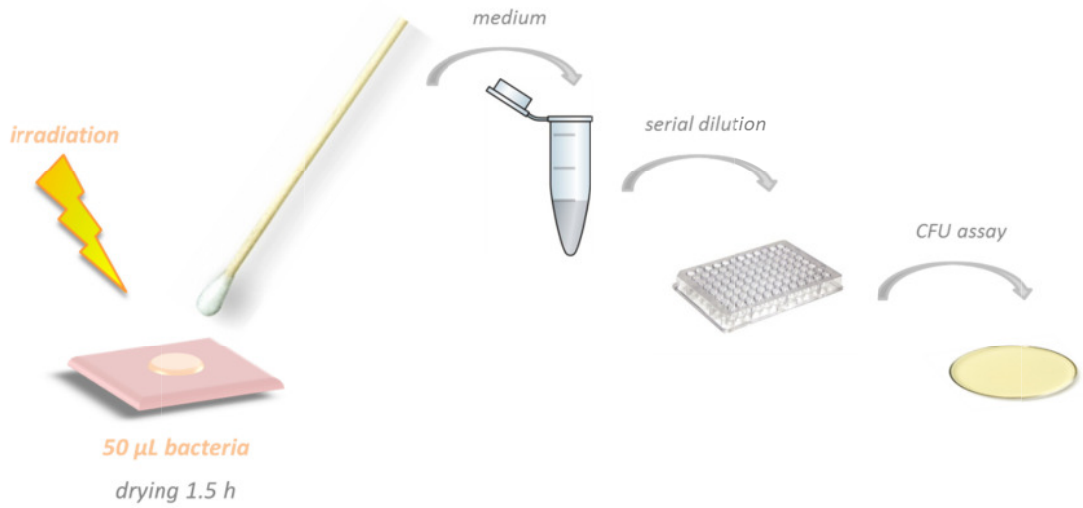

Fig.2.8: Scheme of the phototoxicity experiments on the PU surfaces

After the illumination the bacteria were swapped with a sterile cotton bud and were diluted in 1 mL MH-medium. They were immediately diluted serially in MH-medium and plated on Agar using the method of Miles and Misra [21]. After growing at 37°C for 24 h the colony forming units (CFU) were counted and a mean value depending on the number of experiments was calculated. The number of experiments is reported for each phototoxicity test and the effective errors are reported in the respect chapters.

2.8 REFERENCES

1. Felgenträger, A., *Spektroskopische Untersuchungen an Photosensibilisatoren zur photodynamischen Inaktivierung von Bakterien.* University of Regensburg, 2009: p. 115.
2. Redmond, R.W. and J.N. Gamlin, *A compilation of singlet oxygen yields from biologically relevant molecules.* Photochem Photobiol, 1999. **70**(4): p. 391-475.
3. Frederiksen, P.K., et al., *Two-photon photosensitized production of singlet oxygen in water.* J Am Chem Soc, 2005. **127**(1): p. 255-69.
4. Angeli, N.G., et al., *Meso-substituted cationic porphyrins of biological interest. Photophysical and physicochemical properties in solution and bound to liposomes.* Photochemistry and Photobiology, 2000. **72**(1): p. 49-56.
5. Eichner, A., et al., *Dirty hands: photodynamic killing of human pathogens like EHEC, MRSA and Candida within seconds.* Photochem Photobiol Sci, 2012.
6. Krasnovsky, A.A., Jr., et al., *The photophysics of monomeric bacteriochlorophylls c and d and their derivatives: properties of the triplet state and singlet oxygen photogeneration and quenching.* Photochem Photobiol, 1993. **57**(2): p. 324-30.
7. Oliveros, E., et al., *1h-Phenalen-1-One - Photophysical Properties and Singlet-Oxygen Production.* Helvetica Chimica Acta, 1991. **74**(1): p. 79-90.
8. Nonell, S., M. Gonzalez, and F.R. Trull, *1h-Phenalen-1-One-2-Sulfonic Acid - an Extremely Efficient Singlet Molecular-Oxygen Sensitizer for Aqueous-Media.* Afinidad, 1993. **50**(448): p. 445-450.
9. Marti, C., et al., *Aromatic ketones as standards for singlet molecular oxygen O-2(1 Delta(g)) photosensitization. Time-resolved photoacoustic and near-IR emission studies.* Journal of Photochemistry and Photobiology a-Chemistry, 1996. **97**(1-2): p. 11-18.
10. Redmond, R.W. and J.N. Gamlin, *A compilation of singlet oxygen yields from biologically relevant molecules.* Photochemistry and Photobiology, 1999. **70**(4): p. 391-475.
11. Felgentrager, A., et al., *Hydrogen Bond Acceptors and Additional Cationic Charges in Methylene Blue Derivatives: Photophysics and Antimicrobial Efficiency.* Biomed Res Int, 2013. **2013**: p. 482167.
12. Nilsson, R., P.B. Merkel, and D.R. Kearns, *Kinetic properties of the triplet states of methylene blue and other photosensitizing dyes.* Photochem Photobiol, 1972. **16**(2): p. 109-16.
13. Mosinger, J. and B. Mosinger, *Photodynamic sensitizers assay: rapid and sensitive iodometric measurement.* Experientia, 1995. **51**(2): p. 106-9.
14. Mosinger, J., et al., *Light-induced aggregation of cationic porphyrins.* Journal of Photochemistry and Photobiology a-Chemistry, 2006. **181**(2-3): p. 283-289.
15. Decraene, V., J. Pratten, and M. Wilson, *Cellulose acetate containing toluidine blue and rose bengal is an effective antimicrobial coating when exposed to white light.* Appl Environ Microbiol, 2006. **72**(6): p. 4436-9.
16. Parker, J.G. and W.D. Stanbro, *Dependence of photosensitized singlet oxygen production on porphyrin structure and solvent.* Prog Clin Biol Res, 1984. **170**: p. 259-84.
17. Baier, J., et al., *Theoretical and experimental analysis of the luminescence signal of singlet oxygen for different photosensitizers.* J Photochem Photobiol B, 2007. **87**(3): p. 163-73.
18. Regensburger, J., *Spektroskopische Untersuchungen zur Singulett-Sauerstoff-Lumineszenz in Biomolekülen, Bakterien und Zellen.* University of Regensburg, 2010: p. 200.
19. Harriott, M.M. and M.C. Noverr, *Candida albicans and Staphylococcus aureus form polymicrobial biofilms: effects on antimicrobial resistance.* Antimicrob Agents Chemother, 2009. **53**(9): p. 3914-22.
20. Pereira Gonzales, F., *Photodynamic inactivation of microbial biofilms: impact of Hsp70 expression and non-invasive optical monitoring of oxygen during photodynamic inactivation.* Dissertation, Universität Regensburg, 2013.
21. Miles, A.A., S.S. Misra, and J.O. Irwin, *The estimation of the bactericidal power of the blood.* J Hyg (Lond), 1938. **38**(6): p. 732-49.

Chapter 3

Spectroscopic and Phototoxicity Studies of Phenothiazinium Derivatives

The commonly used phenothiaziniums MB, NMB, DMMB, and TBO were investigated with spectroscopic methods in regard to their photophysical characteristics, including the generation of singlet oxygen. The quantum yields of these photosensitizers were determined with direct spectroscopy for different concentration ranges. Newly synthesized derivatives of MB were characterized in regard to the generation of singlet oxygen and tested on the ability to act as a photosensitizer for aPDT in order to deactivate the Gram(+) and Gram(-) species *S. aureus* and *E. coli* in suspension.

3.1 INTRODUCTION

Methylene blue (MB) and its derivatives were proven to be effective photosensitizers for the inactivation of pathogens in suspension [1-3], e.g. *Candida* species [4, 5], *E. coli* [6, 7], *S. aureus* [8] and *MRSA* [9], tropical diseases [10] or several viruses [11, 12], and therefore finds its application in antimicrobial fields, like blood disinfection [13-16]. *In vivo* the phenothiazinium chromophore system is used with benefit against oral infections [17] performing photodynamic root channel disinfection [18-21] or treatment of periodontitis, inactivating bacteria like *E. faecalis* [22], *P. gingivalis* [23] or *A. actinomycetemcomitans* [24]. As "state of the art" it may be given, that MB and its derivatives like 1,9-dimethylmethylene blue (DMMB), toluidine blue O (TBO) and new methylene blue (NMB) can achieve a log reduction > 6 log_{10}-steps of a bacterium at fluences ranging from $0 - 30\, Jcm^{-2}$, using a fluence rate of 125 $mW\,cm^{-2}$ in a concentration range of $2 - 10\ \mu M$ in suspension [25].

The knowledge about the complex chemical and spectroscopic properties of phenothiazinium photosensitizers is still ambiguous that prevents a broad understanding of their role in antimicrobial photodynamic therapy (aPDT). The basic mechanism of action in aPDT is of mixed nature where type-I, type-II and redox reactions are considered to be the cause of toxic effects, triggered by light. The preferred mechanism depends on several factors like the concentration of the photosensitizer and therefore its dimerisation status [26], the pH-value of the surrounding [27], or the redox potential. On the one hand, the property of phenothiaziniums to generate singlet oxygen via type-II reaction is used as an explanation for the effective killing of several gram-positive and gram-negative bacteria strains, which were extensively investigated by Wainwright *et al*. [7, 8, 28] These papers report rather high singlet oxygen quantum yields of > 0.45 [27, 29-33]. On the other hand, the presence of the hydroxyl radical $HO^{\bullet}$ by irradiation of MB has been shown by Garcez *et al.* indicating a type-I mechanism [34] and proposed to be the dominant antibacterial mechanism of action against bacteria. A phototoxic effect and oxidation of cysteine sulfinic acid, that were formerly ascribed to singlet oxygen, have been described to be paradoxically enhanced by NaN_3 [34-36], which is a singlet oxygen quencher. The role of MB monomers and dimers in photokilling of bacteria has been elucidated by Usacheva *et al*. by correlating the formation of dimers in the presence of bacteria and the photobactericidal efficacy [37].

The phenothiazinium derivatives MB and TBO have been described as agency to act in photoactive surfaces by Wilson *et al*. [38-40] and Wainwright *et al.* [41]. Due to the different

phototoxic mechanisms the action as a singlet oxygen generator in surfaces needs to be clarified.

The indirect method of the reaction of singlet oxygen with 1,3 diphenylisobenzofuran (DPBF) and a subsequent monitoring of its decrease in the fluorescence intensity ($\lambda_{max,fluorescence} = 455\ nm$) after the reaction with singlet oxygen is used frequently to measure the efficiency of singlet oxygen generation by phenothiaziniums [42, 43]. But the influence of DPBF on the investigated system, a necessarily perfect localisation of this probe and reactions with other ROS cannot be excluded with this method [43]. Therefore the quantum yields of MB and the frequently used derivatives NMB, DMMB and TBO were investigated in this work with direct spectroscopic detection of the luminescence of singlet oxygen at $\lambda = 1270\ nm$.

During the investigations on the photophysical properties of the phenothiazinium series, the excitation laser (Nd:YAG laser) with a fixed wavelength of $\lambda = 532\ nm$ was replaced by a tunable laser system, whereby a wavelength could be chosen to irradiate MB or its derivatives at its absorption maximum. To investigate the quantum yields with excitation at $532\ nm$ had required the use of much higher photosensitizer concentrations in comparison to irradiation at the optimal wavelength in the respective absorption maximum (from $600 - 664\ nm$) with concentrations in the range of $1\ \mu M$. Using the new setup it was possible to investigate the effect of photosensitizer dimerisation on the efficacy of the singlet oxygen generation.

New MB-derivatives

New phenothiazinium derivatives have been developed to investigate a structure-response-relationship of the side chains of the molecules regarding efficacy of singlet oxygen generation, adhesion at the bacterial cell wall, and uptake into bacteria cells. Owing to its structure, MB can penetrate cells and can be used as a staining agent in histology [44, 45] or as a chemotherapeutic [46-49]. Binding with cytoplasmic structures within the cell and interference with oxidation/reduction processes [50, 51] may lead to killing of bacteria, funguses, viruses or parasites.

Although MB and its alkyl- and aryl-derivatives are well studied [52-55], not many approaches followed variations of the structure beyond simple modifications [56]. For example, the effect of additional positive charges on the antimicrobial activity and the influence of such substituents on the singlet oxygen yield have not been investigated yet. A

comparison of such photosensitizers with related hydrogen bond acceptor moieties, thus also strongly increasing polarity is lacking, as well as the direct spectroscopic determination of the group's influence on the singlet oxygen quantum yield. More polarity in the structure should cause the molecules to stay outside cell causing only photodynamic damage of the cell wall. Positive charges in addition may lead to better attachment to the exterior of the cell, resulting in shorter process times and higher antimicrobial activity in comparison to MB. Attack from outside the cell also overcomes the problem of reduced photosensitizer activity by efflux mechanisms [57].

The synthesis of MB and its derivatives was summarized [32] and the preparation of phenothiazinium systems with additional positive charges for other purposes was demonstrated [58], but a straight forward, reliable purification protocol without the use of expensive HPLC methods is still missing.

We focused on the synthesis and study of new MB-derivatives with highly polar and/or hydrophilic groups, to extend the field of highly hydrophilic phenothiazinium compounds in aPDT. One substituent in the MB lead structure was changed in order to achieve pursuable variations of the behaviour of the compound.

3.2 EXPERIMENTAL SECTION

3.2.1 Time- and spectrally resolved singlet oxygen luminescence

Time resolved measurement was done according to the description in chapter 2. For the spectrally resolved luminescence detection the Lorentz-shaped function was fitted through the data points yielding a maximum at $\lambda = 1275\ nm$ [59].

3.2.2 Quantum yield of singlet oxygen formation

The emitted singlet oxygen luminescence photons were proportional to the integral of the luminescence curve and a mean value was determined for 3 independent measurements for the same conditions. In this study the lifetime of singlet oxygen is assumed to be constant for the chosen solvent.

MB, TBO, NMB and DMMB

The singlet oxygen quantum yield was determined with direct spectroscopic methods for MB, TBO, NMB and DMMB using different reference photosensitizers, PNS and TMPyP, with known quantum yields (see chapter 2). Each sample was irradiated with a wavelength that fitted its absorption maximum. 33 000 laser pulses at a repetition rate of $f = 1\ kHz$, which equals an irradiation time of 33 s was used to irradiate the photosensitizers in solution of H_2O which was air saturated ($[O_2] = 270\ \mu M$). All photosensitizers were dissolved yielding similar absorption of radiation in a 10 mm quartz cuvette. The power of the tuneable laser system changes with the used wavelength and thus neutral glass filters were used to adapt the applied power. A variation of at least 3 different filters was used to vary the laser power and thus the absorbed energy.

New MB-derivatives

The quantum yields (Φ_Δ) of the new derivatives of MB were compared to the Φ_Δ of MB which is reported in literature being $\Phi_\Delta = 0.52$ in aqueous solution [60]. Therefore a sample of each photosensitizer was diluted to a final absorption of $A = 30\%$ at $\lambda = 600\ nm$ in H_2O.

3 mL (O_2 concentration at air-saturation at 25°C) of each sample was illuminated in a quartz cuvette (path length of 1 cm) with the tunable laser.

3.2.3 Photostability

The photosensitizers were diluted to a final absorption of $A = 30\%$ at the wavelength of $\lambda = 600\ nm$. The samples were irradiated in quartz cuvettes at a path length of 1 cm with the tunable laser at the given parameters with 180 000 laser pulses during magnetic stirring. After the irradiation absorption spectroscopy was done in the range from $200 - 1\,000\ nm$ and the data was compared to the non-illuminated samples.

3.2.4 Bacterial strains

The biochemical analysis of each bacteria strain was done by a VITEK2-System (bioMérieux, Nürtingen, Germany) according to NCCLS (National Committee for Clinical Laboratory Standards) guidelines. The bacterial strains, *S. aureus* (ATCC 25923) and *E. coli* (ATCC 25922) were grown aerobically at 37°C in Mueller-Hinton broth (Gibco Life Technologies GmbH, Eggenstein, Germany). A 500 µL portion of an overnight cell culture (5 mL) was transferred to 50 mL of fresh BHI media and grown at 37°C on an orbital shaker. When the cultures reached the stationary phase of growth, the cells were harvested by centrifugation (200 g, 15 min), washed with phosphate-buffered saline (PBS; Biochrom, Berlin, Germany) at $pH = 7.4$, containing 2.7 $mM\ KCl$ and 0.14 $M\ NaCl$ and suspended in PBS at an optical density of $OD = 0.6$ at 600 nm corresponding to $\approx 10^8$– $10^9\ CFU\ mL^{-1}$ for the use in the phototoxicity experiments.

3.2.5 Light source

The bacteria were illuminated using an incoherent light source PDT1200 provided by Waldmann Medizintechnik (Villingen-Schwenningen, Germany) which covers partially the absorption spectrum of MB and its derivatives (fig. 3). The normalized emission spectrum of the light source was provided by Waldmann Medizintechnik. The maximal fluence rate at the level of the illuminated samples was 50 $mW cm^{-2}$. The samples were illuminated for 10 min (30 $J cm^{-2}$). In order to estimate the effectiveness of the uptake of the light energy by the different derivatives the values of the emission spectrum "Em" was folded with the

values for the absolute absorption "Abs" for the spectral region between $500 - 800\,nm$. According to the following formula an "*effective toxicity*" (*"Eff.Tox."*) was predicted for each derivative:

Eq. 3.1:

$$Eff.Tox. = \left(\sum_{i=500nm}^{800nm} Em_i \cdot Abs_i \right) \cdot \Phi_\Delta$$

Here, it has been taken into account that the effectively absorbed energy (*i.e.* the sum of the product of emission and absorption) of every photosensitizer is used partially to generate singlet oxygen. Therefore, also the quantum yield Φ_Δ was multiplied to the absorbed energy. The results, given as percentage values, are listed in table 3.13.

3.2.6 Phototoxicity assay of the bacteria

A bacterial cell number of $10^8 - 10^9\ CFU\ mL^{-1}$ was incubated for 10 min in the dark with different concentrations of MB-based photosensitizers (0, 1, 10, 50, and 100 μM). At the end of the incubation period, the cells were transferred into a 96-well microtitre plate (200 μL/well) and illuminated for 10 min (50 $mW\,cm^{-2}$; 30 $J\,cm^{-2}$). Controls were neither sensitized with a photosensitizer nor exposed to the light source, or were incubated with the photosensitizer only. After illumination, the survival of the bacteria was determined by CFU assay. Serially diluted aliquots of treated and untreated (no photosensitizer, no light) cells were plated on Mueller-Hinton agar and the numbers of $CFU\ mL^{-1}$ were counted after 24 h of incubation at 37°C.

3.2.7 Data analysis and statistics for cell experiments

Each individual experiment was performed at least in triplicate. All primary data are presented as means with standard deviation of the mean. A reduction of at least 3 orders of magnitude of log_{10} viable median numbers of bacteria cells was considered biologically relevant with regard to the guidelines for hand hygiene [61].

3.3 RESULTS & DISCUSSION

MB, TBO, NMB, DMMB

The literature-known substances MB, TBO, NMB and DMMB were investigated in suspension of H_2O in regard to their photophysical characteristics. For these studies the commercially available powders of the phenothiazinium derivatives were purified by Andreas Späth, Institute of Organic Chemistry, to gain a pureness of > 99% and were compared to the non-purified photosensitizers. With chromatography experiments impureness for all the four compounds was detected and a comparison of the spectroscopic data could exclude any influences.

The absorption cross section was recorded in the range between 200 nm – 1000 nm for different photosensitizer concentrations and after irradiation of the samples to clarify the photostability. In addition direct detection of the singlet oxygen luminescence was done time- and spectrally resolved, in order to determine the rates and rate constants of the coupled system photosensitizer / oxygen in H_2O for each photosensitizer molecule. The singlet oxygen generation was detected at different photosensitizer concentration, oxygen concentration and in the presence of different concentrations of NaN_3. The quantum yields of singlet oxygen formation were determined for low and high photosensitizer concentration in order to estimate the influence of the dimerisation.

New MB-derivatives

New, partly not literature-known phenothiazinium derivatives were synthesized. In order to derive an influence of the structure of the different side chains on the spectroscopic properties and the phototoxic killing efficacy, the data were compared to MB. First, investigations on the absorption of the new photosensitizers and the change of the absorption spectrum with changing photosensitizer concentration were done. Second, the direct detection of the singlet oxygen luminescence at 1270 nm made an estimation of the effectiveness of the singlet oxygen generation possible, and consequently, thirdly, the bacterial killing efficacy against *S. aureus* and *E. coli* was determined. Therefore, the quantity *"effective toxicity"* was introduced, which takes the quantum yield and the overlap with the emission spectrum of the medical broadband lamp and the absorption spectrum of the

photosensitizer into account and might be a more realistic value for the prediction of the outcome in a phototoxic experiment.

3.3.1 Investigation of MB, NMB, DMMB, and TBO

3.3.1.1 Absorption spectra for different photosensitizer concentrations

Phototoxic reactions of MB on microorganisms can involve redox reactions between the photosensitizer and the pathogen, or the generation of reactive oxygen species (ROS) via type-I mechanism or type-II mechanism, *e.g.* direct energy transfer from excited triplet state of the photosensitizer to oxygen, resulting in the formation of singlet molecular oxygen [13, 62]. Both mechanisms are described to be important for an antibacterial effect. The photo-inactivation of bacteria might therefore depend on the aggregation state of the molecule (dimerisation)[63-66] that can be influenced also by the presence of bacteria [67, 68] or other influences like the pH value of the surrounding [5, 27, 69]. Therefore, absorption spectra of the substances MB, NMB, and DMMB were recorded and shown in the following graphs and the absorption maxima are summarized.

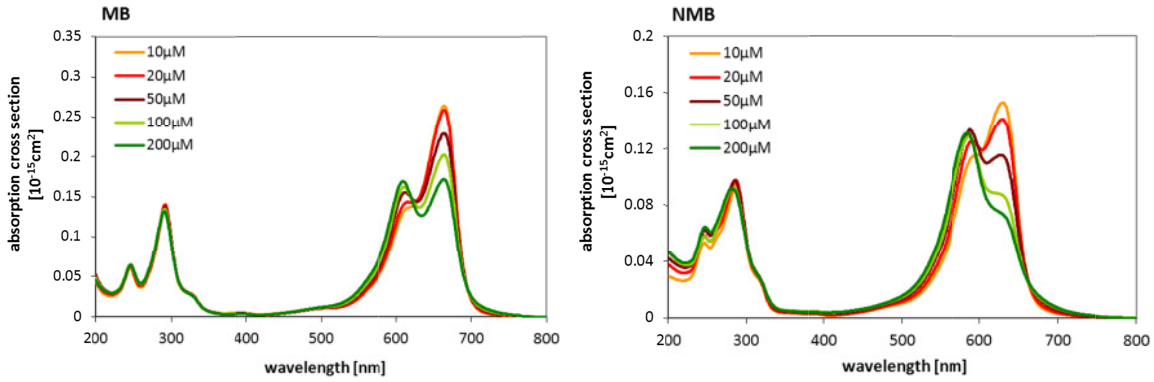

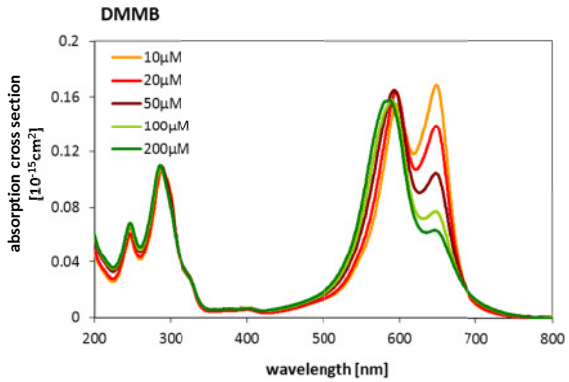

Fig. 3.1: Dependence of the absorption cross section of the non-purified phenothiazines MB, NMB, and DMMB on the wavelength and change of the spectra with different photosensitizer concentrations; the measurements were done in H_2O.

concentration	**[µM]**	**1**	**2**	**5**	**10**	**20**	**50**	**100**	**200**
MB	max_1 [nm]	---	---	---	---	616	612.5	611	609
	max_2 [nm]	664	664	664	664	664	662	663	663.5
NMB	max_1 [nm]	---	---	---	---	591	588	587.5	585.5
	max_2 [nm]	631	632	631	630.5	630	628.5	---	---
DMMB	max_1 [nm]	---	---	---	596.5	595	593.5	588.5	586
	max_2 [nm]	648.5	648.5	648.5	648	648	647.5	647	646

Tab. 3.1: Maxima of the absorption cross section of the non-purified phenothiazines MB, NMB, and DMMB.

Absorption spectra for all substances, MB, NMB, and DMMB, in H_2O showed a dependency of the photosensitizer concentration of the absorption cross section σ. A change of σ can have its origin in aggregation of the photosensitizer molecules, like dimerisation or higher aggregates. The absorption maxima of the non-purified photosensitizers, that are listed in table 3.1, show shifting and in- or decreasing.

The first absorption maximum max_1 shows for all investigated phenothiaziniums a blue-shift for increased concentration, which is described as *hypsochromic effect* and indicates aggregation processes. While the position of the absorption maximum at higher wavelengths, max_2, is not affected by an increase of the concentration within an interval of $\pm 2\ nm$, its intensity decreases and shows the *effect of hypochromicity*.

The absorption spectra were investigated as well for the purified phenothiaziniums, including TBO, and are shown in figure 3.2. The values of their absorption maxima are listed in table 3.2.

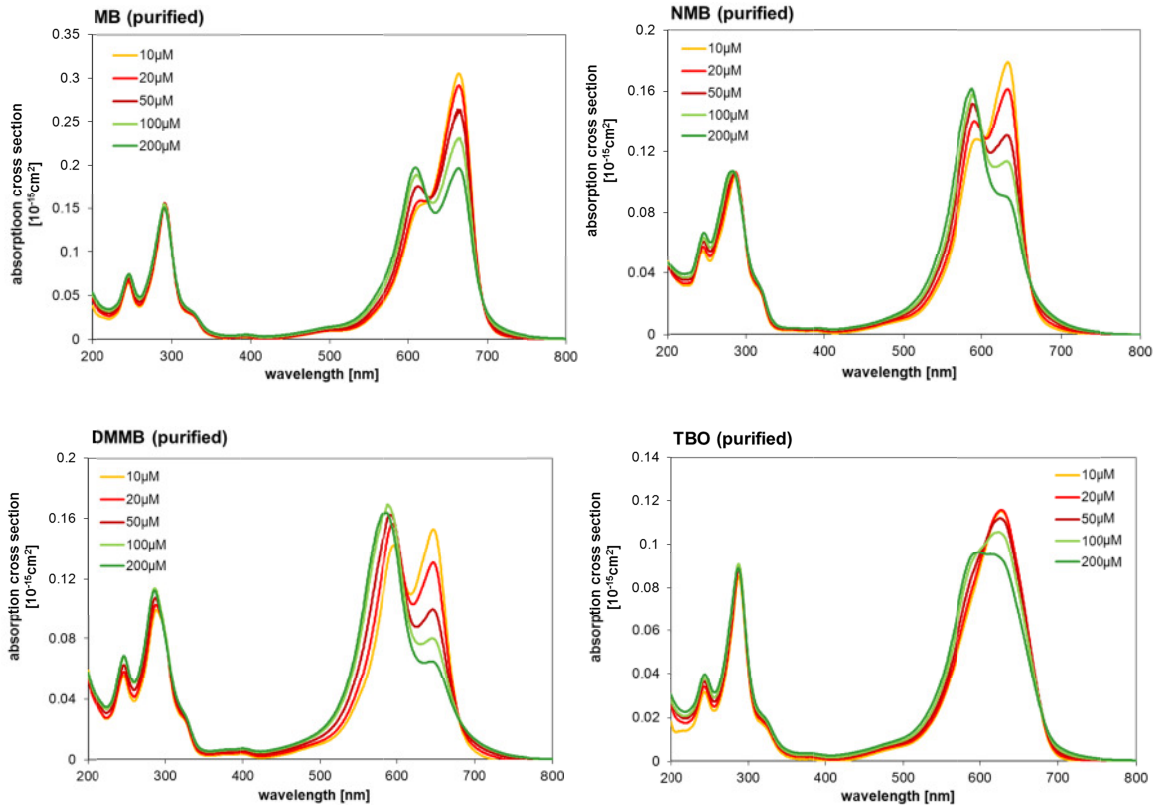

Fig. 3.2: Absorption spectra of the purified phenothiazines MB, NMB, DMMB, and TBO

concentration	**[µM]**	**2**	**5**	**10**	**20**	**50**	**100**	**200**
MB	max_1 [nm]	---	---	---	616.5	613.5	611	610
	max_2 [nm]	664.5	664.5	664	664.5	664.5	663.5	663.5
NMB	max_1 [nm]			593.5	591	588.5	588	587.5
	max_2 [nm]	633	633	633	632.5	632	632	---
DMMB	max_1 [nm]	601.5	598	596	594.5	591.5	588.5	587
	max_2 [nm]	647.5	647.5	647	646.5	646.5	646	644.5
TBO	max_1 [nm]	---	---	---	---	---	---	597.5
	max_2 [nm]	626.5	626.5	627.5	627	625	623.5	---

Tab. 3.2: Maxima of the absorption cross section of the purified phenothiazines MB, NMB, DMMB, and TBO.

Absorption spectra for the purified MB, NMB, DMMB, and TBO in H_2O showed, like their non-purified counterparts, a dependency of the photosensitizer concentration of the

absorption cross section σ. Also here a *hypsochromic* and *hypochromicity effect* was detected for max_1 and max_2, respectively. No influence of possible impurity on and thus change of the absorption spectrum was detected.

Furthermore a change of the absorption cross section σ at $532\,nm$ was investigated in detail, because at this wavelength the Nd:YAG-laser was irradiating the photosensitizers. According to the law of Lambert-Beer

$$T = e^{ac}, \qquad \text{with} \quad a = -\sigma d N_A$$

and assuming that σ is a material constant and therefore independent from the concentration the transmission T which is in the interval of [0;1] decreases exponentially with increasing concentration c, because the factor a is negative.

When assigning the measured values for σ to each concentration a dependency $\sigma(c)$ can be detected. This is expressed in figure 3.3, where (A) represents a non-logarithmic and (B) a logarithmic scaling of the concentration.

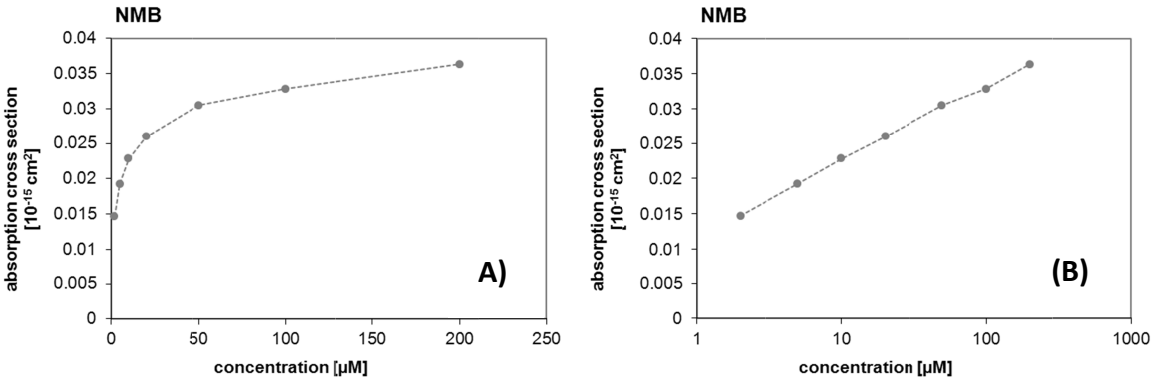

Fig. 3.2: Dependence of the absorption cross section at 532 nm on the concentration of the photosensitizer NMB in H_2O. (A) shows a linear, (B) a logarithmic scaling of the x-axis (concentration).

From figure 3.3 it is clear that the absorption cross section depends on the concentration of NMB which has to be considered in the measurements or for the re-calculation of the molar concentration at known percentaged absorption or transmission value. For the quantum yield measurements a percentaged absorption value is used in order to calculate the absorbed energy at a certain wavelength. With a given dependence of the absorption cross section on the concentration of the photosensitizer the molar concentrations can be re-calculated within the valid range of the law of Lambert-Beer.

Dimerisation of the photosensitizers in the phenothiazine group is used as an explanation for the evolving second absorption peak with increasing concentration in the region of

smaller wavelengths. This explanation is furthermore favoured by many groups and is assigned to a different photophysical behaviour such as a change in the type-I and type-II mechanism and thus in the phototoxic efficacy. It has been described that also the presence of bacteria can enhance this dimerisation behaviour [37]. Nevertheless the dimerisation is controversially discussed by Tafulo *et al*. [70] who assign the appearing shoulder in the absorption spectrum at higher photosensitizer concentration to different ionic strength of the solution.

3.3.1.2 Photostability

Two different methods were used in order to determine the photostability of the photosensitizers. MB, TBO, NMB and DMMB were irradiated with the tuneable laser at different wavelengths and thus different power. Each photosensitizer was irradiated in its absorption maximum and at the same molar concentration of 10 µM, where the dimerization grade was still small for every photosensitizer.

The following figures show the change of the absorption spectrum of each photosensitizer at a concentration of 10 µM for different irradiation times and thus energy doses. For a better overview of the different parameters used for this study, the data are summed up in table 4.3.

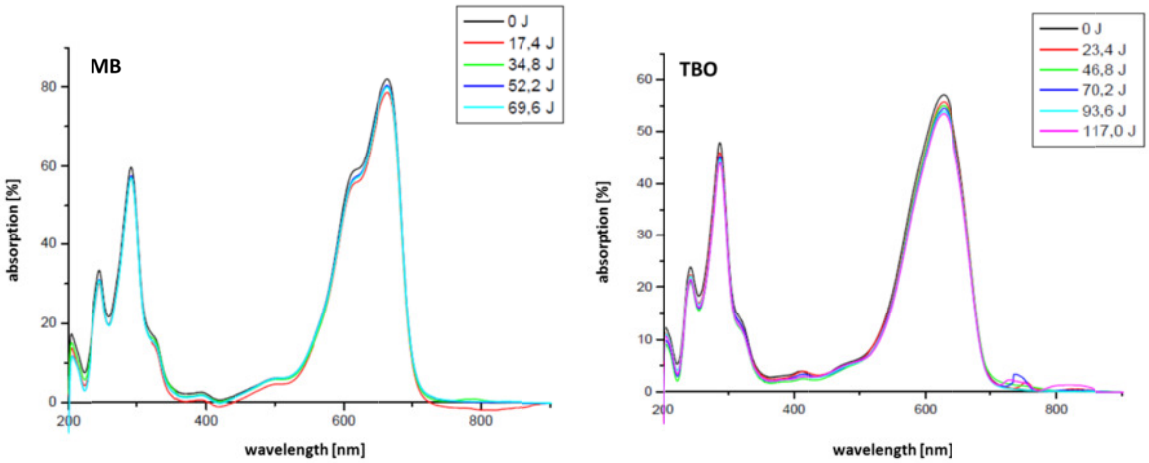

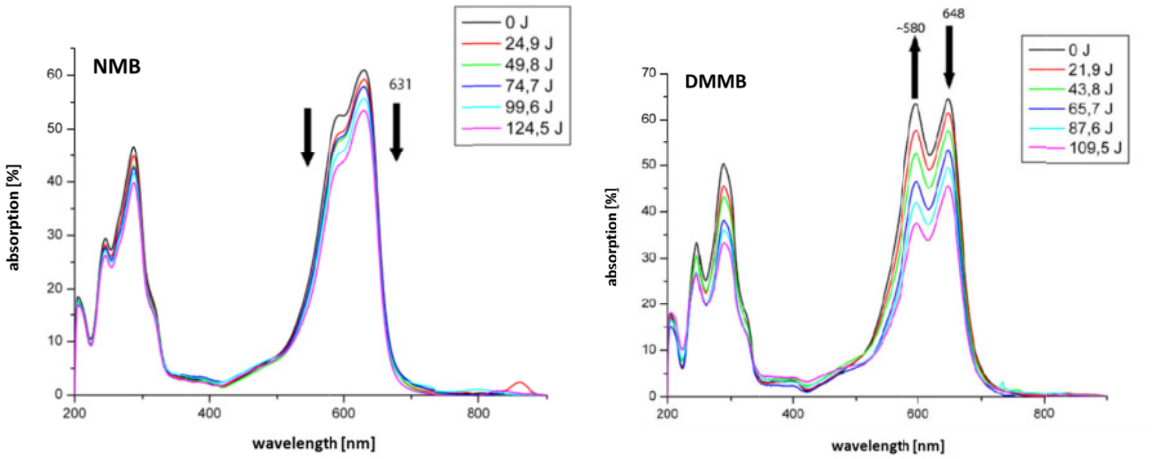

Fig. 3.4: Photostability measurements for MB, TBO, NMB, and DMMB in a quartz cuvette with a photosensitizer concentration of 10 µM. The photosensitizers were irradiated each in its absorption maximum with a constant laser power; every 100 s an absorption spectrum of the solution was recorded. Decrease or increase of an absorption dependent from the irradiation energy is indicated with arrows.

sample	E_{max} [J]	P [mW]	λ [nm]	sigma [cm²]	photostable
MB	69.6	46.4	664	$2.72 \cdot 10^{-16}$	yes
TBO	117	78	627	$1.39 \cdot 10^{-16}$	yes
NMB	124.5	83	631	$1.62 \cdot 10^{-16}$	no
DMMB	109.5	73	648	$1.71 \cdot 10^{-16}$	no

Tab. 3.3: Summary of the parameters for the photostability testing on MB, TBO, NMB, and DMMB; the maximal applied energy E_{max} is given by the irradiation time and the output power P of the laser. λ describes the output wavelength of the laser to irradiate each photosensitizer in its absorption maximum, whereas σ is the absorption cross section at the absorption maximum.

The characteristic absorption spectrum of MB and TBO did not change upon irradiation at the given parameters (see table) within experimental accuracy and therefore they are considered as photostable. In contrast to this NMB and DMMB show both a decrease of the absorption spectrum or bleaching, indicating a change of their photophysical properties. This effect is much stronger for DMMB than for NMB.

3.3.1.3 Time- and spectral resolved direct detection of singlet oxygen

For the investigated substances a singlet oxygen signal was determined both, for irradiating with 532 *nm* and for irradiation into the respective absorption maximum.

In the following section only the rate and rate constants of the non-purified MB, TBO, NMB and DMMB are shown, that were determined in H_2O solution under irradiation of the respective absorption maximum. Due to the optimal irradiation it was, on the one hand, possible to use lower photosensitizer concentrations and on the other, to optimize the signal-to-noise ratio of the singlet oxygen luminescence signal in order to minimize the error in the calculation of the rise and decay times from the time-resolved signals.

The following table sums up the decay times of singlet oxygen that was generated by the different derivatives in H_2O -solution and the respective decay time of the triplet-T_1-state of each photosensitizer that was calculated by extrapolation of the data curves of a variation of the oxygen concentration to anaerobic conditions.

Decay times	**MB**	**TBO**	**NMB**	**DMMB**
τ_Δ **[µs]**	3.57 ± 0.13	3.45 ± 0.12	3.57 ± 0.13	3.57 ± 0.13
τ_{T_1} **[µs]**	526 ± 474	137 ± 113	189 ± 145	42 ± 15

Tab. 3.4: Overview of the decay times of the excited singlet state of oxygen and the excited triplet-T_1-state of the photosensitizer of MB, TBO, NMB, and DMMB by extrapolation to anaerobic H_2O-surrounding.

With values between $3.45 - 3.57\ \mu s$ the determined decay time for singlet oxygen confirmed the findings in literature [71, 72]. The decay times of the triplet states of the different photosensitizers differed significantly from each other. Due to a calculation from reciprocal values of the rates k_Δ and k_{T_1}, which are shown in table 3.5, the errors become very high.

Raten-konstanten Raten	MB	TBO	NMB	DMMB	Einheit
$k_{T_1\Delta} \cdot k_{\Delta T_1}$	$\geq 0,094 \pm 0,086$	$0,454 \pm 0,11$	$0,35 \pm 0,10$	$0,24 \pm 0,10$	$\mu s^{-2} mM^{-2}$
$k_{T_1O_2} + k_{T_1\Delta}$	$2,15 \pm 0,15$	$2,03 \pm 0,14$	$2,25 \pm 0,15$	$1,90 \pm 0,15$	$\mu s^{-1} mM^{-1}$
$k_{\Delta Q}$	$0,48 \pm 0,03$	$0,45 \pm 0,05$	$0,60 \pm 0,05$	$0,55 \pm 0,05$	$\mu s^{-1} mM^{-1}$
k_{T_1Q}	$0,02 \pm 0,01$	$0,025 \pm 0,01$	$0,010 \pm 0,001$	$0,01 \pm 0,01$	$\mu s^{-1} mM^{-1}$
$k_{\Delta S_0} + k_{\Delta T_1}$	$1,5 \pm 1$	$1,5 \pm 1$	$1,5 \pm 1$	≤ 1	$\mu s^{-1} mM^{-1}$
$k_{T_1S_0}$	$1,5 \pm 0,4$	$\leq 2,1$	$0,7 \pm 0,5$	kA	$\mu s^{-1} mM^{-1}$
$K_{T_1}([O_2] = 0)$	$0,025 \pm 0,005$	$0,030 \pm 0,005$	$0,020 \pm 0,005$	$0,027 \pm 0,003$	μs^{-1}
$K_\Delta([O_2] = 0)$	$0,280 \pm 0,005$	$0,290 \pm 0,005$	$0,280 \pm 0,005$	$0,29 \pm 0,01$	μs^{-1}
$K_{T_1}([P] = 0)$	$0,59 \pm 0,05$	$0,57 \pm 0,02$	$0,62 \pm 0,05$	$0,54 \pm 0,05$	μs^{-1}
k_Δ	$0,28 \pm 0,01$	$0,29 \pm 0,01$	$0,28 \pm 0,01$	$0,28 \pm 0,01$	μs^{-1}
k_{T_1}	$0,010 \pm 0,009$	$0,022 \pm 0,018$	$0,013 \pm 0,010$	$0,0275 \pm 0,010$	μs^{-1}

Tab. 4.5: Overview of the results of the rate and rate constants of MB, TBO, NMB, and DMMB [73].

All rates and rate constants for MB, TBO, NMB, and DMMB are presented in the following table 3.5. Therefore, a variation of the photosensitizer concentration with constant oxygen concentration, a variation of the oxygen concentration with constant photosensitizer

concentration and a variation of the concentration of NaN_3 with constant photosensitizer and oxygen concentration was done and evaluated with the coupled differential equation system proposed by Baier *et al.* [71] in order to calculate the rates and rate constants [73].

3.3.1.4 Determination of the singlet oxygen quantum yields by direct methods

The quantum yields of the photosensitizers were determined at different concentrations in H_2O with two different laser systems. Therefore, it was possible to get an idea about the influence of the dimerization on the effectivity of singlet oxygen generation.

With the *Nd-YAG* laser, MB, NMB, and DMMB were irradiated at 532 nm. Since it is not the main absorption band, the concentrations of the photosensitizer had to be adapted, in order to absorb between $30 - 70\%$ of the light. Therefore, the photosensitizer-concentrations used with this setup were 5 – 10 times higher than in the case of irradiating directly in the main absorption band of each molecule.

The quantum yields for singlet oxygen formation of MB, NMB and DMMB were compared in air saturated H_2O to the quantum yield of TMPyP (0.77). Each photosensitizer absorbed the same amount of energy within the same irradiation time. Furthermore the same amount of oxygen in the water surrounding of the molecule was given in order to deactivate the excited triplet state of the photosensitizer. In table the results for the estimation of the quantum yields Φ_Δ of singlet oxygen for all four derivatives are summarized (tab. 3.6).

Photosensitizer	non-purified	purified
MB	0.24-0.28	0.22-0.27
NMB	0.15-0.20	0.18-0.23
DMMB	0.07-0.12	0.06-0.12

Tab. 3.6: Results of the singlet oxygen quantum yield of MB, NMB, and DMMB, irradiated with 532 nm and with a change of the photosensitizer concentration and thus absorbed energy.

The data show the range of the quantum yields for the non-purified, commercially available substances and the purified ones, taking into account the experimental accuracy of the measurement. Within the experimental tolerance the results show the same quantum yields for the purified and the non-purified photosensitizers, but differ significantly from the values from literature.

With the new tunable laser an irradiation in the main absorption band of the phenothiazine-derivatives was possible. The concentration of each photosensitizer was 1 µM and thus the photosensitizers were in their monomeric form.

Photosensitizer	Quantum yield (non-purified)
MB	0.27 ± 0.05
TBO	0.34 ± 0.05
NMB	0.53 ± 0.09
DMMB	0.39 ± 0.07

Tab. 3.7: Results of the singlet oxygen quantum yield of MB, TBO, NMB, and DMMB irradiated in the respective absorption maximum with a change of the laser power and thus absorbed energy.

We found contradictory results for the quantum yields for both measurements, noticing that the method was different. As can be seen in tables 3.6 and 3.7, the result for the quantum yield of MB of 0.27 was reproduced with this measurement, whereas the quantum yield of NMB and DMMB were significantly higher compared to the measurement at 532 nm.

When exciting the photosensitizers with light at absorption maximum using the tuneable laser and varying the power of the irradiating laser beam a concentration of 1 µM was used where the photosensitizer is mainly in its monomeric form. In contrast to that, with the Nd:YAG laser and an irradiation with 532 nm, the concentration of the photosensitizers was varied with a constant laser power. The phenothiaziniums' absorption optima were not irradiated and higher photosensitizer concentrations compared to the experiment with the tuneable laser were used in order to have appropriate energy absorption. The photosensitizers were dissolved to absolute percentaged absorption values between 30% and 70%. Thus, the molar concentrations should be re-calculated from the law of Lambert-Beer, but since the absorption cross section is not constant the values can only be estimated. In order to reach absorption values between $30 - 70\%$, molar concentrations between 40 µM and above 200 µM had to be made. This is already in a range where dimerization was observed and might influence the singlet oxygen quantum yields.

The presence of dimers has to be strongly considered due to the higher concentrations. In case of MB the generation of singlet oxygen does not seem to be dependent on its concentration and thus not on the ratio of monomer/dimer, since the quantum yield was confirmed with the new experimental setup within experimental accuracy. TBO was only investigated with the new laser setup at low molar concentration and is thus not

comparable. Especially NMB and DMMB showed a huge difference of the quantum yields and the measurements thus suggest a more efficient generation of singlet oxygen at low photosensitizer concentrations, i.e. at the monomeric form.

For all investigated phenothiazines the data clearly differ from the values in literature that are listed in the following table 3.8.

Photosensitizer	**Quantum yields**	**citation**
MB	0.6	[29]
	0.52	[30]
	0.443	[33]
	0.5	[27]
TBO	0.86	[31]
	>0.6	[29]
NMB	1.35*	[31]
DMMB	1.22*	[31]
	1.21*	[32]
	0.5-0.75	[27]

*Tab.3.8: Singlet oxygen quantum yields, overview of the results described in literature by various authors. *Wainwright et al. refer here to a MB quantum yield of 1.00.*

The quantum yields were described in literature as rather effective. Especially for MB a quantum yield around 0.27 was determined which 50% of the value mentioned by Wainwright *et al.* and others (see tab. 3.8). Often indirect measurements are performed which results in a change of the quantum yield for singlet oxygen to higher values due to type-I reaction pathways or reaction with other radicals than singlet oxygen. Assuming a literature-given value of 0.52 for MB, the referenced quantum yield according to Wainwright *et al.* for NMB and DMMB would result in 0.70 and 0.63, respectively. The value for DMMB was also confirmed by Chen *et al.* The experimental data via the direct spectroscopic measurement of singlet oxygen give very contradictive results for low and high concentrations for both, NMB and DMMB. NMB shows a quantum yield of 0.53 ± 0.09 for low and values between $0.15 - 0.20$ for higher photosensitizer concentrations. DMMB shows a quantum yield of 0.39 ± 0.07 for low and values between $0.07 - 0.12$ for higher photosensitizer concentrations. Therefore, like MB both photosensitizers differ significantly from the literature values, especially for higher concentrations. They show generally a high influence of the quantum yield on the concentration.

3.3.1.5 Phenothiaziniums and bacteria: attachment and influence on the photosensitizer absorption

Phenothiazinium derivatives were described to be efficient photosensitizers in aPDT. This is referred to the light-triggered generation of singlet oxygen and to the formation of the hydroxyl radical. Since the quantum yields of especially NMB and DMMB are described in literature to be much higher than determined in this study, and therefore a higher activity of DMMB cannot be explained by its quantum yield, we investigated as well the uptake of the four different phenothiaziniums in cells.

Since DMMB was described to be very effective in the photokilling of bacteria by Wainwright *et al.*, even more effective than MB [28, 74], these two substances were compared in their change of absorption when being in contact to microorganisms. It is known that aggregation processes or adhesion might influence the electronic properties of a photosensitizer and therefore might be different when in contact to bacteria. In particular, dimerisation could occur when photosensitizer molecules attach to cell walls or accumulate inside the cells. Therefore, first the influence of PBS on the absorption spectrum of MB and DMMB was studied and this was followed by investigations on the change of the spectrum with time when MB and DMMB being to contact with bacteria.

Uptake of the photosensitizers

The *S. aureus* bacterial cells were diluted to an $OD = 0.6$ resulting in a final concentration of $10^8\ CFU\ mL^{-1}$. $600\ mL$ of each, bacteria suspension and photosensitizer ($20\ \mu M$) were added to an Eppendorf cap. During the incubation procedure they were left under rotation for $1.5\ h$ in the dark. The process resulted in an overall photosensitizer concentration of $10\ \mu M$ for each photosensitizer. After the incubation the bacteria cells were centrifuged in the Eppendorf caps ($15\ min$, $13\,000\ U\ min^{-1}$) and the supernatant (SN) was investigated. Afterwards the cells were diluted again in $1\ mL\ H_2O$ and another centrifugation was done in order to investigate the second supernatant.

The washing procedure was therefore done once and gave a hint of the overall number of photosensitizer molecules that were attached to *S. aureus* or uptaken. In the following table the photosensitizer uptake after the first and second centrifugation are given in percentaged values. The values after the second washing are a sum of the uptake after the first and second centrifugation.

For the estimation of the uptake of photosensitizer molecules the ratio of the extinction of the supernatant after the first washing and of the extinction of the photosensitizer with a concentration of 10 µM was determined. This ratio gave the value for the non-attached photosensitizer molecules. The ratios of the extinction of the supernatant after the second centrifugation and the photosensitizer at 10 µM were likewise determined, that is, the photosensitizer attachment after one complete washing process was determined. Exemplarily for MB, the number of attached photosensitizer molecules was calculated with the following equations:

$$bacteria\ attached\ after\ 1.SN = 100\% - \frac{E_{664\,nm}\ (1.SN)}{E_{664\,nm}\ (10\mu M\ MB)} \cdot 100\%$$

$$bacteria\ attached\ after\ 2.SN = 100\% - \frac{E_{664\,nm}\ (2.SN)}{E_{664\,nm}\ (10\mu M\ MB)} \cdot 100\%$$

Photosensitizer	**max.**	**attachment to bacteria [%]**	
	[nm]	**1. SN**	**2. SN**
MB	664	66	46
TBO	627	77	56
NMB	631	91	81
DMMB	648	98	95

Tab. 3.9: Photosensitizer uptake after investigation of the 1. and 2. supernatant (SN). The calculation bases on a comparison of the extinction coefficients at the respective wavelength of the absorption maximum (max) [73].

Change of the absorption spectrum of MB and DMMB with bacteria

When adding MB or DMMB to a solution with bacteria, the absorption spectrum differs with time and might give a hint of aggregation of the photosensitizer or the localisation due to a characteristic influence of biomolecules. Experiments in regard to the change of the spectrum of a phenothiazinium photosensitizer and *S. aureus* were done and are presented herein. Due to the very low number of experiments the discussion has to be carried out speculatively.

The influence of PBS was investigated by adding to a certain volume of a parent solution of 40 µM MB / DMMB in H_2O the same volume of PBS solution, resulting in a photosensitizer concentration of 20 µM and a PBS-concentration of 50%.

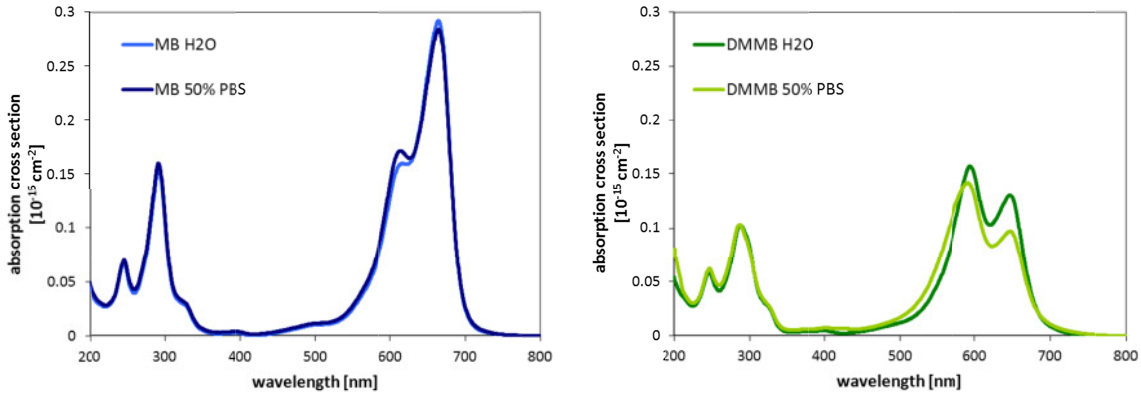

Fig. 3.5: Change of the absorption spectra of MB (left) and DMMB (right), when dissolved in 50% of PBS in H_2O. The photosensitizer concentration was each at 20 µM.

For MB a decrease in its two absorption maxima at 610 nm / 661 nm was detected. For DMMB this effect of decrease was even stronger for both maxima at 591 nm / 642 nm and included also a blue-shift of the maximum at 591 nm of about 6 ± 1 nm.

Bacteria were diluted in PBS to an optical density of $OD_{600} = 0.42$, resulting in a final cell number of $7 \cdot 10^7$ $CFU\ mL^{-1}$, assuming a linear dependence of the optical density and the cell number. The bacteria suspension was added to a solution of MB or DMMB, resulting in an overall photosensitizer concentration of 20 µM. Subsequently the absorption spectrum was recorded after 20 s, 5 min, 15 min, and 30 min.

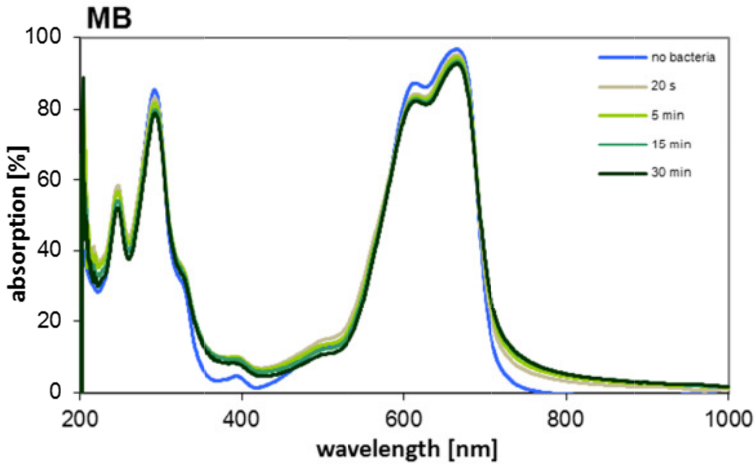

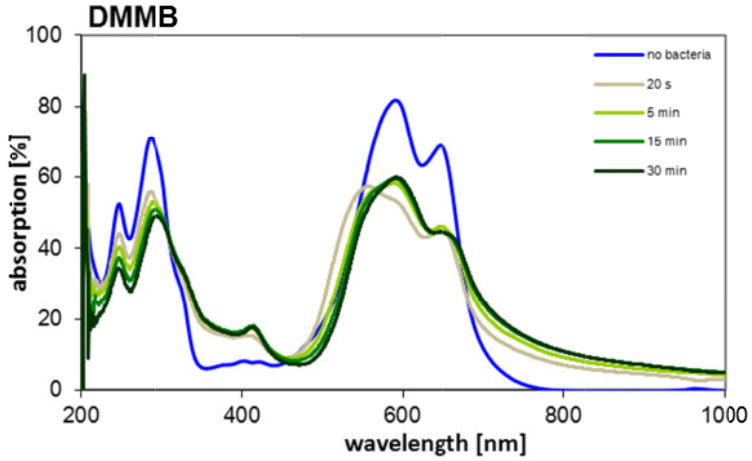

Fig. 3.6: Change of the absorption spectrum of MB and DMMB dependent on the incubation time with S. aureus ($7 \cdot 10^7$ CFU mL^{-1}). The photosensitizers had a final concentration of 20 µM and the overall PBS concentration was 50% in H_2O.

In the spectral range of the absorption maxima of MB (600– 660 nm), the spectrum shows a decrease due to the presence of *S. aureus* in the solution, but not to a high extent. Between 300– 500 nm and 700– 1000 nm the absorption increases. This might also be due to the addition of bacteria. To avoid an influence of the absorption of bacteria a blank with the appropriate concentration of bacteria in 50% PBS was recorded but nevertheless scattering might play a role in this effect.

Compared to MB, DMMB changes its absorption spectrum more drastically in the presence of *S. aureus*. The result is a significant decrease of the absorption between 500– 700 nm. Furthermore shifts of the characteristic absorption peaks can be detected, which are most eye-catching after 20 s of incubation. Shifts of absorption maxima usually indicate aggregation processes, and this would be expected for DMMB due to its high antimicrobial efficacy in the presence of light. The killing efficacy was proven to be light-triggered, but DMMB has also a high dark toxicity, which might be due to its redox-potential. Therefore direct contact between bacteria and photosensitizer is especially necessary. A high attachment of DMMB was also proven in the uptake-studies with an attachment value of 95% compared to 46% for MB after one washing procedure and might be an explanation for the change of the absorption spectrum to a greater extent than in the case of MB. Furthermore, it was described that in the presence of bacteria also dimerisation behaviour might be enhanced [37] and since the attachment value of DMMB is higher a change of the DMMB absorption spectrum to a greater extent can be explained.

Nevertheless a dimerisation of a phenothiazine might and a decrease in the light absorption will lead to a lower singlet oxygen generation via type-II. A decrease of the absorption maxima for DMMB was noticed in figure 3.6 but between 300– 500 nm and 700– 1000 nm the absorption shows an increase and therefore it is not finally clarified how the overall absorption of the respective lamp's emission spectrum changes. This needs further clarification in the future, with a study of the overlap of the emission of the lamp and the absorption of the photosensitizer due to spectral change during bacteria contact.

Furthermore the higher phototoxic efficacy of DMMB might depend notably on the higher quantum yield compared to the yield of MB (0.27), which is around 0.63 in literature (tab. 3.8) and 0.39 for low photosensitizer concentration by own measurements (tab. 3.7). For higher concentrations the quantum yield can drop to values around 0.07 – 0.12 which is lower than the value for MB with 0.27.

3.3.2 New MB-derivatives

3.3.2.1 Absorption spectra for different photosensitizer concentrations

Dimerization of MB and some of its derivatives like TBO has been described in literature [75, 76] and was confirmed as well for NMB and DMMB in the present work. Dimerization has an influence on the photophysical properties of the photosensitizer due to a change of the electronic system and results in different phototoxic efficacies [67]. This effect was also investigated for the new MB derivatives (MB-1 – MB-6), which were dissolved in H_2O with concentrations ranging from 10– 200 μM. The results are shown in the following figures. Table 3.10 displays the absorption maximum of each MB derivative.

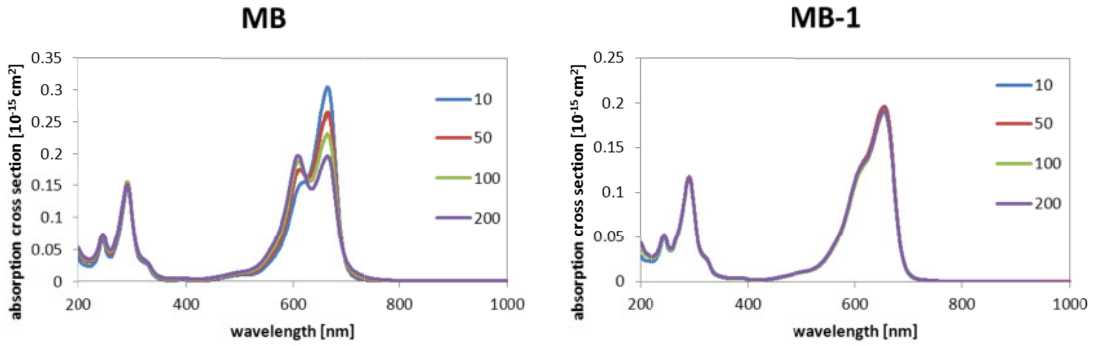

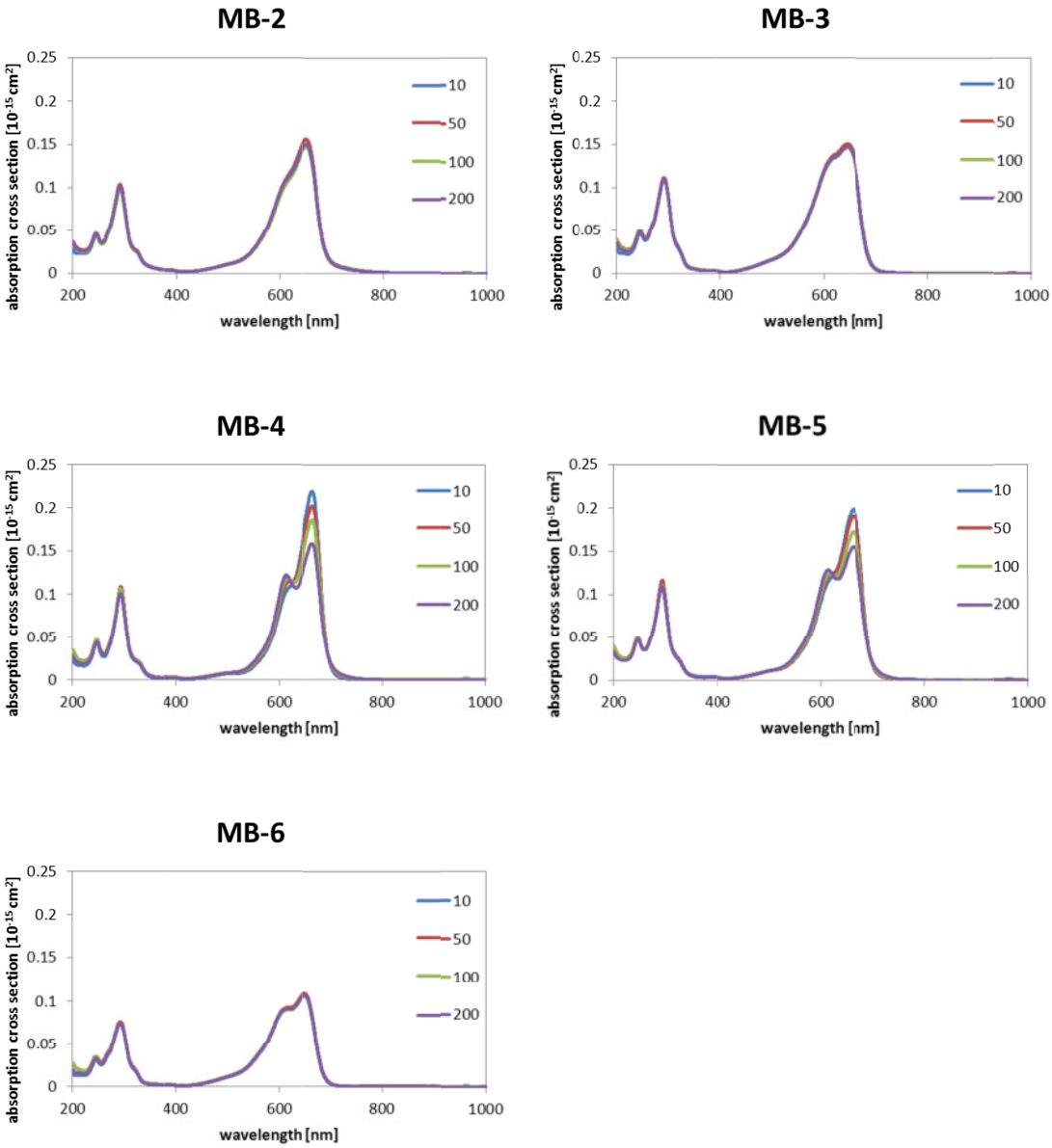

Fig. 3.7: Absorption spectra of MB and its derivatives MB-1 and MB-4 within a concentration range of 10 – 200 µM in H_2O; the measurements show dimerisation for MB, MB-4 and MB-5 in the given concentration range.

PS	**MB**	**MB-1**	**MB-2**	**MB-3**	**MB-4**	**MB-5**	**MB-6**
$\lambda_{abs,max}$ [nm]	664	653.5	650.5	643.5	663.5	662	649

Tab. 3.10: Maxima of the absorption cross section for MB and the new derivatives MB-1 to -6 dissolved in H_2O.

MB-4 and MB-5 closely match the peak of MB at 664 nm. In the given concentration range the derivatives MB-4 and MB-5 show the formation of an additional absorption peak at 613 nm. Under the same circumstances the peak between $662 - 664\ nm$ diminishes with increasing photosensitizer concentration (hypochromicity). The evolving local maximums at

613 nm show each a hypsochromic effect indicating aggregation processes. The peak at 613 nm is considered to be the dimer, as described for MB [75, 76]. MB-1, MB-2, MB-3, and MB-6 do neither show a decrease or increase in any part of their absorption spectrum within experimental accuracy. Since in some newly synthesized phenothiazine derivatives no rising peak at smaller wavelengths was found, it is interesting to have a closer look at the chemical structure of MB-1, -2, -3, and -6 in regard to the argumentation of Tafulo *et al*. [70]. Their reduced ability to dimerize is a benefit of the additional positive charge in this class of compounds. This might enable the use of these phenothiazinium photosensitizers in a broader concentration range in comparison to MB. When the limit of the dimerization process is shifted to higher concentrations or dimerization does not occur at all, the ability for generating singlet oxygen should not change within this concentration range. Therefore, also at higher photosensitizer concentrations the phototoxic effects also might be only linearly dependent on the photosensitizer concentration. Additionally, as was discovered for DMMB, the adsorption to bacteria might affect the dimerization of a photosensitizer. It has to be clarified in further studies if this occurs with contact to bacteria and if this could be an advantage compared to MB or DMMB, respectively.

3.3.2.2 Photostability

The new MB-derivatives were irradiated with the broad-band spectrum of a medical lamp (PDT1200), because also the phototoxicity tests were carried out with this light source. In order to compare the effective light absorption of each derivative an overlay of the emission spectrum of the lamp and the photosensitizers' absorption spectrum was calculated.

Absorption of the lamp emission by the different derivatives of MB

The emission spectrum of the incoherent light source PDT1200 covers partially the absorption spectrum of MB and its derivatives. As an example the overlay of MB with concentrations of 10 µM and 100 µM and the emission spectrum of the PDT1200 are shown in figure 3.8.

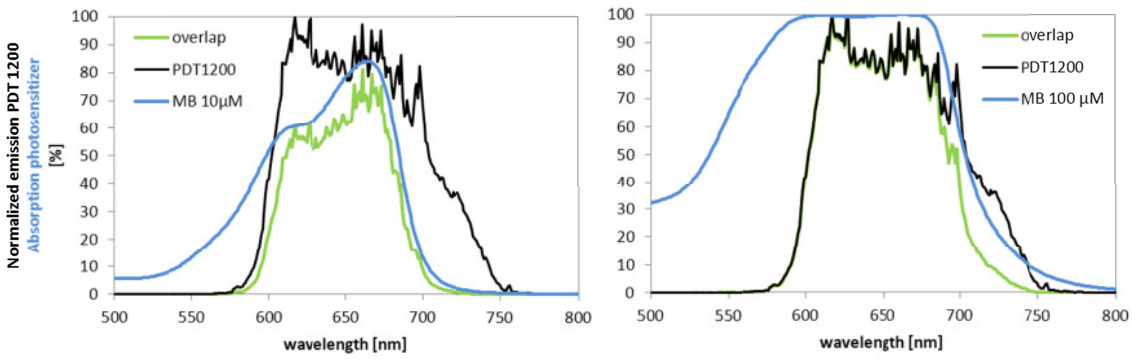

Fig. 3.8: Normalized (100%) emission spectrum of the PDT1200 and absorption spectrum of MB at a concentration of 10 µM (left) and 100 µM (right) in H_2O showing the percentaged absorption. An overlap of these two spectra was calculated by folding the values for emission and absorption for each wavelength and summing up these values.

The effectiveness of light absorption at the molar concentration of 10 μM was calculated with equation 3.1 and the results are listed in table 3.11.

Photosensitizer	overlap [%]
MB	54.4
MB-1	43.1
MB-2	38.7
MB-3	38.4
MB-4	44.5
MB-5	45.4
MB-6	29.6

Tab. 3.11: Calculated overlap of the absorption spectrum of MB (10 µM) with the emission spectrum of the PDT1200.

In table 3.13 in the conclusion one finds the *"overlap"* of emission and absorption and the effective toxicity *"Eff.Tox."*, which estimates the phototoxic effect on microorganisms via singlet oxygen by taking into account the relative singlet oxygen quantum yield $\Phi_{\Delta}^{1.00}$, which describes the part of absorbed energy that generates singlet oxygen. *"Eff.Tox."* describes the predicted "*effective toxicity*" that was calculated by multiplication of $\Phi_{\Delta}^{1.00}$ with the value of the overlap. With this method we assume MB being most active and in descending manner MB (54%) > MB-4 (44%) > MB-1 (37%) > MB-5 (36%) > MB-3 (35%) > MB-2 (28%) > MB-6 (20%).

By diluting MB and its derivatives to a final absorption of $A = 30\%$ at 600 nm the same amount of light energy per time unit is absorbed by each derivative. After irradiation at

600 nm with 180 000 laser pulses (= 3 min), resulting in an energy of $E = 16.2\,J$, the derivatives MB-1 and MB-2 showed a change of absorption around the absorption maxima in the visible spectrum as well as in the UV-range and in the range between 700– 800 nm, while MB and the other derivatives showed photostability.

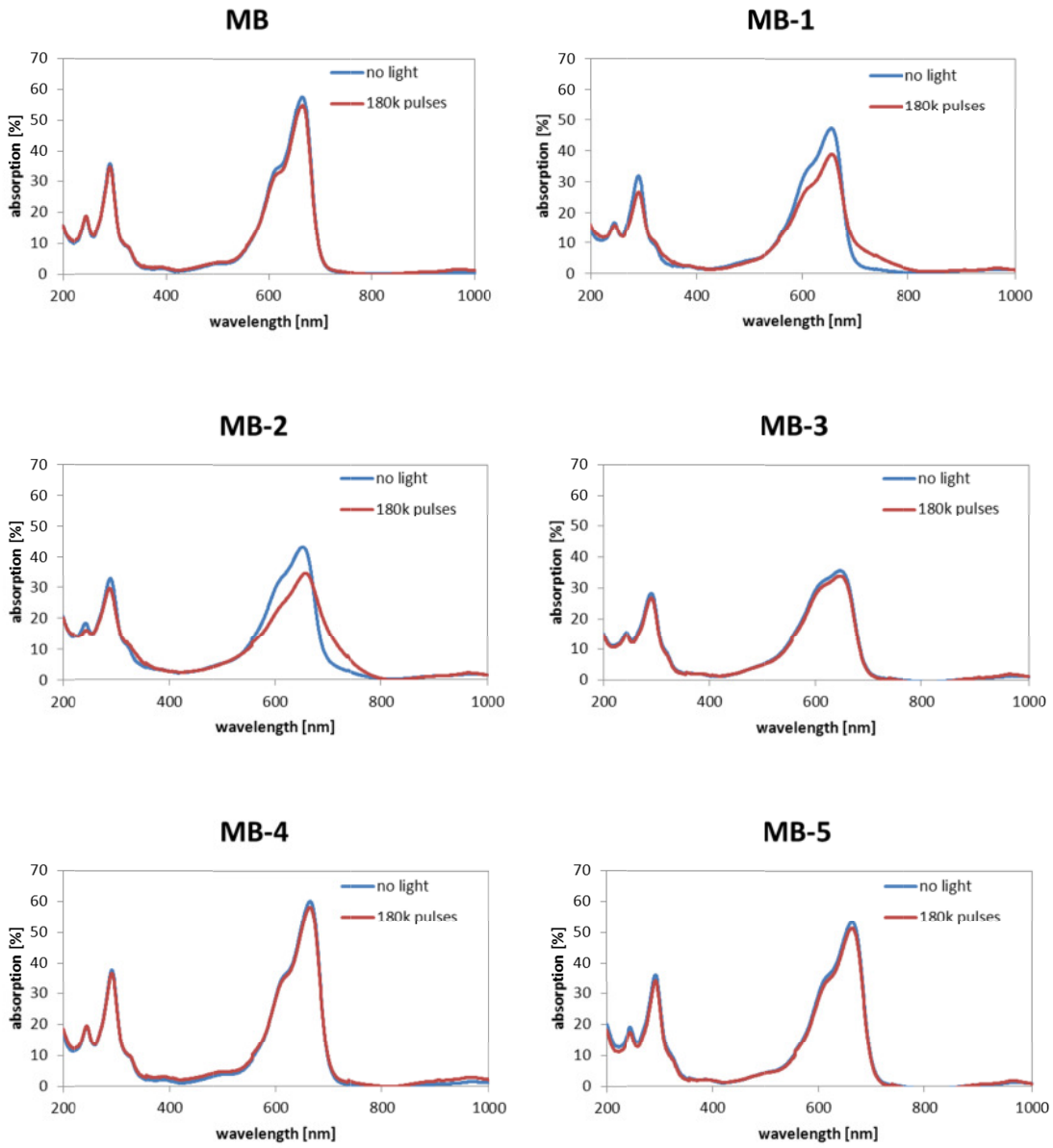

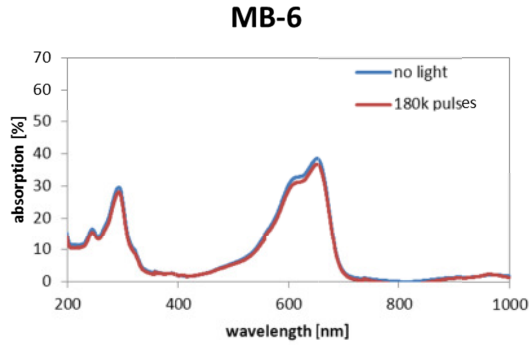

Fig. 3.9: Photostability measurements in a quartz cuvette with an irradiation at 600 nm with 180000 laser pulses; MB-1 and MB-2 show a decrease in the absorption in the visible and in the UV range whereas MB and the other derivatives do not show significant decrease.

The value to estimate photostability was given with the ratio of the absorption maxima after irradiation and before irradiation. The photophysical measurements such as time- and spectrally resolved singlet luminescence did not exceed the amount of energy used for the photostability testing.

3.3.2.3 Time- and spectral resolved direct detection of singlet oxygen

All new MB derivatives MB-1 – MB-6 generated singlet oxygen that was proved by the detection of time- and spectrally resolved luminescence in an air-saturated solution of H_2O at 25°C. 20 000 laser pulses equals an irradiation time of 20 s.

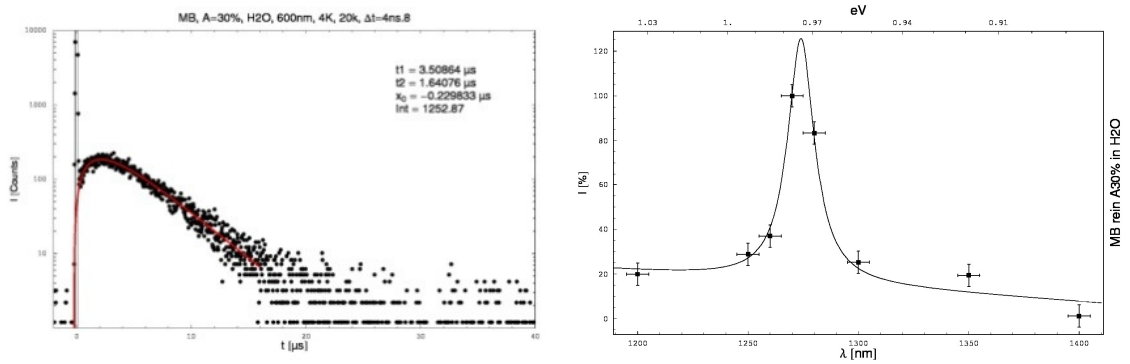

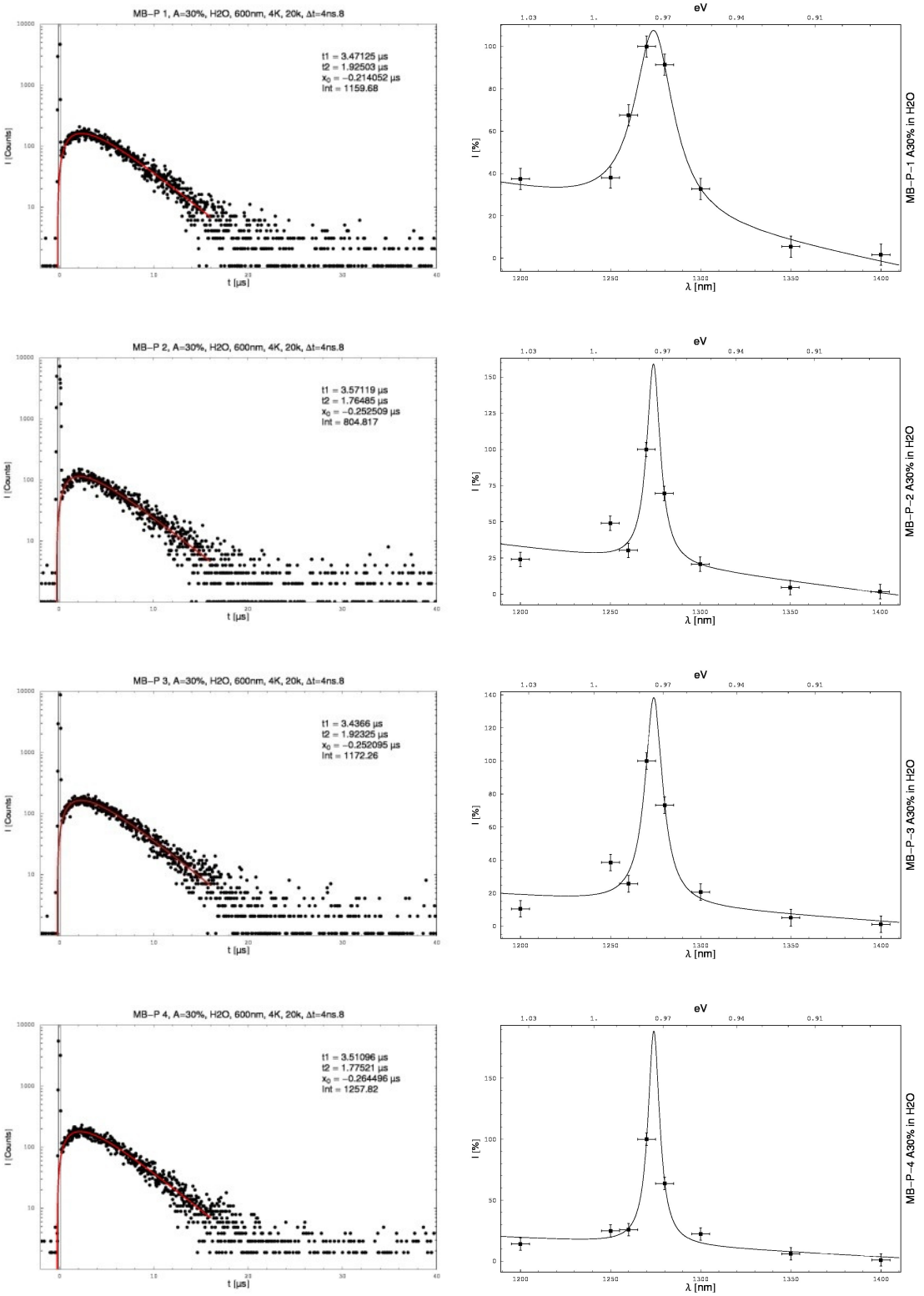
MB–P 1, A=30%, H2O, 600nm, 4K, 20k, Δt=4ns.8
t1 = 3.47125 µs
t2 = 1.92503 µs
x0 = −0.214052 µs
Int = 1159.68
I [Counts]
t [µs]
eV
I [%]
λ [nm]
MB–P–1 A30% in H2O
MB–P 2, A=30%, H2O, 600nm, 4K, 20k, Δt=4ns.8
t1 = 3.57119 µs
t2 = 1.76485 µs
x0 = −0.252509 µs
Int = 804.817
MB–P–2 A30% in H2O
MB–P 3, A=30%, H2O, 600nm, 4K, 20k, Δt=4ns.8
t1 = 3.4366 µs
t2 = 1.92325 µs
x0 = −0.252095 µs
Int = 1172.26
MB–P–3 A30% in H2O
MB–P 4, A=30%, H2O, 600nm, 4K, 20k, Δt=4ns.8
t1 = 3.51096 µs
t2 = 1.77521 µs
x0 = −0.264496 µs
Int = 1257.82
MB–P–4 A30% in H2O

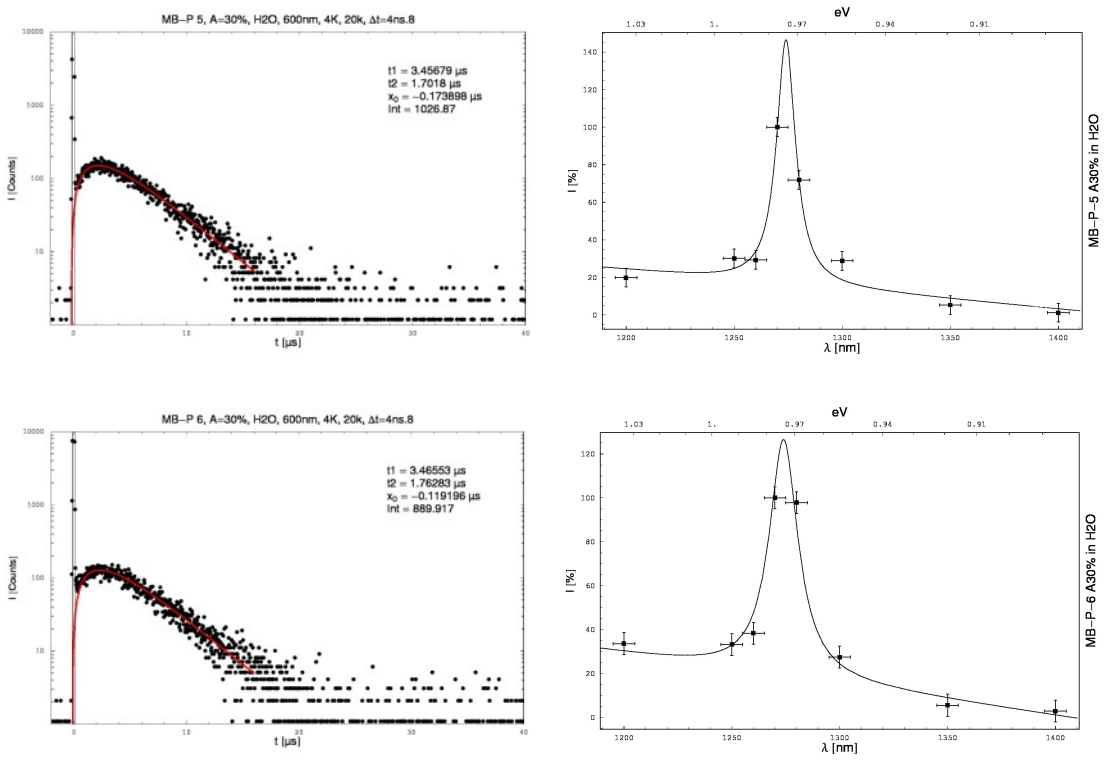

Fig. 3.10: Time- and spectrally resolved singlet oxygen luminescence of MB and its derivatives MB-1 to -6 in air saturated H_2O at 25°C. Singlet oxygen is generated and detected at 1275 nm with a decay time ≈3.5 µs for all derivatives.

Each time-resolved luminescence signal showed a rise and decay time, whereas the rise time differed for each derivative but the decay time was around 3.5 µs, confirming the values in literature for the decay of singlet oxygen in aqueous surrounding [30]. The rise and decay times t_R and t_D are summarized in table 3.13. The maximum of the singlet oxygen luminescence was detected at $\lambda = 1275 \pm 5\ nm$.

3.3.2.4 Determination of the singlet oxygen quantum yields by direct methods

The quantum yields for singlet oxygen formation of the derivatives of MB have been compared in air saturated H_2O to the quantum yield of MB, since it has been described that the quantum yield can be higher in alkaline environment [27]. Each photosensitizer absorbed the same amount of energy within the same irradiation time. Furthermore the same amount of oxygen in the water surrounding of the molecule was given in order to deactivate the excited triplet state of the photosensitizer. Therefore, the singlet oxygen photons give evidence of the effectiveness of each derivative and can be compared to each other. In table 1 the results for the quantum yields Φ_Δ of singlet oxygen for all derivatives are summarized relative to the literature value of the quantum yield for MB of 0.52 [30]. The

quantum yield of MB was then set to 1.00 in this article, as described by $\Phi_{\Delta}^{1.00}$, because it is only needed for reference and comparison purposes. For the values of the quantum yield an error of 10% in regard to the measurement procedure was assumed. Taking into account that the photostability of MB-1 and MB-2 is not given within a range of 180 000 laser pulses we consider an irradiation with 20 000 laser pulses for the quantum yield measurement as an insignificant change in the absorption spectrum ($\approx$ 2%). The Φ_{Δ} of MB-4 is comparable to the yield of MB, whereas the other yields are smaller.

3.3.2.5 Photobiological activity

The irradiation of the Gram-positive *S. aureus* and the Gram-negative *E. coli* upon incubation with different concentrations ($0 - 100\ \mu M$) of MB-1, MB-2, MB-3, MB-4, MB-5 and MB-6, caused a decrease in viability of $CFU\ mL^{-1}$ except for MB-1. An overview of the killing rates after irradiation can be found in the following table 3.12. Since disinfection is considered to reduce the number of viable cells at least 3 log_{10}-steps (99.9%) the table only shows the killing efficacy above this separating line. The exact killing efficacies below 3 log_{10}-steps are shown in figures 3.11.

c [µM]	0	1	10	50	100
			S. aureus		
MB-1	< 3	< 3	< 3	< 3	< 3
MB-2	< 3	< 3	< 3	> 3	> 3
MB-3	< 3	< 3	< 3	> 3	> 6
MB-4	< 3	< 3	> 7	> 7	> 7
MB-5	< 3	< 3	> 7	> 7	> 7
MB-6	< 3	< 3	> 7	> 7	> 7
			E. coli		
MB-1	< 3	< 3	< 3	< 3	< 3
MB-2	< 3	< 3	< 3	> 3	> 3
MB-3	< 3	< 3	> 5	> 5	> 7
MB-4	< 3	< 3	> 5	> 7	> 7
MB-5	< 3	< 3	> 5	> 6	> 6
MB-6	< 3	< 3	< 3	> 7	> 7

Tab. 3.12: Summary of the phototoxic efficacy of the new MB derivatives on S. aureus and E. coli; the table shows only the photodynamic treatment with light (effects of dark toxicity can be found in fig. 3.11 for each photosensitizer). Different concentrations of each photosensitizer were applied and toxic efficacy is described in steps of log_{10}-reduction; therefore "< 3" means a reduction < 3 log_{10} steps (< 99.9%).

Light activation of MB-1 achieved only a reduction of viable bacteria numbers of both bacteria strains of ≈ 1 log_{10} (supplementary figure). Furthermore MB-2 induced only an antibacterial activity of 99.9% using a concentration of 50 µM upon light activation. MB-3 showed a better killing efficacy as compared to MB-2 upon light activation. However, light-activated MB-3 achieved a killing efficacy of > 99.9% at a concentration of 50 µM against both strains, whereas MB-4, MB-5 and MB-6 exhibit the highest killing rate of > 99,999% (5 log_{10}-steps) after irradiation with a concentration > 10 µM.

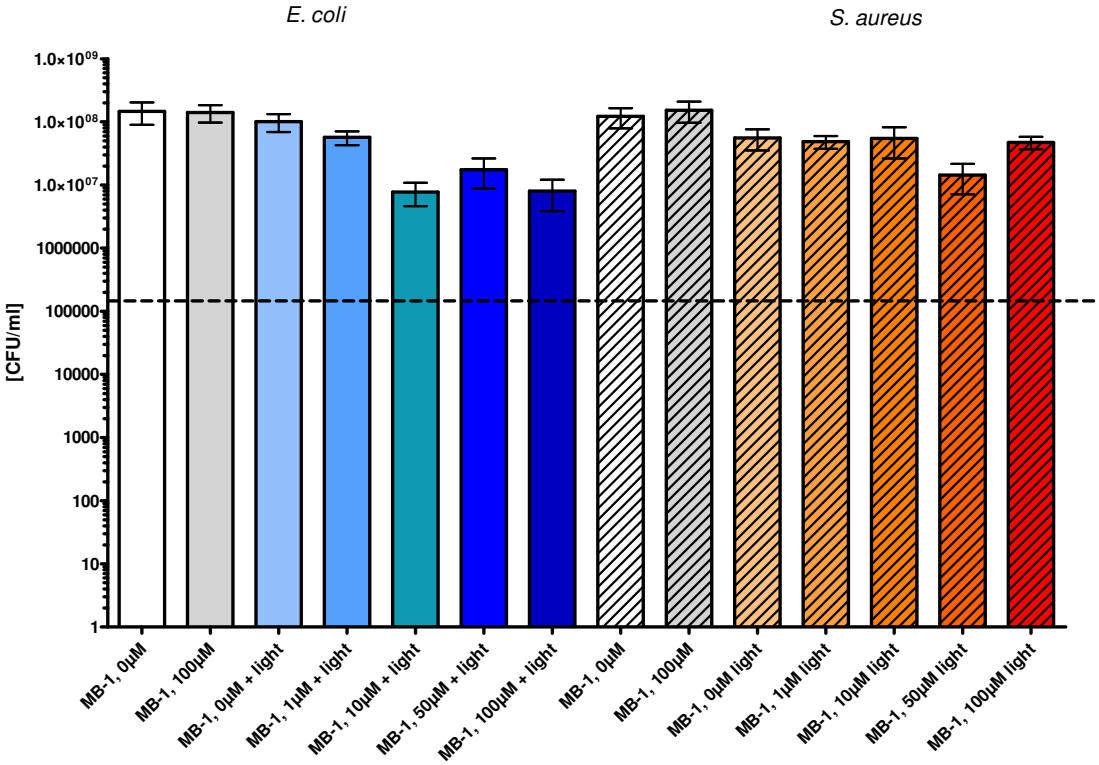

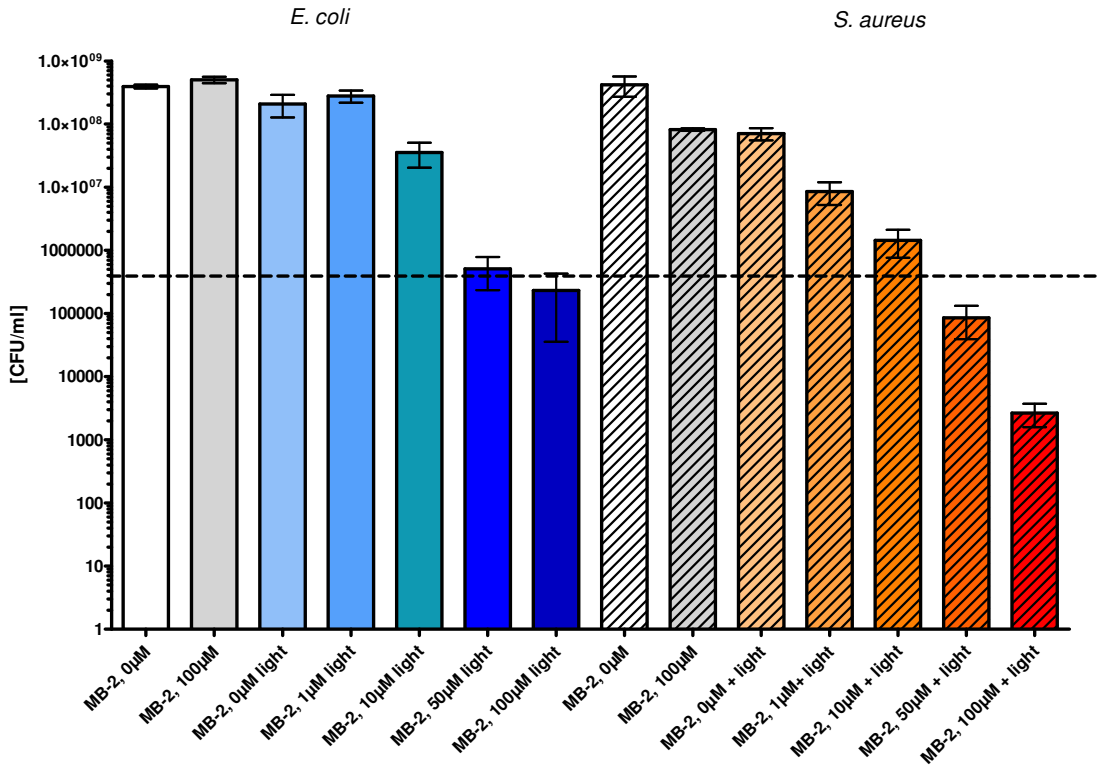
E. coli
S. aureus
[CFU/ml]
1.0×10^09
1.0×10^08
1.0×10^07
1000000
100000
10000
1000
100
10
1
MB-2, 0µM
MB-2, 100µM
MB-2, 0µM light
MB-2, 1µM light
MB-2, 10µM light
MB-2, 50µM light
MB-2, 100µM light
MB-2, 0µM
MB-2, 100µM
MB-2, 0µM + light
MB-2, 1µM+ light
MB-2, 10µM + light
MB-2, 50µM + light
MB-2, 100µM + light

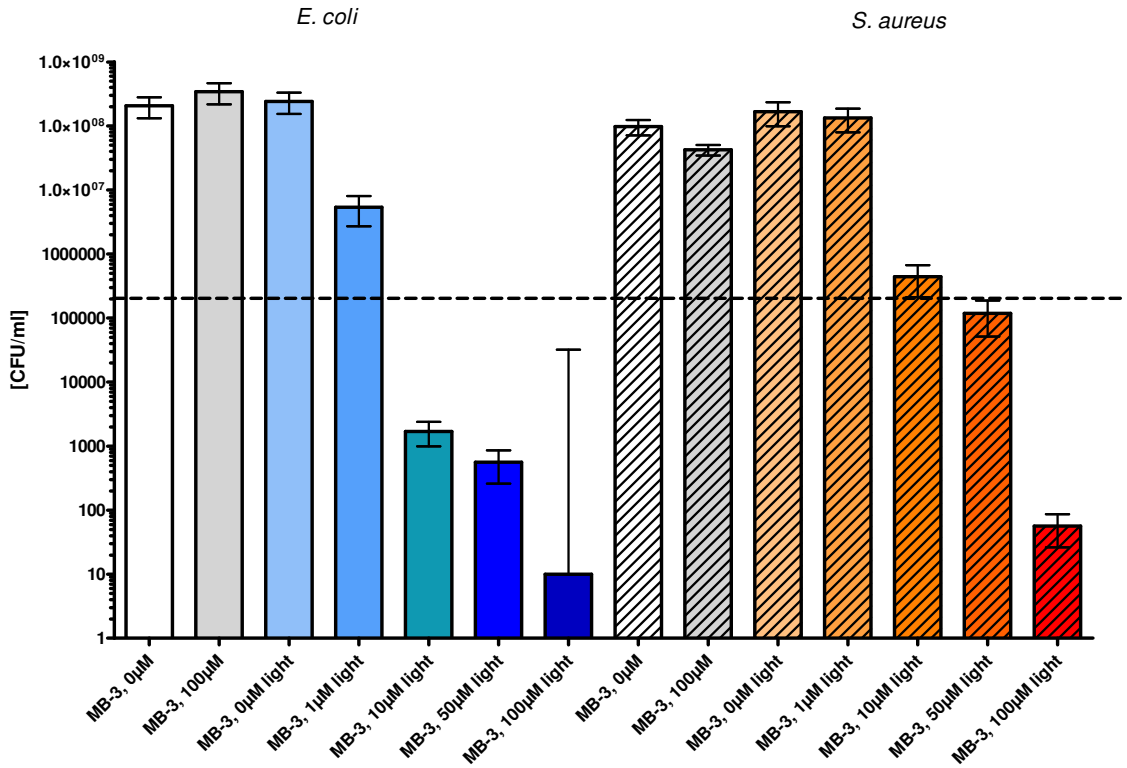
E. coli
S. aureus
[CFU/ml]
1.0×10^09
1.0×10^08
1.0×10^07
1000000
100000
10000
1000
100
10
1
MB-3, 0µM
MB-3, 100µM
MB-3, 0µM light
MB-3, 1µM light
MB-3, 10µM light
MB-3, 50µM light
MB-3, 100µM light
MB-3, 0µM
MB-3, 100µM
MB-3, 0µM light
MB-3, 1µM light
MB-3, 10µM light
MB-3, 50µM light
MB-3, 100µM light

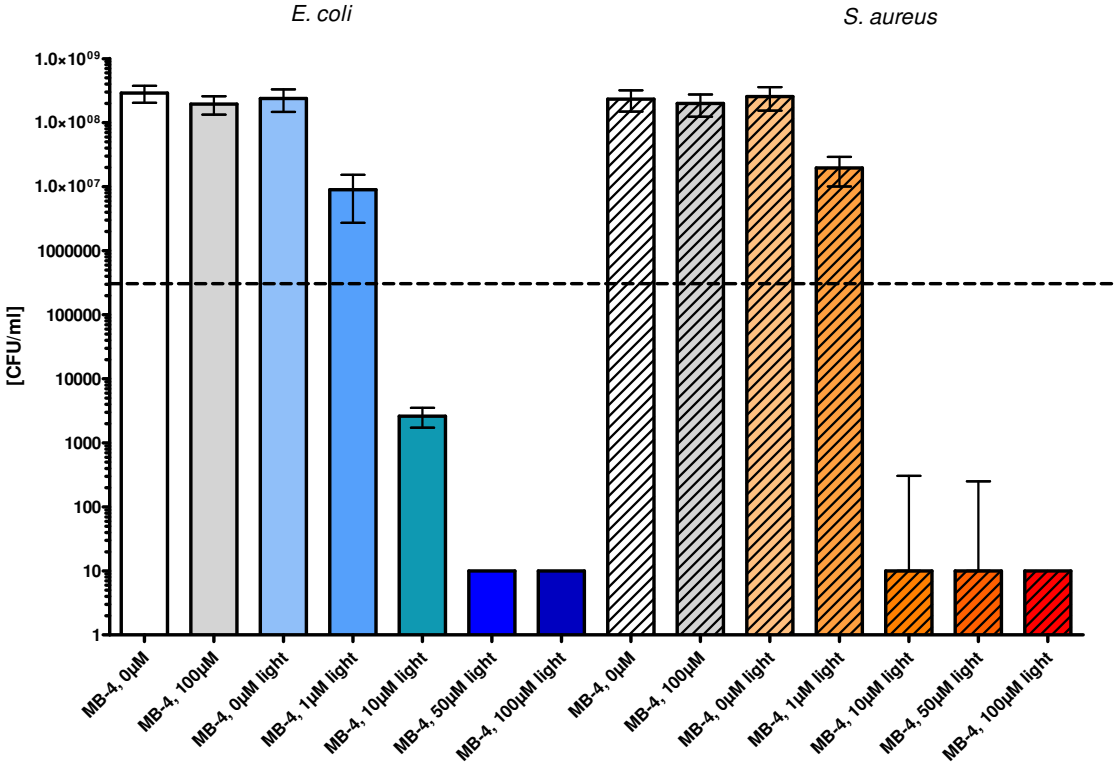
E. coli
S. aureus
[CFU/ml]
1.0×10^09
1.0×10^08
1.0×10^07
1000000
100000
10000
1000
100
10
1
MB-4, 0µM
MB-4, 100µM
MB-4, 0µM light
MB-4, 1µM light
MB-4, 10µM light
MB-4, 50µM light
MB-4, 100µM light
MB-4, 0µM
MB-4, 100µM
MB-4, 0µM light
MB-4, 1µM light
MB-4, 10µM light
MB-4, 50µM light
MB-4, 100µM light

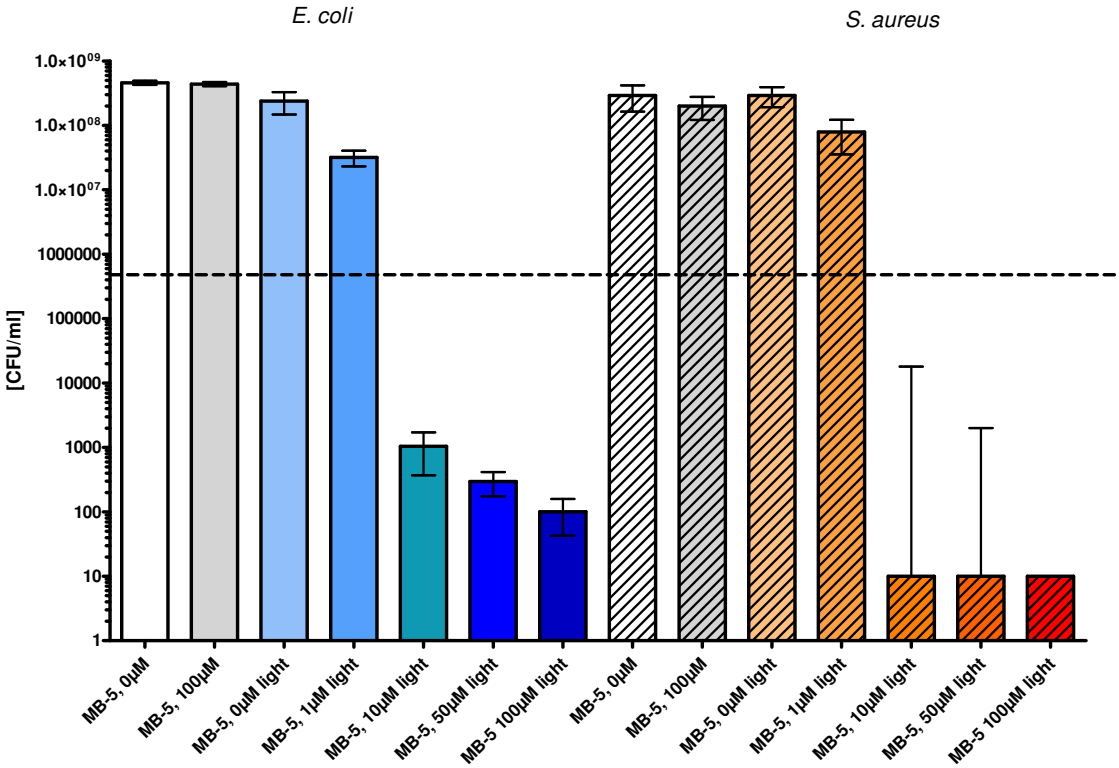
E. coli
S. aureus
[CFU/ml]
1.0×10^09
1.0×10^08
1.0×10^07
1000000
100000
10000
1000
100
10
1
MB-5, 0µM
MB-5, 100µM
MB-5, 0µM light
MB-5, 1µM light
MB-5, 10µM light
MB-5, 50µM light
MB-5 100µM light
MB-5, 0µM
MB-5, 100µM
MB-5, 0µM light
MB-5, 1µM light
MB-5, 10µM light
MB-5, 50µM light
MB-5 100µM light

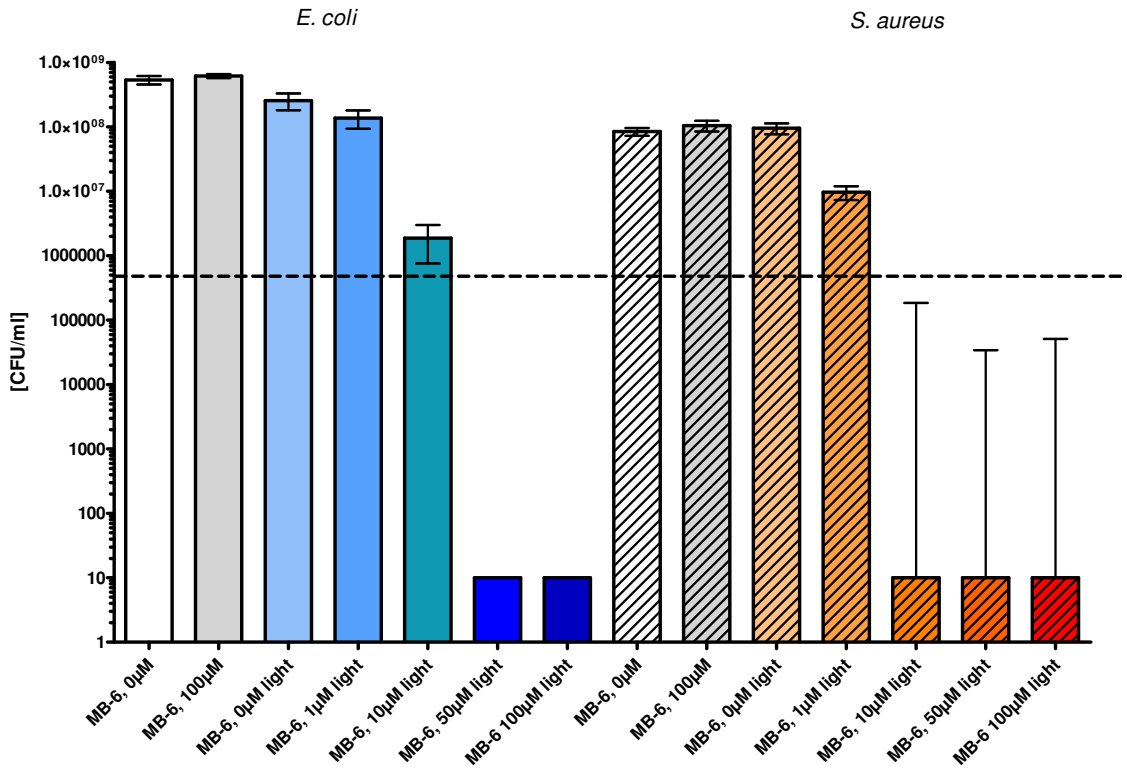

Fig. 3.11: Photodynamic treatment was performed using different concentrations of MB-1 to MB-6 with and without illumination (30 J cm^{-2}). Surviving colonies were counted 24 h later. Black dashed line corresponds to a reduction of 3 log$_{10}$ steps in bacteria numbers (99.9% killing efficacy). White and grey column: controls without illumination. Colored columns: MB-3 + light activation, blue: E. coli; crosshatched: S. aureus. (n = 3 experiments: mean values ± standard deviation)

All bacterial samples that were incubated without photosensitizers exhibited normal growth with or without irradiation, demonstrating that the maximal fluence rate ($50\ mW\,cm^{-2}$) at the level of the irradiated samples alone had no antibacterial effects. In summary, MB-4, MB-5 and MB-6 killed more efficiently both *S. aureus* and *E. coli* compared to MB-1 and MB-2.

The photobiological activity of MB for *S. aureus* and *E. coli* was described for example by Wainwright *et al.* in terms of minimal lethal concentration for $10^6\ CFU\ mL^{-1}$ [2, 28]. To achieve this killing efficacy a concentration of 1 µM for *S. aureus* and 100 µM for *E. coli* an energy dose of 6.3 $J\,cm^{-2}$ was applied (equals 1 h illumination, power of 1.7 $mW\,cm^{-2}$). The phototoxicity data of the derivatives of MB presented herein are comparable to the toxicity of MB as described numerously in literature [1, 2, 25, 28, 29]. The photobiological activities of the derivatives of MB show some dependencies on their photophysical behavior and their chemical properties. Since MB-1 and MB-2 show a decrease in their absorption spectrum when being illuminated (see tab. 3.1), the absorbed amount of light energy decreases as well, which might result in a lower generation of singlet oxygen when compared to the

photostable derivatives. Consequently, a lower phototoxicity compared to the stable derivatives might be the result.

The quantum yield of the photosensitizers gives a value for its efficacy to generate singlet oxygen. But it takes not into account the effective absorption of the light energy. Therefore, the prediction of "*effective toxicity"* - considering the absorbed light energy by the photosensitizers in combination with their quantum yield - is a more realistic value to describe a possible biological killing efficacy. Nevertheless for this study it turned out only for some derivatives to be in line with the measured photobiological activity. MB-4 and MB-1 had a high ranking, predicting effectiveness, whereas MB-6 had a low *"Eff.Tox."* value (tab. 3.13). The toxicity data for MB-4 are in line with the calculations but MB-1 and MB-6 show each the opposite behaviour; while MB-1 did not have any toxic effect at all, but was expected to show toxicity upon irradiation comparable to MB-4, MB-6 was expected to show a low phototoxicity, but inhibited the microorganisms very effectively. In its activity it can be compared to MB-4 and MB-5. A better linking to the cell wall or even uptake into bacteria is therefore supposed for MB-6. Therefore it is interesting to follow the uptake mechanism of each derivative and to investigate the phototoxicity after washing procedures following the incubation process with the photosensitizers in a future study.

The structure-response principle, e.g. the influence of the substituents on the phototoxicity, can be derived from the following considerations:

The antimicrobial efficiency of the derivatives with additional charge in the side chain rises gradually in line, starting from the open chain substituted compounds MB-1 and MB-2 going to the compounds with cyclic substituent MB-3 and MB-6 (MB-1 < MB-2 < MB-3 < MB-6) (tab. 2, see also supporting information). This is in accordance with their photophysical stability (MB-1 = MB-2 < MB-3 = MB-6) (table 3.13, see also supporting information), but not sufficient to explain the findings. The data also show, that going from acyclic to cyclic substituents and moving from primary to secondary to tertiary ammonium charges, an efficiency increase can be achieved. This may be due to better polarity characteristics and in addition a result of the ease of deprotonation of the groups in aqueous media: The pKs values of tertiary ammonium groups (MB-6) are higher than that of secondary (MB-2 and MB-3), which in turn are again higher than that of the primary groups (MB-1). The charges can be seen as more permanent in a pH equilibrium in solution moving from primary to tertiary groups and therefore might have more influence on the attachment to the bacterial cell wall, which is in agreement with the data of the phototoxicity experiments (MB-6 > MB-3 > MB-2).

3.4 CONCLUSIONS

MB, TBO, NMB, DMMB

The photostability of MB, TBO, NMB and DMMB was investigated by irradiating the photosensitizers with a concentration of 10 μM at their respective absorption maximum. In this study only MB and TBO showed photostability within experimental accuracy. NMB and DMMB showed decolourisation expressed in a decrease of absorption cross section σ. The photostability of MB was confirmed, although with lower energy doses, when irradiating and comparing it to the new derivatives at a fixed wavelength of 600 nm. All derivatives except MB-1 and MB-2 showed photostability within experimental accuracy.

In this experimental work the quantum yields were determined with direct spectroscopic methods by comparison with TMPyP or with PNS in H_2O. Since two different experimental setups were used to study the efficacy of singlet oxygen generation, the results were evaluated for high and low photosensitizer concentration at 532 nm and for each photosensitizer in its absorption maximum, respectively.

The maybe most interesting point in the investigations of MB, TBO, NMB, and DMMB was thereby a determination of a much lower quantum yield than described in literature for all the four substances. Due to the fact that many of the quantum yields mentioned in literature were determined with indirect methods, a reaction with other radicals has to be assumed, which influences false-positive the result of the quantum yield.

In case of MB a quantum yield around 0.27 was determined experimentally at high and low photosensitizer concentrations. Due to the "popularity" of this photosensitizer, the easy achievement by industrial companies, and the acceptable quantum yield for singlet oxygen formation, it was worth to test the substance as a singlet oxygen generator also in surfaces, which is described in the following chapter 6. This was done even though type-I reactions, which were investigated in detail by Hamblin *et al*., might lead to a lower outcome in regard to phototoxicity on surfaces and might lead to additional instability for the polymeric surface.

New MB-derivatives

In this study new derivatives of MB derived from modifications of the substituents of MB were described and investigated on their effectiveness for aPDT. These new derivatives should lead to a better insight in the structure-response for aPDT in regard to their different side chains. One substituent in the MB lead structure was changed, in order to achieve pursuable variations of the compound. We focused on the synthesis and study of derivatives with highly polar and/or hydrophilic groups and prepared the compounds in high purity as chloride salts. For this purpose we successfully revised the literature known syntheses and supplied straight forward protocols for preparation and purification of the photosensitizers.

A structure-response relationship was described from a chemical point of view, based on spectroscopic measurements and on investigations of the photobiological activity against *S. aureus* and *E. coli*. Our results point towards a positive influence on the antimicrobial efficacy by hydrogen acceptor bond moieties and additional tertiary charges in the substituent of MB derivatives achieving 7 log_{10}-steps for *S. aureus* and *E. coli* at concentrations of 10 μM with 10 min of irradiation. This can compete with the best examples of known antimicrobial photodynamic agents like porphyrins. The singlet oxygen quantum yields of some compounds are comparable to the yield of MB without overtopping it. Dimerisation of such photosensitizers in solution in a broad concentration range can be suppressed by introducing additional positive charges in the side chains. Table 3.13 summarizes the results for the newly synthesized derivatives of MB, which were described in subunit 3.3.

PS	$\lambda_{abs,max}$	**dim.**	**photo-stab.**	t_D **[µs]**	t_R **[µs]**	Φ_Δ **(ref. MB)**	$\Phi_\Delta^{1.00}$ **(ref. MB)**	**overlap [%]**	**"Eff.Tox." [%]**
MB	664	yes	95%	3.51	1.64	0.52*	1.00	54.4	54
MB-1	653.5	no	82%	3.47	1.93	0.45 ± 0.05	0.87	43.1	37
MB-2	650.5	no	81%	3.57	1.76	0.38 ± 0.04	0.73	38.7	28
MB-3	643.5	no	95%	3.44	1.92	0.47 ± 0.05	0.90	38.4	35
MB-4	663.5	yes	97%	3.51	1.78	0.51 ± 0.05	0.98	44.5	44
MB-5	662	yes	96%	3.46	1.70	0.41 ± 0.04	0.79	45.4	36
MB-6	649	no	95%	3.47	1.76	0.35 ± 0.04	0.67	29.6	20

Tab. 3.13: Characteristic values of MB and its derivatives MB-1 to MB-6, where λ_{max} describes the maximum of the absorption; the dimerisation was detected in a concentration range between 10 – 200 µM; the photostability is described with the ratio of the height of the absorption maximum after irradiation to height of the maximum before irradiation with 180000 laser pulses; t_R and t_D are the rise and decay time of the time resolved singlet oxygen luminescence, respectively; Φ_Δ is the quantum yield of singlet oxygen generation relatively to the quantum yield of MB, which is found in literature to be 0.52 [30]; $\Phi_\Delta^{1.00}$ is the quantum yield of MB set to 1.00, to simplify the comparison. For the values of the quantum yield an error

of 10% in regard to the measurement procedure had to be estimated. "overlap" describes the uptake of the lamp emission spectrum by the different photosensitizers at a concentration of 10 µM. "Eff.Tox." describes therefore the predicted "effective toxicity" that was calculated by multiplication of $\Phi_{\Delta}^{1.00}$ (ref. MB) with the value of the overlap.

Compound MB-4 and MB-5 are comparable in their stability and ability to dimerize, also matching the values of these parameters of MB. Both photosensitizers with hydrogen bond accepting moieties show a high activity against *S. aureus* and *E. coli* in the photodynamic inactivation studies (fig. 3.11), whereas the antimicrobial efficiency of MB-4 is slightly higher than that of MB-5 against *E. coli*. This is in agreement in regard to their singlet oxygen quantum yield and the predicted "*effective toxicity"*, which is summarized in table 3.14.

Predicted *"Effective Toxicity"*	MB > 4 > 1 > 5 > 3 > 2 > 6
Quantum yield	MB > 4 > 3 > 1 > 5 > 2 > 6
Toxicity *S. aureus*	6 = 5 = 4 > 3 > 2 > 1
Toxicity *E. coli*	4 > 5 > 3 > 6 > 2 > 1

Tab. 3.14: Summary of the effectiveness of the new MB-derivatives in regard to their predicted "Effective toxicity", their quantum yield, and their photokilling efficacy against S. aureus and E. coli

From a chemical point of view, compound MB-3 is the most favorable building block for further syntheses at the side chain, *e.g.* coupling to peptides. Its stability is higher than that of its open chain analogues MB-1 and MB-2, the yields in synthesis are also slightly better and the purification is easier. Also the ammonium group is more reactive, than the alcohol in compound MB-4. Since some of the newly synthesized compounds did not show dimerisation in the same concentration range as did MB and also NMB, DMMB and TBO, this might positively influence the effect of phototoxicity also in a higher concentration range. Nevertheless, this has to be clarified in further studies, which also include a direct comparison of MB, NMB, DMMB, and TBO with the newly synthesized MB-1 to MB-6.

A simple method of estimating the effective phototoxicity by taking singlet oxygen quantum yield in combination with the absorbed light energy into account was presented for the new derivatives. Not for all derivatives this value for the effective phototoxicity is in line with the data of the killing rates. Some exhibit a high killing rate which is not supported by spectroscopic data and *vice versa*. Therefore other mechanisms of action have to be assumed and the adhesion to bacteria cell walls and the uptake of the derivatives has to be investigated in a further study, including washing experiments following the incubation period.

3.5 REFERENCES

1. Hamblin, M.R. and G. Jori, *Photodynamic Inactivation of Microbial Pahogens: Medical and Environmental Applications* 2011, London: Royal Society of Chemistry. 450.
2. Wainwright, M., *Photodynamic antimicrobial chemotherapy (PACT).* Journal of Antimicrobial Chemotherapy, 1998. **42**(1): p. 13-28.
3. Maisch, T., *A New Strategy to Destroy Antibiotic Resistant Microorganisms: Antimicrobial Photodynamic Treatment.* Mini-Reviews in Medicinal Chemistry, 2009. **9**(8): p. 974-983.
4. Giroldo, L.M., et al., *Photodynamic antimicrobial chemotherapy (PACT) with methylene blue increases membrane permeability in Candida albicans.* Lasers in Medical Science, 2009. **24**(1): p. 109-112.
5. Carvalho, G.G., M.P. Felipe, and M.S. Costa, *The photodynamic effect of methylene blue and toluidine blue on Candida albicans is dependent on medium conditions.* Journal of Microbiology, 2009. **47**(5): p. 619-623.
6. Menezes, S., M.A.M. Capella, and L.R. Caldas, *Photodynamic-Action of Methylene-Blue - Repair and Mutation in Escherichia-Coli.* Journal of Photochemistry and Photobiology B-Biology, 1990. **5**(3-4): p. 505-517.
7. Singh, H. and D.D. Ewing, *Methylene-Blue Sensitized Photoinactivation of Escherichia-Coli Ribosomes - Effect on Rna and Protein-Components.* Photochemistry and Photobiology, 1978. **28**(4-5): p. 547-552.
8. Cassidy, C.M., R.F. Donnelly, and M.M. Tunney, *Effect of sub-lethal challenge with Photodynamic Antimicrobial Chemotherapy (PACT) on the antibiotic susceptibility of clinical bacterial isolates.* Journal of Photochemistry and Photobiology B-Biology, 2010. **99**(1): p. 62-66.
9. Zolfaghari, P.S., et al., *In vivo killing of Staphylococcus aureus using a light-activated antimicrobial agent.* Bmc Microbiology, 2009. **9**.
10. Baptista, M.S. and M. Wainwright, *Photodynamic antimicrobial chemotherapy (PACT) for the treatment of malaria, leishmaniasis and trypanosomiasis.* Brazilian Journal of Medical and Biological Research, 2011. **44**(1): p. 1-10.
11. Wagner, S.J., et al., *Factors affecting virus photoinactivation by a series of phenothiazine dyes.* Photochemistry and Photobiology, 1998. **67**(3): p. 343-349.
12. Floyd, R.A., J.E. Schneider, and D.R. Dittmer, *Methylene blue photoinactivation of RNA viruses.* Antiviral Research, 2004. **61**(3): p. 141-151.
13. Wainwright, M., *Methylene blue derivatives - suitable photoantimicrobials for blood product disinfection?* International Journal of Antimicrobial Agents, 2000. **16**(4): p. 381-394.
14. Wainwright, M. and K.B. Crossley, *Methylene Blue - a therapeutic dye for all seasons?* Journal of Chemotherapy, 2002. **14**(5): p. 431-443.
15. Wainwright, M., et al., *Phenothiaziniums as putative photobactericidal agents for red blood cell concentrates.* Journal of Chemotherapy, 2001. **13**(5): p. 503-509.
16. Wainwright, M., H. Mohr, and W.H. Walker, *Phenothiazinium derivatives for pathogen inactivation in blood products.* Journal of Photochemistry and Photobiology B-Biology, 2007. **86**(1): p. 45-58.
17. Wilson, M., *Lethal photosensitisation of oral bacteria and its potential application in the photodynamic therapy of oral infections.* Photochemical & Photobiological Sciences, 2004. **3**(5): p. 412-418.
18. George, S. and A. Kishen, *Photophysical, photochemical, and photobiological characterization of methylene blue formulations for light-activated root canal disinfection.* Journal of Biomedical Optics, 2007. **12**(3).
19. Ng, R., et al., *Endodontic Photodynamic Therapy Ex Vivo.* Journal of Endodontics, 2011. **37**(2): p. 217-222.
20. Foschi, F., et al., *Photodynamic inactivation of Enterococcus faecalis in dental root canals in vitro.* Lasers in Surgery and Medicine, 2007. **39**(10): p. 782-787.
21. Jaju, S. and P.P. Jaju, *Newer root canal irrigants in horizon: a review.* International journal of dentistry. **2011**: p. 851359-851359.

22. Soukos, N.S., et al., *Photodynamic therapy for endodontic disinfection.* Journal of Endodontics, 2006. **32**(10): p. 979-984.
23. Fimple, J.L., et al., *Photodynamic treatment of endodontic polymicrobial infection in vitro.* Journal of Endodontics, 2008. **34**(6): p. 728-734.
24. Goulart, R.D., et al., *Comparative Study of Methylene Blue and Erythrosine Dyes Employed in Photodynamic Therapy for Inactivation of Planktonic and Biofilm-Cultivated Aggregatibacter actinomycetemcomitans.* Photomedicine and Laser Surgery, 2010. **28**: p. S85-S90.
25. Ragas, X., et al., *Photodynamic Inactivation of Acinetobacter baumannii Using Phenothiazinium Dyes: In Vitro and In Vivo Studies.* Lasers in Surgery and Medicine, 2010. **42**(5): p. 7.
26. Tardivo, J.P.D.G., A.; de Oliveira, C. S.; Gabrielli, D. S.; Junqueira, H.C.; Batista Tada, D.; Severino, D.; de Fatima Turchiello, R.; Baptista, M.S., *Methylene blue in photodynamic therapy: From basic mechanisms to clinical applications.* Photodiagnosis and Photodynamic Therapy, 2005. **2**: p. 17.
27. Chen, J., T.C. Cesario, and P.M. Rentzepis, *Effect of pH on Methylene Blue Transient States and Kinetics and Bacteria Photoinactivation.* Journal of Physical Chemistry A, 2011. **115**(13): p. 2702-2707.
28. Wainwright, M., et al., *A study of photobactericidal activity in the phenothiazinium series.* Fems Immunology and Medical Microbiology, 1997. **19**(1): p. 75-80.
29. Usacheva, M.N., M.C. Teichert, and M.A. Biel, *Comparison of the methylene blue and toluidine blue photobactericidal efficacy against gram-positive and gram-negative microorganisms.* Lasers Surg Med, 2001. **29**(2): p. 165-73.
30. Wilkinson, F., W.P. Helman, and A.B. Ross, *Quantum Yields for the Photosensitized Formation of the Lowest Electronically Excited Singlet-State of Molecular-Oxygen in Solution.* Journal of Physical and Chemical Reference Data, 1993. **22**(1): p. 113-262.
31. Phoenix, D.A., et al., *The phototoxicity of phenothiazinium derivatives against Escherichia coli and Staphylococcus aureus.* FEMS Immunol Med Microbiol, 2003. **39**(1): p. 17-22.
32. Wainwright, M. and R.M. Giddens, *Phenothiazinium photosensitisers: choices in synthesis and application.* Dyes and Pigments, 2003. **57**(3): p. 245-257.
33. Wainwright, M., *Phenothiazinium photosensitisers: V. photobacterial activities of chromophore-methylated phenothiazinium salts.* Dyes and Pigments, 2007. **73**(1): p. 6.
34. Garcez, A.S., et al., *Antimicrobial mechanisms behind photodynamic effect in the presence of hydrogen peroxide.* Photochem Photobiol Sci, 2011. **10**(4): p. 483-90.
35. Huang, L., et al., *Paradoxical potentiation of methylene blue-mediated antimicrobial photodynamic inactivation by sodium azide: Role of ambient oxygen and azide radicals.* Free Radic Biol Med, 2012. **53**(11): p. 2062-71.
36. Pecci, L., et al., *Methylene blue photosensitized oxidation of cysteine sulfinic acid and other sulfinates: the involvement of singlet oxygen and the azide paradox.* Biochem Biophys Res Commun, 2000. **270**(3): p. 782-6.
37. Usacheva, M.N., M.C. Teichert, and M.A. Biel, *The role of the methylene blue and toluidine blue monomers and dimers in the photoinactivation of bacteria.* J Photochem Photobiol B, 2003. **71**(1-3): p. 87-98.
38. Wilson, M., *Light-activated antimicrobial coating for the continuous disinfection of surfaces.* Infect Control Hosp Epidemiol, 2003. **24**(10): p. 782-4.
39. Decraene, V., J. Pratten, and M. Wilson, *Cellulose acetate containing toluidine blue and rose bengal is an effective antimicrobial coating when exposed to white light.* Appl Environ Microbiol, 2006. **72**(6): p. 4436-9.
40. Perni, S., et al., *Prevention of biofilm accumulation on a light-activated antimicrobial catheter material.* Journal of Materials Chemistry, 2010. **20**(39): p. 8668-8673.
41. Wainwright, M., M.N. Byrne, and M.A. Gattrell, *Phenothiazinium-based photobactericidal materials.* J Photochem Photobiol B, 2006. **84**(3): p. 227-30.
42. Cincotta, L., J.W. Foley, and A.H. Cincotta, *Novel red absorbing benzo[a]phenoxazinium and benzo[a]phenothiazinium photosensitizers: in vitro evaluation.* Photochemistry and Photobiology, 1987. **46**(5): p. 751-8.
43. Carloni, P., et al., *On the Use of 1,3-Diphenylisobenzofuran (Dpbf) - Reactions with Carbon and Oxygen-Centered Radicals in Model and Natural Systems.* Research on Chemical Intermediates, 1993. **19**(5): p. 395-405.
44. Zacks, S.I., *PATHOLOGY OF THE NEURO MUSCULAR JUNCTION.* Annals of Clinical and Laboratory Science, 1975. **5**(3): p. 161-166.

45. Lang, G., *Histotechnik, Praxislehrbuch für die biomedizinische Analytik*2006, Wien: Springer. 427.
46. Kasten, F.H., *Paul Ehrlich: Pathfinder in cell biology .1. Chronicle of his life and accomplishments in immunology, cancer research, and chemotherapy.* Biotechnic & Histochemistry, 1996. **71**(1): p. 2-37.
47. Winau, F., O. Westphal, and R. Winau, *Paul Ehrlich - in search of the magic bullet.* Microbes and Infection, 2004. **6**(8): p. 786-789.
48. Parascandola, J., *The Theoretical Basis of Ehrlich,Paul Chemotherapy.* Journal of the History of Medicine and Allied Sciences, 1981. **36**(1): p. 19-43.
49. Kristiansen, J.E., *Dyes, Antipsychotic-Drugs, and Antimicrobial Activity - Fragments of a Development, with Special Reference to the Influence of Ehrlich,Paul.* Danish Medical Bulletin, 1989. **36**(2): p. 178-185.
50. May, J.M., Z.C. Qu, and C.E. Cobb, *Reduction and uptake of methylene blue by human erythrocytes.* American Journal of Physiology-Cell Physiology, 2004. **286**(6): p. C1390-C1398.
51. Ruck, A., et al., *Nonlinear dynamics of intracellular methylene blue during light activation of cell cultures.* Photochemistry and Photobiology, 1997. **66**(6): p. 837-841.
52. Mellish, K.J., et al., *In vitro photodynamic activity of a series of methylene blue analogues.* Photochemistry and Photobiology, 2002. **75**(4): p. 392-397.
53. Gorman, S.A., et al., *The synthesis and properties of unsymmetrical 3,7-diaminophenothiazin-5-ium iodide salts: Potential photo sensitisers for photodynamic therapy.* Dyes and Pigments, 2006. **71**(2): p. 153-160.
54. Wainwright, M., et al., *Phenothiazinium photosensitisers, Part VI: Photobactericidal asymmetric derivatives.* Dyes and Pigments, 2009. **82**(3): p. 387-391.
55. Wainwright, M., et al., *Phenothiazinium photosensitisers VII: Novel substituted asymmetric N-benzylphenothiaziniums as photoantimicrobial agents.* Journal of Photochemistry and Photobiology B-Biology, 2010. **99**(2): p. 74-77.
56. Wainwright, M., et al., *Phenothiazinium-fluoroquinolone drug conjugates.* International Journal of Antimicrobial Agents, 2010. **35**(4): p. 405-409.
57. Tegos, G.P. and M.R. Hamblin, *Phenothiazinium antimicrobial photosensitizers are substrates of bacterial multidrug resistance pumps.* Antimicrobial Agents and Chemotherapy, 2006. **50**(1): p. 196-203.
58. New, O.M. and D. Dolphin, *Design and Synthesis of Novel Phenothiazinium Photosensitiser Derivatives.* European Journal of Organic Chemistry, 2009(16): p. 2675-2686.
59. Regensburger, J., et al., *A helpful technology - the luminescence detection of singlet oxygen to investigate photodynamic inactivation of bacteria (PDIB).* Journal of Biophotonics, 2010. **3**(5-6): p. 319-327.
60. Redmond, R.W. and J.N. Gamlin, *A compilation of singlet oxygen yields from biologically relevant molecules.* Photochemistry and Photobiology, 1999. **70**(4): p. 391-475.
61. Boyce, J.M. and D. Pittet, *Guideline for hand hygiene in health-care settings - Recommendations of the Healthcare Infection Control Practices Advisory Committee and the HICPAC/SHEA/APIC/IDSA Hand Hygiene Task Force.* American Journal of Infection Control, 2002. **30**(8): p. S1-S46.
62. Foote, C.S., *Mechanisms of Photosensitized Oxidation - There Are Several Different Types of Photosensitized Oxidation Which May Be Important in Biological Systems.* Science, 1968. **162**(3857): p. 963-&.
63. Bartlett, J.A. and G.L. Indig, *Effect of self-association and protein binding on the photochemical reactivity of triarylmethanes. Implications of noncovalent interactions on the competition between photosensitization mechanisms type I and type II.* Photochemistry and Photobiology, 1999. **70**(4): p. 490-498.
64. Gabrielli, D., et al., *Binding, aggregation and photochemical properties of methylene blue in mitochondrial suspensions.* Photochemistry and Photobiology, 2004. **79**(3): p. 227-232.
65. Severino, D., et al., *Influence of negatively charged interfaces on the ground and excited state properties of methylene blue.* Photochemistry and Photobiology, 2003. **77**(5): p. 459-468.
66. Junqueira, H.C., et al., *Modulation of methylene blue photochemical properties based on adsorption at aqueous micelle interfaces.* Physical Chemistry Chemical Physics, 2002. **4**(11): p. 2320-2328.
67. Usacheva, M.N., M.C. Teichert, and M.A. Biel, *The role of the methylene blue and toluidine blue monomers and dimers in the photoinactivation of bacteria.* Journal of Photochemistry and Photobiology B-Biology, 2003. **71**(1-3): p. 87-98.

68. Sabbahi, S., et al., *The role of reactive oxygen species in Staphylococcus aureus photoinactivation by methylene blue.* Water Science and Technology, 2008. **58**(5): p. 1047-1054.
69. Bonneau, R., et al., *Ph-Dependence of Singlet Oxygen Production in Aqueous-Solutions Using Thiazine Dyes as Photosensitizers.* Photochemistry and Photobiology, 1975. **21**(3): p. 159-163.
70. Tafulo, P.A., R.B. Queiros, and G. Gonzalez-Aguilar, *On the "concentration-driven" methylene blue dimerization.* Spectrochim Acta A Mol Biomol Spectrosc, 2009. **73**(2): p. 295-300.
71. Baier, J., et al., *Theoretical and experimental analysis of the luminescence signal of singlet oxygen for different photosensitizers.* J Photochem Photobiol B, 2007. **87**(3): p. 163-73.
72. Frederiksen, P.K., et al., *Two-photon photosensitized production of singlet oxygen in water.* J Am Chem Soc, 2005. **127**(1): p. 255-69.
73. Colmorgen, F., *Spektroskopische Untersuchungen zur Singulett-Sauerstoff-Lumineszenz bei Photosensibilisatoren aus der Phenothiazingruppe.* Master thesis, 2012.
74. Wainwright, M., et al., *Increased cytotoxicity and phototoxicity in the methylene blue series via chromophore methylation.* J Photochem Photobiol B, 1997. **40**(3): p. 233-9.
75. Ruprecht, J. and H. Baumgartel, *The Influence of the Electronic-Structure on the Dimerization of Phenthiazonium Cations in Aqueous-Solution.* Berichte Der Bunsen-Gesellschaft-Physical Chemistry Chemical Physics, 1984. **88**(2): p. 145-150.
76. Michaelis, L.G., S., *Metachromasy of basic dyestuffs.* Journal of the American Chemical Society, 1945. **67**: p. 8.

Chapter 4

Spectroscopic Studies of the Porphyrin XF73

The chapter describes the investigation of the novel cationic porphyrin XF73, which showed high photosensitizing efficacy against multiple microorganisms in low doses, in comparison to the standard porphyrin TMPyP. The photophysical properties in regard to aggregation and the ability to generate singlet oxygen are presented, comparing the influence of H_2O-based with cell physiological solution (PBS). Further, the problems in interpreting the singlet oxygen luminescence signals generated by different photosensitizers in cellular surrounding are outlined.

4.1 INTRODUCTION

Singlet oxygen ($^1O_2$) is an important reactive intermediate in photodynamic reactions, in particular in antimicrobial PDT (aPDT). The detection of singlet oxygen luminescence is frequently used to elucidate the role of singlet oxygen in various environments, in particular in microorganisms and human cells. When incubating *Candida albicans* with porphyrins XF73 (5,15-bis-[4-(3-Trimethylammonio-propyloxy)-phenyl]-porphyrin) or TMPyP (5,10,15,20-Tetrakis(1-methyl-4-pyridinio)-porphyrin tetra(p-toluenesulfonate)), the singlet oxygen luminescence signals were excellent for TMPyP. In case of XF73, the signals showed strange rise and decay times. Thus, singlet oxygen generation of XF73 was investigated and compared to TMPyP.

Absorption spectroscopy of XF73 showed a change of the absorption cross section when changing the concentration from $1 \cdot 10^{-6}\ M$ to $1 \cdot 10^{-3}\ M$ indicating an aggregation process. The addition of PBS substantially changed singlet oxygen luminescence in XF73 solution. Detailed experiments provided evidence that the PBS constituents $NaCl$ and KCl caused the change of singlet oxygen luminescence. The results also indicate that Cl^- ions may cause aggregation of XF73 molecules, which in turn enhances self-quenching of singlet oxygen via photosensitizer molecules.

These results show that some ions, *e.g.* present in cells *in vitro* or added by PBS, can considerably affect the detection and the interpretation of time-resolved luminescence signals of singlet oxygen, in particular *in vitro* and *in vivo*. These effects may occur not only for XF73 but also for other photosensitizers.

The fast development of multiresistant patterns against antibiotics of many species of bacteria has led to novel antibacterial strategies like the antibacterial photodynamic therapy (aPDT) [1, 2]. A lot of work has been done to develop molecular structures and their derivatives that are able to generate reactive oxygen species (ROS), which are the active agents for killing microorganisms [3-7]. The search for photosensitizers (PS) for aPDT has provoked the synthesis of various porphyrin molecules, which have been investigated regarding their photophysics and antimicrobial activity [4, 8, 9]. Naturally occurring porphyrins can be found endogenously, *e.g.* the protoporphyrin IX that is in the prosthetic group of the hemoglobin or the chlorophylls based on the chlorine structure. Some endogenous porphyrins in bacteria are used to treat acne, where *Propionibacterium acnes* is causative for the inflammatory processes [10]. The phototoxicity of the porphyrin TMPyP

has been frequently used for cell staining in order to investigate generation and decay of singlet oxygen [11-13].

Different photosensitizers are considered to localize in different compartments of the cells due to their number of positive charges and structure of the side chain. In order to determine the subcellular localisation of photosensitizers and hence the site of singlet oxygen generation, microscopy is applied by exciting the fluorescence of the respective photosensitizer. Since the resolution of light microscopy is limited, this procedure should fail with small bacteria cells with a diameter of about 1 μm. The direct measurement of singlet oxygen luminescence at 1270 nm might be an alternative candidate to elucidate the cellular action of singlet oxygen because the rise and decay time of singlet oxygen luminescence depend critically on its adjacency [14, 15]. In addition, singlet oxygen luminescence can provide information about the photodynamic process in bacteria during irradiation.

XF73 is a newly synthesized porphyrin molecule that already showed a high potential in antimicrobial PDT that was shown for gram-negative and gram-positive bacteria [16, 17]. However, principal data are lacking regarding its use in singlet oxygen detection in vitro. Thus, it was the goal of the present study to investigate the photophysical properties of XF73 and its potential to monitor photodynamic action in microorganisms. Exemplarily singlet oxygen luminescence detection was analyzed *in vitro* in *C. albicans* cells. The well-known TMPyP was used for reference experiments.

4.2 EXPERIMENTAL SECTION

4.2.1 Chemicals and solvents

The photosensitizers XF73 and TMPyP (see chapter 2) were dissolved in bidistilled water at a stock concentration of $1\,mM$ and stored at $4°C$ until use. NaN_3, Mannitol, $NaCl$, KCl, Na_2HPO_4, KH_2PO_4, and D_2O were used as received. PBS has been used for aggregation experiments. For the NMR spectroscopy a parent solution of the photosensitizer dissolved in D_2O was made and a PBS solution for dilution containing D_2O has been prepared by adding $NaCl$, KCl, Na_2HPO_4, and KH_2PO_4 with the accordant concentrations.

4.2.2 Absorption spectrum

Absorption spectra were recorded at room temperature in a concentration range of $1 \cdot 10^{-6} - 2 \cdot 10^{-3}\ M$. The percentaged transmission has been measured and the absorption cross section $\sigma\ [cm^2]$ was calculated according to equation (2.1).

4.2.3 Photostability

The photosensitizers were illuminated with the broadband lamp UV236. The maximal light intensity was 15.2 $mW cm^{-2}$ at the level of the illuminated samples. The samples were illuminated for either 15 min (13.7 $J cm^{-2}$) or 60 min (54.8 $J cm^{-2}$).

4.2.4 Cell experiments

The *Candida albicans* strain ATCC-MYA-273 was used for the experiments. The planktonic cells of *C. albicans* were diluted to a number of 10^6 CFU mL^{-1}. For the incubation of *C. albicans* the photosensitizer stock solution has been diluted with H_2O. The cells were incubated in the dark for 15 min in H_2O plus 50% PBS in falcons at slow rotation. The cells were rinsed twice with PBS to remove the not included or nonadherent photosensitizer and afterwards solved in pure H_2O. For the singlet oxygen luminescence experiments the planktonic cells were excited with a Nd:YAG-laser.

4.2.5 Fluorescence spectrophotometer

The localisation of XF73 in *C. albicans* was examined by fluorescence microscopy (Zeiss Vario-AxioTech, Goettingen, Germany) with an appropriate dual-band filter set for excitation and emission (Omega Optical, Brattleboro, Vt.) and a $63\times$ magnification. Planktonic *C. albicans* were incubated $2\ h$ with $10^{-4}\ M$ XF73 in PBS and were rinsed twice with PBS.

4.2.6 Singlet oxygen luminescence and quantum yield of singlet oxygen formation (Φ_Δ)

Solutions with photosensitizers were filled in a quartz cuvette; solutions of the planktonic cell suspension were investigated in acrylic cuvettes. The photosensitizers were excited with the Nd:YAG-laser both during magnetic stirring at a wavelength $\lambda = 532\ nm$, power output $P = 50\ mW$, frequency of $f = 2\ kHz$, and therefore an energy per pulse of $E = 2.5 \cdot 10^{-5}\ J$. Every sample was illuminated with 40 000 pulses. The *C. albicans* planktonic cells were excited with the same laser wavelength of $\lambda = 532\ nm$, power output $P = 60\ mW$, frequency of $f = 5\ kHz$, and therefore an energy per pulse of $E = 1.2 \cdot 10^{-5}\ J$. Every sample was illuminated with 100 000 pulses.

Direct detection as described in previous papers [18-20] was done by time resolved measurements at $1270\ nm$ ($30\ nm$ FWHM filter) with using an additional $950\ nm$ cut-off-filter. According to equation (2.1) the singlet oxygen luminescence signal was fitted, and the rise and decay times t_R and t_D were determined.

The luminescence signal was spectrally resolved using interference filters in front of the photomultiplier tube at wavelengths ranging from $1150 - 1400\ nm$ or a monochromator (Horiba, Yobin Yvon Inc., USA) from $1200 - 1350\ nm$ at $10\ nm$ regular steps in case of XF73 in pure H_2O. A Lorentz-shaped function has been fitted through the measurement points, with the maximum at $\lambda = 1270\ nm$, referring to the maximal value in H_2O.

For the determination of Φ_Δ of XF73 in H_2O it is compared to the Φ_Δ of TMPyP in aqueous solution. Therefore 5 probes of each photosensitizer of different concentration (between 30% and 70% absorption at a wavelength of $\lambda = 532\ nm$) are illuminated and the emitted singlet oxygen photons are determined with the integral over the luminescence curve, given with the fit routine mentioned.

4.2.7 NMR-spectra

NMR spectra were recorded on Bruker Avance 600 (1H: 600.1 MHz, 13C: 150.1 MHz, $T = 300\,K$), Bruker Avance 400 (1H: 400.1 MHz, 13C: 100.6 MHz, $T = 300\,K$) or Bruker Avance 300 (1H: 300.1 MHz, 13C: 75.5 MHz, $T = 300\,K$) relative to external standards. NMR spectra were recorded in $CDCl_3$ at 300 MHz (1H) or 75 MHz (13C) unless stated otherwise. The solvent used is reported for each spectrum.

4.3 RESULTS AND DISCUSSION

As a 'first trial' experiment, cells of *C. albicans* were incubated with XF73 or TMPyP for 15 min using a concentration of 100 μM. The cells were washed twice, suspended in H_2O solution, and subsequently excited with the laser at 532 nm in order to determine time-resolved the singlet oxygen luminescence photons.

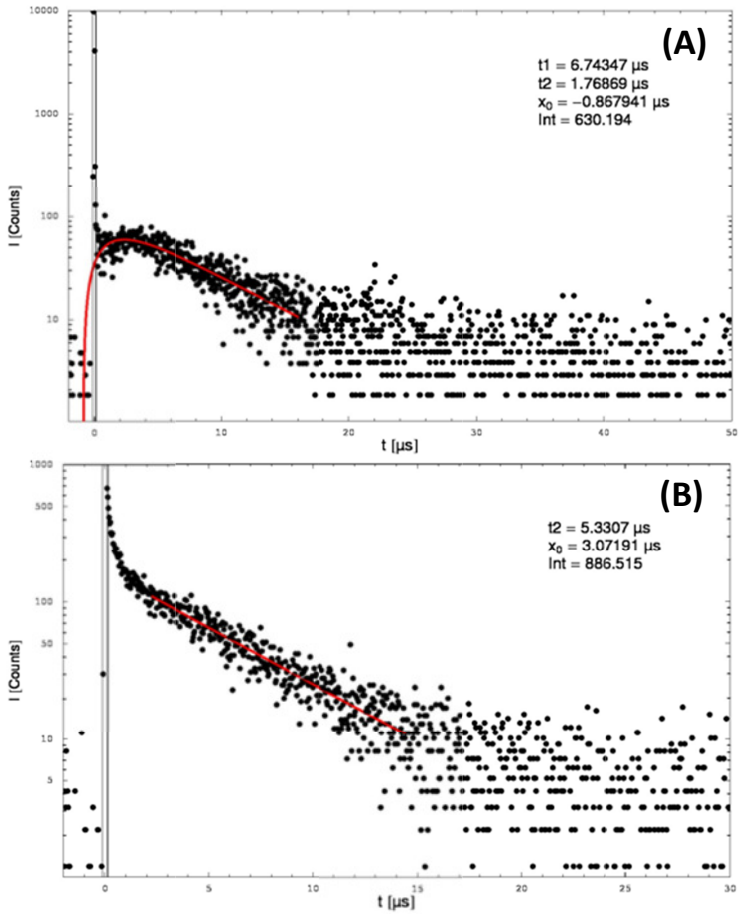

Fig. 4.1: Singlet oxygen luminescence signal of planktonic solution of C. albicans cells incubated with 10^{-4} M of TMPyP (a) and XF73 (b) for 15 min in the dark. The cells were washed and are surrounded by pure H_2O with a cell concentration of 10^6 CFU mL^{-1}.

TMPyP in the cells produced a clear singlet oxygen luminescence signal with a rise time of $t_R = (1.77 \pm 0.2)\mu s$ and a decay time of $t_D = (6.74 \pm 0.7)\mu s$ (fig. 4.1, A). In contrast to that, XF73 in *C. albicans* produced completely different singlet oxygen luminescence signals showing no or a very short rise time, whereas the signal decayed in a multi-exponentially manner. When starting the fit at 2 μs, the decay time was $t_D = (5.33 \pm 0.5)\mu s$ (fig. 4.1, B).

On one hand, XF73 molecules were possibly localized at subcellular sites where high quencher concentrations or low oxygen concentration affected the rise and decay of singlet oxygen luminescence. On the other hand, the photophysical properties of XF73 could have been altered after uptake *C. albicans* cells. It is known for many porphyrin species that photosensitizer molecules can show stacking to *J*- (edge-to-edge) and *H*-aggregates (face-to-face) under certain conditions [18, 19]. Aggregation of porphyrin derivatives is influenced by concentration of inorganic salts, the polarity of the solvents, or the side chains of the porphyrins [20-22], whereas the results are still controversially discussed. Aggregation of photosensitizer like TMPyP should not occur for concentrations of less than 10^{-4} M [23-26]. An overview of the discussions related to the aggregation of TMPyP is given by Vergeldt *et al.*, who described adsorption onto surfaces or aggregation effects due to the impurity of the solvent [27].

Stacking of porphyrin molecules could occur at high photosensitizer concentrations or could be mediated by inorganic salts, which were particularly added with PBS to cells. Photosensitizer stacking may change the rate and rate constants for XF73 molecules and thereby affect the generation and decay of singlet oxygen, which could be detected by time resolved detection of its luminescence.

4.3.1 Absorption spectroscopy in aqueous photosensitizer solution

Changes in the π-electron-system of porphyrin molecules can lead to the change of absorption cross section σ and hence may affect singlet oxygen generation. TMPyP showed a constant absorption cross section in the range from 10^{-6} – 10^{-3} M (data not shown).

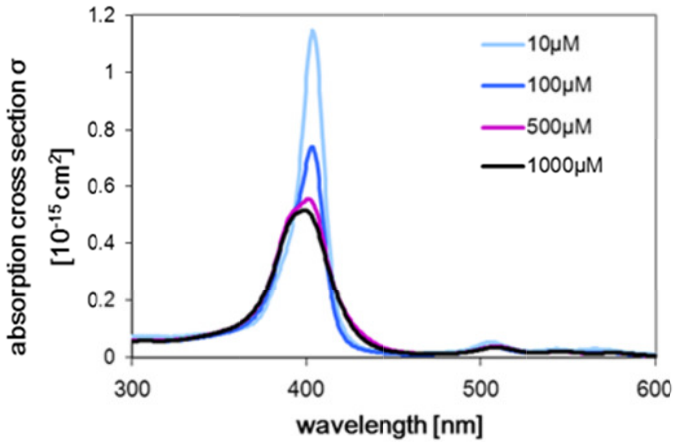

Fig. 4.2: Absorption spectrum of XF73 with increasing photosensitizer concentration. A blue-shift of the absorption maxima of 7 nm was detected when increasing the concentration from 10^{-5} to 10^{-3} M.

In contrast to TMPyP, the absorption spectrum of XF73 in pure H_2O clearly depended on XF73 concentration. The absorption cross section decreased with increasing XF73 concentration from $10^{-5} - 2 \cdot 10^{-3}\ M$ and the absorption maximum (Soret band) shifted to shorter wavelengths ($\approx 7\ nm$) (fig. 4.2). Both effects indicate aggregation of XF73 molecules.

4.3.2 NMR spectra of XF73 and TMPyP in D_2O solution

As a second, independent experiment confirming aggregation of XF73 in comparison to the aggregation of TMPyP, NMR spectroscopy was performed. Therefore, the concentration and the temperature of the solvent of the photosensitizer were varied, in order to break the aggregation effects.

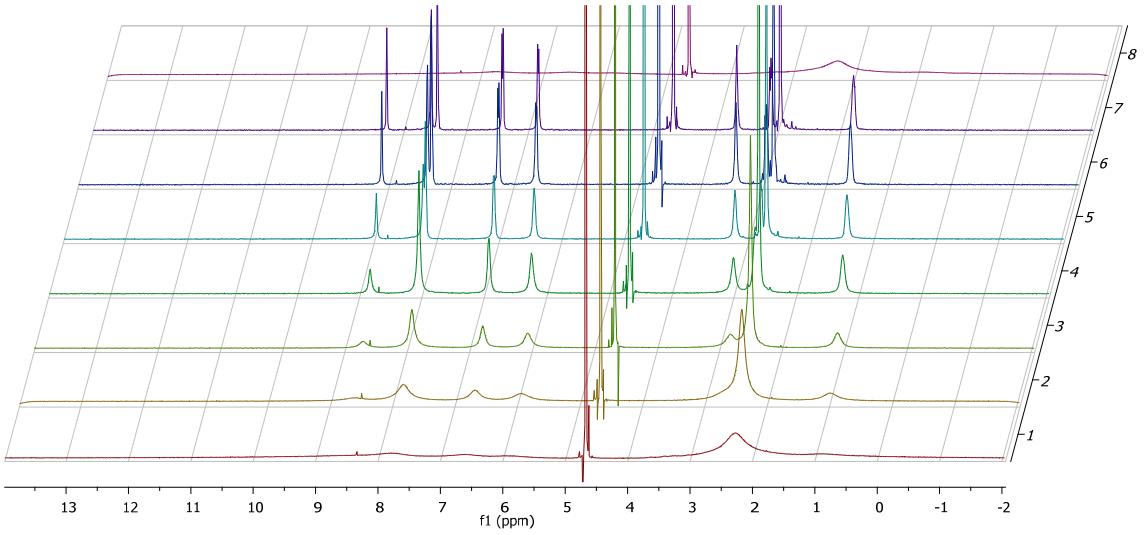

Fig. 4.3: NMR spectra of XF73 in D_2O; heated from room temperature (293 K = 20°C) to 353 K (=80°C).

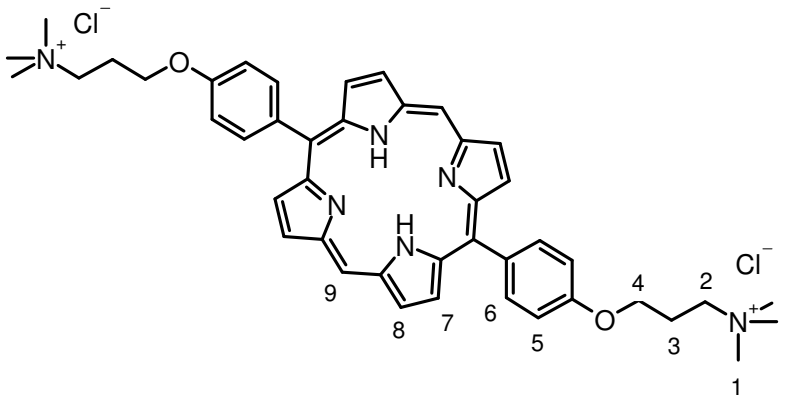

Fig. 4.4: Chemical structure of XF73 and assignment of the molecule regions to the peaks in the NMR spectra in fig. 4.5.

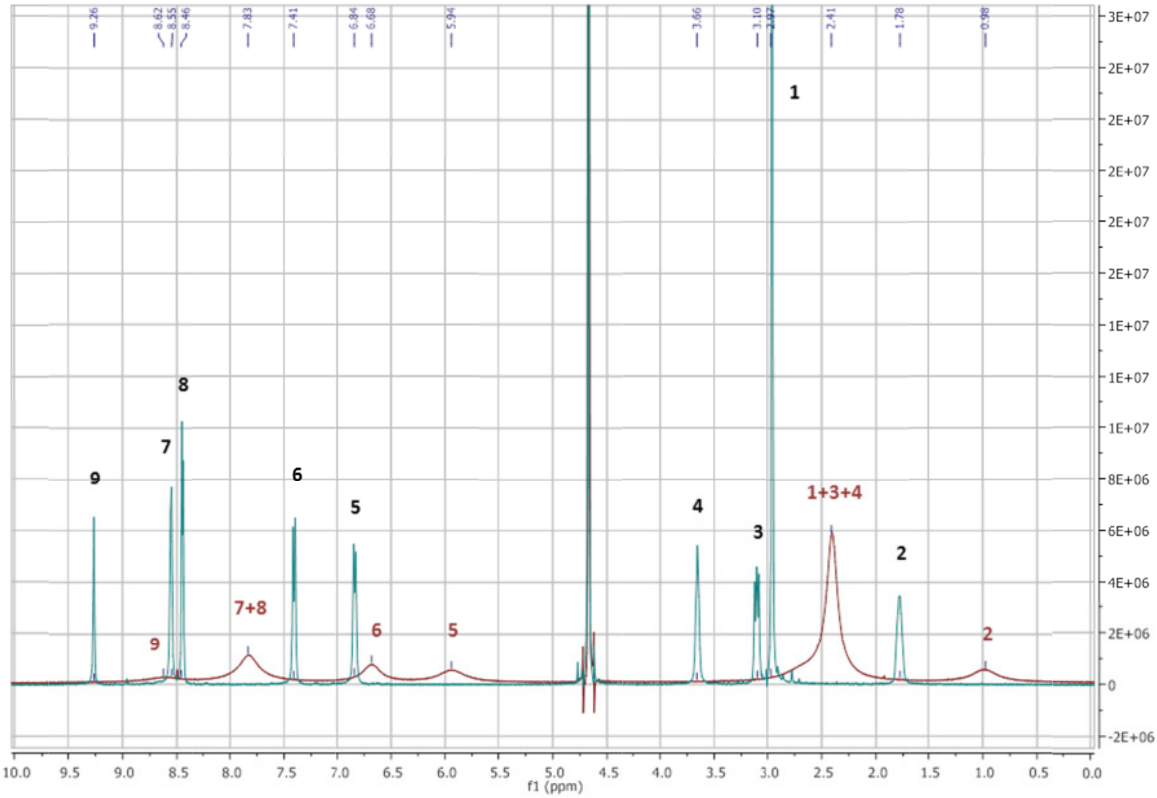

Fig. 4.5: NMR spectra of XF73 in D_2O for the temperatures 313 K (red) and 353 K (green).

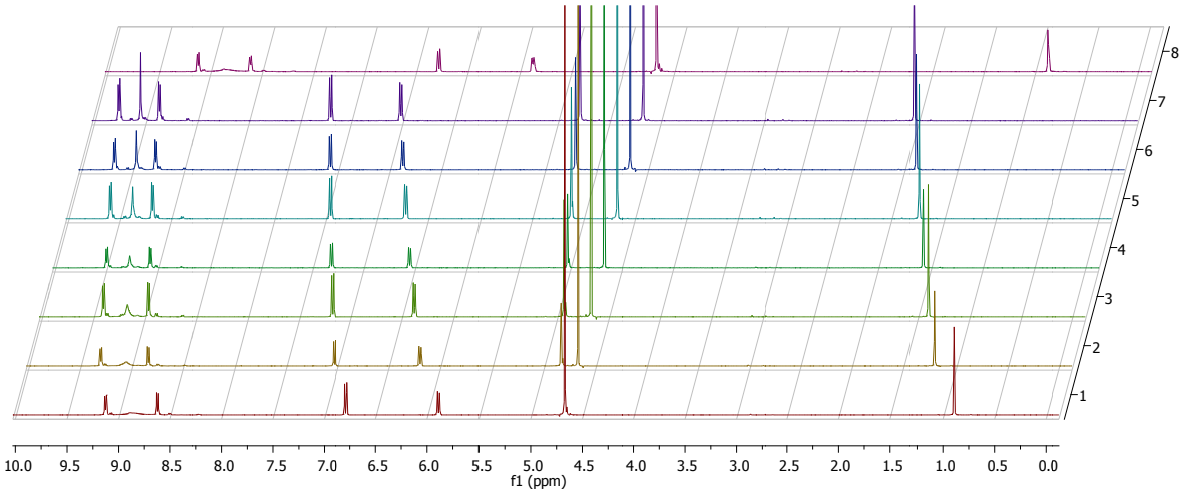

Fig. 4.6: NMR spectra of TMPyP in D_2O; heated from room temperature 293 K (= 20°C) to 353 K (=80°C).

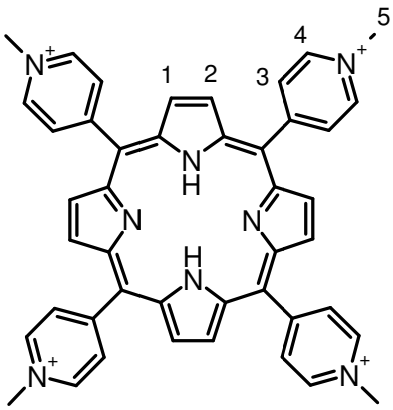

Fig. 4.7: Chemical structure of TMPyP and assignment of the molecule regions to the peaks in the NMR spectra in fig. 4.8.

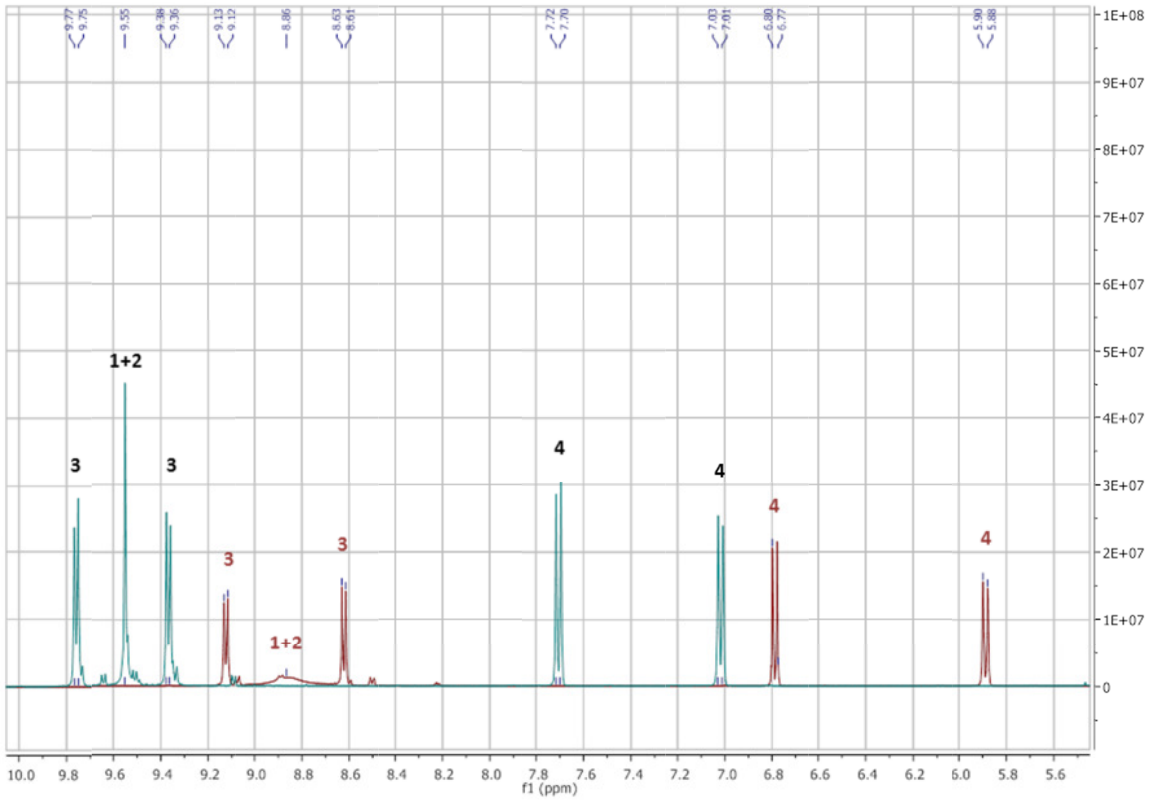

Fig. 4.8: NMR spectra of TMPyP in D_2O for room temperature 293 K (red) and 353 K (green).

From the NMR spectra stacking plot (fig. 4.3) and in the overlay for two exemplary temperatures (fig. 4.5) a continuous breaking of the XF73-porphyrin aggregates due to external heat supply can be followed. At 313 *K* a complete aggregation was detected which was seen from the strong peak-broadening (increase of FWHM). With increasing temperature the π-π-interactions are disturbed increasingly, resulting finally in the presence of XF73-monomers at 353 *K*. There, sharp and clear separated signals of defined

multiplicity were detected, which can be assigned clearly to the respect groups of the molecule (see fig. 4.4).

Although defined dimers cannot directly be detected from the NMR spectrum, their prevalence can be strongly assumed due to a continuous transition from the strong broadening of the spectrum to sharp peaks, not passing any intermediate spectrum.

From the NMR spectra stacking plot of TMPyP (fig. 4.6) and in the overlay for two exemplary temperatures (fig. 4.8) a continuous increase of heat energy supply disturbs increasingly the π-π-interactions. Nevertheless, sharp and clear separated signals of defined multiplicity were detected already at room temperature ($293\ K$), which can be assigned clearly to the respect groups of the molecule (see fig. 4.7). A peak-shift to higher ppm-values was detected.

The strength of the aggregation between the TMPyP molecules is substantially smaller due to the already existing sharp NMR signals. In contrast to that for breaking the XF73-aggregates a higher energy supply is needed. In TMPyP the positively charged, repellent groups are much closer at the aromatic core and fixed in their position and thus inflexible. A higher repulsion due to the positive charges is the consequence. The positive charges in the XF73-molecule are marginal, with a greater distance to the core, and are positioned at a flexible alkyl chain. Therefore, they can elude each other more easily and the aggregation due to the π-π-interactions of the area of the aromatic compound is facilitated.

4.3.3 Absorption spectroscopy in aqueous XF73 solution with PBS or PBS constituents

PBS and cytosol of living cells contain various ions like K^+, Na^+, Cl^-, HCO_3^-, Mg^{2+}, Ca^{2+}, HPO_4^{2-}. As a first approximation to cellular environment, XF73 was dissolved in PBS solutions. As XF73 was not easily soluble in PBS, the maximum concentration of PBS was 50% in H_2O. Absorption spectra of XF73 ($2 \cdot 10^{-5}\ M$) were recorded in pure H_2O, in 50% H_2O plus 50% PBS, and in 100% H_2O adding single constituents of PBS such as KCl, $NaCl$, NaH_2PO_4, or KH_2PO_4 in a concentration of 0.1 M each substance (fig. 4.9).

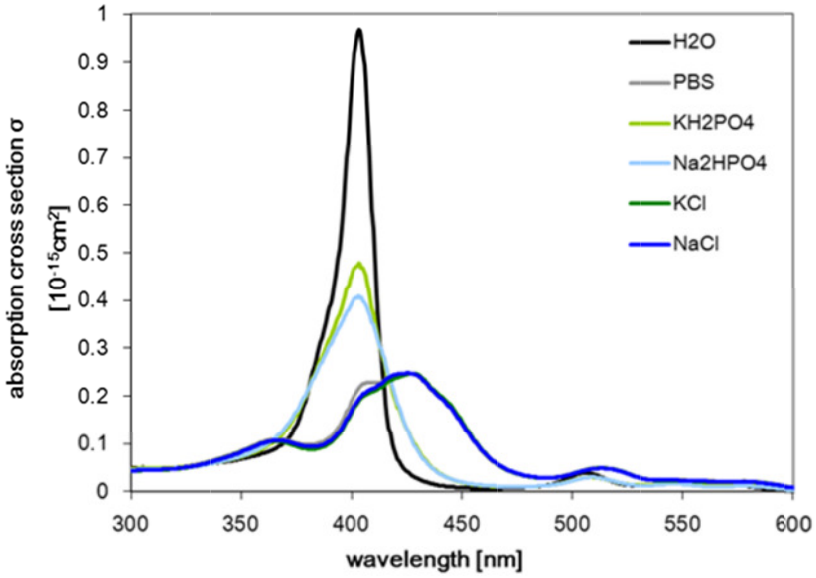

Fig. 4.9: Comparison of the influence of the single components of PBS on the absorption spectrum of XF73. A photosensitizer concentration of $2 \cdot 10^{-5}$ M has been used and NaCl, KCl, KH_2PO_4, and Na_2HPO_4 had each a concentration of 0.1 M. The table shows the wavelengths λ_{max} of the absorption maximum and its value σ_{max} for each component of PBS, for PBS and H_2O.

substance	H_2O	**PBS**	KH_2PO_4	Na_2HPO_4	KCl	$NaCl$
λ_{max} **[nm]**	402	426	403.5	403.5	427.5	425
σ_{max} **[10^{-15} cm²]**	0.71	0.25	0.48	0.41	0.25	0.25

Tab. 4.1: Maxima of the absorption cross section of XF73 at a concentration of $2 \cdot 10^{-5}$ M in different surroundings

In the presence of NaH_2PO_4 or KH_2PO_4, the absorption cross section showed no wavelength shift or new absorption maxima within given experimental accuracy ($\pm 2\,nm$) when compared to pure H_2O. The maximum value of absorption cross section at (402 ± 2) nm decreased from $\sigma_{max} = 0.71 \cdot 10^{-15} cm^2$ (pure H_2O) to $\sigma_{max} = 0.41 \cdot 10^{-15} cm^2$ or $\sigma_{max} = 0.48 \cdot 10^{-15} cm^2$ when NaH_2PO_4 or KH_2PO_4 was added, respectively. When adding PBS, σ_{max} decreased from $0.71 \cdot 10^{-15} cm^2$ to $0.25 \cdot 10^{-15} cm^2$ and shifted to longer wavelengths (red shift) of $\lambda = (24 \pm 2) nm$. When adding $NaCl$ or KCl to XF73 solution, σ_{max} decreased to $0.25 \cdot 10^{-15} cm^2$ for each. In addition, σ_{max} shifted to the red by about $\lambda = (25 \pm 3) nm$. At the same time, the absorption spectrum showed new absorption maxima within the spectral range of the Soret band. Addition of Cl^- led to a fundamental change of the absorption spectrum including a red shift. It is suggested that Cl^- affects the tetrapyrrol ring system and enhances the aggregation, which was already reported for other porphyrin structures [28].

A visible precipitation of the solute started when using >10% (PBS + H_2O). This effect was shown to be reversible by diluting the solution with pure H_2O. As a consequence of this dilution, the absorption spectrum of XF73 in PBS changed back to the absorption spectrum in pure H_2O (data not shown). The precipitation does not affect the absorption measurements because the probes are directly used after being diluted and the precipitation effect needs several hours to develop. No light scattering effect in solutions was detectable by checking the absorption spectrum at shorter wavelengths.

4.3.4 Photostability of XF73

Also the photostability and hence the change of absorption spectrum during irradiation may affect the singlet oxygen luminescence. Therefore, the photostability of XF73 in solution containing PBS was investigated when illuminating the samples with an energy dose of up to 54.8 Jcm^{-2}.

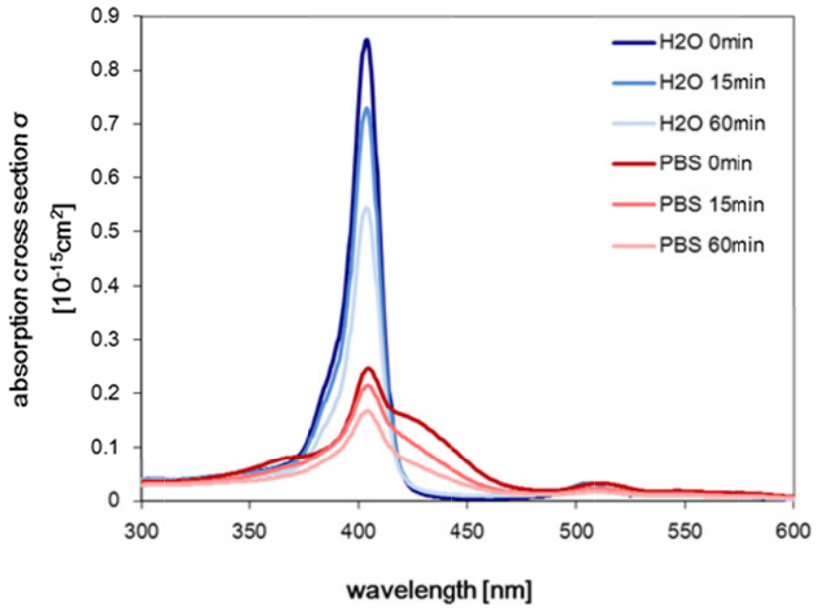

Fig. 4.10: Photostability measurements with XF73 show a decrease of the absorption cross section with the time of illumination and therefore the applied energy. The light source was the Waldmann-UV236 lamp with an applied energy dose of 13.7 J cm^{-2} or 54.7 J cm^{-2} respectively. XF73 with a concentration of 10^{-5} M has been investigated in pure H_2O and in PBS (50% in H_2O).

No changes in the absorption spectrum of TMPyP were noticed within irradiation time of up to 60 min (data not shown). XF73 in H_2O and in 50% (PBS + H_2O) showed a decrease of absorption that was mainly detected in the spectral range of the Soret band (fig. 4.10). Obviously, the presence of PBS, *i.e.* its ions, can additionally reduce radiation absorption of

XF73. These effects may also affect the use of XF73 when applied for photodynamic inactivation of microorganisms.

In case of singlet oxygen experiments (see below), XF73 solutions were irradiated with 1 J of laser energy (532 nm). It is expected that σ values do not significantly change under these experimental conditions.

4.3.5 Singlet oxygen luminescence experiments without PBS

Incubation of bacteria or human cells with XF73 and subsequent irradiation yielded effective cell killing by means of singlet oxygen generation, which was confirmed by adding singlet oxygen quencher NaN_3 that reduced significantly cell toxicity [16]. Since detailed studies on singlet oxygen generation of the novel porphyrin molecule XF73 were missing, we investigated XF73 in pure aqueous solution according to previous studies on other photosensitizers [23].

After dissolving $[XF73] = 5 \cdot 10^{-5}\ M$ in air-saturated ($[O_2] = 2.7 \cdot 10^{-4}\ M$), pure H_2O, the rise and decay part of the time resolved signals could be assigned to the decay time τ_Δ of singlet oxygen and the decay time τ_{T_1} of photosensitizer, respectively. Experiments yielded $\tau_{T_1} = 1.6 \pm 0.2\ \mu s$ and decay time $\tau_\Delta = 3.5 \pm 0.3\ \mu s$ (fig. 4.11). The decay time is in good correlation with the lifetime of singlet oxygen in pure water [29-31].

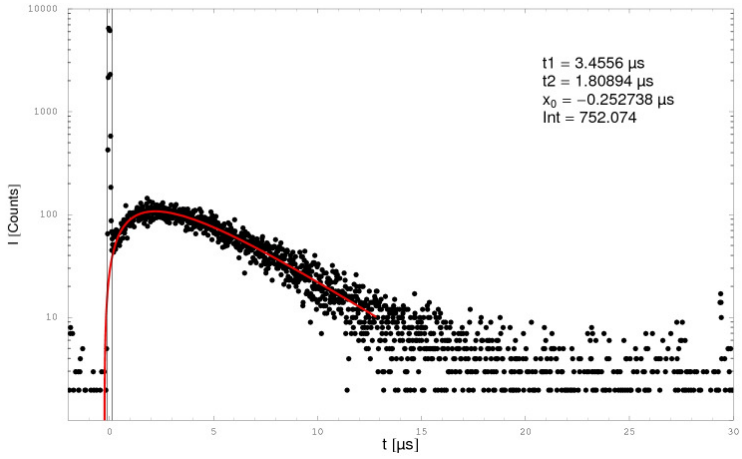

Fig. 4.11: Singlet oxygen luminescence signal of [XF73] = 5·10-5 M in H_2O with an oxygen concentration of [O_2] = 2.7·10-4 M.

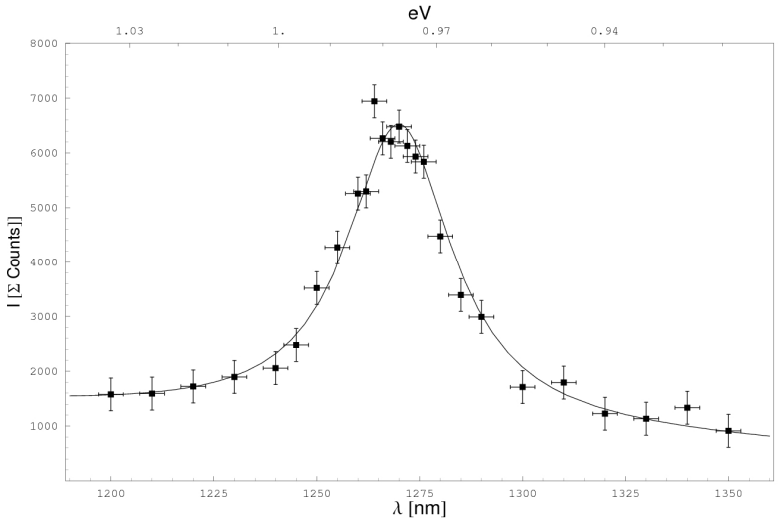

Fig. 4.12: Spectroscopically resolved singlet oxygen luminescence signal, generated by XF73 in H_2O with an oxygen concentration of [O_2] = 2.7·10^{-4} M. A Lorentz-shaped curve has been fitted through the data points.

The spectrally resolved singlet oxygen luminescence revealed a peak at 1270 nm, which clearly confirmed the generation of singlet oxygen (fig. 4.12). The singlet oxygen quantum yield Φ_Δ of XF73 was determined in air saturated, pure H_2O, using TMPyP as reference. The Φ_Δ values of TMPyP are 0.74 [32] and 0.77 ± 0.04 [13]. Using the previously reported technique [32], XF73 showed a value of $\Phi_\Delta = 0.57 \pm 0.06$.

When changing the oxygen concentration in the solution at a constant concentration of $[XF73] = 5 \cdot 10^{-5}\ M$, the meaning of the rates K_Δ and K_{T_1} at $[O_2] = 1.1 \cdot 10^{-4}\ M$ changed according to the decay paths of singlet oxygen and the excited triplet-T_1-state of the photosensitizer (fig. 4.13) [33].

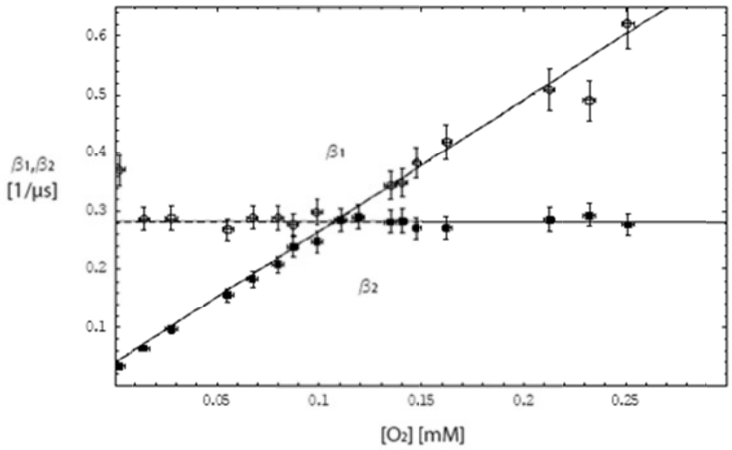

Fig. 4.13: Rates β_1 and β_2 of the time resolved singlet oxygen signal depending on the concentration of O_2. The meaning of the two rates changes at the crossing point of the curves.

This change occurs at a crossing point of t_1^{-1} and t_2^{-1}, which was about $[O_2] = (0.11 \pm 0.02) \cdot 10^{-3}\ M$ for XF73. By extrapolating t_2^{-1}, $K_{T_1}([O_2] = 0\ M) = 0.03\ \mu s^{-1}$ was determined yielding a lifetime of the triplet-T_1-state of $(33 \pm 5)\mu s$ in aqueous solution without oxygen quenching. The quenching rate constant k_q for quenching of the excited triplet state of XF73 by oxygen is therefore $k_q = 2.3 \cdot 10^9\ s^{-1}M^{-1}$ resulting from the Stern-Volmer-plot in figure 4.13 where the oxygen concentration was varied and the triplet decay of XF73 was determined.

As a next step, XF73 concentration was varied from $[XF73] = 10^{-6} - 5 \cdot 10^{-3}\ M$ at $[O_2] = 5.6 \cdot 10^{-5}\ M$ (fig. 4.14).

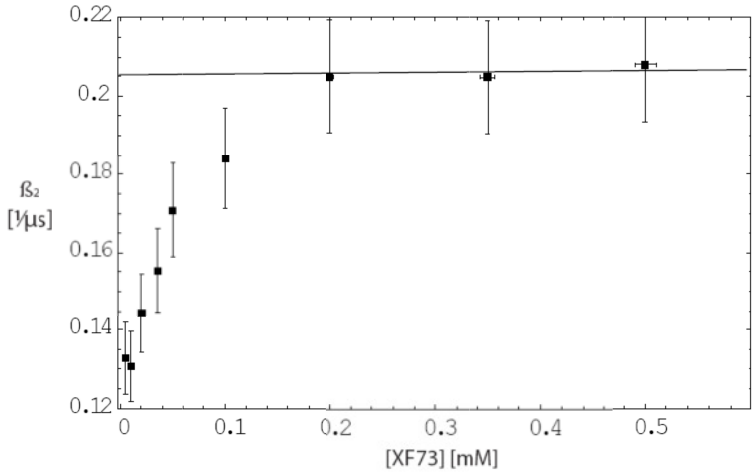

Fig. 4.14: The rate β_2 characterizes the decay time of the triplet-T_1-state and changes with the XF73 concentration; here the oxygen concentration is kept constant at $[^3O_2] = 5.4 \cdot 10^{-5}$ M.

The value of t_2^{-1} increased with increasing concentration that indicated a clear self-quenching effect of the excited triplet-T_1-state for [XF73] up to about $2 \cdot 10^{-4}\ M$. Above this concentration, the quenching effect decreased and reached a plateau at $t_2^{-1} = 0.205\ \mu s^{-1}$ which is equivalent to a decay time of the triplet-T_1-state of $t_{T_1} = 4.9\ \mu s$ (fig. 4.14). According to the absorption spectroscopy data, a stacking of XF73 molecules occurred, which is easily detectable for XF73 concentration higher than $1 \cdot 10^{-4}\ M$ (fig. 4.2). Obviously, the stacking process had already led to the formation of dimers or oligomers of XF73 molecules at this concentration. Besides a different absorption cross section, these aggregates show also a different deactivation of triplet-T_1-state as compared to XF73 monomers (fig. 4.14).

4.3.6 Singlet oxygen luminescence experiments with PBS

In light of the results above, singlet oxygen luminescence signals should be affected by molecule stacking, in particular when the photosensitizer is located in *C. albicans* cells (fig. 4.1). Therefore, we investigated the PBS effect on time-resolved singlet oxygen luminescence generated by XF73 in air-saturated solution at a concentration of $5 \cdot 10^{-5}\ M$, for which stacking due to photosensitizer concentration should be still minimal (fig. 4.2).

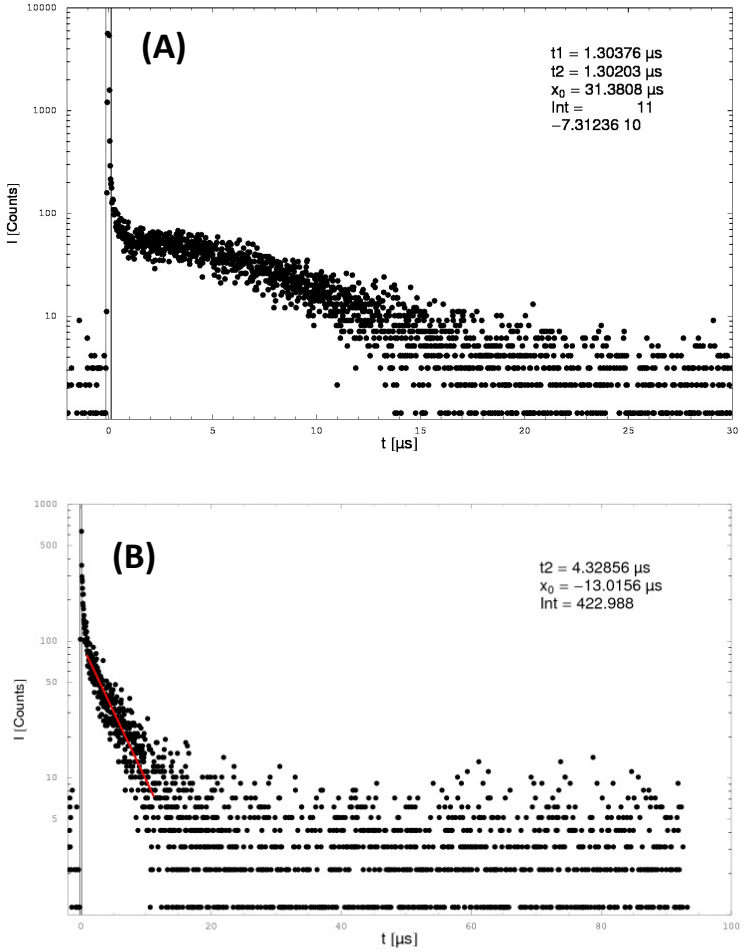

Fig. 3.15: Singlet oxygen luminescence signals of [XF73] = 5·10-5 M with a PBS concentration of (A) 20% and (B) 30% in H_2O with an oxygen concentration of [$^3O_2$] = 2.7·10-4 M

The results clearly show that singlet oxygen luminescence substantially changed with increasing PBS concentration (fig. 4.11, 4.15). From 0% to 50% PBS in H_2O, the rising part of singlet oxygen luminescence signal disappeared, whereas the decaying part shortened. Now, the luminescence signals at higher PBS concentrations (fig. 4.15, B) were similar to those recorded for XF73 in *C. albicans* cells (fig. 4.1, B) yielding again a multi-exponential decay.

When adding singlet oxygen quencher NaN_3 [34, 35] to the 20 % PBS solution up to a high concentration of $2 \cdot 10^{-3}\, M\ \ NaN_3$, the singlet oxygen luminescence signal almost disappeared.

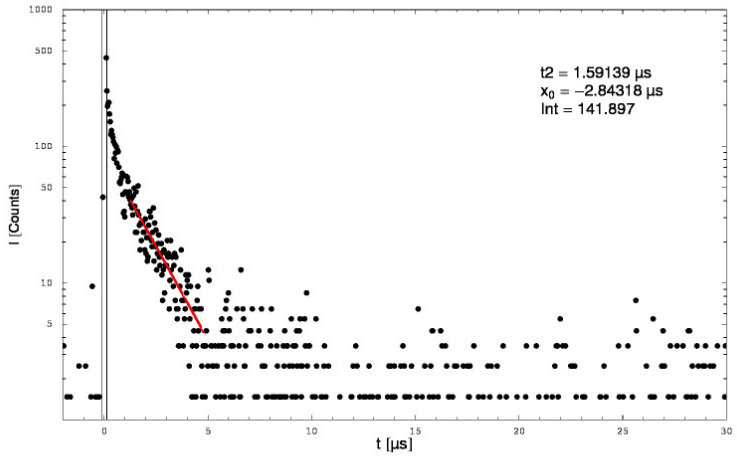

Fig. 3.16: Singlet oxygen luminescence generated by XF73 in H_2O + 20% PBS at 1270 nm with 2·10^{-3} M NaN_3 in solution.

The residual signal should not originate from singlet oxygen luminescence (see fig. 4.16). The same residual signal was detected in solutions without NaN_3 and without oxygen (data not shown).

The singlet oxygen luminescence was also recorded spectrally resolved for PBS 0% and 50% in H_2O (fig. 4.12, 4.17). A Lorentz-shaped function was fitted through the measurement points and the values were normalized to the maximal value. Without PBS, the fit shows a clear maximum at 1270 nm which confirms the generation of singlet oxygen [36].

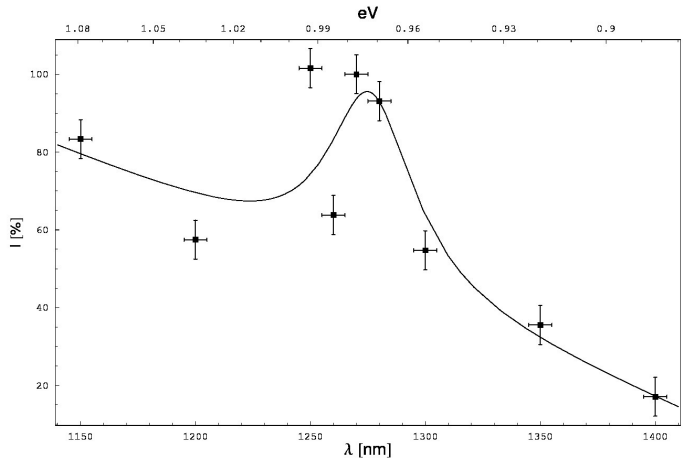

Fig. 4.17: Spectroscopically resolved singlet oxygen luminescence signal, generated by XF73 in 30% PBS + H_2O with an oxygen concentration of [O_2] = 2.7·10^{-4} M. A Lorentz-shaped curve has been fitted through the data points.

At 50% PBS, the maximum at 1270 nm almost disappeared, the baseline moved for wavelengths $< 1270\,nm$, and the signal-to-noise ratio decreased which indicates a substantial decrease of singlet oxygen generation.

Comparable to absorption spectroscopy, the changes of time- and spectral resolved singlet oxygen luminescence signals, induced by PBS, could be simply reversed by diluting the used solutions with H_2O and hence reducing the PBS concentration. A high degree of dilution of PBS concentration yielded time- and spectrally resolved singlet oxygen luminescence signals comparable to figures 4.11 and 4.12.

Scattering of photons within solution might also cause a singlet oxygen luminescence signal equal to the one in figure 4.16, and might be originating from precipitation due to the stacking of the porphyrins. To exclude any scattering effects, the scattering agent SiO_2 was added to aqueous solutions containing $5 \cdot 10^{-5}\ M$ XF73 or TMPyP. No effect on the shape of the singlet oxygen luminescence signal and no change of the rise and decay times were detected for both photosensitizers. Additionally there was no scattering effect visible in the absorption spectrum of XF73 in H_2O + 50% PBS.

4.3.7 Fluorescence microscopy of *C. albicans* incubated with XF73

Fluorescence microscopy showed the overall attachment of XF73 to the cell after washing, however, the low spatial resolution of optical microscopy impedes the evaluation of the subcellular photosensitizer localisation.

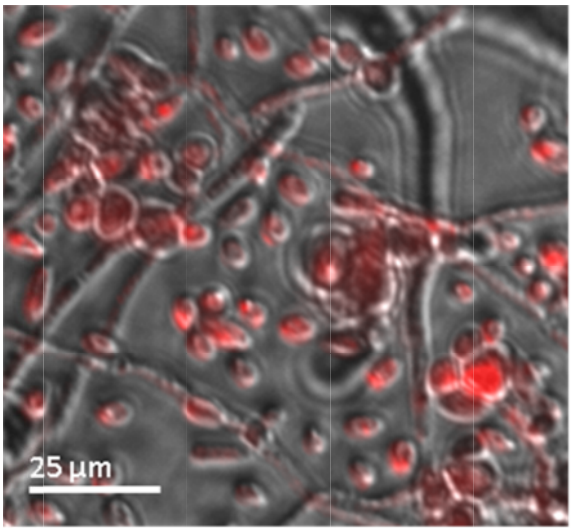

Fig. 4.18: Fluorescence image of C. albicans; cells were incubated 2 h with 10^{-4} M XF73 in PBS and rinsed twice. An attachment of XF73 to the cells can be seen.

4.4 CONCLUSIONS

The detection of singlet oxygen by its luminescence is a great tool to show the action of singlet oxygen even in cells or bacteria. In this context it is important to have a detection procedure that provides reliable data from inside such cells, in particular when knowing that cellular constituents can substantially affect singlet oxygen luminescence. The interaction of porphyrins with *C. albicans* is controversially discussed that ranges from no uptake to tight binding or even internalisation [37-41]. Many porphyrins are lipophilic and hence should accumulate in cellular membranes but the high water-solubility of XF73 suggests localisation in the cytoplasm as well. Fluorescence microscopy showed the overall attachment of XF73 to the cell after washing, however, the low spatial resolution of optical microscopy impedes the evaluation of the subcellular photosensitizer localisation (fig. 4.18). Thus, it would be of importance to gain additional insight by evaluating the singlet oxygen luminescence data.

However, XF73 showed substantial stacking of molecules that affected light absorption as well as the generation and decay of singlet oxygen. Stacking already occurred in pure H_2O along with the increase of the photosensitizer concentration. The stacking is additionally forced by the ionic pressure of Cl^-. Such ions are either present in cells and are usually added in cell experiments *in vitro* via PBS to protect the cells from osmosis. Therefore, it is impossible to exclude such ions when investigating photosensitizers in cell experiments.

Depending on the uptake mechanisms and the chemical structure, a photosensitizer localizes in cellular membranes or in the cytoplasm close to any cellular structures [42, 43]. Cytoplasm shows a similar concentration of Cl^- like PBS, therefore, it is very likely that aggregation of XF73 occurs in cells such as *C. albicans*. The time-resolved detection of the singlet oxygen luminescence in a solution of planktonic *C. albicans* cells incubated with XF73 and surrounded by pure H_2O has been done (fig. 4.1, B). In fact, the luminescence signal is similar to the signal of XF73 generating singlet oxygen in 30% PBS (fig. 4.15) showing a multi-exponential decay. This signal indicates a surrounding of XF73 within *C. albicans* cells whose ionic concentration is similar to that of > 30% PBS. Usually, the rise and decay times of luminescence provides information about the localisation of singlet oxygen and hence of the photosensitizer applied due to the short diffusion length of singlet oxygen in cells. As the molecule XF73 is strongly influenced by the salts of the phosphate buffer PBS, such interpretations could be misleading at the moment. This problem may also occur for any other photosensitizer that undergoes stacking in the presence of ions such as Cl^-.

Despite the results with XF73, the singlet oxygen luminescence detection in cells is a great tool to elucidate photodynamic processes. The porphyrin TMPyP showed neither stacking in the investigated range of concentration, nor interference with the salts of PBS. After attached to or taken up by *C. albicans,* the generated singlet oxygen could be easily detected by its luminescence with clear rise and decay components. The decay time of the singlet oxygen luminescence in figure 4.1(A) of $t_D = (6.74 \pm 0.5)\mu s$ is clearly longer than the decay of the signal in pure air-saturated water (which is assigned to singlet oxygen, $\tau_\Delta = 3.5\ \mu s$) and can thus be most likely attributed to the decay time of the excited T_1-state of TMPyP. If so, a triplet state decay time of $\tau_{T_1} = 6.74\ \mu s$ suggests an oxygen concentration in its surrounding of $[O_2] = 8 \cdot 10^{-5} M$ which is then 30% of $[O_2]_{sat} = 2.7 \cdot 10^{-4} M$ which is the oxygen concentration at its saturation level in H_2O.

Nevertheless the striking phototoxic effect of XF73 in bacteria was demonstrated [16]. *In vitro* experiments showed a substantial reduction of bacteria (≈ 8 $\log_{10}$ steps), which were incubated very small XF73 concentrations ($10^{-8}\ M$) for 5 min and subsequently irradiated with an energy dose of 13.7 Jcm^{-2}. The action of singlet oxygen was proven with the addition of the singlet oxygen quencher NaN_3, however, the photodynamic effect could not be completely inhibited by the quencher. In addition, the rather small XF73 concentration in the range of $0.01 - 10\ \mu M$ in those bacteria experiments could have minimized the stacking effect and therefore maximized phototoxicity by an effective singlet oxygen generation.

Aggregation effects influence also the fluorescence of a dye, which has recently been described by López-Chicón *et al.* with an investigation of Hypericin in different species of *Candida* [44]. The grade of aggregation depends on the surrounding and the fluorescence is low or not existent at a high photosensitizer aggregation, which occurs in H_2O-environment. Upon incubation of different species of *Candida* with Hypericin one can draw a conclusion about the localisation of the photosensitizer by monitoring the radiative decay, here the fluorescence that depends on the aggregation status.

Recently, with an optimized experimental setup singlet oxygen generation in *C. albicans* cells was detected by irradiating directly the Soret-band of the porphyrin TMPyP at 420 nm [45] (see chapter 5). With irradiation of the absorption maximum it is possible to detect singlet oxygen generation and decay at already very low photosensitizer concentrations in the range of few μM offering a concentration range where aggregation effects are expected to be low and thus the singlet oxygen generation is effective.

Since the phototoxic efficacy depends on the localisation and also on the aggregation status of the photosensitizer, which is influenced by ions, further investigations and comparative studies on the change of the singlet oxygen luminescence in different species of microorganisms should lead to better insights about the change of the decay times due to the localisation.

4.5 REFERENCES

1. Hart, C.A. and S. Kariuki, *Antimicrobial resistance in developing countries.* BMJ, 1998. 317(7159): p. 647-50.
2. Wise, R., et al., *Antimicrobial resistance. Is a major threat to public health.* BMJ, 1998. 317(7159): p. 609-10.
3. Wainwright, M., *Photodynamic antimicrobial chemotherapy (PACT).* J Antimicrob Chemother, 1998. 42(1): p. 13-28.
4. Lang, K., J. Mosinger, and D.M. Wagnerova, *Photophysical properties of porphyrinoid sensitizers non-covalently bound to host molecules; models for photodynamic therapy.* Coordination Chemistry Reviews, 2004. 248(3-4): p. 321-350.
5. Hamblin, M.R. and T. Hasan, *Photodynamic therapy: a new antimicrobial approach to infectious disease?* Photochem Photobiol Sci, 2004. 3(5): p. 436-50.
6. Niedre, M., M.S. Patterson, and B.C. Wilson, *Direct near-infrared luminescence detection of singlet oxygen generated by photodynamic therapy in cells in vitro and tissues in vivo.* Photochem Photobiol, 2002. 75(4): p. 382-391.
7. Jori, G. and S.B. Brown, *Photosensitized inactivation of microorganisms.* Photochem Photobiol Sci, 2004. 3(5): p. 403-5.
8. Bonnett, R., *Photosensitizers of the Porphyrin and Phthalocyanine Series for Photodynamic Therapy.* Chemical Society Reviews, 1995. 24(1): p. 19-33.
9. Bonnett, R. and M. Berenbaum, *Porphyrins as Photosensitizers.* Ciba Foundation Symposia, 1989. 146: p. 40-59.
10. Nouri, K. and L.M. Villafradez-Diaz, *Light/laser therapy in the treatment of acne vulgaris.* J Cosmet Dermatol, 2005. 4(4): p. 318-20.
11. Feese, E. and R.A. Ghiladi, *Highly efficient in vitro photodynamic inactivation of Mycobacterium smegmatis.* J Antimicrob Chemother, 2009. 64(4): p. 782-5.
12. Frederiksen, P.K., et al., *Two-photon photosensitized production of singlet oxygen in water.* J Am Chem Soc, 2005. 127(1): p. 255-69.
13. Snyder, J.W., J.D. Lambert, and P.R. Ogilby, *5,10,15,20-tetrakis(N-methyl-4-pyridyl)-21H,23H-porphine (TMPyP) as a sensitizer for singlet oxygen imaging in cells: characterizing the irradiation-dependent behavior of TMPyP in a single cell.* Photochem Photobiol, 2006. 82(1): p. 177-84.
14. Ragas, X., M. Agut, and S. Nonell, *Singlet oxygen in Escherichia coli: New insights for antimicrobial photodynamic therapy.* Free Radic Biol Med, 2010. 49(5): p. 770-6.
15. Silva, E.F., et al., *Irradiation- and Sensitizer-Dependent Changes in the Lifetime of Intracellular Singlet Oxygen Produced in a Photosensitized Process.* Journal of Physical Chemistry B, 2011.
16. Maisch, T., et al., *Photodynamic effects of novel XF porphyrin derivatives on prokaryotic and eukaryotic cells.* Antimicrob Agents Chemother, 2005. 49(4): p. 1542-52.
17. Pereira Gonzales, F. and T. Maisch, *XF drugs: A new family of antibacterials.* Drug News Perspect, 2010. 23(3): p. 167-74.
18. Ricchelli, F., *Photophysical properties of porphyrins in biological membranes.* J Photochem Photobiol B, 1995. 29(2-3): p. 109-18.
19. Zenkevich, E., et al., *Photophysical and photochemical properties of potential porphyrin and chlorin photosensitizers for PDT.* Journal of Photochemistry and Photobiology B-Biology, 1996. 33(2): p. 171-180.
20. Kadish, K.M., K.M. Smith, and R. Guilard, *The porphyrin handbook*2000, San Diego: Academic Press.
21. Maiti, N.C., et al., *Fluorescence Dynamics of Noncovalently Linked Porphyrin Dimers and Aggregates.* Journal of Physical Chemistry, 1995. 99(47): p. 17192-17197.
22. Sirish, M. and H.J. Schneider, *Supramolecular chemistry, part 93 - Electrostatic interactions between positively charged porphyrins and nucleotides or amides: buffer-dependent dramatic changes of binding affinities and modes.* Chemical Communications, 2000(1): p. 23-24.
23. Pasternack, R.F., et al., *On the aggregation of meso-substituted water-soluble porphyrins.* J Am Chem Soc, 1972. 94(13): p. 4511-7.

24. Kano, K., et al., *Evidence for Stacking of Cationic Porphyrin in Aqueous-Solution.* Chemistry Letters, 1983(12): p. 1867-1870.
25. Brookfield, R.L., H. Ellul, and A. Harriman, *Luminescence of Porphyrins and Metalloporphyrins .9. Dimerization of Meso-Tetrakis(N-Methyl-4-Pyridyl)-Porphine.* Journal of Photochemistry, 1985. 31(1): p. 97-103.
26. Kadish, K.M., B.G. Maiya, and C. Araullomcadams, *Spectroscopic Characterization of Meso-Tetrakis(1-Methylpyridinium-4-Yl)Porphyrins, [(Tmpyp)H2]4+ and [(Tmpyp)M]4+, in Aqueous Micellar Media, Where M = Vo2+, Cu(Ii), and Zn(Ii).* Journal of Physical Chemistry, 1991. 95(1): p. 427-431.
27. Vergeldt, F.J., et al., *Intramolecular Interactions in the Ground and Excited-State of Tetrakis(N-Methylpyridyl)Porphyrins.* Journal of Physical Chemistry, 1995. 99(13): p. 4397-4405.
28. De Luca, G., A. Romeo, and L.M. Scolaro, *Role of counteranions in acid-induced aggregation of isomeric tetrapyridylporphyrins in organic solvents.* Journal of Physical Chemistry B, 2005. 109(15): p. 7149-7158.
29. Rodgers, M.A.J. and P.T. Snowden, *Lifetime of O-2(1delta-G) in Liquid Water as Determined by Time-Resolved Infrared Luminescence Measurements.* J Am Chem Soc, 1982. 104(20): p. 5541-5543.
30. Egorov, S.Y., et al., *Rise and Decay Kinetics of Photosensitized Singlet Oxygen Luminescence in Water - Measurements with Nanosecond Time-Correlated Single Photon-Counting Technique.* Chemical Physics Letters, 1989. 163(4-5): p. 421-424.
31. Baumler, W., et al., *The role of singlet oxygen and oxygen concentration in photodynamic inactivation of bacteria.* Proceedings of the National Academy of Sciences of the United States of America, 2007. 104(17): p. 7223-7228.
32. Wilkinson, F., W.P. Helman, and A.B. Ross, *Quantum Yields for the Photosensitized Formation of the Lowest Electronically Excited Singlet-State of Molecular-Oxygen in Solution.* Journal of Physical and Chemical Reference Data, 1993. 22(1): p. 113-262.
33. Baier, J., et al., *Theoretical and experimental analysis of the luminescence signal of singlet oxygen for different photosensitizers.* J Photochem Photobiol B, 2007. 87(3): p. 163-73.
34. Kanofsky, J.R., et al., *Biochemical requirements for singlet oxygen production by purified human myeloperoxidase.* J Clin Invest, 1984. 74(4): p. 1489-95.
35. Butorina, D.N., A.A. Krasnovskii, and A.V. Priezzhev, *Investigation of the kinetic parameters of singlet molecular oxygen in aqueous porphyrin solutions. influence of detergent and the quencher sodium azide.* Biofizika, 2003. 48(2): p. 201-209.
36. Wessels, J.M., P. Charlesworth, and M.A. Rodgers, *Singlet oxygen luminescence spectra: a comparison of interferometer- and grating-based spectrometers.* Photochem Photobiol, 1995. 61(4): p. 350-2.
37. Mitra, S., et al., *Effective photosensitization and selectivity in vivo of Candida Albicans by meso-tetra (N-methyl-4-pyridyl) porphine tetra tosylate.* Lasers Surg Med, 2011. 43(4): p. 324-32.
38. Ito, T., *Photodynamic action of hematoporphyrin on yeast cells--a kinetic approach.* Photochem Photobiol, 1981. 34(4): p. 521-4.
39. Cormick, M.P., et al., *Mechanistic insight of the photodynamic effect induced by tri- and tetra-cationic porphyrins on Candida albicans cells.* Photochem Photobiol Sci, 2011. 10(10): p. 1556-61.
40. Cormick, M.P., et al., *Photodynamic inactivation of Candida albicans sensitized by tri- and tetra-cationic porphyrin derivatives.* Eur J Med Chem, 2009. 44(4): p. 1592-9.
41. Oriel, S. and Y. Nitzan, *Mechanistic Aspects of Photoinactivation of Candida albicans by Exogenous Porphyrins(dagger).* Photochem Photobiol, 2012.
42. Pasternack, R.F., et al., *A spectroscopic and thermodynamic study of porphyrin/DNA supramolecular assemblies.* Biophys J, 1998. 75(2): p. 1024-31.
43. Kubat, P., et al., *Interaction of novel cationic meso-tetraphenylporphyrins in the ground and excited states with DNA and nucleotides.* Journal of the Chemical Society-Perkin Transactions 1, 2000(6): p. 933-941.
44. Lopez-Chicon, P., et al., *On the mechanism of Candida spp. photoinactivation by hypericin.* Photochem Photobiol Sci, 2012. 11(6): p. 1099-107.
45. Eichner, A., et al., *Dirty hands: photodynamic killing of human pathogens like EHEC, MRSA and Candida within seconds.* Photochem Photobiol Sci, 2012.

Chapter 5

Spectroscopic Studies of Porphyrins in Planktonic Cells and Biofilms

In this chapter *Candida albicans* cells were incubated with the porphyrin TMPyP and the singlet oxygen luminescence was directly detected. These experiments were performed with planktonic cell samples in solution, as well as for the first time in biofilms, which form a surface and therefore are a challenging subject. Two different laser setups were used and the different results gave rise to a model proposed for the photosensitizer localisation and decay of singlet oxygen in planktonic cells.

5.1 INTRODUCTION

In the last years the direct detection of singlet oxygen by its luminescence at 1270 nm has become sensitive enough to detect singlet oxygen generated in eukaryotic or prokaryotic cells that have been incubated with photosensitizers [1-5]. In these studies, also the role of oxygen and bacterial concentration on the singlet oxygen phosphorescence kinetics and the effect for aPDT has been investigated [4]. The intensity of these singlet oxygen luminescence signals depend critically on the given irradiation parameters, as such the irradiation wavelength, laser power and absorption of the photosensitizer at the respective wavelength, and the overall number of laser pulses. In this study the singlet oxygen luminescence generated in fungal and bacterial cells under different irradiation parameters are compared.

The antifungal activity of singlet oxygen generated by photosensitizers, especially against *Candida albicans*, has been investigated widely in planktonic cell suspensions [6, 7]. In reality most of the time *C. albicans* will form biofilms that are much more difficult to destroy by the photodynamic effect due to an extracellular matrix within the biofilm [6, 8]. The biofilm matrix is a three-dimensional layer of cells and mainly consists of extracellular polysaccharides, specifically β-1,3 glucan for *C. albicans*. This gel-like material is highly hydrated and partly negatively charged due to the presence of carboxyl, sulphate or phosphate groups [9, 10]. In addition, such a biofilm, which is incubated with a photosensitizer, represents a surface model comparable to PU/PMMA system that is doped with porphyrins or PN molecules (see chapter 6).

In the present work, the luminescence signal of singlet oxygen from photosensitizer-incubated *C. albicans* both growing as planktonic cells and as biofilm was detected directly by time-resolved measurements at 1270 nm. Planktonic cell suspensions as well as biofilms of *C. albicans* in polystyrene Petri dishes were investigated with this method, the latter for the first time.

Most of the measurements regarding the detection of the singlet oxygen luminescence were performed by irradiating *Candida* in suspension containing TMPyP and XF73. As described in chapter 3, PBS alone, due to the presence of Cl^-, leads already to a change of the rise component of the XF73-based singlet oxygen luminescence. Due to the dramatic influence of PBS on the stacking of XF73 that influences the singlet oxygen luminescence, the herein presented data are restricted to the results achieved with TMPyP. TMPyP did not show any change of the singlet oxygen luminescence when dissolved in PBS and has furthermore a

high photostability and a well investigated phototoxic effect against a variety of microorganisms [11]. TMPyP was recently described as effective photosensitizer for photodynamic inactivation of *Candida* in both liquid suspensions or localized on a surface [7] as well as an effective photosensitizer against bacteria [11, 12]. Thus, we assume that TMPyP is at least attached at the cell membrane of these microorganisms.

During the experiments, a new tunable laser system was purchased that allowed the adaption of the excitation wavelength to the absorption spectrum of the applied photosensitizers. Due to the high number of data investigated under different conditions, this chapter describes results exemplarily, beginning with the singlet oxygen detection in planktonic solutions of *Candida* and in biofilms with the Nd:YAG laser, followed by the detection with the new tunable laser system. Mainly, the difficulties and issues in analysing and interpreting the singlet oxygen luminescence in *Candida* are described in regard to the photosensitizer concentration, the oxygen concentration and the site of the deactivation of the excited photosensitizer triplet state.

5.2 EXPERIMENTAL SECTION

5.2.1 Chemicals

TMPyP (5,10,15,20-Tetrakis(1-methyl-4-pyridinio)porphyrintetra(p-toluene sulfonate), purity > 97%) and NaN_3 were purchased from Sigma–Aldrich (Steinheim, Germany). Different photosensitizer concentrations have been prepared in pure H_2O by dilution of a stock solution of 1 mM.

5.2.2 Fungi cells

Candida albicans strain ATCC-MYA-273 was used for the singlet oxygen luminescence detection.

Preparation for the experiments with the Nd:YAG laser

The planktonic cell samples were grown as described in detail in chapter 2 and prepared as follows: *C. albicans* with a concentration of $10^7\ CFU\ mL^{-1}$ were diluted in PBS before mixed 1:1 with different concentrations of TMPyP dissolved in H_2O, resulting in a cell concentration of $0.5 \cdot 10^7\ CFU\ mL^{-1}$ and a PBS concentration of 50%. A volume of cell suspension of $2\ mL$ each measurement was used for the singlet oxygen luminescence detection.

The biofilm formation was prepared as follows: *C. albicans* were diluted in 25% of fetal bovine serum (FBS) to $10^6\ CFU\ mL^{-1}$ [13]. The cells were transferred to cell culture dishes (Petri dish, 35, 0/10 mm, Cellstar, Greiner bio-one, Frickenhausen, Germany) which consist of Polystyrene free of heavy metal. The cells were covering a growth area of 8.7 cm^2 and were incubated for 24 h at 37°C to allow biofilm formation. The biofilm was washed twice with PBS to remove nonadherent cells and subsequently incubated with different concentrations of the photosensitizer for 1 h. The biofilm cells were washed once or non-washed after incubation with TMPyP. To gain visible dryness, some biofilm samples were left for 1 h under the laminar flow of a sterile work bench.

Preparation for the experiments with the new tunable laser system

The *C. albicans* cells were diluted in PBS to yield a concentration of $10^7\ CFU\ mL^{-1}$ before mixed 1:1 with the photosensitizer. *C. albicans* was incubated with TMPyP dissolved in H_2O leading to a final concentration of 1, 10, and 100 µM of the photosensitizer in a total volume of 2 mL for each sample. Furthermore, this dilution resulted in an overall PBS concentration of 50% in each sample.

5.2.3 Singlet oxygen luminescence detection by direct spectroscopic methods

Both, the Nd:YAG laser and the tunable laser system were used to irradiate incubated *C. albicans*. Different conditions were used for irradiation of the photosensitizers in *C. albicans* in order to generate singlet oxygen. These conditions are described separately for each experiment.

Experiments with the Nd:YAG laser

C. albicans planktonic solutions incubated with TMPyP ($0.5 \cdot 10^7\ CFU\ mL^{-1}$, if not stated otherwise) or in biofilms was excited with a frequency-tripled Nd:YAG-laser at $\lambda = 532\ nm$, a laser power of $P = 60\ mW$, a repetition rate of $f = 5\ kHz$, and 100 000 laser pulses ($= 20\ s$ irradiation time) with a pulse duration of 70 ns and a pulse energy of 12 µJ. During the irradiation with the laser the planktonic cells were magnetically stirred and the oxygen concentration in the surrounding of the cells was determined with an oxygen needle sensor.

Additionally, for some samples of the planktonic solutions of *C. albicans* the singlet oxygen quencher NaN_3 was incubated in parallel with TMPyP. Therefore, first a solution with NaN_3 and TMPyP with a concentration of 2.8 mM and 200 µM was made in H_2O, before mixing it 1:1 with the cell suspension, as described above.

The singlet oxygen luminescence experiments with *C. albicans* planktonic solution and biofilms were immediately performed after incubation and one washing step in acrylic cuvettes (planktonic solutions) or on polystyrene Petri dishes (biofilms). For both plastic materials no singlet oxygen generation was detected within the noise level of the PMT when excited at 532 nm under the given experimental conditions (data not shown). On the biofilm samples in the Petri dishes the spot size of the excitation laser was expanded using an optical lens yielding an irradiation area of $\approx 7\ cm^2$ in regard to the size of the biofilm in the

Petri dishes. The singlet oxygen luminescence was detected directly time-resolved at 1270 nm using a FWHM = 30 nm filter (LOT Oriel GmbH, Darmstadt, Germany).

Experiments with the new tunable laser system

C. albicans planktonic solutions incubated with TMPyP ($0.5 \cdot 10^7\ CFU\ mL^{-1}$) with an overall volume of 2 mL was excited either in its Soret band at $\lambda = 420\,nm$ or it its Q-band at $\lambda = 520\,nm$ with a tunable laser yielding a laser power of $P = 360\,mW$ for each wavelength. The laser works with a repetition rate of $f = 1\ kHz$, and 10 000 laser pulses ($= 10\ s$ irradiation time) were applied to the cells samples with a $4 - 7\ ns$ pulse width. With the given parameters an energy of 360 µJ per pulse was applied.

Immediately after mixing the cells with TMPyP (incubation $< 1\,min$), the samples were irradiated in acrylic cuvettes (Sarstedt, Nümbrecht, Germany) during magnetic stirring and the oxygen concentration in the surrounding of the cells was determined with an oxygen needle sensor. The singlet oxygen luminescence was detected time-resolved at 1270 nm using a FWHM = 30 nm filter (LOT Oriel GmbH, Darmstadt, Germany). Biofilm samples were not investigated with the tunable laser system.

5.3 RESULTS & DISCUSSION

In this chapter for the first time the singlet oxygen luminescence was directly detected at its transition at 1270 nm with spectroscopic methods first in incubated planktonic cells of *C. albicans* and secondly in *C. albicans* biofilms. In addition to the standard laser system with excitation wavelengths of 355 or 532 nm, a new tunable laser setup was used, which provided light pulses at a wavelength at which the photosensitizer TMPyP in *C. albicans* planktonic cells could be irradiated in its absorption maximum (Soret band). Thus, the luminescence in cell suspensions could be precisely detected even at TMPyP concentrations below 5 µM with a high signal-to-noise ratio. This offers more accurate determinations of the rise and decay times of singlet oxygen luminescence signals, which might be especially helpful for low photosensitizer concentration after cell washing procedures.

The *C. albicans* cells were incubated with TMPyP for different time spans and both, planktonic cell suspensions and biofilms, were either passed through one washing step or remained unwashed. The biofilms were investigated additionally under wet and dry (visible dryness) conditions. The determined rise and decay times for all samples were compared to pure TMPyP in H_2O. In order to assign the rise and decay time of the singlet oxygen luminescence signals, generated by irradiation with a Nd:YAG laser, some samples of the planktonic *C. albicans* solutions contained the singlet oxygen quencher NaN_3.

With a new tunable laser setup irradiation of TMPyP in its Soret band was performed in planktonic *Candida* solutions. Therefore, *C. albicans* were incubated with different photosensitizer concentrations and the singlet oxygen luminescence signals were compared for non-washed cells and very short incubation time. Moreover, the different absorption properties of TMPyP in its Soret band and in its Q-band and the influence on the singlet oxygen luminescence signals were compared.

5.3.1 Fluorescence imaging of TMPyP in C. albicans planktonic cells and biofilm

Prior to the singlet oxygen detection, fluorescence microscopy was performed to confirm uptake or attachment of TMPyP-molecules by planktonic or biofilm growing *C. albicans* [14]. Therefore, both planktonic cells and biofilm were incubated each with a TMPyP concentration of 100 µM for 60 min. Subsequently, the cells were washed once in order to remove non-adherent photosensitizer molecules. Figure 5.1 (A) shows the bright field image

of planktonic cells, which was overlaid with the fluorescence of TMPyP in (B). The cell wall (A, black arrow) and the cell nucleus (A, white arrow) can be detected clearly. Figure 5.1 (C) shows the bright field image of the biofilm. The corresponding fluorescence image was overlaid with the bright field image (D). The polyphenic character of *C. albicans* can be seen by the presence of ovoid yeast cells, pseudohyphae and hyphae (invasive form). Figure 5.1 (E) shows only the TMPyP fluorescence as detected in the biofilm (fig. 5.1 C), which could not be defined accurately in regard to the depth of focus due to the 3-dimensional formation of the biofilm. In summary, the data shows uptake of TMPyP in both, planktonic cells and biofilm, to a certain extent [14].

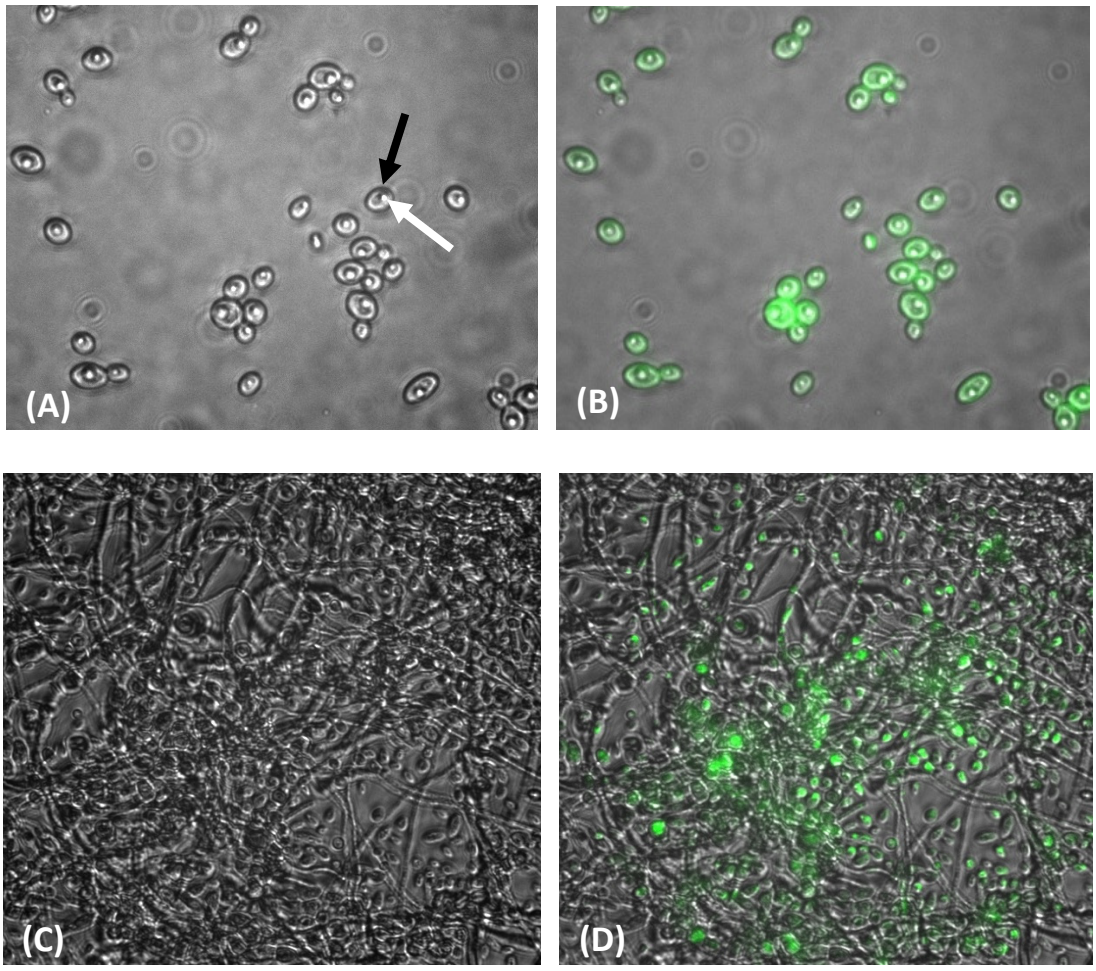

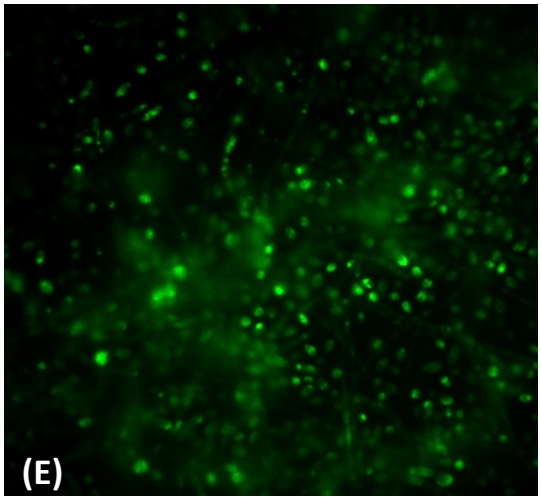

Fig. 5.1: Fluorescence microscopy of C. albicans (A-B) planktonic cells and (C-E) biofilm incubated with 100 µM TMPyP and washed once to remove non-adherent photosensitizer molecules; (A) bright field image planktonic cells (B) overlay of TMPyP fluorescence with bright field image planktonic cells (C) bright field image biofilm (D) overlay TMPyP fluorescence with bright field image biofilm (E) fluorescence TMPyP incubated in biofilm [14].

5.3.2 Direct spectroscopic detection of singlet oxygen in TMPyP dissolved in H_2O

TMPyP with a concentration of 10 μM was investigated in pure air-saturated H_2O with an oxygen concentration of $[O_2] = 0.27 \cdot 10^{-6}\ M$ and revealed a rise and decay time (data not shown). The decay time of singlet oxygen is $\tau_\Delta = (3.5 \pm 0.4)\mu s$ which correlates to the literature values of singlet oxygen decay in H_2O [1]. The decay time of the excited triplet-T_1-state of TMPyP is $\tau_{T_1} = (2.1 \pm 0.2)\mu s$. Spectroscopically resolved singlet oxygen measurements in H_2O gave a peak at 1270 nm [11] and are together with the time resolved measurement an evidence for the generation of singlet oxygen.

5.3.3 Direct spectroscopic detection of singlet oxygen in planktonic *C. albicans* cells with the Nd:YAG laser

C. albicans planktonic cell solutions were incubated with TMPyP resulting in a final concentration of 10 or 100 µM in the solution. Since the wavelength of the Nd:YAG laser was restricted to 532 nm, only the first Q-band of TMPyP could be irradiated. In order to have an appropriate photosensitizer absorption and therefore a good signal-to-noise ratio of the singlet oxygen luminescence signal these photosensitizer concentrations were used. The incubated *C. albicans* cells were either investigated non-washed or were washed once

before they were exposed to laser irradiation. This was done in order to detect differences in the rise and decay times, which depend critically on the localisation of the photosensitizer and to avoid a dominance of the singlet oxygen generated by non-adherent TMPyP molecules in the H_2O surrounding of the cells.

First, the rise and decay time of the singlet oxygen luminescence of non-washed cell suspensions incubated with 10 and 100 µM of TMPyP (incubation time: 15 min) were determined from a signal with a high signal-to-noise ratio. Exemplarily, the time-resolved singlet oxygen luminescence with 100 µM TMPyP is shown in the following figure 5.2 together with the deviation of the bi-exponential fit-curve (least square fit). Rise and decay times are summarized in table 5.1, displaying the mean value of three independent experiments with an experimental accuracy of 10%. As determined with the oxygen needle sensor, the oxygen concentration in the surrounding of the cells was at air-saturation ($[O_2] = 0.27\ mM$) during the irradiation with 100 000 laser pulses (= irradiation time of 20 s).

The rise and decay times of the cell samples that were incubated with TMPyP and non-washed showed the characteristic rise and decay time for both photosensitizer concentrations in a pure air-saturated solution of H_2O. Since the cells were not washed after incubation, a great deal of photosensitizer molecules should have been located in the water in between the cells. Thus, singlet oxygen was mainly generated in the water, which correlates with the decay time of the detected luminescence signal ($\approx$ 3.5 µs).

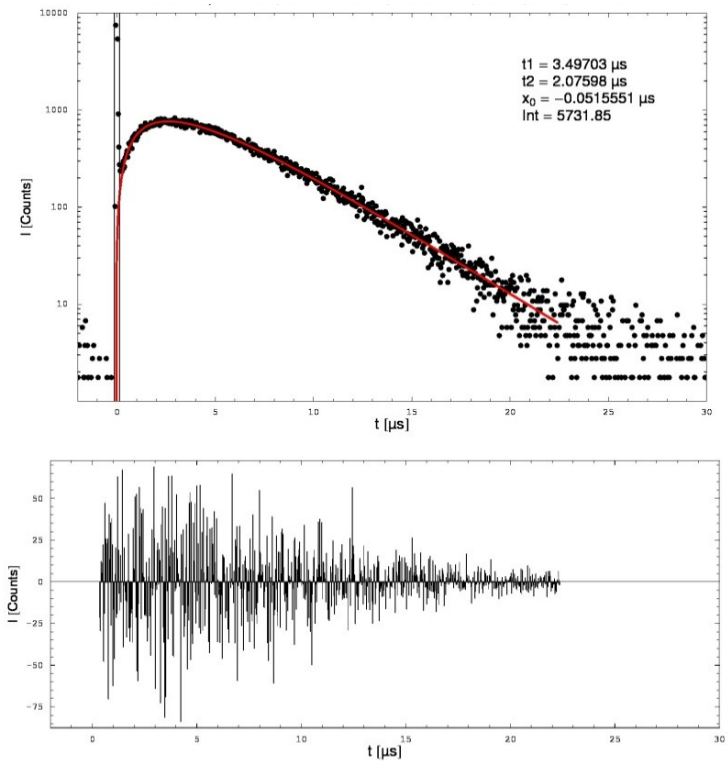

Fig. 5.2: Singlet oxygen luminescence signal generated by TMPyP incubated in a C. albicans planktonic solution by irradiation with λ = 532 nm, P = 60 mW, f = 5 kHz, and 100 000 laser pulses in an acrylic cuvette; TMPyP was incubated for 15 min with a concentration of 100 µM and the cells were non-washed; cell concentration of 0.5·10⁷ cells per mL; the deviation of the fit-curve is shown below the singlet oxygen luminescence signal.

planktonic

c [µM]	t_R [µs]	t_D [µs]
10	2.0	3.5
100	2.0	3.7

Tab. 5.1: Rise and decay times of the singlet oxygen luminescence generated by a concentration of c = 10 and 100 µM of TMPyP in a C. albicans planktonic cell suspension containing 0.5·10⁷ cells per mL; the cells were incubated 15 min and non-washed. (for 10 µM: n = 3, for 100 µM: n = 5; exp. accuracy: 10%)

After one washing step the results for the singlet oxygen luminescence vary. For 10 µM TMPyP, singlet oxygen luminescence was not detected, but for 100 µM the detection succeeded, yielding rather different luminescence intensities or signal-to-noise ratios. An example of a singlet oxygen luminescence signal of a washed planktonic cell suspension after 15 min of TMPyP-incubation is shown in figure 5.3. The detection criteria, although, changed ($f = 2\ kHz$, $P = 50\ mW$, 40 000 laser pulses) and thus the results summarized in

table 5.1 might be compared carefully (intensity of the signals are not comparable due to the use of different laser power, frequency and number of pulses).

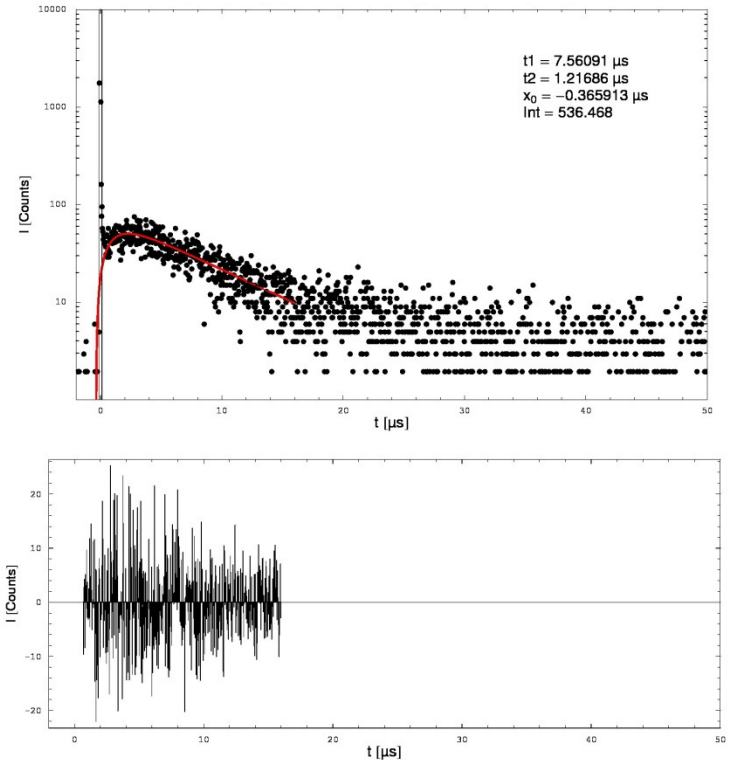

Fig. 5.3: Singlet oxygen luminescence signal generated by TMPyP incubated in a C. albicans planktonic solution by irradiation with λ = 532 nm, P = 50 mW, f = 2 kHz, and 40 000 laser pulses in an acrylic cuvette; TMPyP was incubated for 15 min with a concentration of 100 µM and the cells were washed once; cell concentration of 0.5·10⁷ cells per mL; the deviation of the fit-curve is shown below the singlet oxygen luminescence signal.

In this example (fig. 5.3) singlet oxygen luminescence yielded a rise and decay time of $t_R = (1.5 \pm 0.2)\mu s$ and $t_D = (7.2 \pm 0.7)\mu s$ (mean of two experiments). During the measurement ($20\ s$) the oxygen concentration in the suspension decreased from $[O_2] = 0.30\ mM$ to $[O_2] = 0.27\ mM$ ($\approx 10\%$). Compared to the results summed up in table 5.1 the rise time becomes shorter and the decay time longer. At the site of the photosensitizer due to the value t_D an oxygen concentration in the range of $[O_2] = (0.067 - 0.081) mM$ ($\triangleq$ 25 – 30%) is proposed by comparison of the values of an oxygen variation for TMPyP in H_2O.

Reflecting the findings of Regensburger *et al.* of TMPyP in bacteria, a similar behaviour was obtained herein with *C. albicans* (tab. 5.2). An oxygen variation in the surrounding of the bacteria suggested that the decay times of the signals could be assigned to the triplet-T_1-

state of the photosensitizer and a decay of singlet oxygen, τ_Δ, was in the range of $1.7 - 2.9\ \mu s$ [15].

	t_R [μs]	t_D [μs]	$[O_2]_{H_2O\ surrounding}$
S. aureus	1.76	6.39	$90\% \triangleq 0.24\ mM$
E. coli	1.83	4.22	$100\% \triangleq 0.27\ mM$

Tab. 5.2: Rise and decay times of the singlet oxygen luminescence signal generated by TMPyP in bacteria; S. aureus and E. coli were incubated 60 min and subsequently washed once to remove non-adherent TMPyP [15].

Nevertheless, the effectivity of the uptake of TMPyP into *C. albicans* is not finally clarified with the so far presented measurements. No singlet oxygen generation was detected with a TMPyP concentration of 10 μM which suggested a weak attachment to the exterior cell wall of *C. albicans* or signal under the detection limit. Quiroga *et al.* report that the amount of cell-bound TMPyP reached the highest value around 15 min of incubation but an enhancement of the incubation time did not lead to higher uptake. They reported a decrease of TMPyP molecules of about 70% after one washing step with 5 μM TMPyP and an incubation time of 15 min. Nevertheless, their phototoxic studies of once washed *C. albicans* cells that were incubated with 5 μM TMPyP for 30 min showed a killing efficiency of $\approx 2.5\ log_{10}$-steps (irradiation conditions: 15 min, 90 $mW cm^{-2}$) [7]. Therefore, also at low photosensitizer concentrations like 5 μM, a singlet oxygen luminescence signal should be detected after one washing procedure. In our experiments, after one washing step, the amount of generated singlet oxygen luminescence photons might have been below the detection limit, since the photosensitizer was also not irradiated properly at its highest absorption in the Soret band.

In order to assign the rise and decay time of the luminescence signal to the decay of singlet oxygen or the excited triplet-state of the photosensitizer (tab. 5.1), the singlet oxygen quencher NaN_3 was added to the cell suspension with an overall concentration of 1.4 mM in the solution. This is a typical quencher concentration value, where a shortening of the singlet oxygen decay time occurs. Again, the oxygen concentration in the surrounding of the cells was determined to be equal with air-saturated pure H_2O ($[O_2] = 0.27\ mM$).

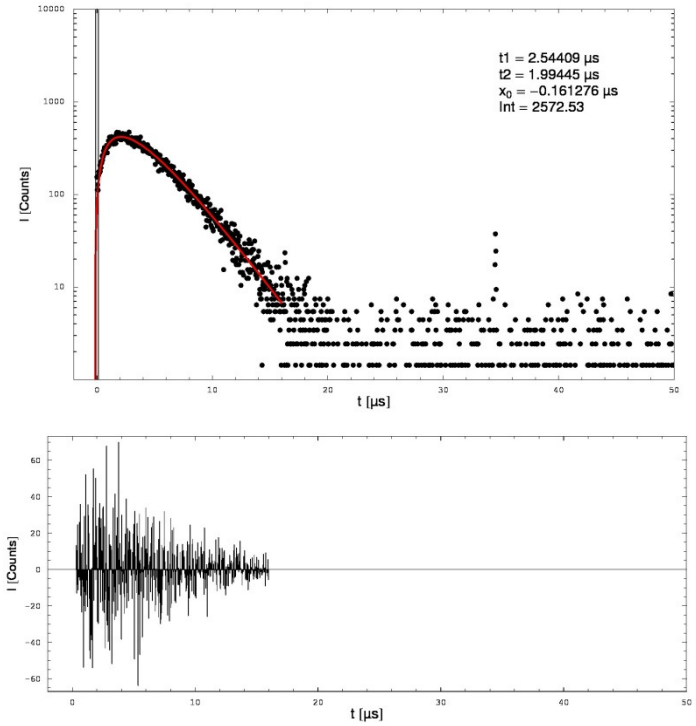

Fig. 5.4: Singlet oxygen luminescence signal, generated by TMPyP incubated in a C. albicans planktonic solution by irradiation with λ = 532 nm, P = 60 mW, f = 5 kHz, and 100 000 laser pulses with a NaN_3 concentration of 1.4 mM in an acrylic cuvette; TMPyP was incubated for 15 min with a concentration of 100 µM and the cells were non-washed; cell concentration = $0.3 \cdot 10^7$ cells per mL; the deviation of the fit-curve is shown below the singlet oxygen luminescence signal.

After adding 1.4 mM of NaN_3 in the cell suspension the singlet oxygen luminescence signal has a good signal-to-noise ratio and the fit deviation is equally distributed (fig. 5.4). Due to the influence of NaN_3 the decay time $t_1 = t_D = (2.5 \pm 0.3)\mu s$ becomes shorter, whereas the rise time $t_2 = t_R = (2.0 \pm 0.2)\mu s$ does not change. From this effect we conclude that $t_1 = \tau_\Delta$ and $t_2 = \tau_{T_1}$, because NaN_3 quenches predominantly the singlet oxygen decay time.

In conclusion for these singlet oxygen luminescence experiments, the results from the non-washed cells with and without NaN_3 suggest a decay of singlet oxygen predominantly in H_2O-surrounding, with a decay time around 3.5 μs. According to Regensburger et al. the quenching of singlet oxygen due to the presence of proteins within the cell would lead to faster singlet oxygen decay and thus it is assumed that the herein presented measurements singlet oxygen was generated most likely predominantly in the aqueous environment outside the cell [15]. This consideration fits with the short rise time determined in *C. albicans* after one washing step, where the number of TMPyP molecules in contact with proteins increased. Nevertheless, the weak signal-to-noise ratio for 10 μM does not allow precise determinations of the rise and decay time, received with washed cells, and thus has to be enhanced.

5.3.4 Detection of singlet oxygen in biofilms with the Nd:YAG laser

C. albicans biofilms were incubated for 1 h with 10 or 100 µM TMPyP after biofilm formation. The incubated *C. albicans* cells in the biofilm were either investigated non-washed or were washed once by rinsing with PBS before they were exposed to laser irradiation. This was done in order to see changes in the singlet oxygen luminescence signal which might give a hint on the attachment of the photosensitizer and also its localisation.

Exemplarily, the time-resolved singlet oxygen luminescence generated by 100 µM TMPyP in the *C. albicans* biofilm, non-washed and washed, are shown in the figure 5.5. The biofilm was surrounded by air at room temperature, before the irradiation.

The signal-to-noise ratio is sufficient in order to determine a bi-exponential fit of the singlet oxygen luminescence signal for the non-washed and washed biofilm samples. Three independent measurements yielded rise and decay times and are represented in table 5.3.

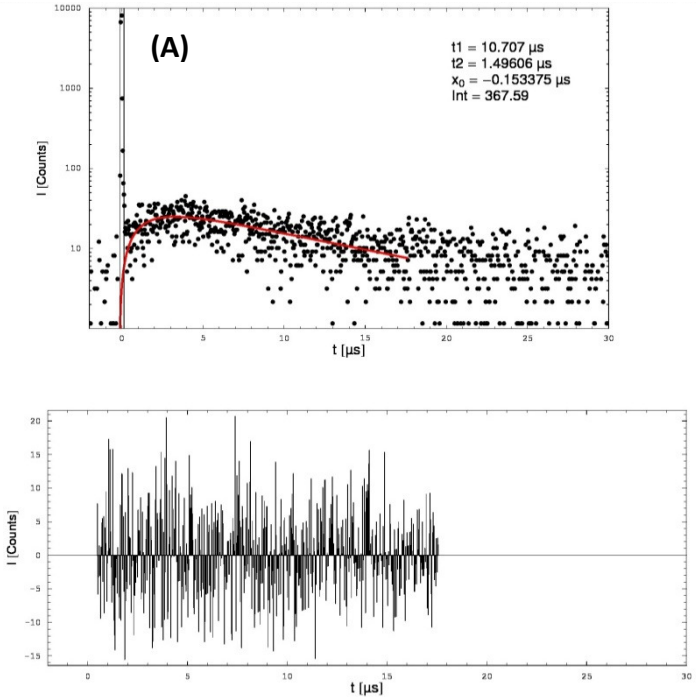

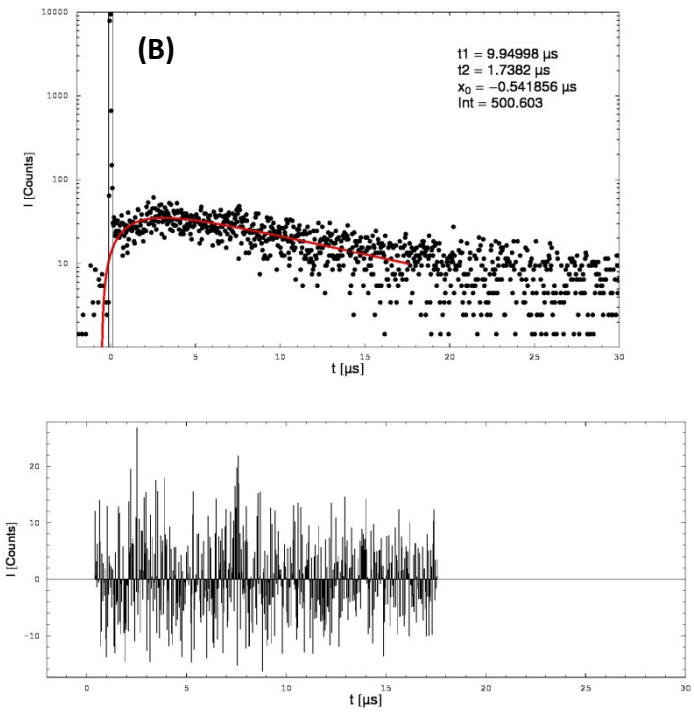

Fig. 5.5: Singlet oxygen luminescence signal generated by TMPyP incubated in a C. albicans biofilm by irradiation with λ = 532 nm, P = 60 mW, f = 5 kHz, and 100 000 laser pulses in a polystyrene petri dish; TMPyP was incubated after biofilm formation for 1 h with a concentration of 100 µM, the supernatant was removed and the biofilm was (A) non-washed or (B) washed with PBS once; the deviation of the fit-curve is shown below the singlet oxygen luminescence signal.

biofilm

	t_R [µs]	t_D [µs]
non-washed	1.5	10.9
washed	1.3	10.5

Tab. 5.3: Rise and decay times of the singlet oxygen luminescence signals generated by TMPyP-incubated biofilms; (n = 3, exp. accuracy: 10%)

For the non-washed, but wet biofilms a rise time of $t_R = (1.5 \pm 0.2)\mu s$ and a decay time of $t_D = (10.9 \pm 1.1)\mu s$ was detected. Thus, the rise time is about 0.5 µs shorter compared to the cells in planktonic solution, which is a difference that is beyond the experimental accuracy of 10%; the decay part becomes approximately 7.5 µs longer in the biofilm compared to planktonic solution.

Furthermore, the washing procedure does neither lead to a change in rise and decay time nor in the intensity of the luminescence. This suggests penetration of TMPyP into the biofilm, as confirmed by fluorescence microscopy (fig. 5.1, C, D, E). It was detected that the

photosensitizer molecules were not washed away easily with the applied gentle washing method.

In planktonic cells singlet oxygen luminescence was detected predominantly after incubation with a rather high concentration of 100 μM, which was also confirmed by fluorescence microscopy (fig. 5.1, A, B) attachment of TMPyP after 15 min of incubation was found only in some samples, and. Biofilms form an additional extracellular matrix and the biofilm samples were incubated longer than the planktonic cells. On the one hand, an enhancement of the incubation period to 1 h might be more effective for photosensitizer penetration. On the other hand, the additional matrix structure of biofilms has different constituents compared to the *C. albicans* cell membrane and therefore TMPyP might be linked also in the matrix and thus have a better attachment to a biofilm than to planktonic cells due to the fact that the biofilm matrix consists mainly of polysaccharides, specifically β-1,3 glucan, which is hydrophilic like TMPyP.

Drying out the biofilm for 1 h under a laminar flow of a sterile work bench was done in order to exclude the H_2O-environment. A comparison of the so achieved dry biofilms with the non-dry samples leads to almost similar rise and decay of the singlet oxygen luminescence, as can be seen in table 5.4.

	biofilm, dry	
	t_R [μs]	t_D [μs]
non-washed	1.4	11.2
washed	1.6	13.0

Tab. 5.4: Rise and decay times of the singlet oxygen luminescence signals generated by TMPyP-incubated biofilms; the biofilms were dried for 1 h under a laminar flow of a sterile work bench. (n = 3, exp. accuracy: 10%)

Both, rise and decay time, do not change within experimental accuracy compared to the non-dry biofilm samples. In the non-dry biofilms the amount of H_2O surrounding the cells and surrounding the singlet oxygen generator TMPyP is less compared to cells in planktonic solution. As the amount of H_2O in the biofilm cannot be estimated properly it is not clear how much the remaining H_2O influences the singlet oxygen decay time. After drying the biofilm 1 h under the laminar flow the signals and thus the decay time of the photosensitizer and singlet oxygen do not change within experimental accuracy. This leads to the assumption that a similar surrounding of the photosensitizer is given compared to the non-dry biofilms. The extracellular matrix might keep a constant amount of water within the 1 h

drying process. It is known, that the gel-like matrix is highly hydrated, which enhances the lifetime of the cells under dry conditions [9].

Polysaccharides, specifically β-1,3 glucan, are a main component of the *C. albicans* biofilm matrix. Degrading of polysaccharides by ROS such as singlet oxygen has been reported [16, 17]. A decay time of $t_D \approx 11\ \mu s$ (tab. 5.3, 5.4) reported herein for both, non-dry and dry biofilm samples, is close to a decay time of singlet oxygen in lipid environment as determined by Baier *et al.* to be $\approx 14\ \mu s$ with lipid spreads on quartz glass [1]. The singlet oxygen luminescence of these dry lipid samples compared to their non-dry counterparts revealed also an almost unchanged decay time of singlet oxygen of $14\ \mu s$ and thus an influence of H_2O was also there excluded to a great extent [1]. However, a shorter decay time compared to the decay in H_2O $(= 3.5\ \mu s)$ might be reasonable as well with characteristic singlet oxygen quenching features of polysaccharides [18, 19].

5.3.5 Detection of singlet oxygen in planktonic *C. albicans* cells with the tunable laser system and a gas flow unit

During the cell study the experimental was optimized with a tunable laser system and a gas flow unit. On the one hand, it is well-known that high cell concentrations consume oxygen, especially under irradiation, which influences dramatically the singlet oxygen generation [4]. With a gas flow unit, flooding with a constant ratio of O_2 and N_2 and a constant volume per time unit, the oxygen concentration in the cell surrounding, especially with a high concentration of cells, could be adjusted and kept constant. Therefore, the same oxygen conditions in the exterior of the planktonic cells could be adjusted and kept during the singlet oxygen measurement. In order to have a fast diffusion of the O_2/N_2 in the cell solution the gas flow is accompanied by magnetic stirring.

On the other hand, with the tunable laser every photosensitizer could be irradiated optimally. Thus, it was possible to irradiate TMPyP directly in its Soret band at $420\ nm$. Irradiation with the appropriate wavelength leads to an effective absorption causing higher signal intensity of the singlet oxygen luminescence which can be evaluated properly. Especially low photosensitizer concentrations $(< 5\ \mu M)$ led usually to an already low signal-to-noise ratio for irradiation with the Nd:YAG laser at $532\ nm$. Very low photosensitizer concentrations can be found particularly when incubated cells undergo washing processes and the remaining photosensitizer attached to cells is spectroscopically investigated. Quiroga *et al.* reported a binding saturation value of $1.7\ nmol\ 10^{-6}$ *C. albicans* cells after

incubation with 5 µM TMPyP for 30 min incubation time [7]. In that example very low photosensitizer concentrations are reached which are the basis for direct spectroscopic singlet oxygen detection. Additionally, high photosensitizer concentrations might cause dark toxicity during the incubation process, which was reported by Maisch *et al.* for the porphyrin XF73 [20]. By avoiding high photosensitizer concentrations, the probability of the singlet oxygen luminescence being detected in vital cells might be enhanced also by a lower probability of possible self-quenching of the photosensitizer.

Due to the high cell concentration of $0.5 \cdot 10^7\ CFU\ mL^{-1}$ for *C. albicans* the oxygen consumption by the microorganisms has to be compensated by flooding the planktonic cell solutions under magnetic stirring with a constant gas flow of $0.1\ L\ min^{-1}$ of O_2 and $0.4\ L\ min^{-1}$ of N_2 (≙ air-saturation level of oxygen) in order to keep a constant amount of oxygen in the solution comparable to that in air-saturated water. The probes were irradiated with two different wavelengths of $\lambda = 420\ nm$ and 520 nm which correspond to the absorption maximum of TMPyP (Soret-band) and its first Q-band, respectively. TMPyP solutions were added to the cell suspensions immediately before the irradiation with no washing procedure and therefore the overall incubation time did not exceed 1 min.

5.3.5.1 Irradiation with 520 nm in the first Q-band of TMPyP

First, optimal irradiation of the first Q-band of TMPyP was done at 520 nm to compare the findings of the setup with the Nd:YAG laser, which also irradiated the first Q-band, but non-optimally at 532 nm. Therefore, the percentaged absorption of 10 µM changed from 17.4% (at 532 nm) to 22.3% (at 520 nm) and for 100 µM from 15.5% (at 532 nm) to 25.6% (at 520 nm), respectively. The new tunable laser is working with a much higher laser power of 360 mW (Nd:YAG, 60 mW) but at a lower frequency of 1 kHz (Nd:YAG, 5 kHz). Further, the irradiation time was shorter and 10 000 laser pulses (= 10 s) were used for collecting the singlet oxygen photons within one measurement instead of 100 000 pulses (= 20 s) in case of the Nd:YAG laser. Figures 5.6 (A) and (B) show the singlet oxygen luminescence for 10 and 100 µM TMPyP that was incubated in *C. albicans* with an incubation time of $< 1\ min$.

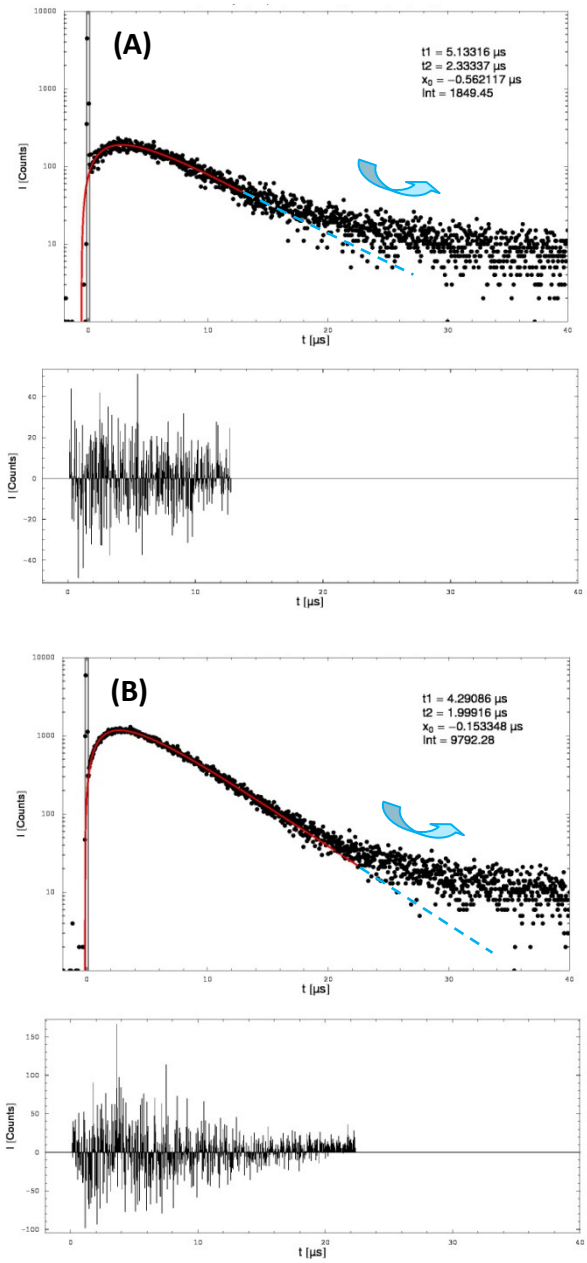

Fig. 5.6: Singlet oxygen luminescence signals generated by TMPyP incubated in a C. albicans planktonic cell suspension (2 mL) by irradiation the first Q-band of the photosensitizer at λ = 520 nm, P = 360 mW, f = 1 kHz, and 10 000 laser pulses in an acrylic cuvette containing 50% PBS in H_2O; TMPyP was incubated < 1 min with a final concentration of 10 µM (A) or 100 µM (B); the planktonic cells were not washed; cell concentration $0.5 \cdot 10^7$ cells mL^{-1}; the deviation of the fit-curve is shown below the singlet oxygen luminescence signal; the blue dashed line indicates a mono-exponential decay and the blue arrow indicates the deviation from that mono-exponential decay pattern.

The detected singlet oxygen luminescence signals had a high signal-to-noise ratio and therefore the rise and decay times could be determined accurately. For a concentration of 10 µM $t_1 = t_D = (5.1 \pm 0.5)\mu s$ is the decay time and $t_2 = t_R = (2.3 \pm 0.2)\mu s$ is the rise time of the luminescence signal. A deviation from an only mono-exponential decay (as indicated

with the blue dashed line) can be seen in figure 5.6 (A, arrow), but a second decay time could not be fitted. A deviation from a mono-exponential decay is even more prevalent in figure 5.6 (B, arrow), using a concentration of 100 µM. Also there, $t_1 = t_D = (4.3 \pm 0.4)\mu s$ is the decay time and $t_2 = t_R = (2.0 \pm 0.2)\mu s$ the rise time of the luminescence signal. Both rise times for the two different TMPyP concentrations are in good agreement with the values for the rise time of TMPyP in pure H_2O at air saturation, within experimental accuracy (see sub-chapter 5.3.2). The decay time of the signal obtained with 100 µM is as well in agreement with the data for singlet oxygen generated by TMPyP in pure H_2O, and therefore is assigned to the singlet oxygen decay time.

Compared to the *C. albicans* planktonic cell solution that was incubated for 15 min and irradiated at 532 nm, the cells were now incubated for less than 1 min. Therefore, one might expect less uptake of the photosensitizer TMPyP and a rise and decay time of the singlet oxygen luminescence signal close to the values in pure H_2O. Nevertheless, for 10 µM, a decay time value of $t_D = 5.1\ \mu s$ was obtained which might reflect, that a higher proportion of singlet oxygen molecules is quenched very close or attached to the *C. albicans* cells. Thus, a decay time of singlet oxygen in H_2O ($\tau_\Delta = 3.5\ \mu s$) and the influence of lipids ($\tau_\Delta = 14\ \mu s$) on the decay might lead to a mixed value of $t_D = 5.1\ \mu s$.

Furthermore, a higher sensitivity of the signal might be the case due to higher irradiation power, coupled with higher absorption at 520 nm, a different handling in the cell preparation and slight fluctuation in the cell concentration. An additional underlying signal might therefore have not been detectable with the old setup. The additional slight bend in the decay part of the luminescence signals for both photosensitizer concentrations (fig. 5.6, arrows) might be then reasonable for the deviation of the value for the decay time, resulting in longer decay times compared to figure 5.2. Also, the higher laser power during the measurement might have an influence on the integrity of the cells. Nevertheless, the signals with the new setup are considered to be more sensitive due to the additional bend in the decay part of the signal, possibly indicating a further decay time of singlet oxygen or the photosensitizer in the given system of H_2O and cells. So far, the difference of the signals at 532 nm and 520 nm can only be followed by additional measurements, varying the laser power, the irradiation time, the cell concentration, the photosensitizer concentration, or the oxygen concentration in the surrounding.

5.3.5.2 Irradiation with 420 nm in the Soret band of TMPyP

In order to compare the outcome of the experiments with the new setup with the results presented for the Nd:YAG laser in 5.3.2 the same concentrations for TMPyP of 10 µM and 100 µM were used. Due to a higher sensitivity by the irradiation in the Soret band of the photosensitizer ($\lambda = 420\,nm$), additionally a concentration of 1 µM was investigated as minimal photosensitizer concentration. Irradiation in the Soret-band of the photosensitizer is therefore reasonable in regard to the use of lower photosensitizer concentrations.

The following 3 graphics show the singlet oxygen luminescence for the 3 different concentrations of TMPyP (fig. 5.7) irradiated with $\lambda = 420\,nm$. The oxygen concentration in the surrounding of the samples was on an air-saturation level.

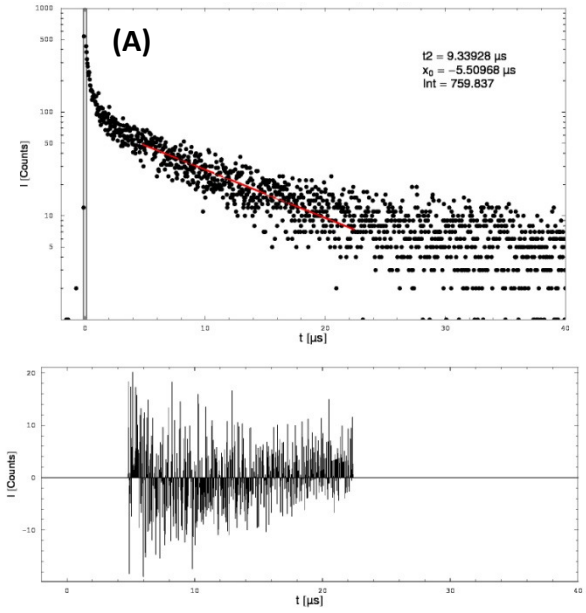

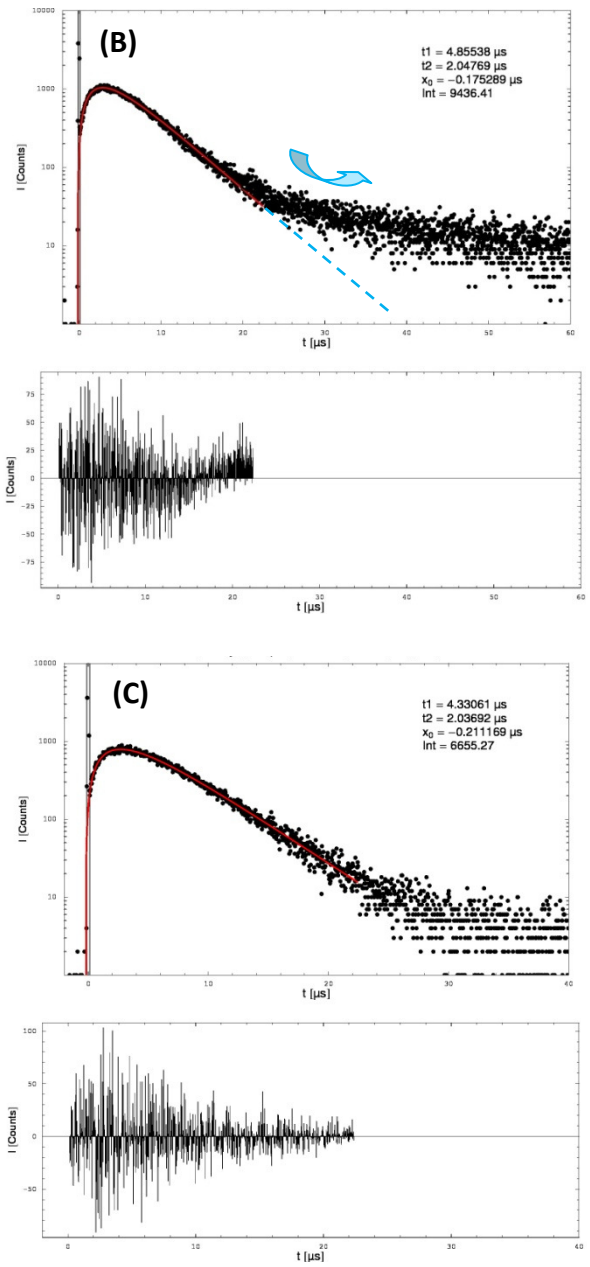

Fig. 5.7: Singlet oxygen luminescence signals generated by TMPyP incubated in a C. albicans planktonic cell suspension (2 mL) by irradiation with λ = 420 nm, P = 360 mW, f = 1 kHz, and 10 000 laser pulses in an acrylic cuvette containing 50% PBS in H_2O; TMPyP was incubated < 1 min with a final concentration of 1 µM (A), 10 µM (B) or 100 µM (C); the planktonic cells were not washed; cell concentration $0.5 \cdot 10^7$ cells mL^{-1}; the deviation of the fit-curve is shown below the singlet oxygen luminescence signal; the blue dashed line indicates a mono-exponential decay and the blue arrow indicates the deviation from that mono-exponential decay pattern.

All of the detected singlet oxygen luminescence signals had a high signal-to-noise ratio and therefore the rise and decay times could be determined accurately and are summarized in table 5.5. Most eye-catching are probably the change in the shape of the singlet oxygen luminescence signals and the change of their rise and decay time(s) depending on the concentration of TMPyP in the cell solution.

	C. albicans	
c [µM]	**t_1 [µs]**	**t_2 [µs]**
1	---	9.2
10	4.8	2.0
100	4.2	2.1

Tab. 5.5: Rise and decay times of the singlet oxygen luminescence generated by TMPyP incubated in a C. albicans planktonic cell suspension (2 mL) by irradiation the Soret band of the photosensitizer at λ = 420 nm, P = 360 mW, f = 1 kHz, and 10 000 laser pulses in an acrylic cuvette containing 50% PBS in H_2O; TMPyP was incubated < 1 min with a final concentration of 1, 10, and 100 µM; the planktonic cells were not washed; cell concentration $0.5 \cdot 10^7$ cells mL^{-1}; the oxygen concentration in the cell surrounding was kept constant between 90% and 100% of the air-saturation. (exp. accuracy: 10%)

In a *C. albicans* planktonic solution incubated with 1 µM of TMPyP only one decay time of $t_D = (9.2 \pm 0.9)\mu s$ was detected. For a concentration of 10 µM of TMPyP the signal shows decay in a multi-exponential manner and was fitted as a bi-exponential fit in the first part (count 5 – 700) with a rise and decay time of $t_R = (2.0 \pm 0.2)\mu s$ and $t_{D1} = (4.8 \pm 0.5)\mu s$ (see fig. 5.7 (B)), and also with a mono-exponential fit in the second part (count 800 – 1500) with a $t_{D2} = (22 \pm 2)\mu s$ (fig. 5.8).

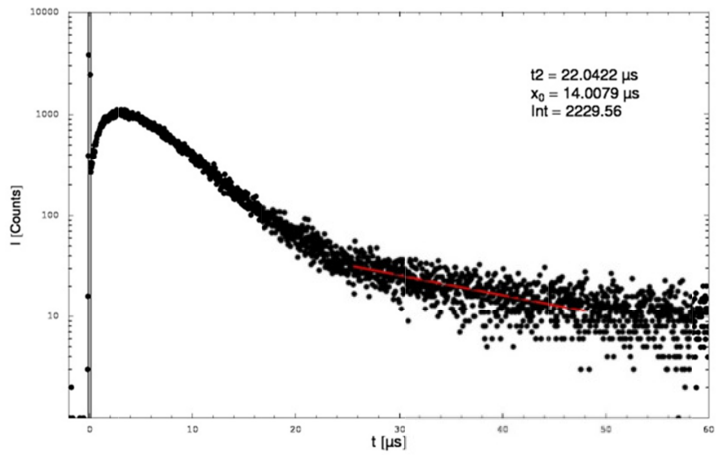

Fig. 5.8: Singlet oxygen luminescence signal of 10 µM TMPyP in planktonic C. albicans cells with a cell concentration of $5 \cdot 10^6$ cells mL^{-1}; the O_2 concentration in the surrounding of the cells was 88% compared to air saturated H_2O; a mono-exponential curve was fitted in the second part (count 800-1500).

A bi-exponential fit of the singlet oxygen luminescence signal in the presence of 100 µM TMPyP gave a rise and decay time of $t_R = (2.1 \pm 0.2)\mu s$ and $t_D = (4.2 \pm 0.4)\mu s$ (see tab. 5.5). The decay of the collected singlet oxygen luminescence photons are clearly dominated by an air-saturated water-surrounding, which is consistent with a decay time for singlet

oxygen around 3.5 µs and a photosensitizer decay time of 2 µs, as was shown in previous experiments (see 5.3.1).

When irradiating 10 µM of TMPyP in the planktonic cell suspension with 520 nm (fig. 5.6 (A)) a bi-exponential decay can only be slightly detected, whereas it was dominant for the irradiation with 420 nm. The oxygen concentration in the surrounding, the $CFU\ mL^{-1}$ and the photosensitizer concentration were kept constant, as well as the laser parameters for 420 nm and 520 nm, respectively. The absorption of TMPyP was over-saturated at 420 nm for both, 10 µM and 100 µM. A higher sensitivity for 10 µM TMPyP in planktonic cell suspension was already detected.

When enhancing the photosensitizer concentration up to 100 µM additional effects might disturb the higher sensitivity with the appropriate irradiation in the absorption maximum of a photosensitizer. As can be seen from figure 5.6 (B) the signal for 100 µM TMPyP irradiated with 520 nm also differs from the one detected at the irradiation wavelength of 420 nm (fig. 5.7 (C)). The irradiation at 520 nm in the Q-band of TMPyP leads to a singlet oxygen signal where a bi-exponential decay is clearly indicated. The high concentration of TMPyP might have a shielding effect for the majority of the cells, which might be even more drastically than illustrated in figure 5.9.

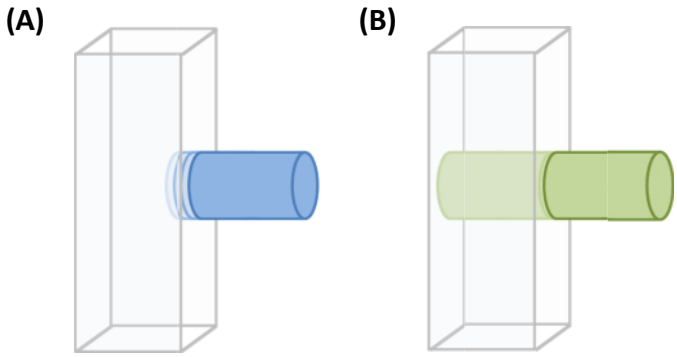

Fig. 5.9: Illustration of the irradiation of TMPyP with a concentration of 100 µM within a quartz cuvette at different wavelengths; (A) 420 nm; shielding effect due to a high absorption resulting in irradiation of a small volume; (B) 520 nm: low absorption resulting in an irradiation of an optimal volume.

The irradiation of TMPyP in the Soret band at 420 nm is followed by a high absorption and might lead to a low irradiated volume within the solution. Irradiation with 520 nm, which is 70% transparent for light at this wavelength, leads to a higher illuminated volume and therefore more cells. This shielding effect was confirmed by a lower signal intensity that was

detected when irradiating with 420 nm, compared to 520 nm. For these artificially high concentrations it might be good for signal recording to irradiate in wavelength regions of the photosensitizer, that are transparent to a certain extent in order to avoid effects of photosensitizer over-saturation and to guarantee a full irradiation of the sample.

Nevertheless, high concentrations in the range of 100 µM are only of scientific interest, especially when characterizing the photosensitizer and its properties. For obtaining the vitality of cells in the presence of photosensitizer molecules, lower concentrations are preferred. On the one hand, dark toxicity can be avoided and the influence of the photodynamic effect during singlet oxygen detection and the laser irradiation might also be minimized. On the other hand, as already mentioned very low binding saturation values (1.7 $nmol/10^6$ cells) of TMPyP to *C. albicans* have been reported by Quiroga *et al.* [7]. Therefore, irradiation with the appropriate wavelength enhances the generation of singlet oxygen dramatically. Exemplarily, the concentration of 1 µM TMPyP was incubated in *C. albicans*. The singlet oxygen luminescence signal detected for this low concentration at an irradiation wavelength of 420 nm shows only one decay time of $t_D = (9.2 \pm 0.9)\mu s$, but a rise time was not detected. However, this decay time is controversially discussed. Baier *et al.* reported a decay of ≈ 9 µs to be the decay time of singlet oxygen in aqueous suspensions of lipid droplets, or in aqueous suspensions of human colonic cancer cells (HT29) when incubated with the porphyrin Photofrin [1]. In contrast to that, a decay time of $t_D = (9.4 \pm 0.9)\mu s$ was assigned to the decay of the excited triplet-T_1-state of TMPyP by Regensburger *et al.* They showed a singlet oxygen luminescence signal from HT29 ($4 \cdot 10^6\ CFU\ mL^{-1}$) which were incubated 60 min with TMPyP (250 µM) while keeping the solution at an air-saturation level for oxygen [15]. Regensburger *et al.* detected the localisation of TMPyP within the cytoplasm of HT29 cells in non-specified vesicles via fluorescence microscopy after incubation with 250 µM for 60 min. Neither a localisation in the plasma membrane nor in the cell nucleus was observed. From this Regensburger *et al.* concluded a singlet oxygen decay time shorter than in pure water due to the presence of proteins in the cytoplasm, which act as singlet oxygen quencher and the decay time of singlet oxygen was estimated to be below 0.5 µs [15]. To confirm this assumption, a variation of the oxygen concentration in the surrounding of the cells was done. An oxygen decrease to 70% of the air-saturation led to an increase of the decay time of the signal to 14 µs which indicated the assignment to the excited triplet state of the photosensitizer.

A similar behaviour was observed with the porphyrin XF73 in HT29 cells, which was detected also in the cell membrane by fluorescence microscopy [15]. In the XF73 study the decay time was increasing with decreasing oxygen concentration in the extracellular

surrounding and was hence assigned to the decay time of the excited triplet-T_1-state of the photosensitizer [15]. These contrary interpretations of the decay time of singlet oxygen luminescence signals in HT29 cells by Baier and Regensburger was due to different handling and knowledge about the oxygen concentration and consumption during the singlet oxygen detection [4, 5, 21]. Therefore one important point must be the constancy of the oxygen concentration. With the needle sensor and the new gas flow unit, the extracellular oxygen concentration can now be well defined during the singlet oxygen detection.

Similar findings are reported as well by Regensburger *et al.* for TMPyP in prokaryotic cells but the comparison with these cells and HT29 cannot help to explain the rise and decay times detected in suspensions with *C. albicans*, since it has different cell wall properties and thus different possible localisation of TMPyP. A final assignment of the decay time detected in *C. albicans* for 1 μM TMPyP at 420 nm can be done only with additional measurements like a variation of the extracellular oxygen concentration or the addition of sodium azide. Since the sensitivity in the detection of singlet oxygen was increased by the optimal irradiation wavelength (tunable laser system), much smaller amounts of photosensitizer molecules can be used.

The presence of at least 2 decay times in the singlet oxygen luminescence generated by 10 μM of TMPyP and irradiated with 420 nm and additionally the difference to the signal for 1 μM and 100 μM TMPyP lead to the assumption that the deactivation of the photosensitizer and singlet oxygen takes place in different surroundings. The prevalence of the respective decay times seems to be dependent on the photosensitizer concentration. Since a low concentration of porphyrins is offered to the cells they might be not yet saturated with 1 μM and an uptake of almost every TMPyP molecule might occur. Enhancing the photosensitizer concentration an over-saturation might start, leaving TMPyP in the exterior of the cells.

The difference in the surrounding might be for example a high and low oxygen concentration or two environments of which one is dominated by water and the other one by lipids. The latter hypothesis might be supported by a study of Ragàs *et al.* who detected a double localisation of TMPyP, at DNA (inside) and the cell wall (outside) of *E. coli* cells. Furthermore, they stated that singlet oxygen is able to cross the cell wall of these microorganisms [3]. Although these findings might not be directly conferrable to *C. albicans*, they show that TMPyP has the ability to localize at different sites of the cell.

In addition, assuming two different oxygen concentrations at two sites of singlet oxygen generation by two different localisations of TMPyP might also lead to a change of the meaning of the rise and decay time(s) of the singlet oxygen luminescence signal. From previous studies with TMPyP in pure H_2O it is known that a change of the meaning of rise and decay times occurs around 50% of air saturation ($[O_2] = 135\ \mu M$). The smaller the oxygen concentration the lower is the possibility for the deactivation of the excited triplet-T_1-state of TMPyP and therefore its decay time becomes longer.

If the TMPyP is located inside and outside the *Candida* cell and assuming that the oxygen concentration in the cell is below 135 μM we consider the following model. In that model the complex cellular environment is simplified by neglecting the presence of chemical singlet oxygen quenchers and only the oxygen concentration influences the signal. In the intracellular region with an assumed oxygen concentration below 135 μM the rise time of the singlet oxygen luminescence signal is assigned to singlet oxygen and the decay time to the triplet-T_1-state of TMPyP. In the extracellular region at air-saturation these times are assigned the opposite way (see tab. 5.6).

region	intracellular	extracellular, H_2O
$\boldsymbol{[O_2]}$	$< 135\ \mu M$	$270\ \mu M$
$\boldsymbol{t_R}$	singlet oxygen	TMPyP triplet-T_1-state
$\boldsymbol{t_D}$	TMPyP triplet-T_1-state	singlet oxygen

Tab. 5.6: Overview of the assignment of the rise and decay time of the singlet oxygen luminescence signal in the intracellular region with low oxygen concentration and in the extracellular region with high oxygen concentration.

If now these two singlet oxygen luminescence signals overlay, two rise and two decay times might be mixed and the evaluation technique might be not sufficient. Similar findings were presented by Baier *et al.* who investigated a model of singlet oxygen decay in different surroundings by irradiating a photosensitizer at the same time in H_2O and in lipids under exclusion of interfusion of the two 'solvents'. In that study a singlet oxygen luminescence signal with a normal rise but a clear bi-exponential decay was observed with two inherent singlet oxygen decay times of $(3.5 \pm 0.5)\mu s$ in H_2O and $(16.5 \pm 2.5)\mu s$ in lipids [22]. For our data determined by irradiation of *Candida* at 420 nm with a TMPyP concentration of 10 μM, we obtained a bi-exponential decay (fig. 5.7 (B)). In our model, the decay time $t_{D2} = 22\ \mu s$ describes the deactivation of the excited photosensitizer in the intracellular and the shorter decay time $t_{D1} = 4.8\ \mu s$ describes the decay of singlet oxygen in the extracellular region. For

the rise time this applies *vice versa*, but an effect can not directly be detected since the more intense signal seems to overlay the other one completely for the rise part.

If the obtained two decay times at 10 μM are due to different oxygen concentrations in the extracellular and intracellular region of *Candida*, a variation of the oxygen concentration in the cell surrounding might lead to a disappearance of the second decay time because then the photosensitizer would be in two different cellular regions but there the oxygen concentration would be equal. With this experiment also the intracellular oxygen concentration could be estimated.

5.4 CONCLUSIONS

Different quenching of singlet oxygen leads to different decay times in different parts in or in adjacency to the microorganism. The diverse quenching possibilities of singlet oxygen by proteins, fatty acids, polysaccharides, *etc.*, or water depend on the localisation of the photosensitizer. The rise and decay times of the singlet oxygen luminescence signal in *C. albicans* biofilm and planktonic cells are both different from the decay times generated by pure TMPyP in H_2O.

Experiments with the Nd:YAG laser

Singlet oxygen luminescence signals from non-washed planktonic solutions with TMPyP had clear rise and decay components which were accurately evaluable. There, the singlet oxygen decay is dominated by a water environment and is in the range around 3.5 μs, which might be anticipated. For washed cells a greater variation of signals was detected, ranging from no signal mainly for 10 μM to evaluable signals for 100 μM of the used photosensitizer concentration. It can be assumed from these measurements that the photosensitizer is not strongly attached to the exterior of the cells. Nevertheless, photokilling of planktonic *C. albicans* cells after one washing procedure is described in literature [7].

A singlet oxygen luminescence generated after incubation with TMPyP in wet and dry, or washed and non-washed biofilms were detected for the first time within this study. The signal-to-noise ratio was proper enough to evaluate a rise and decay time. The singlet oxygen luminescence from *C. albicans* biofilms did not strongly depend on a washing procedure or a drying of the biofilm for 1 h and revealed almost unchanged rise and decay times. This can be understood, because the biofilm matrix is developed in order to protect the cells from external influences and therefore it is gel-like and highly hydrated due to the presence of hydrophilic polysaccharides [9].

Interpretations of the meaning of the rise and decay time are still under debate. The accuracy of experiments with biofilms, which are complex surfaces, critically depends on accurate preparation methods and optimisation of the experimental setup due to its geometry. Slightly different criteria like shorter irradiation time, different laser pulse frequency or irradiation power and especially different geometry of irradiation and detection of the singlet oxygen photons leads to dramatic changes in the intensity of the

singlet oxygen luminescence. Scattering processes due to different biofilm consistency, *e.g.* biofilm thickness or growth properties in the Petri dish are still a challenge for the detection of singlet oxygen luminescence.

Experiments with the new tunable laser system – planktonic cell suspensions

The experimental setup for detecting singlet oxygen was optimised with a tunable laser system and a gas flow unit. Therefore, photosensitizer concentrations below 5 µM can be used, because they can be irradiated properly in their absorption maxima. Very low photosensitizer concentrations usually are found after cell washing. In this study the setup was tested first on non-washed *C. albicans* cells with a photosensitizer concentration of 1 µM. A higher sensitivity resulting in a better signal-to-noise ratio was detected even at this low concentration. Nevertheless, when dealing with artificially high concentrations, as was done herein with 100 µM, an irradiation in the Q-band should be preferred due to over-saturation in the absorption when irradiating in the Soret-band. This avoids possible 'shielding' effects which would result in a decrease of the irradiated volume and thus total number of cells in the laser irradiation volume (fig. 5.9).

Different rise and decay times of the singlet oxygen signals were detected in *C. albicans* cell suspensions dependent on the photosensitizer concentration. Interpretations of the rise and decay times are still controversially discussed. For example a decay time of ≈ 9 µs detected after irradiation of a cell suspension with 1 µM TMPyP might be assigned as well to the photosensitizer triplet decay in a cellular region with low oxygen concentration as shown by Regensburger *et al.* or a decay of singlet oxygen in lipid environment as described by Baier *et al.* for HT29 cells [1, 15].

Based on the findings for 10 µM TMPyP irradiated at 420 nm a model is proposed, explaining the bi-exponential decay with a possible double localisation of TMPyP in the intra- and extracellular region resulting in different oxygen concentrations in the environment of the photosensitizer. However, this model does not take chemical quenching into account. The different rise and decay parts in dependency of the different photosensitizer concentration suggest either different oxygen concentrations in the surrounding of the photosensitizer due to bi-localisation or singlet oxygen decay in lipid-/ water–/ protein-containing surrounding, respectively. Probably these effects also have to be taken into account together, which illustrates how fast the complexity for the theoretical description of a luminescence signal when working with cells is growing.

The addition of the singlet oxygen quencher sodium azide as well as triplet spectroscopy should be conducted in future experiments to clarify the assignment of the rise and decay times. Additionally the change of the extracellular oxygen concentration influences the decay time of the photosensitizer in the extracellular region.

The gradual change of the photosensitizer concentration in the cell suspension can be followed in smaller concentration steps and might give additional insights in the uptake process. A washing procedure should be carried out, in order to eliminate photosensitizer molecules in the H_2O surrounding and to detect singlet oxygen luminescence generated only by adherent photosensitizer molecules.

With the new experimental setup a dose finding would be interesting, finding the minimal photosensitizer concentration that has to be used in order to detect singlet oxygen luminescence from cells. Therefore a variation of the

- photosensitizer concentration
- incubation time
- extracellular oxygen concentration
- cell concentration
- laser parameters (power, irradiation time)

might be carried out. With the enhanced sensitivity of the tunable laser an enhancement of the cell concentration, which was usually done for having a higher overall photosensitizer concentration after the washing procedure might be obsolete then.

One of the main ideas of the investigation of the singlet oxygen luminescence in cell suspensions was at first to use different photosensitizers, which locate at different sites of the cell. Since the porphyrins TMPyP and XF73 might tend to localize in different cellular structures, the site of singlet oxygen generation can be different and might provide information about the respective surrounding depending on the decay time of the excited triplet-T_1-state and the decay of singlet oxygen. The phototoxicity tests in combination with luminescence measurements should provide a better understanding of the effectiveness of different photosensitizers regarding photodynamic inactivation of microorganisms. Such a comparison should elucidate the subcellular location of the photosensitizers and the site of singlet oxygen generation, which in turn may help to optimize the chemical structure of photosensitizers with chemical design of specific photosensitizers for better penetration and attachment.

5.5 REFERENCES

1. Baier, J., et al., *Time-resolved investigations of singlet oxygen luminescence in water, in phosphatidylcholine, and in aqueous suspensions of phosphatidylcholine or HT29 cells.* J Phys Chem B, 2005. **109**(7): p. 3041-6.
2. Baier, J., et al., *Direct detection of singlet oxygen generated by UVA irradiation in human cells and skin.* J Invest Dermatol, 2007. **127**(6): p. 1498-506.
3. Ragas, X., M. Agut, and S. Nonell, *Singlet oxygen in Escherichia coli: New insights for antimicrobial photodynamic therapy.* Free Radic Biol Med, 2010. **49**(5): p. 770-6.
4. Maisch, T., et al., *The role of singlet oxygen and oxygen concentration in photodynamic inactivation of bacteria.* Proc Natl Acad Sci U S A, 2007. **104**(17): p. 7223-8.
5. Regensburger, J., et al., *A helpful technology--the luminescence detection of singlet oxygen to investigate photodynamic inactivation of bacteria (PDIB).* J Biophotonics, 2010. **3**(5-6): p. 319-27.
6. Pereira Gonzales, F. and T. Maisch, *Photodynamic inactivation for controlling Candida albicans infections.* Fungal Biol, 2012. **116**(1): p. 1-10.
7. Quiroga, E.D., M.G. Alvarez, and E.N. Durantini, *Susceptibility of Candida albicans to photodynamic action of 5,10,15,20-tetra(4-N-methylpyridyl)porphyrin in different media.* FEMS Immunol Med Microbiol, 2010. **60**(2): p. 123-31.
8. Baillie, G.S. and L.J. Douglas, *Matrix polymers of Candida biofilms and their possible role in biofilm resistance to antifungal agents.* J Antimicrob Chemother, 2000. **46**(3): p. 397-403.
9. Flemming, H.C. and J. Wingender, *The biofilm matrix.* Nat Rev Microbiol, 2010. **8**(9): p. 623-33.
10. Al-Fattani, M.A. and L.J. Douglas, *Biofilm matrix of Candida albicans and Candida tropicalis: chemical composition and role in drug resistance.* J Med Microbiol, 2006. **55**(Pt 8): p. 999-1008.
11. Eichner, A., et al., *Dirty hands: photodynamic killing of human pathogens like EHEC, MRSA and Candida within seconds.* Photochem Photobiol Sci, 2012. **12**(1): p. 135-47.
12. Maisch, T., et al., *Fast and effective: intense pulse light photodynamic inactivation of bacteria.* J Ind Microbiol Biotechnol, 2012. **39**(7): p. 1013-21.
13. Harriott, M.M. and M.C. Noverr, *Candida albicans and Staphylococcus aureus form polymicrobial biofilms: effects on antimicrobial resistance.* Antimicrob Agents Chemother, 2009. **53**(9): p. 3914-22.
14. Pereira Gonzales, F., *Photodynamic inactivation of microbial biofilms: impact of Hsp70 expression and non-invasive optical monitoring of oxygen during photodynamic inactivation.* Dissertation, Universität Regensburg, 2013.
15. Regensburger, J., *Spektroskopische Untersuchungen zur Singulett-Sauerstoff-Lumineszenz in Biomolekülen, Bakterien und Zellen.* Dissertation, Universität Regensburg, 2010: p. 202.
16. Duan, J. and D.L. Kasper, *Oxidative depolymerization of polysaccharides by reactive oxygen/nitrogen species.* Glycobiology, 2011. **21**(4): p. 401-9.
17. Kon, S.S., S., *Depolymerization of polysaccharides by active oxygen species derived from a xanthene oxidase system.* Journal of Food Biochemistry, 1977. **1**: p. 12.
18. Egorov, S.Y. and A.A. Krasnovskii, *Quenching of Singlet Molecular-Oxygen by Components of Media Used for Isolation of Chloroplasts and Investigation of Their Photosynthetic Activity.* Soviet Plant Physiology, 1986. **33**(1): p. 5-8.
19. Kuimova, M.K., G. Yahioglu, and P.R. Ogilby, *Singlet oxygen in a cell: spatially dependent lifetimes and quenching rate constants.* J Am Chem Soc, 2009. **131**(1): p. 332-40.
20. Maisch, T., et al., *Photodynamic effects of novel XF porphyrin derivatives on prokaryotic and eukaryotic cells.* Antimicrob Agents Chemother, 2005. **49**(4): p. 1542-52.
21. Baier, J., et al., *Time dependence of singlet oxygen luminescence provides an indication of oxygen concentration during oxygen consumption.* J Biomed Opt, 2007. **12**(6): p. 064008.
22. Baier, J., *Lumineszenz-Untersuchungen zur Generierung und Relaxation von Singulett-Sauerstoff in zellulärer Umgebung.* Dissertation, 2005: p. 184.

Chapter 6

Spectroscopic and Phototoxicity Studies of Photosensitizers in Surfaces

Polymeric surfaces of different material were doped with photo-sensitizers in order to create self-disinfecting surfaces using the aPDT principle. The properties of the photosensitizers after polymerization were investigated with different spectroscopic methods. The generation of singlet oxygen was determined and the decay of the excited triplet-T_1-state of the photosensitizer and the decay of singlet oxygen were monitored. The challenge in the assignment of rise and decay time of the singlet oxygen luminescence signal is described in detail. The photosensitising properties of the surfaces were investigated with a phototoxicity assay of *Staphylococcus aureus*.

6.1 INTRODUCTION

In 1986 Dahl *et al.* already described a method to follow the toxicity of singlet oxygen without the influence of other reactive species generated via type-I mechanisms with physical separation of the photosensitizer and bacteria [1]. Being a neutral molecule, singlet oxygen is assumed to show normal diffusion in air, contrarily to the other reactive oxygen species, and the lifetime of singlet oxygen is only limited by collisions with other air molecules. In that study, the half-life of singlet oxygen was determined by changing the distance of the site of singlet oxygen generation and the position of the bacteria to be killed by singlet oxygen. These experiments yielded a half-life for singlet oxygen of $(24 \pm 6)\ ms$ which confirmed findings of the singlet oxygen decay time in the range of milliseconds $(35 - 86\ ms)$. That range was detected by the same group in water-saturated air at $5°C$ with $1\ atm$ pressure in 1983 [2]. These studies provide insights into an interesting field of antimicrobial PDI, where photosensitizer and pathogen are separated during the photokilling in contrast to the phototoxicity experiments as described for example in chapter 3. The generated singlet oxygen molecules reach the pathogen by diffusion, and the diffusion length or radius of biologically relevant action is limited by the lifetime of singlet oxygen. That concept is considered as the basis for the herein introduced investigations.

The effect of photokilling of bacteria without direct contact of photosensitizer and microorganisms offers many interesting features and potential application. Antibacterial surfaces or also self-cleaning surfaces, which work with the PDI principle, are of great interest due to their preventive character for infections (see chapter 1). Such surfaces may help to reduce the transmission of multi-resistant microorganisms, which is a great issue in hospital hygiene. Since the photodynamic process of such surfaces in theory does not lead to a consumption of photosensitizer if abrasion and photobleaching is ideally neglected, a long-term, constant prevention of microorganism settlement and growth will be given.

Photoactive surfaces were developed and investigated in this study in regard to possible antibacterial properties by doping polymeric layers with photosensitizers. The active surfaces are applied as a varnish in order to cover the surface of solid material. It has been reported that upon polymerisation of a photosensitizer oligomerisation and thus self-quenching could be prevented, leading to enhanced quantum yields for singlet oxygen formation as well as a higher photostability [3]. The study on the physical and chemical characteristics of photosensitizers linked to surfaces necessitated the detection of the singlet

oxygen generation that is performed directly via its luminescence at 1270 *nm* and indirectly via the formation of tri-iodide [4].

Different types of surfaces with different classes of photosensitizers were produced and investigated in regard to photostability, singlet oxygen generation and phototoxicity against bacteria. Some known photosensitizers like TMPyP, MB, PN or TPP have been studied already in simple solutions and in regard to their photophysical properties influencing singlet oxygen generation and their phototoxic efficacy. TMPyP, MB, and TPP were therefore polymerized into cellulose acetate (CA) surfaces. This material was used as a complete surface and did not cover another material. Derivatives of PN or TPP (TPP-O-A/B and PN-O-A/B) were newly synthesized with the addition of side chains and were polymerized into polyurethane (PU) via chemical linking into the polymer network. PU was investigated as a varnish layer on the common carrier material poly-methylmethacrylate (PMMA).

The aims of the surface studies were to dope different photosensitizers into two different polymers (CA alone or PU as a layer on PMMA) and

(1) to investigate a possible photosensitizer leaking out of the surface,
(2) to detect singlet oxygen generated in these surfaces directly via its luminescence and indirectly via the use of chemicals,
(3) to determine and assign the rise and decay part of the luminescence signal to the photosensitizer triplet decay or the decay of singlet oxygen,
(4) to investigate the structure of the surfaces via microscopic techniques,
(5) and to determine the phototoxic effect exemplarily against *Staphylococcus aureus* in dependency of the photosensitizer concentration and the irradiation time.

The decay time of singlet oxygen in air is estimated to be in the range of milliseconds [1, 2] and cannot be detected with the present experimental setup due to the high repetition frequency of the used excitation laser. Therefore, only indirect methods like the formation of tri-iodide or a phototoxic assay with microorganisms was used to detect singlet oxygen that escaped the surface layer by diffusion. However, singlet oxygen molecules, which are decaying inside the polymeric surface layer, can be detected by its luminescence that allows an estimation of possible quenching effects on either the photosensitizer or singlet oxygen. Without knowing the oxygen concentration in the polymeric surface layer it is nonetheless difficult to interpret the singlet oxygen luminescence signals in regard to the assignment of rise and decay times, which might exhibit a multi-exponential manner (non-first order kinetics).

6.2 EXPERIMENTAL SECTION

6.2.1 Chemicals

The water-soluble phenothiazine MB and porphyrin TMPyP, the non-water-soluble porphyrin TPP and NaN_3 were purchased from Sigma–Aldrich (Steinheim, Germany). TPP-O-A/B and PN-O-A/B were synthesized in cooperation with the Institute of Organic Chemistry, University of Regensburg.

6.2.2 Surfaces

6.2.2.1 Cellulose acetate (CA) doped with photosensitizer

Cellulose acetate was doped with MB, TMPyP or TPP at a concentration of $2.5 \cdot 10^{-5}\ M$ or $10^{-4}\ M$. Therefore, 360 mg of cellulose acetate and 7 mL acetone were mixed resulting in a concentration of approximately 50 $mg\ mL^{-1}$. The photosensitizers MB and TMPyP were dissolved in *acqua dist.* and TPP was dissolved in benzene, each with the appropriate concentration between 10– 250 µM before the drying process of the surface (see 2.2.1).

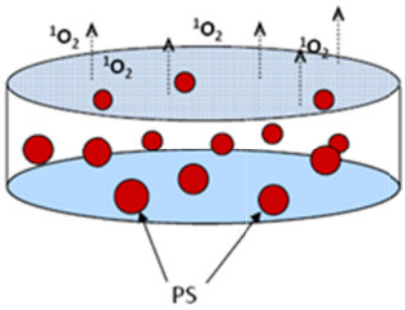

Fig. 6.1: Cellulose acetate doped with photosensitizer (PS) molecules; singlet oxygen ($^1O_2$) is generated upon light exposure by the PS and its diffusion from the surface is indicated by the arrows.

6.2.2.2 Polyurethane (PU) doped with photosensitizer on PMMA polymer plate

TPP-O-A/B and PN-O-A/B were polymerized via linking hydroxyl groups ($-OH$) with isocyanates ($-CNO$) into polyurethane (PU) as described in 2.2.2. PU was sprayed as a layer onto a PMMA polymer plate of 2 mm thickness (fig. 6.2). Different photosensitizer

concentrations and different thicknesses of the PU layer were prepared and are listed in table 2.1.

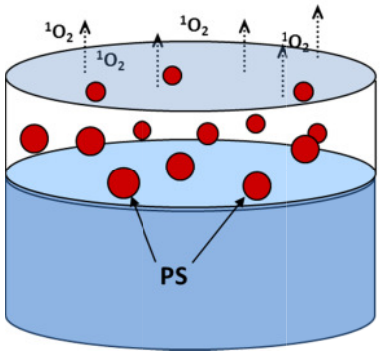

Fig. 6.2: Polyurethane (PU) doped with photosensitizer (PS) molecules; PU (thicknesses: 20-70 µm) was sprayed as a layer onto a PMMA polymeric plate (thickness: 2 mm); singlet oxygen ($^1O_2$) is generated upon light exposure by the PS and its diffusion from the surface is indicated by the arrows.

6.2.3 Singlet oxygen luminescence detection by direct spectroscopic methods

The cellulose acetate surfaces were irradiated with a Nd:YAG-laser at $\lambda = 532\,nm$, laser power output of $P = 50\,mW$, repetition rate of $f = 2\,kHz$, and 50 000 laser pulses ($= 25\,s$ irradiation time) with a pulse duration of $70\,ns$. With the given parameters an energy of $E_p = 2.5 \cdot 10^{-5}\,J$ was applied.

The PMMA polymer plates coated with a photosensitizer-doped PU-layer were excited with a tunable laser system at $\lambda = 420\,nm$, laser power output $P = 360\,mW$, repetition rate of $f = 1\,kHz$, and 10 000 laser pulses ($= 10\,s$ irradiation time) with a pulse duration of $4 - 7\,ns$. With the given parameters an energy of $E_p = 3.6 \cdot 10^{-4}\,J$ per pulse was applied.

Singlet oxygen luminescence was detected using an interference filter with a maximal transmission at $1270\,nm$ and a spectral width of FWHM = $30\,nm$ in front of the photomultiplier. To achieve spectral resolution, the luminescence was measured at different wavelengths using different interference filters in the range of $1100 - 1400\,nm$. The resulting values were fitted with Lorentz-shaped function yielding a maximum at $\lambda = 1275\,nm$.

6.2.4 Photostability

The PMMA polymer plates coated with a photosensitizer-doped PU-layer were irradiated with a broadband lamp (Waldmann PIB 3000, see 2.6.3) with a power of 50 $mW\,cm^{-2}$ at the level of the samples. After the irradiation absorption spectroscopy was carried out and compared to the non-irradiated samples.

6.2.5 Indirect detection of singlet oxygen with potassium iodide (KI)

An overall volume of 3 mL KI with a concentration of 0.12 M in H_2O was filled in a glass surrounding a polymer plate. In case of the PMMA polymer plates with PU-layer the photoactive side was turned upside. The samples were irradiated for 0, 5, 10, 15, and 30 min and after each time point 2 mL of the solution was spectrally recorded, in order to monitor the formation of tri-iodide I_3^-. After absorption spectroscopy the solution was filled back into the glass for further irradiation and monitoring steps.

6.2.6 Transmission electron microscopy (TEM)

In order to investigate the microscopic structure of the PU-layer on PMMA with and without the photosensitizer and obtain differences of non-irradiated and irradiated samples, TEM was used in cooperation with the Central EM Lab at the University Hospital Regensburg (see 2.5.2). TEM was carried out with the photosensitizer TPP-O-A; as irradiation parameters 60 min of irradiation time with 50 $mW\,cm^{-2}$ at the level of the samples (Waldmann PIB 3000, see 2.6.3) were chosen.

6.2.7 Phototoxicity experiments

In this study the bacterium *S. aureus* was exemplarily used. As described in sub-unit 2.7.4, 50 µl of *S. aureus* suspension ($OD = 0.6 \triangleq 5 \cdot 10^6 – 5 \cdot 10^7\ CFU\ mL^{-1}$) was dropped on the PU-surface containing TPP-O-A or PN-O-A and dried 1.5 h under a laminar flow. Samples were illuminated with the Waldmann PIB 3000 (emission $\lambda > 400\ nm$) with a maximal light intensity of 50 $mW\,cm^{-2}$ at the level of the illuminated samples. 3 different irradiation times (10, 30, 60 min) with photosensitizer concentrations of 0, $1 \cdot 10^{-4}$, and $2 \cdot 10^{-4}\ M$ were used. For each condition the dark control was the reference.

6.3 RESULTS AND DISCUSSION

In this sub-unit first, the results from investigations on cellulose acetate are presented, because they were produced and investigated before the PU-surfaces and therefore, the results and discussion will be used as the basis for the PU studies.

Different diffusion coefficients of oxygen in different surroundings like air, H_2O, PMMA, or CA at 1 atm are displayed in the following table 6.1. These values give an overview how the diffusion coefficient of oxygen can change by orders of magnitude in different solvents or materials.

solvent/ material	**diffusion coefficient** $[cm^2\ s^{-1}]$	**temperature [°C]**	**citation**
air	2.09×10^{-1}	25	[5]
air	2.04×10^{-1}	20	[5]
H_2O	2.10×10^{-5}	25	[5]
H_2O	2.38×10^{-5}	20	[5]
PU	3.2×10^{-7}	-	[6]
PMMA, film	3.5×10^{-8}	25	[7]
PMMA, bulk glass	3.3×10^{-9}	25	[7]

Tab. 6.1: Diffusion coefficients for oxygen in different solvents and materials.

In addition to table 6.1, Wolinska-Grabczyk *et al.* investigated the diffusivity coefficients for oxygen in structurally different polyurethane (PU) membranes at 30°C and reported values in the range of $10^{-7}\ cm^2 s^{-1}$ [8] which are consistent with the value reported by Jesenska *et al.* [6].

6.3.1 Cellulose acetate (CA) with MB, TMPyP and TPP

Cellulose acetate (CA) was doped with MB, TMPyP or TPP at concentrations of 25 µM for all photosensitizers and additionally a concentration of 100 µM in case of TMPyP. For the investigations with spectroscopic methods the CA-surface was kept in different surroundings that are listed in table 6.2.

Photosensitizer	**concentration [μM]**	**surrounding**
TMPyP	25	**air**
	25	H_2O
	25	H_2O + 4 mM NaN_3
	25	H_2O + 10 mM NaN_3
	100	**air**
	100	$EtOH$
	100	H_2O + 1 mM NaN_3
MB	25	**air**
	25	H_2O
	25	H_2O + 1 mM NaN_3
	25	H_2O + 4 mM NaN_3
	25	H_2O + 10 mM NaN_3
	25	$EtOH$
TPP	25	**air**
	25	H_2O
	25	D_2O
	25	$EtOH$

Tab. 6.2: Overview of the CA-surfaces doped with different photosensitizers; the concentrations, the surrounding of the probes are given as well.

6.3.1.1 Absorption spectra of MB, TMPyP, and TPP in CA

The absorption spectra of the photosensitizers MB, TMPyP and TPP with a concentration of 25 μM in CA were determined and compared to the spectra in solution. Within experimental accuracy (2 nm) no shifts of the absorption maxima of either TMPyP or TPP were recorded. MB showed a red-shift at its absorption peak at 664 nm of 2.5 nm. Shifts in the spectrum indicate a change in the electronic system of the PS and might suggest aggregation or dimerisation effects, which was shown for MB to occur in solution (chapter 3). An increase of the sharpness of all absorption peaks (smaller half-width) was detected, which is a typical behaviour for substances in the solid-state due to less degree of freedom for the molecule (data shown in [9]).

Leakage of the photosensitizers

The CA surfaces were tested for their antibacterial properties and therefore, it is essential to know how stable the photosensitizers are cross-linked with the polymer. Especially MB and TMPyP are water-soluble and were not chemically linked to the polymer; thus a release of the PS into the water-surrounding was investigated. The surfaces were placed for $2\,h$ in H_2O. After that, the aqueous solvent was investigated by absorption spectroscopy.

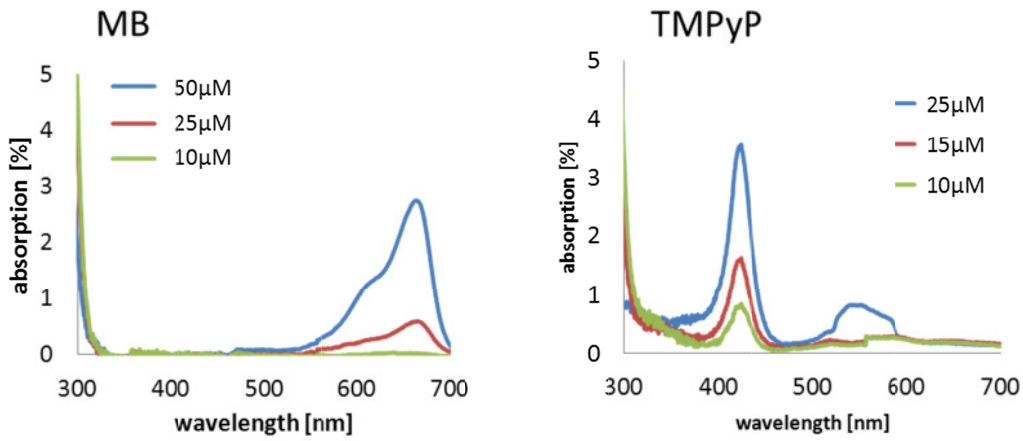

Fig. 6.3: Absorption spectra of the aqueous solvent in the surrounding of cellulose acetate films containing (left) MB and (right) TMPyP with different photosensitizer concentrations between 10 µM and 50 µM; the polymeric films were kept in H_2O for 2 h before the spectroscopy of the aqueous solvent [9].

For both, MB and TMPyP, the aqueous solvent showed peaks at the characteristic absorption maxima at 600 nm (MB) and 420 nm (TMPyP) and a release of photosensitizer in the surrounding water was proven. The release of the photosensitizer molecules increased with increasing photosensitizer concentration in CA. In order to estimate the amount of released photosensitizer molecules, the intensity of the absorption maxima for MB and TMPyP at low concentrations ($0.5 - 10\ \mu M$) in H_2O was compared with the aqueous solvent.

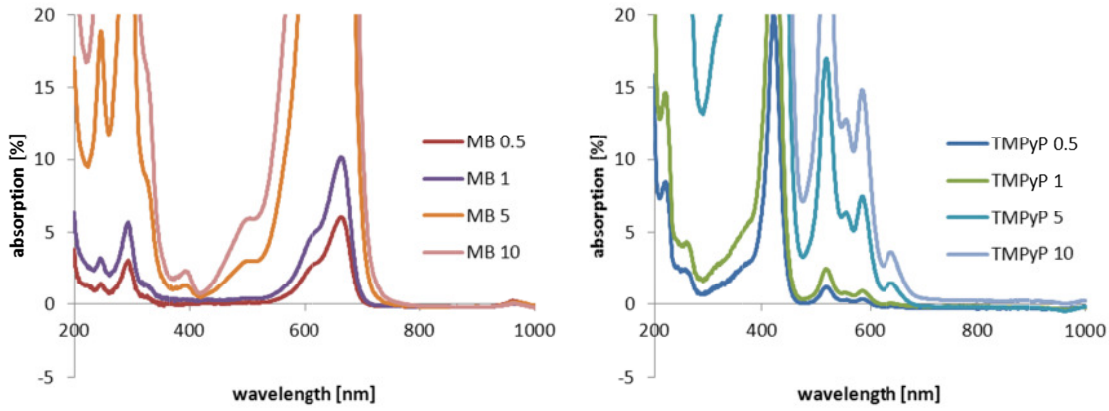

Fig. 6.4: Absorption spectra of solutions of (left) MB and (right) TMPyP in H_2O; the unit of the concentrations is given in µM.

From figure 6.4 in comparison of the percentaged absorption of both photosensitizer maxima at 660 nm (MB) and 420 nm (TMPyP), respectively, the maximal photosensitizer concentration of released from the CA surfaces (aqueous solvent) was below 0.5 µM.

The leakage of the non-water-soluble porphyrin TPP into the aqueous solvent was performed using concentrations between 10– 250 µM. Contrarily to TMPyP and MB, TPP did not show a leakage up to a concentration of 250 µM from the CA-surface.

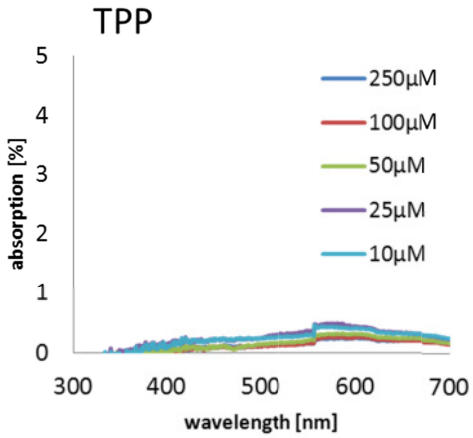

Fig. 6.5: Absorption spectrum of the aqueous solvent in the surrounding of cellulose acetate films containing TPP with different photosensitizer concentrations between 10 µM and 250 µM; the polymeric films were kept in H_2O for 2 h before the spectroscopy of the aqueous solvent [9].

6.3.1.2 Direct detection of the singlet oxygen luminescence at 1270 nm

MB and TMPyP in CA-surfaces

The CA-surfaces containing MB and TMPyP with a concentration of 25 µM were placed and irradiated in quartz cuvettes at $\lambda = 532\,nm$ in order to generate singlet oxygen and to determine the rise and decay times of the singlet oxygen luminescence at 1270 nm. First the luminescence of CA samples that were equilibrated with air at room temperature were recorded. The time-resolved singlet oxygen luminescence signals generated by MB and TMPyP are shown in the following figure 6.6. There, t_1 and t_2 describe the rise or decay times, x_0 the start of the fit and Int is a value that is proportional to the number of singlet oxygen luminescence photons.

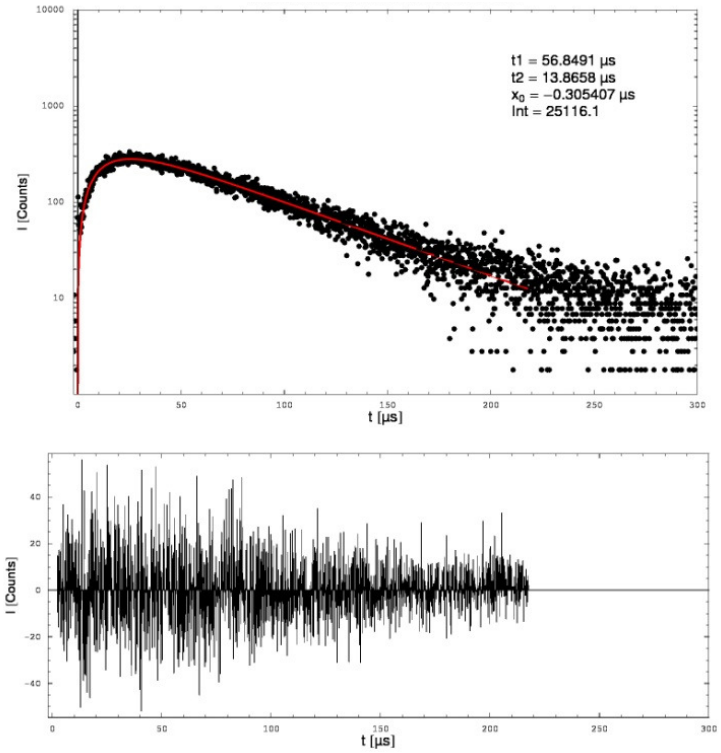

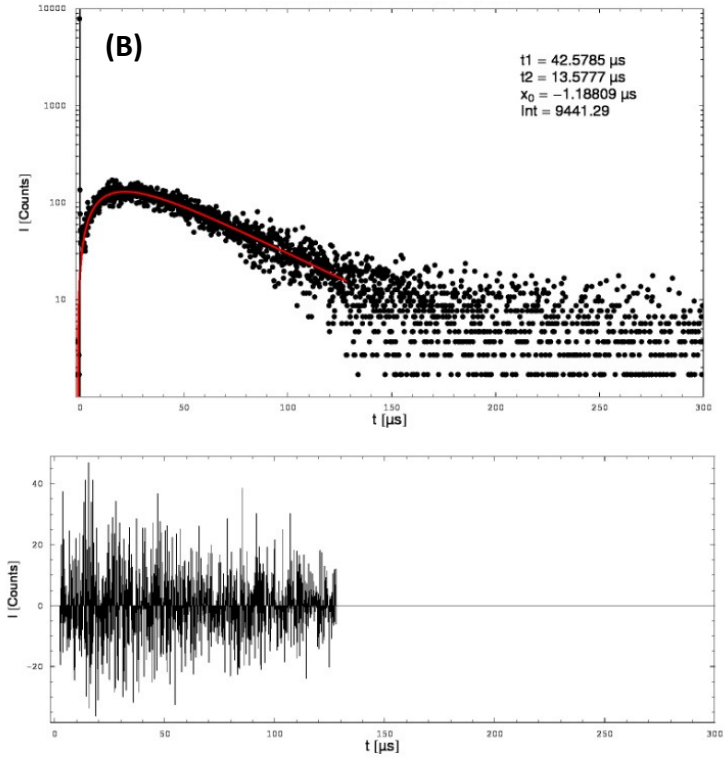

*Fig. 6.6: Time-resolved singlet oxygen luminescence signal, generated by CA-surfaces containing each 25 µM of (A) TMPyP and (B) MB; the CA-surface was irradiated with a Nd:YAG-laser at λ = 532 nm with 50 000 pulses (= 25 s) in a quartz cuvette in air-surrounding at room temperature; herein, $\boldsymbol{t_1}$ and $\boldsymbol{t_2}$ describe the rise or decay times, $\boldsymbol{x_0}$ the start of the fit and **Int** a value that is proportional to the number of singlet oxygen luminescence photons; the deviation of the fit-curve is shown below each singlet oxygen luminescence signal.*

The time-resolved signals have a good signal-to-noise ratio and the rise and decay times were accurately determined and are summarized in table 6.3. In order to attribute the time-resolved signal to the luminescence of singlet oxygen and to exclude any phosphorescence of the photosensitizer spectral resolved single photon counting was performed. Exemplarily, a spectral resolved monitoring of the singlet oxygen luminescence generated by a CA-surface containing 25 µM TMPyP is shown in figure 6.7.

The fit of the spectral resolved luminescence signal with a Lorentz-shaped function (fig. 6.7) clearly yielded a maximum at 1275 nm. It is characterized by a flat bottom line between $1150 - 1400\,nm$ and thus, additional phosphorescence of the photosensitizer was not detected within this measurement.

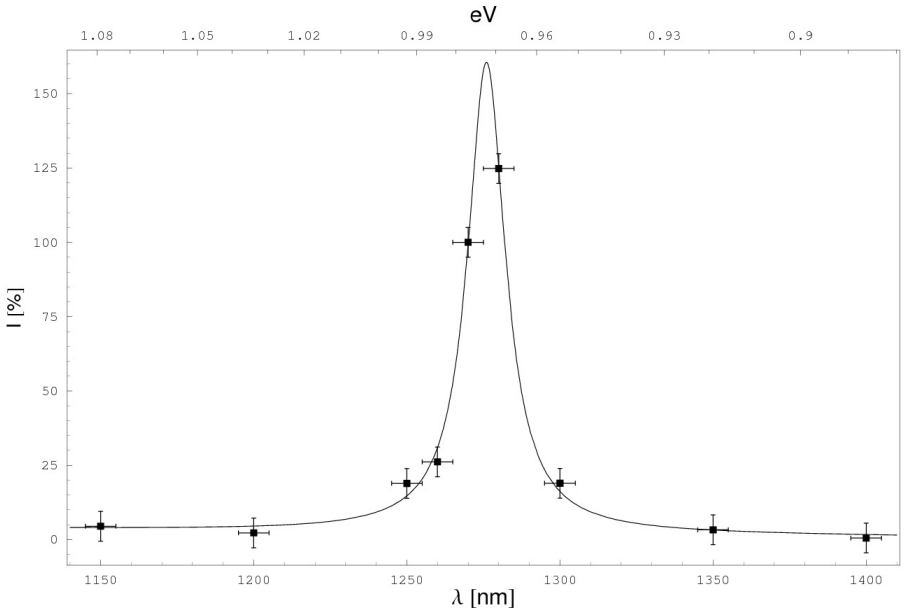

Fig. 6.7: Spectral resolved singlet oxygen luminescence of CA-surfaces containing 25µM TMPyP; the CA-surface was irradiated with a Nd:YAG-laser at λ = 532 nm with 50 000 pulses (= 25 s) in a quartz cuvette in air-surrounding at room temperature; the luminescence was measured using different interference filters in the range of 1100 to 1400 nm; the resulting values were fitted with a Lorentz-shaped function.

As a further step, the external of the CA-surfaces was changed to allow different surroundings such as normal air, H_2O, $EtOH$, or H_2O containing NaN_3 at different concentrations to influence the singlet oxygen luminescence signal of the polymer specimen. For each surrounding condition a new sample of a CA-polymer was used. Table 6.3 displays the results for the rise and decay times of the luminescence signal for the different conditions.

Surrounding of CA polymeric film	**TMPyP (25 µM)**		**MB (25 µM)**	
	t_D [µs]	t_R [µs]	t_D [µs]	t_R [µs]
air	57	14	43	14
$EtOH$	52	15	35	14
H_2O	34	12	23	17
H_2O + 1 mM NaN_3	27	9	24	14
H_2O + 4 mM NaN_3	32	10	28	11
H_2O + 10 mM NaN_3	32	9	28	11

Tab. 6.3: Rise and decay times, t_R and t_D, determined from the singlet oxygen luminescence signals generated by CA-surfaces containing each 25 µM of TMPyP or MB; the CA-surface was irradiated with a Nd:YAG-laser at λ =

532 nm with 50 000 pulses (= 25 s) in a quartz cuvette at room temperature; as different surroundings air, H_2O, EtOH, or H_2O containing different concentrations of NaN_3 were used (experimental accuracy: 15%).

A change in the rise and decay times of the singlet oxygen luminescence signal was detected when altering the surrounding medium of the CA-surface containing TMPyP or MB. For the measurement the CA-surfaces were kept $\approx 1\ min$ before the measurement in the solution. The interpretation of the results will be done by neglecting the diffusion of a small amount ($< 0.5\ \mu M$ for $2\ h$) of photosensitizer molecules into the surrounding medium, as described in 6.3.1.1.

The rise and decay time of the singlet oxygen luminescence signal generated by TMPyP in CA-surfaces remained almost unchanged for $EtOH$-surrounding. Although the decay value t_D of the signal was not reproduced for MB-doped surfaces and the decay time decreased from 43 μs to 35 μs, it must be considered as neglectable change within the experimental accuracy of 15%.

In the investigations of the CA-surfaces with H_2O surrounding for both photosensitizers a shorter decay time t_D compared to air surrounding was obtained, whereas the rise time was constant within experimental accuracy. The rise and decay times of singlet oxygen luminescence generated by 25 μM TMPyP in H_2O were investigated in previous studies in our group in dependency on the oxygen concentration. There a decay time of the excited triplet-T_1-state of TMPyP of $\tau_{T_1} = 34 \mu s$ (as detected for CA-surface doped with TMPyP and surrounded by H_2O), resulting in a rate constant of 0.029 μs^{-1} would indicate an oxygen concentration of 25 μM in H_2O. Furthermore, a variation of the oxygen concentration was carried out with 10 μM MB in H_2O and subsequently a decay time of the excited triplet-T_1-state of MB of $\tau_{T_1} = 34 \mu s$, resulting in a rate constant of 0.043 μs^{-1} would indicate an oxygen concentration of 14 μM in H_2O. Since the photosensitizers in the CA-surface might have a different photophysics due to their solid-state surrounding, the estimations for the oxygen concentration in H_2O are not readily transferrable to the existing oxygen concentrations in CA.

Interestingly, the differences in the concentration of NaN_3, ranging between 1– 10 mM, do not have an influence on decay time t_D of the singlet oxygen signal but a slight decrease above experimental accuracy of the rise time t_R was obtained for TMPyP in the CA-surfaces. Since a decrease in the rise time was not detected for MB in the CA-surfaces, it might be an artefact. In order to see differences in the rise and decay time due to the presence of NaN_3 the concentration range might be chosen higher.

The partial pressure for oxygen is the same in different surroundings like air, H_2O or EtOH. The same applies for polymers. A difference in the partial pressure leads to a diffusion of oxygen from the region with a higher p_{O_2} to a region with a lower p_{O_2} until the difference is 0. The p_{O_2}-value of air at a pressure of 1013 $mbar$ and an oxygen concentration of 20.95% is

$$p_{O_2} = 0.2095 \cdot 1013\ hPa = 212\ hPa = 159\ mmHg = 159\ Torr$$

Diffusion of oxygen is dependent on the diffusion coefficient for each gas, liquid or material like polymers. The equilibrium oxygen concentration in polymers can be determined by multiplication of the solubility S_{O_2} for oxygen with p_{O_2} [10].

Eq. 6.1

$$[O_2] = p_{O_2} \cdot S_{O_2}$$

In most polymers S_{O_2} does not differ to a great extent [11]. Consequently according to equation 6.1 the oxygen concentration in the polymers should not differ to a great extent, assuming a constant p_{O_2}. Taking into account that the oxygen permeability can be expressed with

Eq. 6.2

$$P_{O_2} = S_{O_2} \cdot D_{O_2}$$

and that the solubility S_{O_2} does not vary very much, the permeability for oxygen and therefore the quenching ability of the excited triplet-T_1-state is strongly determined by the diffusion coefficient D_{O_2} in the respective material [11]. Typical diffusion coefficients in polymers are in the range of 10^{-9}– $10^{-8}\ cm^2 s^{-1}$ [12]. As stated by Clough *et al.* diffusion coefficients for oxygen can be up to 4 orders of magnitude smaller than in their liquid counterpart, *e.g.* the diffusion coefficient of a glassy PMMA polymer was described to be $D_{O_2}(glassy\ PMMA, 25°C) = 3.3 \cdot 10^{-9}\ cm^2 s^{-1}$ and for the respective solute cyclohexane is $D_{O_2}(cyclohexane, 30°C) = 5.3 \cdot 10^{-5}\ cm^2 s^{-1}$ [7]. With that, a less quenching of the triplet-T_1-state of the photosensitizer in polymers and thus longer τ_{T_1} decay times can be explained. The decay time of the triplet-T_1-state of a photosensitizer in a solid-state like a glassy polymer was described to be longer than in fluid surrounding, because deactivation of the triplet-T_1-state, such as collisional deactivation, has a lower probability [11].

An equation that takes the influencing parameters for photosensitizer triplet-state quenching into account is given by Lu *et al.* There, for samples in equilibrium with oxygen in the gas phase the following relation is given by a Stern-Volmer-plot

Eq. 6.3

$$\frac{\tau^0}{\tau} = 1 + \frac{4}{1000}\pi\sigma\alpha N_A \tau^0 (S_{O_2} \cdot D_{O_2}) p_{O_2}$$

with τ = decay time of the photosensitizer triplet-T_1-state, τ^0 = decay time of triplet-T_1-state in absence of oxygen, σ = collision radius of the oxygen-dye complex, α = probability that a collision leads to quenching, and N_A = Avogadro number [10, 13, 14].

Some aspects have not been considered for the quenching of the triplet-state or singlet oxygen within the polymer material. As long as it is not yet clear to which amount H_2O, $EtOH$, or especially NaN_3 can diffuse into the surface, the interpretations have to be speculative. Further, MB and TMPyP are both water-soluble and a leakage from the material was detected, but was neglected for this discussion. It is also not clear how much this influences the rise and decay time of the singlet oxygen luminescence signal by a then resulting second overlaying signal. Here, contrary effects might lead to data which are not easily interpretable without additional measurements like triplet spectroscopy.

TPP in CA-surfaces

It was shown that CA-surfaces doped with non-water soluble TPP did not exhibit TPP diffusion into an aqueous surrounding. Therefore, these surfaces were spectroscopically investigated separately, but following the same experimental methods as for TMPyP and MB. Therefore, the TPP-plates were therefore left in different surroundings like H_2O, $EtOH$ and additionally in D_2O. Since NaN_3 did not show any effect in the rise and decay times for TMPyP and MB-containing CA-surfaces, it was not used in this study.

The time-resolved singlet oxygen luminescence signal of TPP in CA-surfaces is shown in figure 6.8. From this measurement the rise and decay time of the luminescence were determined.

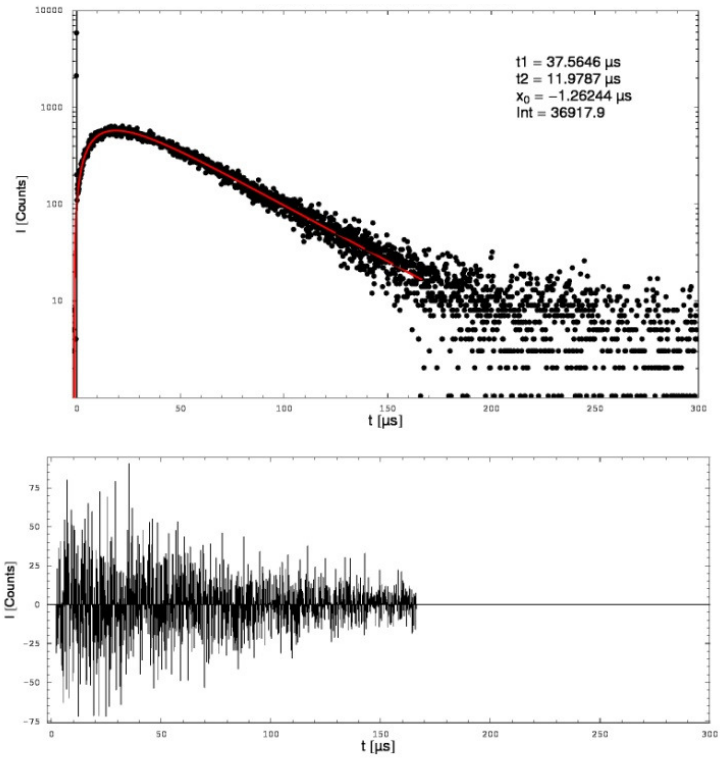

*Fig. 6.8: Time-resolved singlet oxygen luminescence signal, generated by CA-surface containing 25 µM of TPP; the CA-surface was irradiated with a Nd:YAG-laser at λ = 532 nm with 50 000 pulses (= 25 s) in a quartz cuvette in air-surrounding at room temperature; herein, $\boldsymbol{t_1}$ and $\boldsymbol{t_2}$ describe the rise or decay times, $\boldsymbol{x_0}$ the start of the fit and **Int** a value that is proportional to the number of singlet oxygen luminescence photons; the deviation of the fit-curve is shown below each singlet oxygen luminescence signal.*

The time-resolved signal of TPP in cellulose acetate shows a clear rise and decay time without a significant deviance from the theoretical bi-exponential fit-model. The rise and decay time of the singlet oxygen signal generated by irradiation of TPP in CA show a value of $t_D(air) = 37.4\ \mu s$ and $t_R(air) = 12.2\ \mu s$, respectively. When adding H_2O in the surrounding of the surface, the decay time of the signal decreased to $t_D(H_2O) = 29.0\ \mu s$, but $t_R(H_2O) = 10.6\ \mu s$ does not change significantly within experimental accuracy. Interestingly when using D_2O in the surrounding, which is known to enhance the lifetime of singlet oxygen, the $t_D(D_2O) = 38\ \mu s$ is again in the range of $t_D(air)$ and $t_R(D_2O) = 14.2\ \mu s$ just slightly differs from that value determined in air. $t_D(EtOH) = 29.5\ \mu s$, then is again in the range of the value of water, as can be almost confirmed also for $t_R(EtOH) = 8.3\ \mu s$. All rise and decay values are summarized in table 6.4.

Surrounding of polymeric film	TPP (25 μM)		oxygen concentration in solvent [μM]	typical values for τ_Δ in solvent
	t_D [μs]	t_R [μs]		
air	37	12		$1-100\ ms$
H_2O	29	11	270	3.5 μs
D_2O	38	14	238	68 μs
$EtOH$	30	8	1850	14 μs

Tab. 6.4: Rise and decay times, t_R and t_D, determined from the singlet oxygen luminescence signals that were generated by irradiating 25 μM TPP doped into CA-polymer; as different surroundings air, H_2O, Ethanol, and D_2O were used; the singlet oxygen decay in air is estimated according to the literature [2]; the values for H_2O, EtOH, D_2O are taken from [15, 16]. (experimental accuracy: 15%)

From the findings for MB, TMPyP, and also TPP in CA-surfaces, it can first be noticed that the rise time for all singlet oxygen luminescence signals is in the range of 12 μs and therefore comparable within experimental accuracy. It is considered to reflect the singlet oxygen decay time in CA, which is strongly dependent on its surrounding and only in cases of oxidation or other types of quenching by the photosensitizer additionally influenced. This was shown in previous experiments with TMPyP and MB dissolved in H_2O, where at concentrations in the μM-range both photosensitizers yielded a singlet oxygen decay time of 3.5 μs.

For CA-surfaces doped with TPP and placed in H_2O a decrease of t_D was obtained, but might be an artefact due to the experimental accuracy of only 15%.

In D_2O neither the rise, nor the decay time change fundamentally. It is known from several studies in solution that the decay of singlet oxygen in D_2O is longer (68 μs) than in H_2O (3.5 μs). If the solvents H_2O or D_2O were able to penetrate in a sufficient amount into the polymeric film due to the permeability of diffusion constant for H_2O or D_2O into CA, a change for both, rise and the decay time, would be expected. A lower / higher oxygen concentration in the polymer due to H_2O or D_2O within the material would lead to an increased / decreased decay time of the triplet-T_1-state of the photosensitizer and the presence of either solvent would lead to a de- or increase of the singlet oxygen lifetime in the polymer. To study this assumption the dependency of the rise and decay times on the diffusion time of the surrounding solvent into the polymer should be monitored.

6.3.1.3 Indirect detection of the generation of singlet oxygen with potassium iodide

When generating singlet oxygen in a solution containing KI, a chemical reaction, which was described in detail by Mosinger *et al.*, would lead to the formation of tri-iodide, I_3^- [4]. This molecule shows in H_2O two characteristic absorption peaks at 287 nm and 350.5 nm, and the absorption value is correlated with concentration. Using this method TPP-doped polymeric CA-films were tested on its ability to generate singlet oxygen that diffused from the surface into the surrounding medium, H_2O, which contained potassium iodide. This assay also delivers information of the amount of generated singlet oxygen. CA-films doped with TMPyP and MB were excluded from this iodometric assay, because of the above detected leakage effect that results in direct contact with the PS and the potassium iodide in solution. Consequently, a clear separation of singlet oxygen generated in CA or generated outside CA in the surrounding H_2O would be not possible.

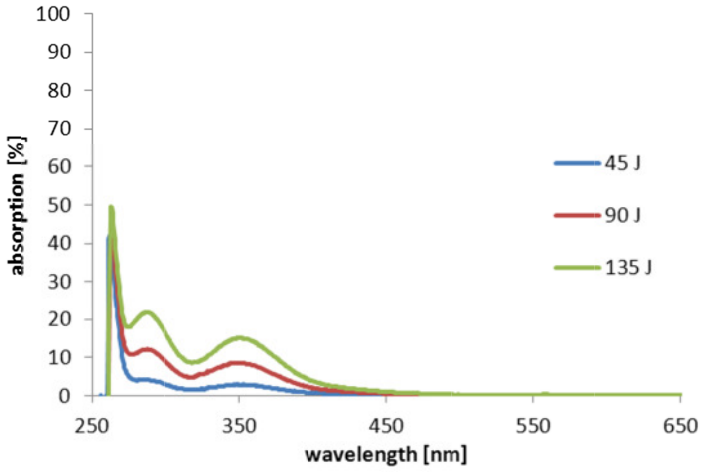

Fig. 6.9: Absorption spectrum of the supernatant (20 mM potassium iodide, dissolved in H_2O) of 25 µM TPP doped into CA after irradiation with 45, 90, or 135 J cm^{-2}.

From figure 6.9, the formation of I_3^- can be clearly followed by the evolving spectroscopic maximum at 287 nm and 350.5 nm. In order to follow the increase of the absorption with time, the percentaged absorption value at 287 nm and 350.5 nm is shown with its dependency on the irradiation time in figure 6.10.

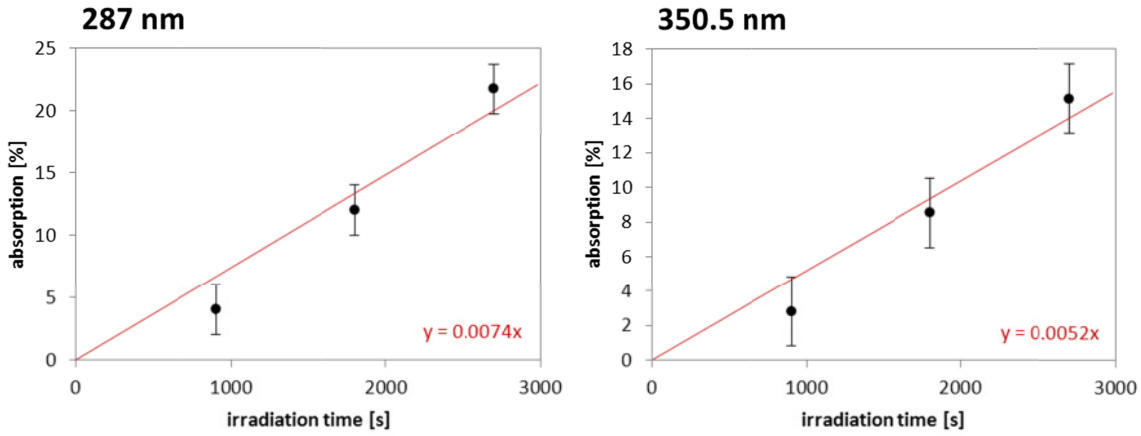

Fig. 6.10: Formation of tri-iodide by 25 µM TPP doped into CA; dependence of the absorption at the characteristic absorption maxima on the irradiation time; the concentration of potassium iodide in H_2O was 120 mM, its absorption was recorded at 287 nm and 350.5 nm (error: Δy = 2%, Δx = 2s).

Here, a linear dependency of the absorption of tri-iodide and the irradiation time of the cellulose acetate film containing TPP was detected. The slope of the linear fit of the data for 287 nm was calculated as $7.4 \cdot 10^{-3}$ and for the data for 350.5 nm as $5.2 \cdot 10^{-3}$. The intersection with the y-axis is expected to be at (0/0%) and therefore a linear fit was using that point. The values are in good agreement within experimental accuracy, accepting an error of 2% for the absorption. With a known photosensitizer concentration and a calibration line a quantification of singlet oxygen molecules would be possible. Obligatory, the size of the polymer plates and the irradiation parameters such as the geometry must be equal.

Similar findings were confirmed with measurements with TPP-O-A/B and PN-O-A/B in the following section.

6.3.2 Polyurethane (PU) with TPP-O-A/B and PN-O-A/B

The porphyrin TPP and the perinaphthenon PN were chemically modified with a linker that enabled the polymerisation of these photosensitizers into polyurethane (see chapter 2). Although PN is water-soluble a leakage effect might be avoided completely.

6.3.2.1 Absorption spectra and photostability

Before choosing PMMA as the basic material different polymer materials were investigated in regard to their transparency at different wavelengths between $200 - 1000\,nm$. It is optimal to have at least a window in the visible part of the electromagnetic spectrum ($400 - 700\,nm$), where the transparency of the underground material is given.

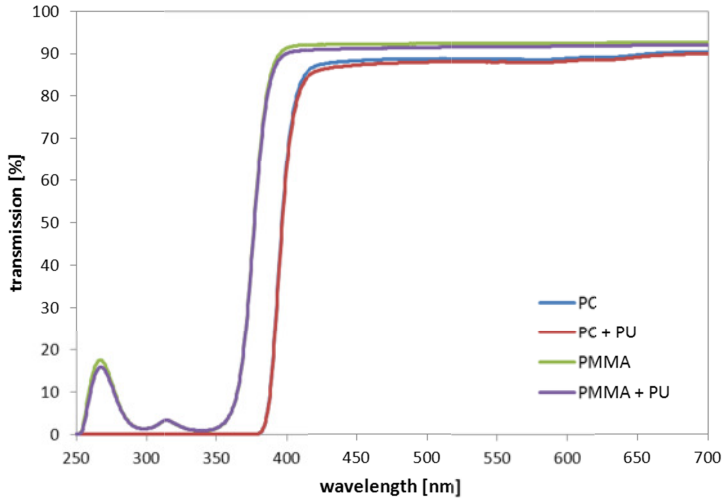

Fig. 6.11: Absorption spectra of the polymers polycarbonate (PC) and poly-methylmethacrylate (PMMA) materials with and without PU-layer.

PMMA had the best absorption properties to be used as basic polymer material for a PU-layer, because its absorption band is below $380\,nm$, whereas the absorption band of polycarbonate (PC) starts already at $400\,nm$. For both polymers we find transparency in the visible region, but absorption at lower wavelengths is preferred, since some medical broadband lamps used in our laboratory start to emit at $380\,nm$ and this might affect the polycarbonate materials.

The chemical structure of PN-O-A and PN-O-B, which are displayed in chapter 2, show the water-solubility of these two photosensitizers. Therefore, the absorption spectra were determined first in H_2O and compared to the spectrum of the well-known photosensitizer PNS in solution. Figure 6.12 shows the absorption cross section in dependency on the wavelength. Later potential shifts in the absorption spectra after polymerisation into PU might give insights into the photophysical properties.

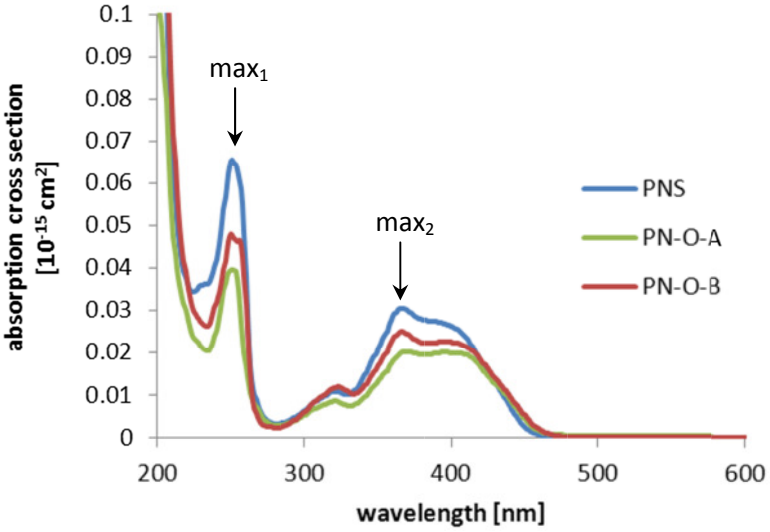

Fig. 6.12: Dependence of the absorption cross section of PNS, PN-O-A, and PN-O-B on the wavelength; the photosensitizers were dissolved in H_2O with a concentration of 50 µM.

The absorption maxima (max_n) of PNS and the two derivatives PN-O-A and –B are within a tolerance of $\pm 2\ nm$ at the same wavelength and are summarized in table 6.5.

sample	max_1 [nm]	max_2 [nm]
PNS	251	366
PN-O-B	252	368
PN-O-A	250	365

Tab. 6.5: Maxima of the absorption cross section for PNS, PN-O-A, and PN-O-B dissolved in H_2O with a concentration of each 50 µM.

Exemplarily, the absorption spectrum of PN-O-A linked in PU was investigated for 4 different PS concentrations ranging from 10– 200 µM (fig. 6.13). Air was used as a blank measurement which was then subtracted from the spectra of the PU-plates. The positions of the characteristic maxima for the linked PN-O-A are summarized in table 6.6.

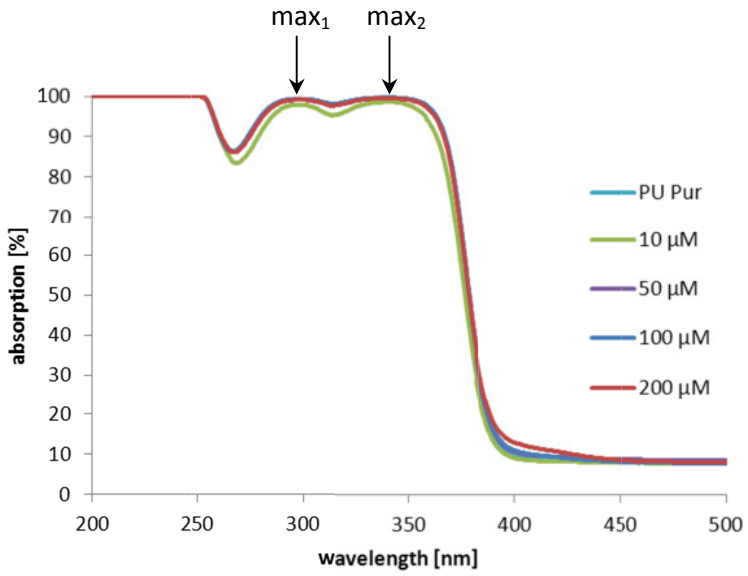

Fig. 6.13: Absorption spectra of PN-O-A in different concentrations (10 – 200 µM) in a PU-layer polymerized on PMMA with a thickness of 50 µm.

sample	max_1 $[nm]$	max_2 $[nm]$	**concentration** $[\mu M]$
PUR	296.5	338.5	---
PU + PN-A	298.0	338.5	10
PU + PN-A	297.5	337.5	50
PU + PN-A	299.0	341.5	100
PU + PN-A	299.5	342.0	200

Tab. 6.6: Absorption maxima of PU Pur (PUR) and PU+PN-O-A in different concentrations (0 – 200 µM) in PU-layer polymerized onto PMMA with a thickness of 50 µm.

It can clearly be noticed that these values are at the same position and describe the absorption maxima of the pure PU layer. The absorption spectrum of PU on PMMA covers completely the absorption maxima of the PN-derivatives which are in H_2O at $\approx 250\ nm$ and $\approx 366\ nm$. Only a slight increase in the absorption depending on the concentration was detected between $400 - 450\ nm$ for 100 μM and 200 μM where the PN-derivatives seem to dominate the absorption of the pure PU layer. This finding is enforced by a zoom into the graphic, shown in figure 6.14.

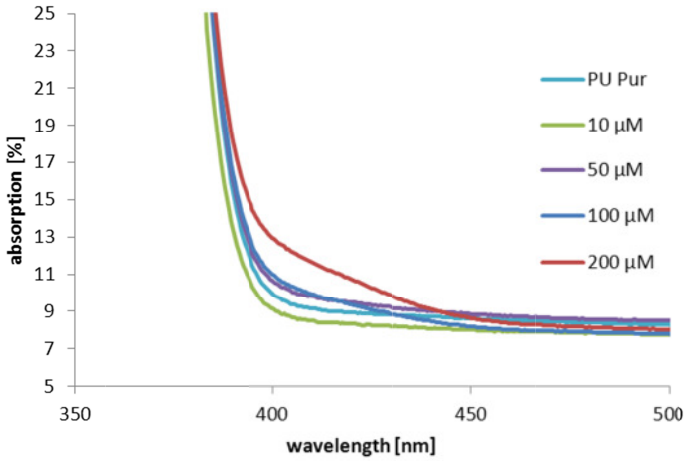

Fig. 6.14: Zoom of the absorption spectra of PN-O-A in different concentrations (0 – 200 µM) in PU-layer polymerized onto PMMA with a thickness of 50 µm, between 400 nm and 450 nm.

Due to the domination of the absorption of PU when trying to determine the absorption spectrum of PN-O-A, a change due to long-term irradiation might be non-detectable. Therefore, for the photostability tests, that base on the change of the absorption spectrum after irradiation, this technique is not appropriate enough.

TPP-O-A in solution and doped into PU

The derivatives of TPP, doped into PU, were not soluble in H_2O and the data of the absorption spectra were compared to findings in the literature. Brückner *et al.* reported an absorption maximum of TPP in Chloroform ($CHCl_3$) at a wavelength of S (Soret) = 416 nm (Q_1 = 515 nm, Q_2 = 550 nm, Q_3 = 593 nm, Q_4 = 646 nm) [17], which was confirmed by Korinek *et al.* [18] in air-saturated acetone. The absorption spectrum of TPP-O-A in the PU-polymer was detected by subtraction of PU/PMMA absorption spectrum without the photosensitizer (fig. 6.16). The main absorption bands of TPP-O-A in the PU-polymer were detected at S (Soret) = 419.5 nm, Q_1 = 515.5 nm, Q_2 = 551 nm, Q_3 = 592 nm, Q_4 = 647 nm. TPP-O-A in the PU-polymer does not show a significant difference in its absorption spectrum compared to TPP in solution. The determined absorption maxima were therefore in good agreement to the findings solution [19, 20]. No red or blue shifts were observed, indicating that no aggregation processes were involved during the preparation of the coating [21, 22]. This is important, because aggregation of photosensitizers might result in a loss of the ability to generate singlet oxygen, as was described for the porphyrin XF73 in chapter 4. The two absorption maxima between $250 - 380\ nm$ are ascribed to the absorption of the pure PU-plate, as was determined in previous investigations.

Overlap of TPP-O-A with the PIB 3000 and photostability

TPP-O-A in PU (PS concentration of $10^{-4}\ M$, PU-layer thickness of 30 μm) was irradiated with the PIB 3000 broadband lamp (see chapter 2) during the phototoxicity tests. In order to clarify the effect of the lamp on TPP-O-A, the plates were irradiated under the same conditions without bacteria and the absorption spectra before and after illumination were compared. The emission spectrum of the PIB 3000 was normalized to its maximal value (= 100%) and overlaid with the absorption spectrum of TPP-O-A in PU (fig. 6.15).

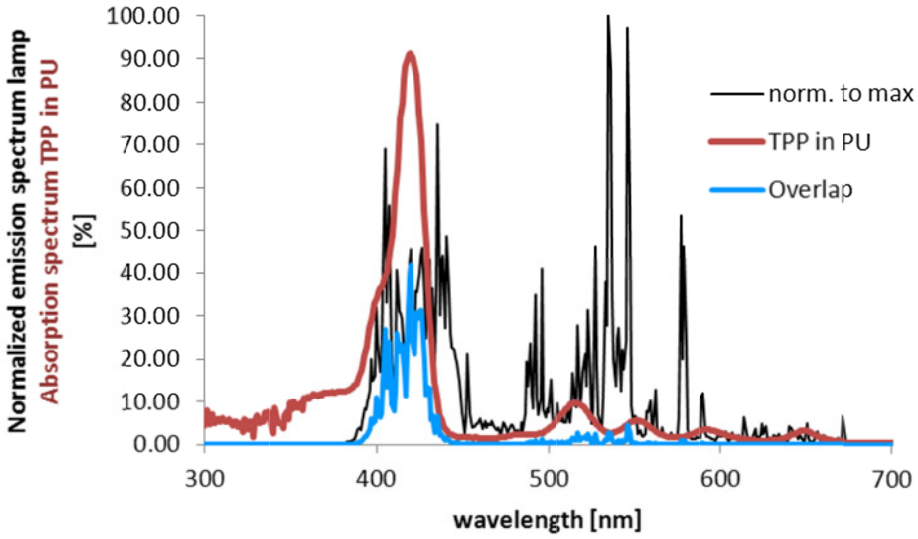

Fig. 6.15: Overlap of the normalized emission spectrum of the Waldmann PIB 3000 (black line) and the absorption spectrum of TPP-O-A in PU (red line). The blue line represents the overlap of both spectra, calculated by spectral folding.

An overlap of 21.5 % was calculated. Since the lamp emitted with an overall power of $P = 50\ mW\,cm^{-2}$. Figure 6.16 shows the absorption spectrum of the non-irradiated sample of TPP-O-A in PU in comparison to irradiated samples.

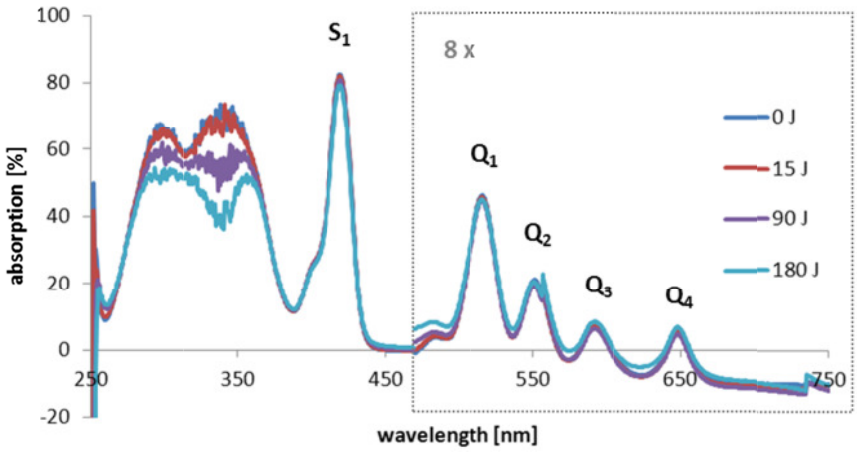

Fig. 6.16: Percentaged absorption of TPP-O-A in the PU-polymer in the range between 250 – 750 nm; a variation of the applied energy dose between 0 – 180 J cm^{-2} was done with the PIB 3000, with irradiation times between 0 – 60 min; TPP-O-A had a concentration of 10^{-4} M and the PU-layer thickness was 55 µm; for a better view, the Q-bands were magnified 8-fold in y-axis starting from 470 nm; S_1 describes the Soret-band; the blank was a PU-polymer without photosensitizer.

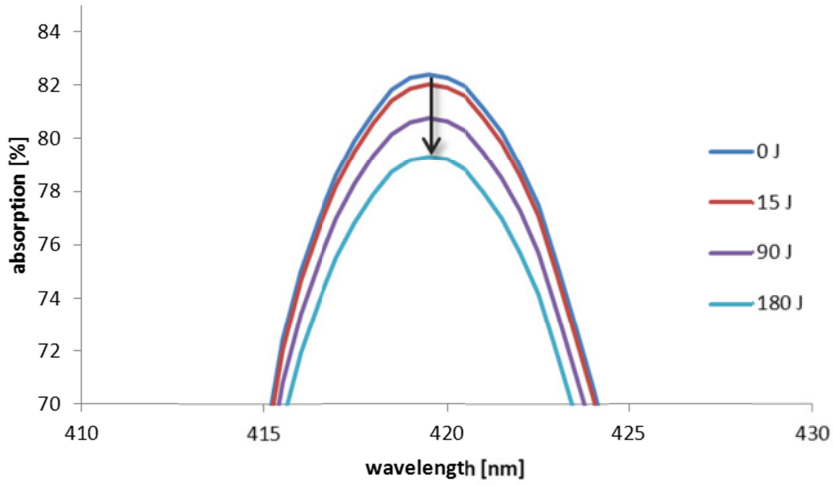

Fig. 6.17: Magnification of the Soret-band (absorption maximum) of the absorption spectrum in figure 6.16; the arrow indicates the decrease of the absorption maximum.

Irradiation of the plates between 5 min and 60 min ($E = 15\,Jcm^{-2}$ and $180\,Jcm^{-2}$) did not lead to a significant change in the absorption spectrum of TPP-O-A. As blank measurement another PU-polymer without containing photosensitizer molecules was used. There, the thickness of the surface or the drying procedure should be equal. Since the values for the absorption are negative in the red and IR-region, as presented in figure 6.16, it has to be considered that the samples are not identical and might have slight differences in their absorption or scattering properties.

By irradiation the absorption maximum decreased 4%, as indicated by the arrow in figure 6.17. The absorption data for the Q-bands are displayed 8-fold magnified compared to the absorption at 420 nm. Even with this magnification no decrease of the singlet bands was detected. From these data the photosensitizer is considered to be photostable within the limits of the experimental accuracy.

Leakage of the photosensitizer

Since bacteria in aqueous suspension were applied to the surface for phototoxicity tests, it is essential to know the leakage of the PS because this critically influences the phototoxicity results. Such a leaching was already detected for CA surfaces and non-linked, water-soluble photosensitizers. The polymer plate with TPP-O-A was placed for 1 week in H_2O and the absorption spectrum of the supernatant was recorded. No typical absorption bands of TPP-O-A were detected in the supernatant which can be explained by the fact that TPP-O-A is not soluble in H_2O and is linked with PU.

6.3.2.2 Direct detection of the singlet oxygen luminescence

After the PU-surface was doped with TPP-O-A, the plate was spectroscopically investigated to understand the process of the singlet oxygen generation in such a PU-surface. The singlet oxygen luminescence was detected time- and spectrally resolved in air-saturated samples at 25°C. Therefore, the oxygen concentration in the air-surrounding of the plates was calculated to be at $[O_2] = 8.54 \cdot 10^{-3}\ mol\ L^{-1}$. 10 000 laser pulses are equal to an irradiation time of 10 s and were used for each measurement.

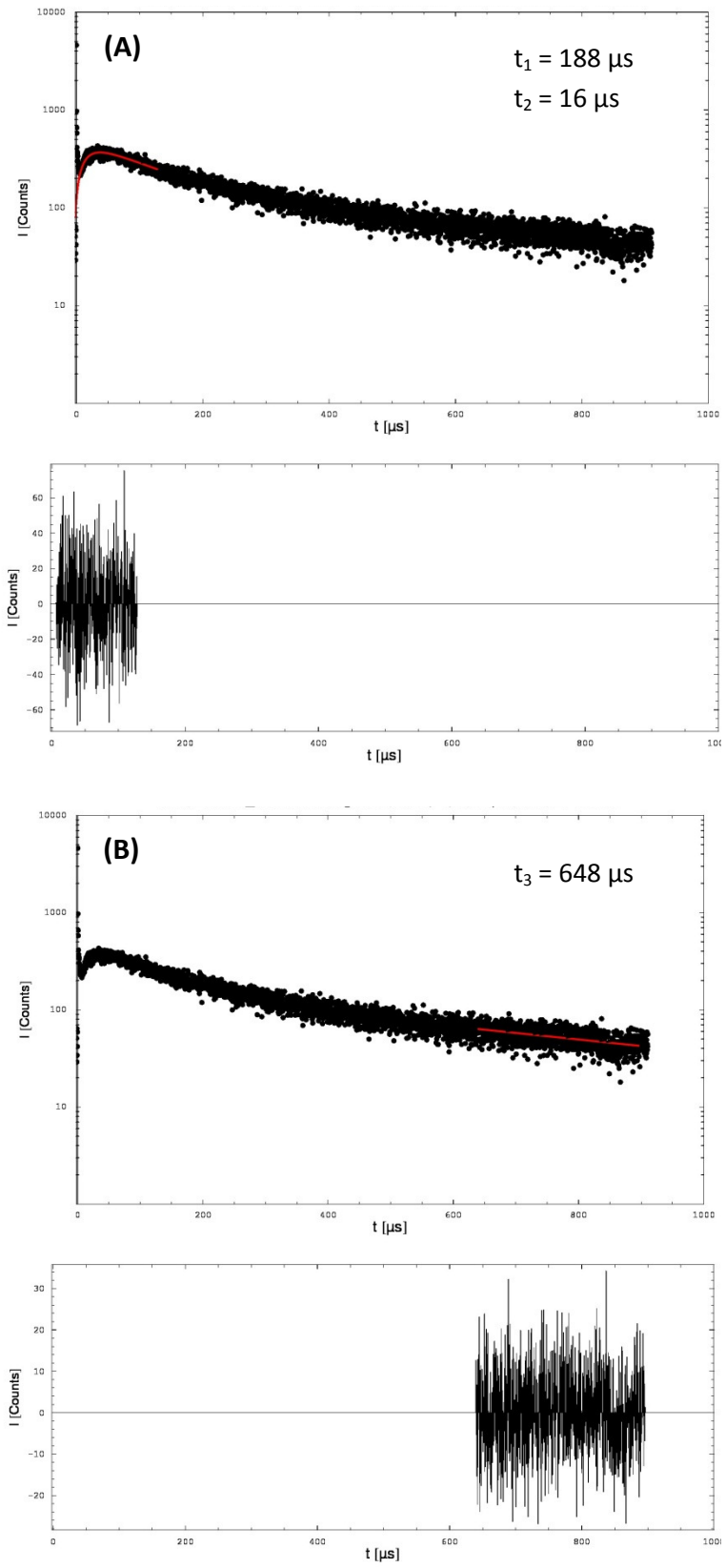

Fig. 6.18: Time-resolved direct detection of singlet oxygen generated by TPP-O-A in PU with a concentration of 10^{-4} M and a PU layer thickness of 50 µm; the samples were air saturated at a temperature of 25°C. In (A) t_1 and t_2 were obtained by a bi-exponential fit in the first part of the luminescence signal; in (B) the second

part of the decay of the signal was fitted with a single-exponential fit gaining t_3; the deviation of the fit-curve is shown below the singlet oxygen luminescence signal.

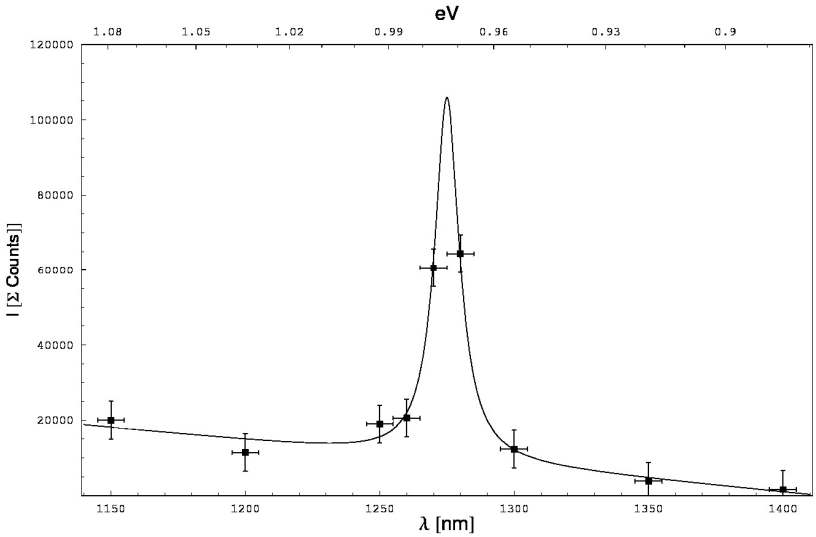

Fig. 6.19: Spectrally resolved direct detection of singlet oxygen generated by TPP-O-A in PU with a concentration of 10^{-4} M and a PU layer thickness of 30 µm; the samples were air-saturated at a temperature of 25°C; a Lorentz-function was fitted through the data points yielding a maximum at 1275 nm.

The maximum of the singlet oxygen luminescence was detected at 1275 nm (fig. 6.19). In combination with the time-resolved measurement at 1270 nm (fig. 6.18), the generation of singlet oxygen was directly proven. The high signal intensity compared to photosensitizer in solution would facilitate an accurate determination of the rise and decay time of the signal with a bi-exponential function.

The rise part of the signal was detected as single-exponential whereas the signal decays in a multi-exponential manner. Since one rise time but at least 2 decay times seem to be inherent, the exact determination of the rise and decay times is challenging. The fit of the time-resolved signals has been done according to the bi-exponential equation (2.2), for the first part of the luminescence signal. The second part was fitted with a single-exponential function. These resulted in a decay of $t_{D_1} = t_1 = (188 \pm 19)\mu s$, $t_R = t_2 = (16 \pm 1.6)\mu s$ (first part) and $t_{D_2} = t_3 = (648 \pm 65)\mu s$ (second part). Due to more than one rise and one decay time as usually obtained in simple solutions with dissolved photosensitizer in H_2O or $EtOH$ the interpretation of the data for the PU-surfaces are difficult.

These measurements do not finally assign rise and decay time. Therefore in the following sub-chapter a variation of the external oxygen concentration was done with the monolayer samples.

Influence of the oxygen concentration on the decay times

The oxygen concentration influences predominantly the deactivation of the excited triplet-T_1-state of the photosensitizer. In order to assign the decay times to the decay of singlet oxygen and the triplet state of the photosensitizer, a variation of the external oxygen concentration in the surrounding air was done with a gas-flow unit. With that instrumentation, flooding with a constant ratio of O_2 and N_2 and a constant volume per time unit ($L\ min^{-1}$) the oxygen concentration in the polymer surrounding could be adjusted and kept constant.

As a preliminary investigation, the measurement of the oxygen concentration in pure H_2O was performed when changing the oxygen partial pressure in the air used for bubbling the solution by changing the ratio of O_2 and N_2. Therefore, the volume of O_2 and N_2 was kept at a constant volume flow of $O_2 + N_2 = 0.8, 0.5, 0.2\ L\ min^{-1}$, respectively. The oxygen concentration in the control suspension H_2O was detected with an oxygen sensor with the principle of the dynamic fluorescence deactivation.

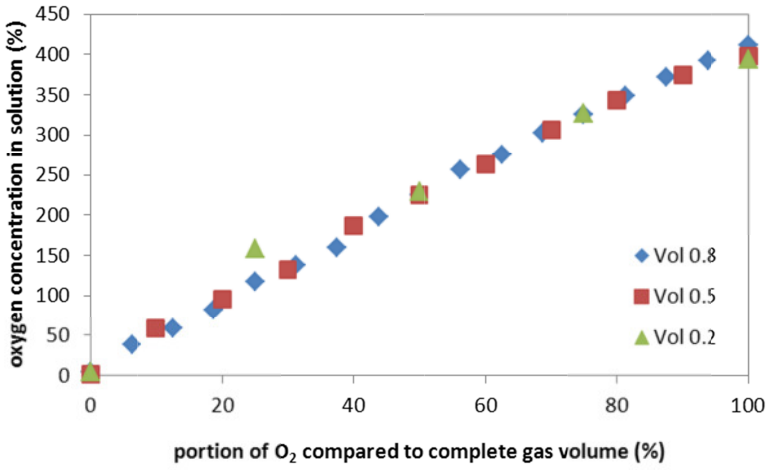

Fig. 6.20: Dependency of the portion of O_2 in a complete gas volume to the oxygen concentration which is then solved in a control solution of H_2O; the dependency was investigated for 3 different gas flows at a constant volume per time unit of 0.8, 0.5, and 0.2 L min^{-1}.

The percentaged value of oxygen in the gas volume is shown in dependency of the oxygen concentration in the H_2O solution. From the graph in figure 6.20 it can be seen that independently of the constant gas volume of 0.8, 0.5, or 0.2 $L\ min^{-1}$ for the same percentaged volume of oxygen in the gas respectively the same amount of oxygen in the suspension was detected. Thus, only the ratio of O_2/N_2 is important for the oxygen concentration in the sample (solution), independent from the overall volume flow ($L\ min^{-1}$) of gas.

Then, the partial pressure of oxygen was varied with that gas-flow unit in the surrounding of the PU polymeric plates. Therefore, a polymer plate containing TPP-O-A was placed diagonally into a quartz cuvette and covered with a cap. At a constant gas flow of $1\ L\ min^{-1}$ the ratio of O_2 and N_2 was varied from 0% to 100% O_2 in 10%-steps. For each step 10 min after adjusting the oxygen concentration the singlet oxygen luminescence was detected and the rise and decay time of the signals were determined. Exemplarily, figure 6.21 shows the time resolved singlet oxygen luminescence signals for decreasing oxygen concentration at 100%, 20% and 0% oxygen in the air surrounding the PU-polymer containing TPP-O-A.

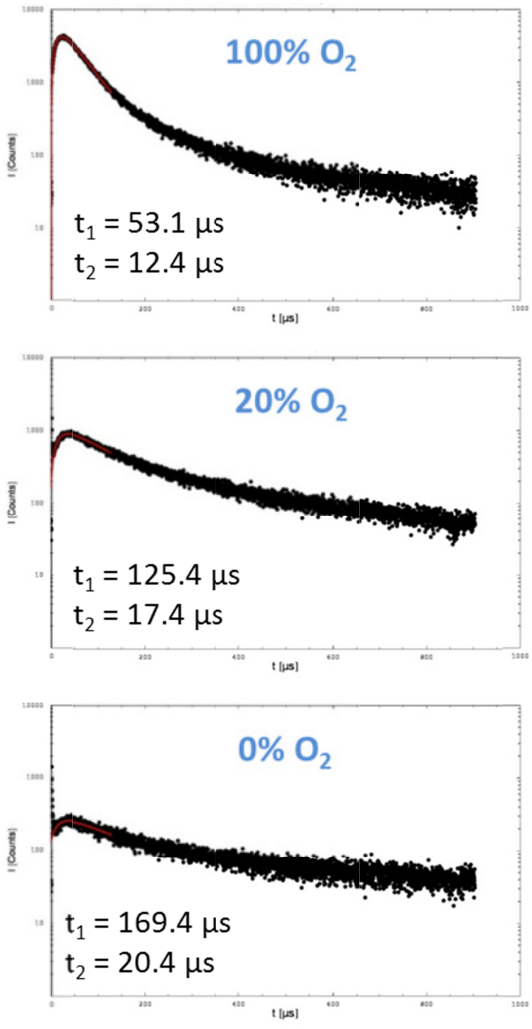

Fig. 6.21: Change of the shape of the time-resolved singlet oxygen luminescence signal with the oxygen concentration in the surrounding air; exemplarily shown for 100%, 20%, and 0% O_2.

The percentaged oxygen concentration of was re-calculated to the concentration with the unit [mol] with the given constants and parameters and the following considerations. The equivalent n of a gas can be calculated with the ideal gas law:

Eq. 6.4

$$p \cdot V = n \cdot R \cdot T$$

$$\Leftrightarrow$$

$$n = \frac{p \cdot V}{R \cdot T}$$

and

$$V_m := \frac{R \cdot T}{p}$$

is defined as the molar volume.

With the parameters

$$R = 8.314 \cdot 10^6\ Pa\ cm^3\ mol^{-1}\ K^{-1}$$

$$T = 25°C = 298\ K$$

$$V = 4\ cm^3$$

$$p = 101325\ Pa\ (= 7.5006 \cdot 10^{-3}\ Torr)$$

into equation (6.1) this leads to an equivalent of

$$n = \frac{V}{V_m} = 3.42 \cdot 10^{-5}\ mol$$

of oxygen in the cuvette. The absolute values of the equivalents were referred to the percentaged values with

$$20.9\%\ O_2 \triangleq 3.42 \cdot 10^{-5}\ mol$$

…

$$100\%\ O_2 \triangleq 16.36 \cdot 10^{-5}\ mol$$

Therefore, the figure 6.22 shows the change of the rise and decay time of the singlet oxygen luminescence signal that depends on the oxygen concentration [mol].

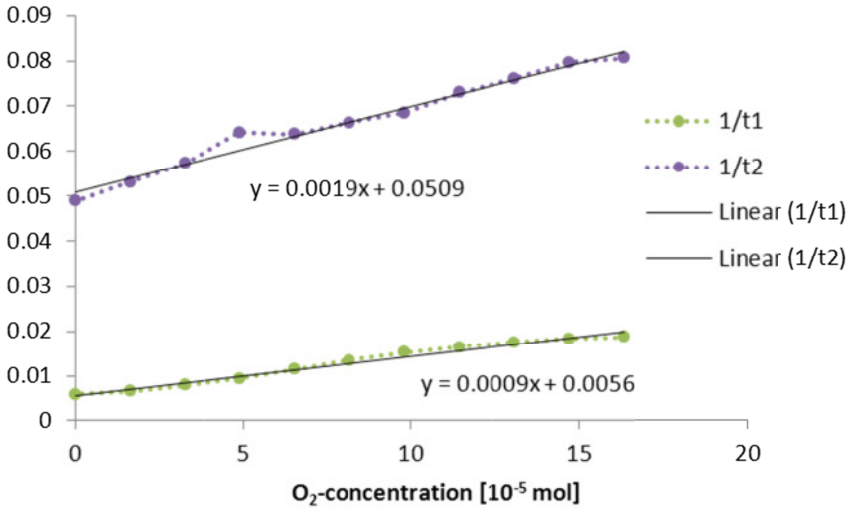

Fig. 6.22: Change of the rise and decay time of the singlet oxygen luminescence signal with oxygen concentration; the inverted rise and decay time was fitted linearly and thus the slope of the curve k_q is determined.

According to equation (2.3) the quenching rate constant for triplet state quenching by oxygen was determined with a linear fit as $k_{q,1} = 9 \cdot 10^{-10} s^{-1}\, mol^{-1}$. With the measurements of the variation of the oxygen concentration a second quenching rate constant was determined that was calculated as $k_{q,2} = 1.9 \cdot 10^{-9} s^{-1}\, mol^{-1}$.

With the assumption that one decay time is the decay of the excited triplet-T_1-state, but the other is the singlet oxygen state, it has to be consequently assumed that singlet oxygen is also quenched by oxygen. This effect of singlet oxygen quenching by oxygen, which exhibited a nonlinear dependency, the rate constants of singlet oxygen depopulation by oxygen was described by Dedic *et al.* [23] using the photosensitizer $TPPS_4$ in potassium phosphate buffer of $pH = 7.4$. Nevertheless this effect is, from the quantum mechanical perspective, very unlikely, so that as well other effects have to be considered and discussed.

Photosensitizer aggregates in different forms, with different triplet decay patterns, or different local oxygen concentration around the photosensitizers, or different local deactivation of singlet oxygen due to no constant micro-geometry might influence the luminescence signal to a great extent, so that for some singlet oxygen luminescence photons the rise time is referred to the decay of singlet oxygen and the decay time is referred to the excited triplet-T_1-state of the photosensitizer, whereas for other luminescence photons this is vice versa and therefore a mixed luminescence signal will be the result, having an influence of both, excited triplet state and singlet oxygen state in each, the rise and decay part of the signal.

Sandwich polymer plates

The PU-layer of the polymeric plate is in contact to air, having a specific oxygen concentration, and is also in contact to PMMA, having probably a different oxygen concentration. Thus, an oxygen gradient has to be assumed that starts from air through PU-layer into PMMA. In order to determine if and to which amount this influences the singlet oxygen luminescence signal, a "sandwich"-polymer plate, whose structure can be seen in the following figure 6.23, was prepared and investigated due to its generation of singlet oxygen and the change in the singlet oxygen luminescence signals.

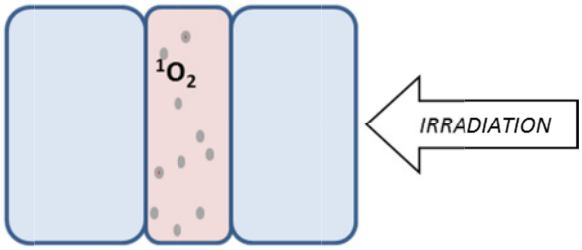

Fig. 6.23: Scheme of a "sandwich" polymer plate; the blue areas left and right indicate the PMMA material with a thickness of 2 mm each plate; the red-doped area in the middle shows the PU-layer with the different linked photosensitizers and a thickness around 50 µm.

The sandwich polymer plate is irradiated as indicated by the arrow through the three separate layers. Upon irradiation of the PU-layer, singlet oxygen is generated in the PU-layer and may diffuse inside PU, or escape into either air or PMMA. Due to the size of the sandwich polymer plate, the contact area of the PU-layer with air surrounding is $4 \times (50 \cdot 10^{-4}\, cm \times 4\, cm) = 8 \cdot 10^{-2}\, cm^2$ and the contact area with PMMA gives $2 \times (4\, cm \times 4\, cm) = 32\, cm^2$, which is then 400-fold bigger. Therefore, the amount of singlet oxygen molecules diffusing into air might be neglectable in the PU-sandwich structures.

Table 6.7 summarizes the rise and decay times of the singlet oxygen luminescence of the different PU-monolayer samples and the PU-sandwich structures for TPP-O-A/B and PN-O-A/B. For the summary of the data of rise and decay times the data were collected as illustrated in the following figure 6.24. A bi-exponential fit according equation (2.2) used in the time interval, in which mono-exponential decay can be supposed and the deviation of the fit is equally distributed around a medium value (see deviation in fig. 6.18 (A)).

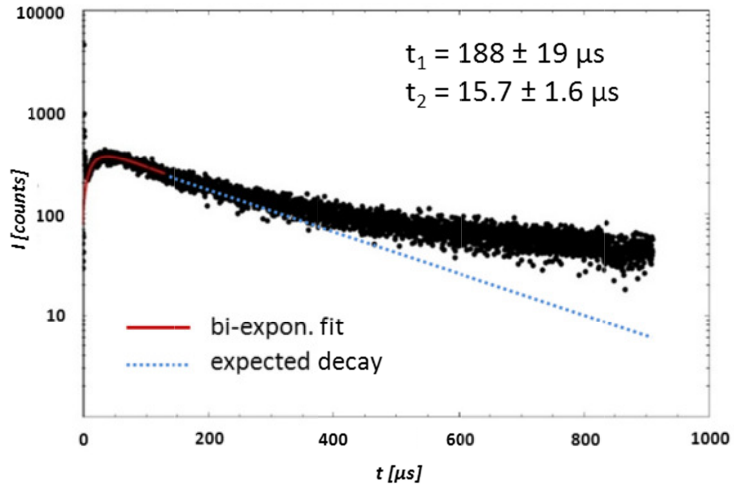

Fig. 6.24: Time-resolved direct detection of singlet oxygen generated by TPP-O-A in a PU-layer with a concentration of 10^{-4} M and a PU-layer thickness of 30 µm as also shown in (6.19, A) with the deviation of the fit; the rise and decay time, t_2 and t_1, respectively, of the time resolved signal were obtained by fitting the data.

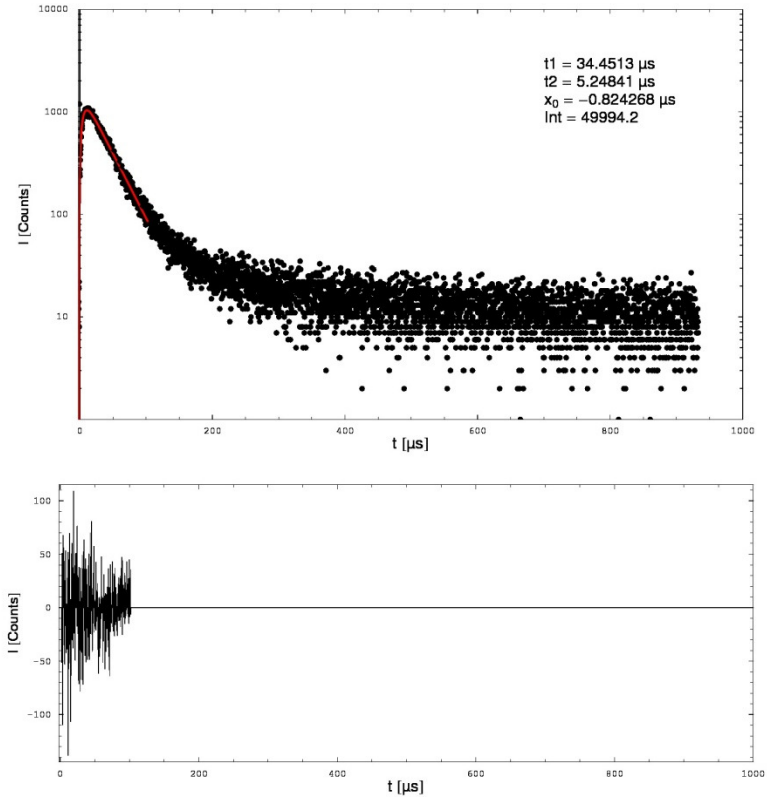

Fig. 6.25: Time-resolved direct detection of singlet oxygen generated by TPP-O-A in a PU sandwich polymer (1A) with a concentration of 10^{-4} M and a PU layer thickness of 50 µm; the samples were air saturated at a temperature of 25°C. t_1 and t_2 were obtained by a bi-exponential fit in the first part of the luminescence signal; the deviation of the fit-curve is shown below the singlet oxygen luminescence signal and an increased deviation can be followed with increasing time.

Figure 6.25 shows a singlet oxygen luminescence signal that was generated by TPP-O-A in a PU sandwich polymer (1A) exhibiting a high signal-to-noise ratio. It shows a remarkable decrease around 80% in the decay time to $t_D = (34 \pm 3)\mu s$ and further a decrease of ≈ 50% of the rise time to $t_R = (6 \pm 1)\mu s$ in comparison to TPP-O-A in a monolayer PU-polymer (1A).

Monolayer		**t_1 [µs]**	**t_2 [µs]**	**Sandwich**		**t_1 [µs]**	**t_2 [µs]**
TPP-O-A	**1A**	157	10	**TPP-O-A**	**1A**	34	6
	1B	195	12		**1B**	35	6
	1C	175	13		**1C**	27	4
	1D	199	13		**1D**	32	6
TPP-O-B	**2A**	150	10	**TPP-O-B**	**2A**	30	5
	2B	170	9		**2B**	33	6
	2C	130	11		**2C**	27	5
	2D	140	9		**2D**	32	5
PN-O-A	**3A**	204	16	**PN-O-A**	**3A**	31	4
	3B	193	17		**3B**	26	3
	3C	---	---		**3C**	29	< 0.5*
	3D	---	---		**3D**	27	6

*Tab. 6.7: Rise and decay time, t_2 and t_1, of the time-resolved singlet oxygen luminescence signals for the PU-monolayer samples and the PU-"sandwich" structures. There, 'A' equals a photosensitizer concentration in PU of $1 \cdot 10^{-4}$ M, 'B' = $2 \cdot 10^{-4}$ M, 'C' = $1 \cdot 10^{-5}$ M, and 'D' = $5 \cdot 10^{-5}$ M. * t_2 was not resolvable.*

In case of the monolayer samples for both, TPP-O-A and -B, a rise and decay time was determined of a signal with a good signal-to-noise ratio. In case of PN-O-A only with PS-concentrations of $1 \cdot 10^{-4}\,M$ and $2 \cdot 10^{-4}\,M$ singlet oxygen generation was detected, although with a lower intensity compared to the TPP-O-A/B samples; nevertheless, rise and decay times were evaluable. A decrease for both, rise and decay time, was detected when using the sandwich structures for TPP-O-A/B and PN-O-A compared to the monolayer PU-plates. Additionally, also the samples 3C and 3D of the sandwich polymers containing PN-O-A showed now singlet oxygen generation, but exhibited a low signal-to-noise ratio. PN-O-B did not show singlet oxygen generation for all 4 concentrations and for monolayer and sandwich samples.

The photosensitizer PN is known for its high quantum yield for singlet oxygen formation [24]. Hence, the lower singlet oxygen luminescence intensity cannot be understood by a simple comparison of the quantum yields that have been determined only in solution. PN is known to consume oxygen while being irradiated [25]. Therefore, effects like oxidisation

might lead to a fast decrease of the oxygen in the material and thus low signal intensity. Moreover, due to additional side chains or the chemical linking in the PU-polymer, PN-O-B might have changed its electronic structure and hence its rate and rate constants resulting in no or very low generation of singlet oxygen. Since the absorption of the photosensitizer is not detectable due to the overlap with the light absorption of PU (see section 6.3.2.1), this explanation remains however speculative. Fluorescence detection or triplet spectroscopy with the polymer plate and the photosensitizer might elucidate the reason of the absence of detectable singlet oxygen generation.

What can be noticed further for all determined singlet oxygen luminescence signals, is an increase in the intensity of the signal. For the determination of the rise and decay time of each sample neither the photosensitizer concentration nor the thickness of PU-layer were changed. Together with the obtained shortage in the rise and decay times, a model is proposed with a comparison of the monolayer with the "sandwich" structures. In that model we exclude a general change of the oxygen concentration or the diffusion constant when adding a second PMMA-layer onto PU. Since both, rise and decay time become shorter, the probabilities for singlet oxygen and triplet-T_1-state deactivation must be consequently higher. The first basic change when adding a second PMMA-layer is, as determined above by calculation, the exclusion of air-surrounding for PU. Therefore, singlet oxygen might not have the possibility to be deactivated in air exhibiting a very long decay time ($\approx\ ms$). Thus, a higher proportion of singlet oxygen decays within PU or PMMA, which is detectable on our time scale in the time-resolved singlet oxygen detection method. This can be an explanation for the sudden higher signal intensity, which can be expressed in simple terms as a 'compression' of the time-resolved luminescence signal along the time-scale (x-axis).

Further, the system was simplified by excluding the air-contact and a decay of singlet oxygen in PMMA has now a stronger influence on the signal and the photon statistic is changed. Therefore it might also seem that the triplet decay time becomes shorter, which might be not the case; the long singlet oxygen decay in air might overlay the triplet state decay and lead to false assumptions in regard to the triplet decay, similar to the findings in chapter 5, where an overlay of different singlet oxygen luminescence signals from cells in suspension.

6.3.2.3 Indirect detection of the generation of singlet oxygen with potassium iodide

In the presence of singlet oxygen, iodide is transformed into tri-iodide which is an indirect proof of the generation of this reactive oxygen species. TPP-O-A in PU with a concentration of $10^{-4}\ M$ and a PU-layer thickness of 30 μm was irradiated in a solution of H_2O with potassium iodide for 0, 5, 10, 15 and 30 min. After each illumination time the solution was spectroscopically investigated following the formation of tri-iodide at its maximal absorption at 287 nm and 350.5 nm (fig. 6.26).

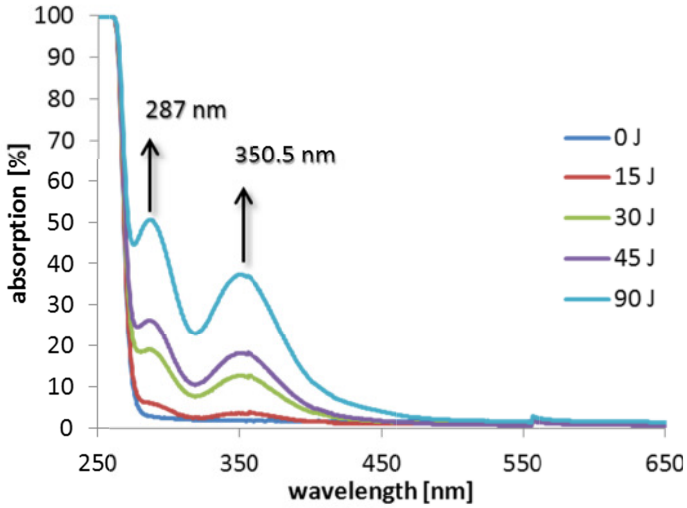

Fig. 6.26: Detection of tri-iodide following irradiation of TPP-O-A with a concentration of 10^{-4} M linked in PU with a layer thickness of 30 µm; the plates were irradiated with the PIB 3000 with P = 50 mW cm^{-2} at the level of the irradiated samples; the concentration of potassium iodide in H_2O was 120 mM.

With increasing irradiation time and therefore applied light energy the typical absorption maxima for tri-iodide at 287 nm and 350.5 nm increase as well. The following two graphs show the dependence of the irradiation time, and thus applied light energy, and the absorption due to the formation of tri-iodide.

A linear dependence of the absorption at 287 nm and 350.5 nm of tri-iodide was detected. With a linear fit the slope of the graph was calculated as $(2.85 \pm 0.3) \cdot 10^{-2}$ and $(2.05 \pm 0.2) \cdot 10^{-2}$. From the time kinetics with this method the rate constant for the formation of tri-iodide can be determined, which is the slope of the curve in the graphs in figure 6.27. If the materials that are compared have different absorption, the rate constant has to be adapted according to the absorbance of the correspondent wavelength [6]. For a comparison also the size of the samples should be equal.

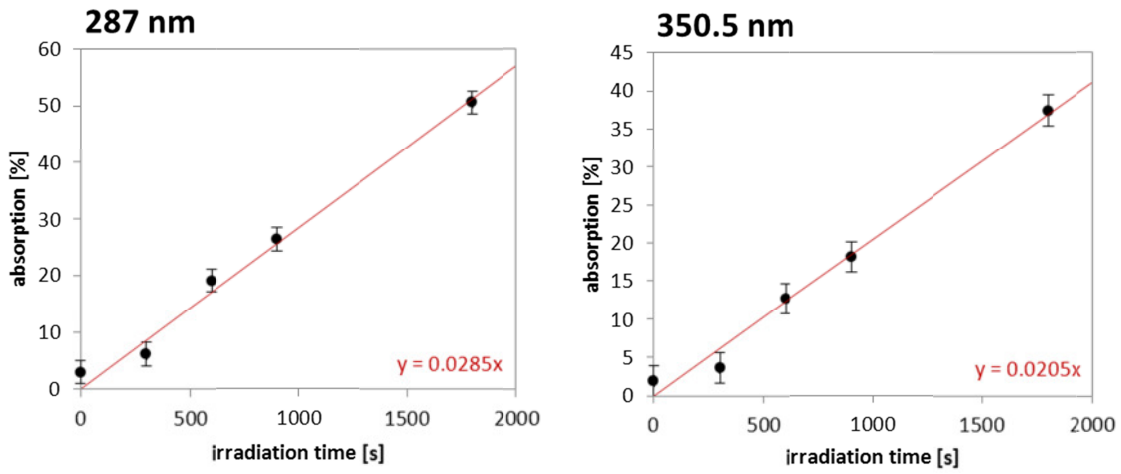

Fig. 6.27: Dependence of the absorption of tri-iodide on the irradiation time of TPP-O-A with a concentration of 10^{-4} M linked in PU with a layer thickness of 30 µm; the plates were irradiated with the PIB3000 with P = 50 mWcm^{-2} at the level of the irradiated samples; the concentration of potassium iodide in H_2O was 120 mM its absorption was recorded at 287 nm and 350.5 nm (error: Δy = 2%, Δx = 2s).

As control experiment, the PU polymer surface (PUR) without photosensitizer was tested in regard to its ability to lead to the formation of tri-iodide. The following graphic shows the dependence of the absorption value of tri-iodide from the irradiation time of PUR.

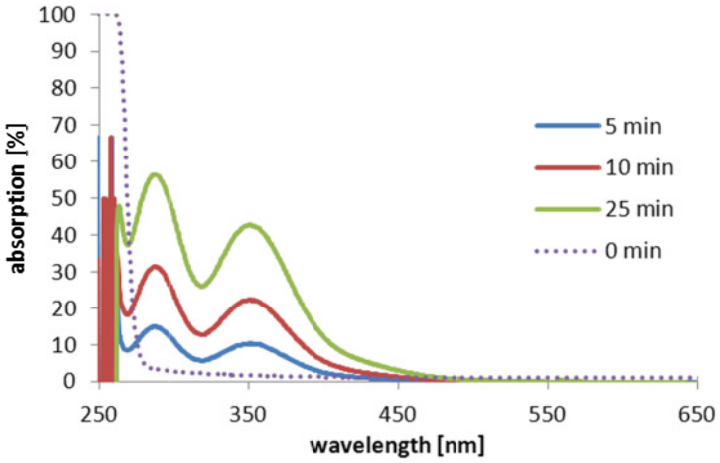

Fig. 6.28: Dependence of the absorption of tri-iodide on the irradiation time of a PU polymeric surface (PUR) without a photosensitizer with a layer thickness of 30 µm; the plates were irradiated with the PIB3000 with P = 50 mW cm^{-2} at the level of the irradiated samples; the concentration of potassium iodide in H_2O was 120 mM.

The dotted line for 0 min irradiation time indicates the absorption of 120 mM potassium iodide in H_2O, where pure H_2O was used as blank. The values for 5, 10 and 25 min of irradiation were calculated by subtracting the non-irradiated solution of 120 mM potassium

iodide in H_2O (blank). The formation of tri-iodide can clearly be followed by the absorption peaks at 287 nm and 350.5 nm after irradiating the PUR sample with the PIB 3000 using 50 $mW\,cm^{-2}$. The absorption value increases with the irradiation time.

From these findings we concluded that (i) either singlet oxygen is generated by irradiating the samples, or (ii) another reactive species is formed which reacts with potassium iodide, resulting in the formation of tri-iodide.

Point (1) was tested by direct spectroscopic investigation of the PU polymeric plates without photosensitizer (PUR). There, by irradiation of the samples with a wavelength of 420 nm, which was also used in order to irradiate TPP-O-A in its Soret band, no singlet oxygen was detected with the PUR samples. Therefore, we consider point (2) as rather probable. One of the possible candidates for another reactive species would be H_2O_2, which was detected by Jesenska *et al*. in their study of PU material [6]. It plays furthermore an important role in the reaction mechanism in the formation of tri-iodide as presented in scheme 2.1.

6.3.2.4 Fluorescence of TPP-O-A in PU

Fluorescence microscopy of the TPP-O-A containing PU polymeric plates was done to investigate the homogeneity of photosensitizer distribution in the PU layer. This experiment was in the end considered to be not sensitive enough to determine the micro-structure and therefore the homogeneity, but photobleaching of the fluorescence can be detected with this system.

Thus, fluorescence microscopy the photobleaching by irradiation with the tunable laser system at 420 nm for 38 min of TPP-O-A (PS concentration of 10^{-4} M, PU-layer thickness of 30 µm) in PU was investigated. Figure 6.29 shows the fluorescence in false colour images at different localisations around the irradiation centre, which was hit by the laser beam. The findings were only obtained qualitatively.

After irradiation of 38 min with the laser at the given conditions a bleaching of the fluorescence has been detected in the irradiated area. The polymer plate with TPP-O-A was scanned from right to left as indicated by the arrow in picture 0. The most right position is therefore picture 1 and the most left position is picture 8. Picture 1 is already close to the irradiated area and therefore in dark blue colour, that indicates a low fluorescence. Following the direction towards the centre of the laser spot and therefore the point of

highest irradiation, no fluorescence is detected anymore. When going towards the area of low to no irradiation intensity, from picture 4 to 7 an increase in the fluorescence intensity was detected. Finally in picture 8 a non-irradiated part of the polymer plate shows the highest fluorescence intensity indicated by the yellowish-orange colour.

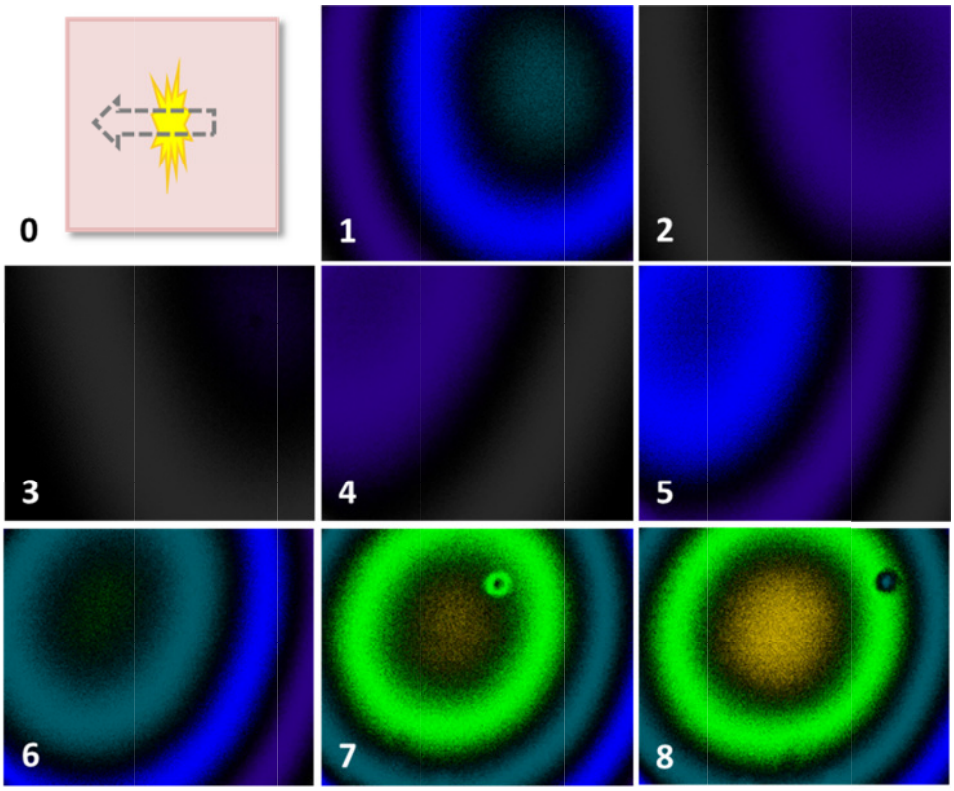

Fig. 6.29: Fluorescence of TPP-O-A in PU shown in false colour image. The fluorescence of the illuminated sample was investigated at different locations along the indicated direction (0). The illuminated part is indicated by the yellowish coloured figure resulting in a darkening, which can be seen in (1) – (3). After scanning over the illuminated part the fluorescence again reaches its maximal value (4) – (8). The observed ring structures are due to the geometry of the microscope illumination.

6.3.2.5 Transmission electron microscopy

TEM microscopy was carried out in order to clarify the micro-structure of the PU polymer surfaces containing TPP-O-A.

The TEM samples were cut or scraped off with a diamond microtome according to figure 6.30. There it was important to find the optimal thickness of the produced polymer films, because due to electrostatic interaction the specimen might curl. After scraping off the thin

films, they were fixated onto a standardized grid for the TEM microscopy. There, according to figure 6.31 an electron beam was guided through the sample, in which heavy atoms led to a higher scattering and thus a darkening of the 'photo' (collected microscopy data).

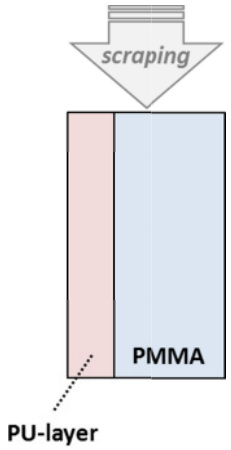

Fig. 6.30: Scraping off a polymeric thin film from the PU polymeric surface containing 10^{-4} M of TPP-O-A with a diamond microtome for TEM measurements; the cutting direction is indicated with the grey arrow.

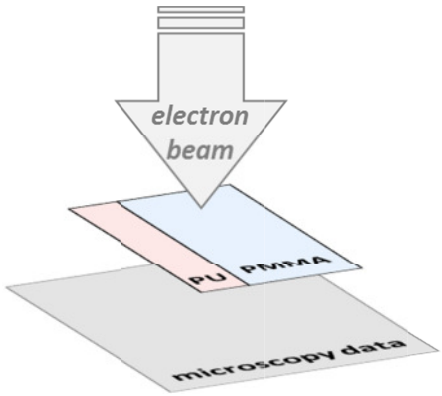

Fig. 6.31: TEM electron beam sent through the polymeric thin film from the PU polymeric surface containing 10^{-4} M of TPP-O-A; the direction of the beam and the collection of the microscopy data (photo) are indicated.

With this method, PU polymeric films with and without TPP-O-A were investigated, as well as probes containing TPP-O-A, which were irradiated with the same conditions as done for the phototoxicity tests, using a power of 50 $mWcm^{-2}$ for 60 min (applied energy dose of 180 Jcm^{-2}).

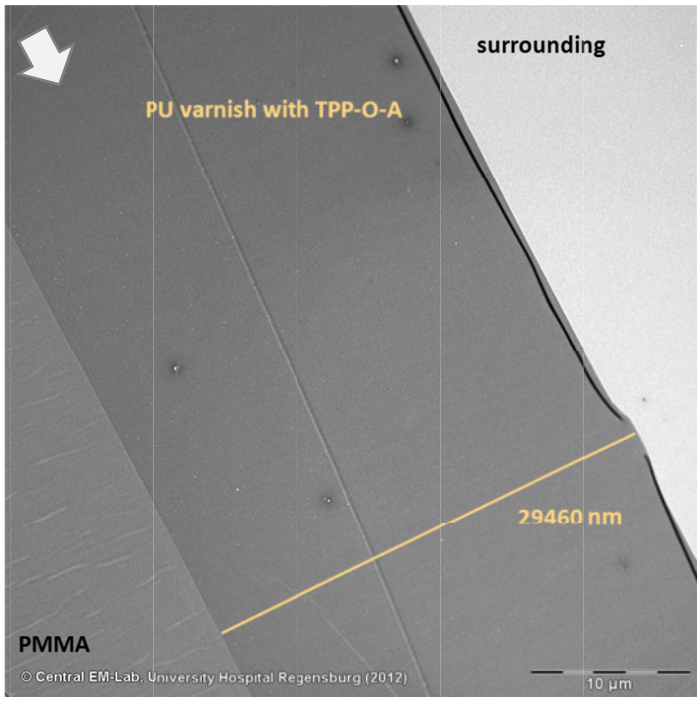

Fig. 6.32: TEM photo of a PU polymeric surface containing TPP-O-A with a concentration of 10^{-4} M and with a PU layer thickness of 30 µm; untreated with light (dark control); a 1000× magnification was used.

From TEM microscopy at a 1000 × magnification (fig. 6.32) a homogenous shadowing of the PU-layer can be seen. Since the containing atoms are not heavily different regarding their atomic weight, aggregates of TPP molecules were not detectable with this method. The area of PMMA shows a lighter grey-tone compared to the area containing TPP-O-A, because the scattering of electrons in the two different polymers and additionally due to the photosensitizer is different. The PMMA-region further shows a "wave"-like shaping. Most probably this is due to the cutting process, which is indicated by the arrow in figure 6.32 and shows an angle of 90° compared to the "waves". Furthermore, a very precise contact area between the PU-layer and PMMA was detected and a constant thickness of the PU-layer could be confirmed. Lines in the direction of the arrow are considered as scratches due to the process of manufacturing the thin polymeric films with the diamond microtome.

Small white spots were detected and investigation of the probe at a 5000 × magnification (fig. 6.33) on its edge revealed more details.

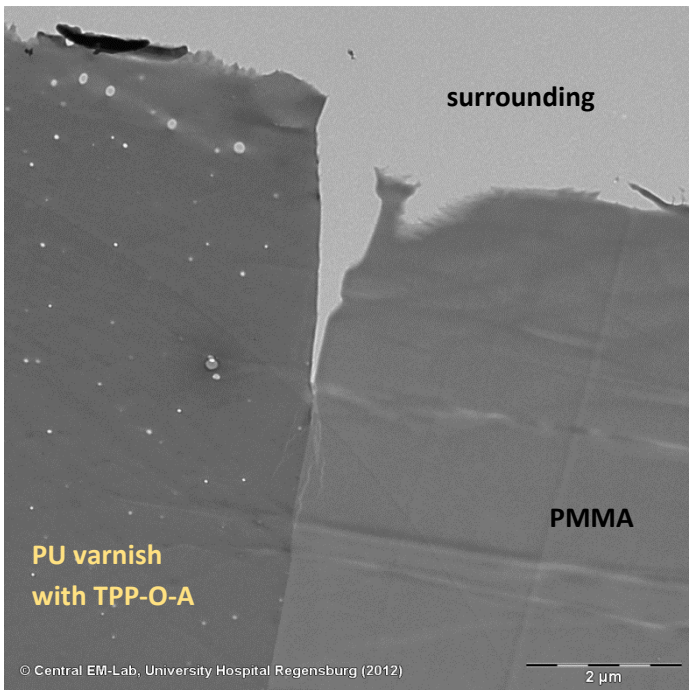

Fig. 6.33: TEM photo of the edge of a PU polymeric surface containing TPP-O-A with a concentration of 10^{-4} M and with a PU layer thickness of 30 µm; untreated with light (dark control); a 5000× magnification was used.

The small white spots in the region of the PU varnish are considered as air bubbles which probably are created during the polymerisation process and thus fixed into the material. Before the polymerisation, the PU-varnish contains different ingredients which have to be fully dissolved and mixed. During the mixing process and probably also the airbrushing procedure air will be forced into the material and forms these bubbles. In PMMA these white spots are missing, indicating another process of production.

6.3.3 Phototoxicity experiments on surfaces

Phototoxicity experiments with surfaces show the effectivity of the light induced generation of radicals (type-I and type-II reactions) and their ability to kill microorganism depending on the irradiation time and the applied power. The photophysical experiments showed generation of singlet oxygen in the materials CA and PU after irradiation. With indirect methods, the diffusion of singlet oxygen (without exclusion of other ROS) was determined. Therefore, a photokilling effect is expected for both materials. The determination of the reduction of bacteria on the surface is a second proof of the generation of singlet oxygen (or other ROS), that are able to escape the surface, and can be used as a quantification of the effectiveness of ROS generation. The corresponding experimental procedure, however, is more complex as compared to the testing of phototoxicity of photodynamic killing of

microorganisms in aqueous suspension. Thus, lower experimental accuracy of the results was expected requiring a larger number of independent experiments. The procedure is described in chapter 2. There, the handling of the recovery of bacteria, and within this especially the swapping technique is considered as source of the high errors.

In contrast to TPP the investigated CA surfaces containing MB and TMPyP showed a weak photosensitizer leakage from the material (fig. 6.3). Therefore, only TPP in CA was investigated in our group in regard to its phototoxicity (data not shown). Upon irradiation of *S. aureus* for $10\,min$ (OmniCure®Series 2000, $50\,mW\,cm^{-2}$, $30\,J\,cm^{-2}$) on a CA-surface containing $250\,\mu M$ of TPP a photodynamic inactivation due to the presence of the photosensitizer of $\leq 2\ log_{10}$-steps was achieved and a dependency of the photokilling effect on irradiation time and TPP concentration was determined [9]. However, a loss of bacteria was reported on the CA-samples not containing any photosensitizer of up to $4\ log_{10}$-steps only upon irradiation for 30 min. The reason for that has not finally been clarified [9].

The PU-polymer surfaces can be used as a coating due to the simple application technique. They are considered as an improvement of the CA surfaces, because the photosensitizers are chemically linked to PU. Furthermore, the loss of bacteria is expected to be lower compared to the findings with CA due to a change of the polymer material. In a first study, exemplarily the effective killing of *S. aureus* by TPP-O-A and PN-O-A doped in PU under irradiation was investigated and is presented herein. Therefore, 3 different irradiation times (10, 30, 60 min) and 3 different photosensitizer concentrations (0, 10^{-4}, $2 \cdot 10^{-4}\ M$) were used with a constant irradiation power of $50\,mW\,cm^{-2}$ using the PIB 3000 for both, TPP-O-A and PN-O-A. For each condition a dark control was the reference.

The values for the reduction of *S. aureus* presented herein are given in logarithmic steps, x, of the logarithm with the base 10 and were calculated using the following formula

Eq. 6.5

$$x = log_{10}\left(\frac{DK}{LK}\right)$$

with DK and LK being the $CFU\ mL^{-1}$ of the respective dark control and light control and therefore the difference in direction of the y-axis in a typical diagram showing the

$CFU\ mL^{-1}$ in a phototoxicity test, as exemplarily done in the following graph (fig. 6.34). There the reduction of x log_{10}-steps is illustrated by the arrow.

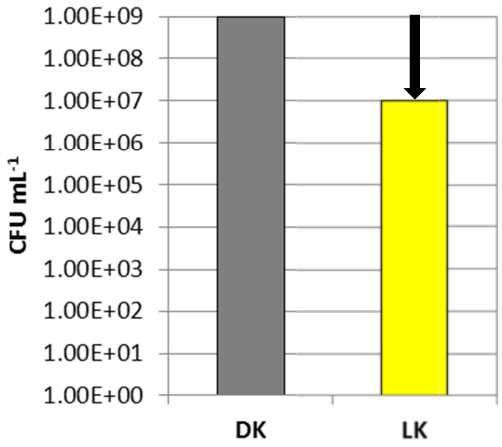

Fig. 6.34: Example of a reduction of bacteria; the CFU mL-1 are on a logarithmic scale and the dark control (DK) and light control (LK) are compared; the arrow indicates the reduction in log_{10}-steps.

The values x, symbolizing consequently the log_{10}-step reduction, can be transferred in a percentaged value with the following considerations

Eq. 6.6

$$100\% \cdot \left(1 - \frac{1}{10^{x}}\right)$$

And therefore, a reduction of 0.23 log_{10}-steps equals a percentaged reduction of

$$100\% \cdot \left(1 - \frac{1}{10^{0.23}}\right) = 41.1\%$$

6.3.3.1 Recovery from the PU-surface and fluctuation of the dark control

In order to quantify the photodynamic inactivation of bacteria on the PU-surfaces, following recovery experiments were performed. Droplets of bacteria suspensions with known concentration were applied on surfaces, the surface was irradiated and bacteria were wiped off again to determine the number of surviving bacteria by colony forming units (CFU). This recovery procedure served as test to determine possible diffusion of bacteria into the PU surface. Those bacteria would have been lost for quantification of the photodynamic procedure and would have led to false positive effects. The experiments were started with an idealized polystyrene surface. Like already described in the material and methods section

the dried bacteria suspension was kept for 30 min in the dark. Then the $CFU\ mL^{-1}$ were calculated and summarized in the following graph.

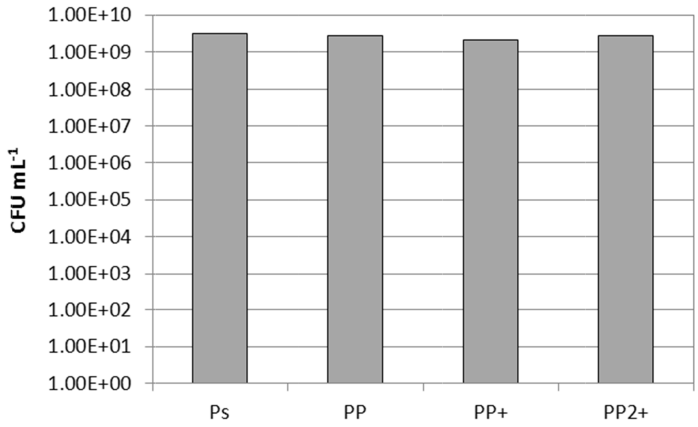

Fig. 6.35: Results of the recovery experiments using S. aureus bacteria. The surfaces were polystyrene without photosensitizer (Ps). The PU polymeric surfaces contained 0 M (PP), 10^{-4} M (PP+), or $2 \cdot 10^{-4}$ M (PP2+) of TPP-O-A.

This experiment shows that the recovery of bacteria from the PU-surfaces is comparable to the recovery from the idealized polystyrene surfaces. Furthermore, the bacteria suspension contained cells in a concentration in the range of $10^9\ CFU\ mL^{-1}$, which were found in the same range after the recovery process with the sterile cotton bud and subsequent dilution and plating process.

6.3.3.2 Phototoxicity efficacy of TPP-O-A in PU

Irradiation of the PU plates containing TPP-O-A with the PIB 3000 for 10 min and 50 $mW\,cm^{-2}$ did not exhibit noteworthy killing effects against *S. aureus* within the experimental accuracy of 0.5 log_{10}-steps.

Irradiation of 30 min with the PU samples without photosensitizer (PUR plates) led to a reduction of 0.23 log_{10}-steps ($n = 4$), which is considered as no effect within the above given experimental accuracy. Figure 6.36 shows the reduction of *S. aureus* on the TPP-O-A surfaces for the irradiation time of 30 min. The values are the average of 3 independent measurements ($n = 3$) and refer to the dark control. The dark control was in the range of $\approx 10^9\ CFU\ mL^{-1}$ for all samples.

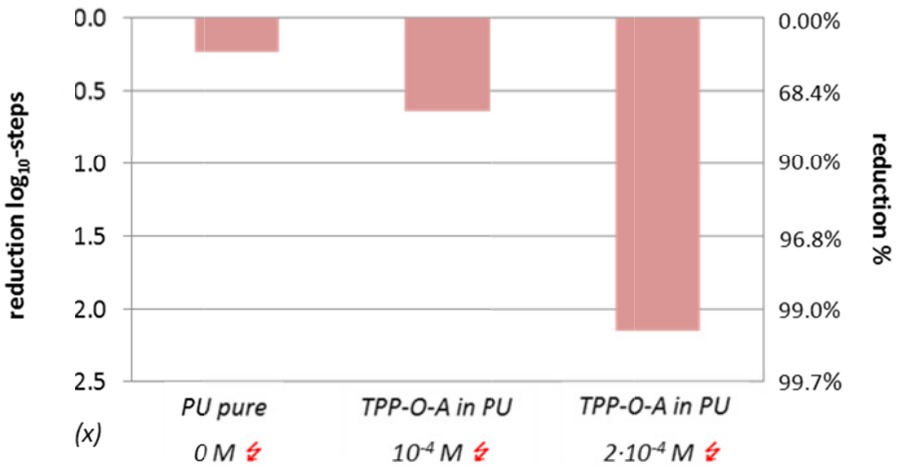

Fig. 6.36: Irradiation of TPP-O-A doped into PU; irradiation time = 30 min with P = 50 mW cm^{-2}; as reference a dark control for each condition was used which was each ≈ 10^{9} CFU mL^{-1} (n = 3, error: 0.5 log$_{10}$-steps).

A phototoxic effect was clearly demonstrated on the PU surface containing TPP-O-A. Since the experimental accuracy is given with 0.5 log_{10}-steps the killing efficacy of 0.6 log_{10}-steps with the photosensitizer concentration of $10^{-4}\ M$ is not considered as biologically relevant, whereas for $2 \cdot 10^{-4}\ M$ TPP-O-A solved in PU a reduction of 2.2 log_{10}-steps ($n = 3$) was reached. Therefore, a dependency of the killing efficacy on the photosensitizer concentration was demonstrated.

The phototoxic results with 60 min irradiation time showed a tendency of the photokilling effect (data not shown), which is comparable to the findings with 30 min. Nevertheless, a much bigger fluctuation of the $CFU\ mL^{-1}$ for both, light and dark control, were detected, maybe due to the additional drying which occurs at 60 min of irradiation. Due to these fluctuations also a comparison of the effectiveness with 30 min irradiation was not possible. Comparing the effective cell killing after 10 min and 30 min clearly a dependency of the killing rate with the irradiation time was detected.

6.3.3.3 Toxicity efficacy of PN-O-A in PU

Irradiation of 30 min of the PU samples without photosensitizer (PUR plates) led to a reduction of 0.5 log_{10}-steps ($n = 4$), which is considered as no effect within the above given experimental accuracy. Figure 6.37 shows the reduction of *S. aureus* on the PN-O-A surfaces for the irradiation time of 30 min. These results are the average value of 3 independent measurements ($n = 3$). The following graph shows the reduction of $CFU\ mL^{-1}$ in log_{10}-steps and in per cent.

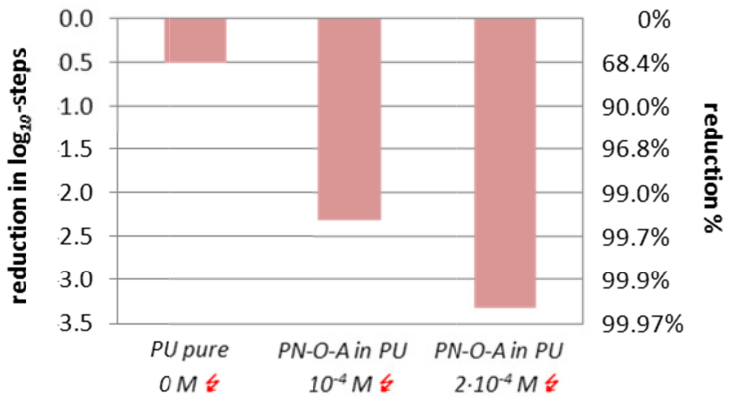

Fig. 6.37: Irradiation of PN-O-A doped into PU; irradiation time = 30 min with P = 50 mW cm^{-2}; as reference a dark control for each condition was used which was each ≈ 10^{9} CFU mL^{-1} (n = 3, error: 0.5 log$_{10}$-steps).

When using PN-O-A as photosensitizer in the surface, clear photodynamic killing of bacteria on the surfaces was achieved. Compared to TPP-O-A, a higher reduction of *S. aureus* on the surface under the same conditions was possible. The phototoxic effect increased with the photosensitizer concentration and a reduction of 2.3 log_{10} for $10^{-4}\ M$ and 3.3 log_{10}-steps with $2 \cdot 10^{-4}\ M$ was determined.

Although the singlet oxygen luminescence signals showed lower intensity when PN-O-A was doped in PU instead of TPP-O-A, as discussed in sub-unit 6.3.2.2, the phototoxicity experiments unequivocally show that the generation of ROS is more effective in the PN-samples. The reason for that can only be clarified by exclusion of the presence of other radical species with quenchers, and the enhancement of the spectroscopy studies, such as determination of a change in phosphorescence or fluorescence of the photosensitizer after doped in PU.

6.4 CONCLUSIONS

Microorganisms are frequently distributed via contaminated surfaces, which are in alternating contact with different individuals. It would be of great importance to interrupt this transmission pathway of microorganisms by a self-cleaning effect of surfaces, in which photodynamically generated singlet oxygen could play an important role. To achieve this goal, surfaces can be coated with polymer films containing photosensitizers with an appropriate concentration, which generates singlet oxygen upon irradiation with visible light. The aim of this chapter was the scientific investigation of singlet oxygen generation in such polymer films. The major physical issues in this process were the investigation of singlet oxygen production in different polymer films, its quenching and the impact of diffusion processes of oxygen followed by first microbiologically testing of such surfaces with regard to their efficacy against bacteria.

On one hand, photoactive surfaces and hence the doped photosensitizers require sufficient oxygen supply from either outside air or from inside polymer. On the other hand, the generated singlet oxygen should escape, as much as possible, from the photoactive surface to kill the microorganisms on the surface. Thus, diffusion of oxygen or oxygen permeability of substrates plays an important role.

At present, the oxygen permeability of the investigated material can be estimated by a comparison to similar materials, listed in tables such as in the polymer handbook [12], but theory and knowledge of luminescent oxygen sensors help to elucidate the oxygen concentration within a polymer. In these devices the luminescence of a photosensitizer in a polymer film is quenched by oxygen, whereas the quenching efficacy depends on the oxygen concentration and the diffusion coefficient. Following Lu *et al.* the quenching kinetics can be described completely in terms of parameters that can be determined independently: the excited triplet-T_1-state lifetime of the photosensitizer and the permeability P_{O_2} and diffusion coefficient D_{O_2} of oxygen in the polymer [10].

Describing the mobility of molecular oxygen in polymers and the consequences for triplet-state quenching is complex but some basic information, which might helpful in understanding the singlet oxygen lifetime in polymers, are provided by Boersma *et al.* [26, 27]. For many industrial purposes it is important to enhance the resistance of the polymer products, especially against oxidation, and the mobility of oxygen is described to be such a critical factor that may lead to instability of the material. Thus, they studied a change in the

amount of free volume within the polymer by monitoring the oxygen permeation. It is also in line with these studies that the change in the diffusion coefficient with temperature can be explained by the change in the free volume [28]. This might be a good starting point when trying to understand the generation and decay of singlet oxygen in materials such as the present polymeric layers that are doped with photosensitizer molecules.

In general diffusion seems to play a critical role in the quenching processes of singlet oxygen and especially the excited photosensitizer. Despite low diffusion coefficients in polymers, in comparison to air or liquid surrounding, a rather rapid oxygen diffusion into polystyrene, ($D_{PS} = (2.3 \pm 0.2) \cdot 10^{-7} cm^2 s^{-1}$, $25°C$, $1\ atm$) was reported by Poulsen *et al.* Their polymer film reached an equilibrium within 5 s after exposure of a degassed 10 µm thick polystyrene film to oxygen [29]. The time for reaching an equilibrium of oxygen in the material might be strongly dependent on the thickness of the polymer.

Singlet oxygen detected by direct spectroscopic methods

After doping the polymers CA or PU with the respective photosensitizers, the generation of singlet oxygen was clearly detected directly by its luminescence, except for the photosensitizer PN-O-B, with a rather high signal-to-noise ratio. Thus, an accurate evaluation of the rise and decay times was possible. The rise and decay times were in the range of µs and thus the deactivation of singlet oxygen most probable occurred within the samples, since a decay in surrounding air should have been substantially longer in the range of milliseconds [2].

The singlet oxygen luminescence signals detected for the photosensitizers in CA showed a bi-exponential behaviour. For all photosensitizers, MB, TMPyP, and TPP, the rise time was in the range of $12 - 13$ µs, which is considered as the range of decay time of singlet oxygen in the CA material.

	t_1 [µs]	t_2 [µs]
MB	42.6	13.6
TMPyP	56.9	13.9
TPP	37.4	12.3

Tab. 6.7: Rise and decay time of MB, TMPyP, and TPP in CA. Each experiment was done in triplicate with an assumed error of 10%.

For all photosensitizers, MB, TMPyP, and TPP, the rise time was in the range of $12 - 13\ \mu s$. Schiller *et al.* report values for the singlet oxygen lifetime in polymers to be in the range between $10 – 50\ \mu s$ [30]. Jesenska *et al.* obtained a singlet oxygen lifetime in PU nanofibers doped with TPP of $11.6\ \mu s$ and a decay time of the triplet-T_1-state of $17\ \mu s$ [6]. And these decay times for singlet oxygen are in good agreement with the herein presented findings for CA-polymers or PU-layers on PMMA. Although the assignment of the rise and decay times of the singlet oxygen luminescence signals is still challenging, decay times of $12\ \mu s$ in CA and $14\ \mu s$ in PU are reasonable from the present measurements.

In the case of the TPP derivatives in PU polymer a multi-exponential decay of the singlet oxygen luminescence signal was detected which made an exact evaluation impossible with the fit-curve basing on a bi-exponential model (eq. 2.2). Nevertheless, when taking only the first part of the signal into account (fig. 6.21), an estimation of rise and decay time was possible. The multi-exponential decay gives room for speculation: as one assumption singlet oxygen might decay in different micro-environments, which might differ in the oxygen concentration or in the size of the free volume within the polymer. Dependence of the oxygen solubility on the free volume has been shown by Boersma *et al.* on glassy polymers [26] and might lead to multi-exponential decay manner of the detected luminescence signals of singlet oxygen. Despite to the assumption of different decay times of singlet oxygen Clough *et al.* state that singlet oxygen has an intrinsic decay time within a polymer and thus exhibits first-order decay kinetics, whereas the excited triplet-T_1-state decays in non-first-order kinetics [7].

In case of the PU polymeric surfaces a rather complex system with two different boundary layers, comparable to the biofilm surfaces, was described. Once generated in PU, deactivation of singlet oxygen within PU, PMMA or air is possible, considering an additional probability for singlet oxygen to be reflected into the respective material/surrounding. Due to the shape of the singlet oxygen luminescence signals we assume that singlet oxygen is deactivated in the PMMA material after diffusion from the boundary layer with PU in a non-neglectable amount and the deactivation in air gives rise to a long decay of the signal, until its disappearance in the noise of the photomultiplier and limited by the time resolution of the experimental setup. Like in biofilms, representative surfaces comparable to the PU-polymer surfaces, the singlet oxygen luminescence should be considered composed of spatially separated photon emission sources (PMMA, PU, air), each being more or less dominant and influencing rise and decay of the other signals to a certain extent. The experiments with the sandwich structures showed under exclusion of the air surrounding a considerable change of both, rise and decay time (tab. 6.6). Although the decay time in air

cannot be resolved in its whole decay part in time and thus disappears in the noise signal of the photomultiplier, its influence on the whole luminescence signal might be visible by affecting the decay times by overlay of such different luminescence sources.

Exclusion or minimisation of the possibilities of singlet oxygen to decay in other surroundings than PU is helpful to understand the deactivation mechanism. Therefore, the proposed model has to be checked with future experiments like direct photosensitizer triplet spectroscopy in order to determine the decay time of the photosensitizer. A change of the material surrounding PU (glass, polymers allowing no oxygen diffusion, *etc.*) and a variation of the PU thickness might lead to characteristic changes of the decay times of photosensitizer triplet-state and singlet oxygen. The change of the decay times from a fluid to a solid state of the polymer might give additional insight as would do a change of the oxygen pressure, with respect to the diffusion of oxygen in the material.

To summarize, the production of different polymeric samples and a simplification of the herein presented complex surfaces by excluding decay possibilities, supported by computer simulation methods of these interfaces, describing the behaviour of the coupled differential equation system of 'photosensitizer-oxygen', is inevitable.

Singlet oxygen monitoring by indirect methods

A reaction of oxygen radicals with a solution of potassium iodide leads to the formation of tri-iodide which can be detected via absorption spectroscopy. This reaction can be used to detect the presence of singlet oxygen, but it is also sensitive to H_2O_2. In our measurements also the irradiation of pure PU on PMMA led to the formation of tri-iodide, which - without photosensitizer - should not be due to singlet oxygen generation. Experiments with additional quenchers for singlet oxygen, H_2O_2 or further reactive oxygen species might therefore exclude certain reaction pathways and give a clear evidence of the involved substances. Although the formation of a potential radical in the PU surfaces without photosensitizer was shown with the formation of tri-iodide, a phototoxic effect with these surfaces was not detected within experimental accuracy of 0.5 log_{10}-steps.

Phototoxicity

The photokilling effectiveness of the PU polymeric surfaces depended on the irradiation time and the concentration of the photosensitizer. Although the first results of the present

photoactive surfaces are very promising an optimum of the photosensitizer concentration, irradiation time and irradiation power is an important goal for the near future.

The PU-polymer surfaces doped with TPP-O-A showed for all concentrations a singlet oxygen luminescence signal with high intensity. Nevertheless, the samples showed a killing effectivity of slightly more the 2 log_{10}-steps only with a concentration of $2 \cdot 10^{-4}\ M$ and an irradiation time of 30 min. For $10^{-4}\ M$ the killing effectivity is already below 0.5 log_{10}-steps and is therefore considered as not biologically relevant.

PN-O-A in PU-polymer surfaces showed, despite lower intensity of the singlet oxygen luminescence signals, an increased effectivity in photoinduced cell killing compared to TPP-O-A. With a concentration of $10^{-4}\ M$ a reduction of $> 2\ log_{10}$-steps and with $2 \cdot 10^{-4}\ M$ a reduction of $> 3\ log_{10}$-steps was determined within 30 min. A reduction rate of at least 3 orders of magnitude of log_{10} is considered already as biologically relevant according to the hand hygiene guidelines [31]. The 'self-disinfecting' surfaces rather prevent microorganism settlement and growth than destroying already present colonies or biofilm structures. Thus, it is noteworthy to mention that the definition of cell killing on surfaces, in terms of effectivity, must be reconsidered and cannot directly be compared to photokilling efficacy in solution.

6.5 REFERENCES

1. Dahl, T.A., W.R. Midden, and P.E. Hartman, *Pure singlet oxygen cytotoxicity for bacteria.* Photochem Photobiol, 1987. **46**(3): p. 345-52.
2. Midden, W.R. and S.Y. Wang, *Singlet Oxygen Generation for Solution Kinetics - Clean and Simple.* Journal of the American Chemical Society, 1983. **105**(13): p. 4129-4135.
3. Wahlen, J., et al., *Solid materials as sources for synthetically useful singlet oxygen.* Advanced Synthesis & Catalysis, 2004. **346**(2-3): p. 152-164.
4. Mosinger, J. and B. Mosinger, *Photodynamic Sensitizers Assay - Rapid and Sensitive Iodometric Measurement.* Experientia, 1995. **51**(2): p. 106-109.
5. Denny, M., *Air and Water: The Biology and Physics of Life's Media.* Princeton University Press, 1993.
6. Jesenska, S., et al., *Antibacterial nanofiber materials activated by light.* J Biomed Mater Res A, 2011. **99**(4): p. 676-83.
7. Clough, R.L., et al., *Behavior of Singlet Molecular-Oxygen (1-Delta-G02) in a Polymer Matrix - Effects of Temperature, Matrix Rigidity, and Molecular Composition.* Macromolecules, 1989. **22**(9): p. 3620-3628.
8. Wolinska-Grabczyk, A. and A. Jankowski, *Gas transport properties of segmented polyurethanes varying in the kind of soft segments.* Separation and Purification Technology, 2007. **57**(3): p. 413-417.
9. de Jonge, L., *Inaktivierung von Bakterien auf einer photodynamisch aktiven Oberfläche mittels unterschiedlicher Photosensibilisatoren.* Dissertation, University of Regensburg, 2013.
10. Lu, X. and M.A. Winnik, *Luminescence quenching in polymer/filler nanocomposite films used in oxygen sensors.* Chemistry of Materials, 2001. **13**(10): p. 3449-3463.
11. Mills, A., *Controlling the sensitivity of optical oxygen sensors.* Sensors and Actuators B-Chemical, 1998. **51**(1-3): p. 60-68.
12. Brandrup, J., E.H. Immergut, and E.A. Grulke, *Polymer handbook*. 4th ed1999, New York: Wiley.
13. Sugunan, S.K., M.F. Paige, and R.P. Steer, *Determination of oxygen permeabilities in thin polymer films using quenching of upconverted fluorescence in porphyrins.* Canadian Journal of Chemistry-Revue Canadienne De Chimie, 2011. **89**(2): p. 195-202.
14. Amao, Y., *Probes and polymers for optical sensing of oxygen.* Microchimica Acta, 2003. **143**(1): p. 1-12.
15. Engl, R., *Die Erzeugung und Relaxation von Singulett-Sauerstoff in homogenen Lösungen sowie Lipid- und Zellsuspensionen.* Dissertation, University of Regensburg, 2003.
16. Baier, J., *Lumineszenz-Untersuchungen zur Generation und Relaxation von Singulett-Sauerstoff in zellulärer Umgebung.* Dissertation, University of Regensburg, 2005.
17. Bruckner, C., et al., *A spectroscopic and computational study of the singlet and triplet excited states of synthetic beta-functionalized chlorins.* Chemical Physics, 2003. **294**(3): p. 285-303.
18. Korinek, M., et al., *Luminescence study of singlet oxygen production by meso-tetraphenylporphine.* J Fluoresc, 2004. **14**(1): p. 71-4.
19. Barnett, G.H., M.F. Hudson, and K.M. Smith, *Concerning Meso-Tetraphenylporphyrin Purification.* Journal of the Chemical Society-Perkin Transactions 1, 1975(14): p. 1401-1403.
20. Rousseau, K. and D. Dolphin, *Purification of Meso-Tetraphenylporphyrin.* Tetrahedron Letters, 1974(48): p. 4251-4254.
21. Pasterna.Rf, et al., *Aggregation of Meso-Substituted Water-Soluble Porphyrins.* Journal of the American Chemical Society, 1972. **94**(13): p. 4511-&.
22. Zenkevich, E., et al., *Photophysical and photochemical properties of potential porphyrin and chlorin photosensitizers for PDT.* Journal of Photochemistry and Photobiology B-Biology, 1996. **33**(2): p. 171-180.
23. Dedic, R., et al., *Singlet oxygen quenching by oxygen in tetraphenyl-porphyrin solutions.* Journal of Luminescence, 2006. **119**: p. 209-213.
24. Nonell, S., M. Gonzalez, and F.R. Trull, *1h-Phenalen-1-One-2-Sulfonic Acid - an Extremely Efficient Singlet Molecular-Oxygen Sensitizer for Aqueous-Media.* Afinidad, 1993. **50**(448): p. 445-450.

25. Felgenträger, A., *Spektroskopische Untersuchungen an Photosensibilisatoren zur photodynamischen Inaktivierung von Bakterien.* University of Regensburg, 2009: p. 115.
26. Boersma, A., D. Cangialosi, and S.J. Picken, *Mobility and solubility of antioxidants and oxygen in glassy polymers. III. Influence of deformation and orientation on oxygen permeability.* Polymer, 2003. **44**(8): p. 2463-2471.
27. Boersma, A., D. Cangialosi, and S.J. Picken, *Mobility and solubility of antioxidants and oxygen in glassy polymers - II. Influence of physical ageing on antioxidant and oxygen mobility.* Polymer Degradation and Stability, 2003. **79**(3): p. 427-438.
28. Boersma, A., *Mobility and solubility of antioxidants and oxygen in glassy polymers. I. Concentration and temperature dependence of antioxidant sorption.* Journal of Applied Polymer Science, 2003. **89**(8): p. 2163-2178.
29. Poulsen, L., et al., *Oxygen diffusion in bilayer polymer films.* Journal of Physical Chemistry B, 2003. **107**(50): p. 13885-13891.
30. Schiller, K. and F.W. Muller, *Singlet Oxygen Lifetime in Polymer-Films.* Polymer International, 1991. **25**(1): p. 19-22.
31. Boyce, J.M. and D. Pittet, *Guideline for Hand Hygiene in Health-Care Settings. Recommendations of the Healthcare Infection Control Practices Advisory Committee and the HIPAC/SHEA/APIC/IDSA Hand Hygiene Task Force.* Am J Infect Control, 2002. **30**(8): p. S1-46.

Chapter 7

Conclusions

The commercially available phenothiazinium derivatives showed a quantum yield which was substantially below the values reported in literature. Since the quantum yields differed with concentration, an influence of dimerisation on the ability to generate singlet oxygen is suggested. New derivatives of methylene blue were synthesized and dimerisation could be suppressed in some of these molecules. The phototoxic efficacy of the derivatives is comparable to methylene blue, however, some of the new synthesized photosensitizers showed additionally a higher photostability, which is together with an absent dimerisation behaviour a new, promising batch of phenothiaziniums. Nevertheless, uptake experiments of these photosensitizers will give further insights in the interaction with microorganisms, supporting the aPDT effect.

An aggregation of the porphyrin XF73 was determined, which was higher compared to the reference porphyrin TMPyP, most probable due to its flexible side chains. Stacking of XF73 was substantially enhanced by Cl^- ions, which can be found in high concentration in cell physiological solution like PBS. The effect of aggregation leads to a dramatic increase in the ability to generate singlet oxygen and the singlet oxygen luminescence signals reveal a changed rise and decay time. Therefore, an interpretation of the luminescence signals becomes a challenging undertaking. The experimental data suggests that even at the same localisation of two similar photosensitizers, the singlet oxygen luminescence generated by these can differ to a great extent, because the surrounding of the photosensitizer might not only affect singlet oxygen, but the electronic system of the photosensitizer. The study on the effects of PBS on photosensitizer might help to elucidate the mode of action in cellular surrounding as for example absent phototoxic effects in suspension.

The singlet oxygen luminescence signal, detected directly at 1270 nm, was substantially improved with a new laser setup. Now, the singlet oxygen generated in cells can be monitored with a higher signal-to-noise ratio. This is especially important, because the photosensitizer concentrations after incubation and washing procedures can be rather low (few nm to μM). We could evaluate accurately the rise and decay time of a singlet oxygen luminescence signal in a cell suspension incubated with 1 μM of TMPyP.

Further, singlet oxygen luminescence signals of photosensitizers doped into *Candida albicans* biofilms were presented, which were recorded for the first time. The signals of washed and non-washed, and additionally dry and non-dry biofilms did not change to a

great extent and thus it was suggested, that the biofilm matrix, which is highly hydrophilic, keeps a constant surrounding like the amount of water, to maintain its features and TMPyP is linked efficiently into the matrix-cell-structure.

Polymer surfaces using the principle of PDI were produced with different photosensitizers and polymers. The generation of singlet oxygen within these surfaces was confirmed by direct spectroscopic methods. A discrepancy from the bi-exponential fit model used in this thesis was determined, having its accruement without much doubt in the complexity of the polymeric surface system, the oxygen diffusion and the deactivation probability of the electronically excited triplet state of the photosensitizer. It might be stated that the investigation of these physical and chemical parameters of polymer surfaces doped with photosensitizers is still a challenge, especially with regard to the assignment of rise and decay time of the singlet oxygen luminescence signals, which might not be answered by the methods proposed in this work alone, but ask for cooperation with polymer chemistry and microbiology. A model to consider the determined rise and decay times was proposed, but should be tested in future experiments with assistance of computer simulations.

Further, after excluding the surfaces exhibiting a leaking of photosensitizers upon contact with water, the phototoxic efficacy was tested exemplarily on *Staphylococcus aureus*. A dependence of bacteria cell killing on the photosensitizer concentration and the irradiation time was confirmed and a reduction of $> 3\ log_{10}$-steps (>99.9%) was determined after 30 min at 50 $mW\,cm^2$, which is considered as biologically relevant.

PUBLICATIONS IN JOURNALS

Gonzales F, Felgenträger A, Regensburger J, Bäumler W, Maisch T. **Fungicidal photodynamic effect on planktonic and biofilm-growing Candida albicans cells using two positively charged porphyrins: an in vitro study.** *(Future Microbiology 06/2013; 8:785-797.)*

Felgenträger A, Gonzales F, Maisch T, Bäumler W. **Ion induced stacking of photosensitizer molecules can remarkably affect the luminescence detection of singlet oxygen in *C. albicans* cells.** Journal of Biomedical Optics 18(4), 045002 (April 2013)

Felgenträger A, Maisch T, Dobler D, Späth A. **Hydrogen bond acceptors and additional cationic charges in methylene blue derivatives – photophysics and antimicrobial efficiency.** Biomed Research International, Vol. 2013.

Eichner A, Gonzales F, Felgenträger A, Regensburger J, Holzmann T, Schneider-Brachert W, Bäumler W and Maisch T. **Dirty hands: photodynamic killing of human pathogens like EHEC, MRSA and *Candida* within seconds.** Photochem. Photobiol. Sci., 2012, Advance Article.

Maisch T, Spannberger F, Regensburger J, Felgenträger A, Bäumler W. **Fast and effective: intense pulse light photodynamic inactivation of bacteria.** J Ind Microbiol Biotechnol. 2012 Jul; 39(7):1013-21.

Bäumler W, Regensburger J, Knak A, Felgenträger A, Maisch T. **UVA and endogenous photosensitizers - the detection of singlet oxygen by its luminescence.** Photochem Photobiol Sci. 2011 Oct 11.

Maisch T, Hackbarth S, Regensburger J, Felgenträger A, Bäumler W, Landthaler M, Röder B. **Photodynamic inactivation of multi-resistant bacteria (PIB) - a new approach to treat superficial infections in the 21st century.** J Dtsch Dermatol Ges. 2011 May; 9(5):360-6.

Regensburger J, Maisch T, Felgenträger A, Santarelli F, Bäumler W. **A helpful technology--the luminescence detection of singlet oxygen to investigate photodynamic inactivation of bacteria (PDIB).** J Biophotonics. 2010 Jun; 3(5-6):319-27.

CONTRIBUTION TO CONFERENCES

9th International Symposium on Photodynamic Therapy and Photodiagnosis in Clinical Practice. Bressanone / Italy. October 2012.

ORAL PRESENTATION "Singlet Oxygen Luminescence in a Polyurethane Matrix and its Phototoxic Efficacy on *S. aureus*"

(Felgenträger A, Maisch T, Bäumler W)

POSTER PRESENTATION "Hydrogen bond acceptors and additional cationic charges in methylene blue derivatives – photophysics and antimicrobial efficiency"

(Felgenträger A, Dobler D, Maisch T, Späth A)

"Beyond TMPyP: Derivatives and analogues with altered attachment properties to bacterial cell walls"

(Späth A, Felgenträger A, Maisch T, Bäumler W)

"Photodynamic inactivation of *S. aureus* on Cellulose Acetate containing *meso*-Tetraphenylporphine (TPP)"

(De Jonge L, Felgenträger A, Maisch T, Bäumler W)

American Society for Photobiology (ASP) - Conference, Montréal, CA. June 2012.

ORAL PRESENTATION "Singlet oxygen luminescence originating from polymeric matrices"

(Felgenträger A, Regensburger J, Maisch T, De Jonge L, Bäumler W)

"Beyond TMPyP: Derivatives and analogues with altered attachment properties to bacterial cell walls"

(Späth A, Bäumler W, Maisch T, Felgenträger A)

Arbeitsgemeinschaft Dermatologische Forschung (ADF) – Jahrestagung, Marburg / Germany. March 2012.

POSTER PRESENTATION "Detection of singlet oxygen luminescence in *Candida albicans* biofilm and phototoxic efficacy of the photodynamic inactivation"

(Felgenträger A, Gonzales F, Regensburger J, Bäumler W, Maisch T)

"Photodynamic fungicidal effect of a two-fold positive charged porphyrin-derivative and visible light against *Candida albicans*"

(Gonzales F, Felgenträger A, Lehner K, Maisch T)

BioMedIGS (International Graduate School) – Summer School, Regen / Germany. November 2011.

POSTER PRESENTATION "Investigation of (new) photosensitizers for self-disinfection of surfaces"

(Felgenträger A)

International Photodynamic Association (IPA) – Conference, Innsbruck / Austria. March 2011.

ORAL PRESENTATION "Photophysical Characteristics of the Porphyrin XF73 and Singlet Oxygen Luminescence in Cells"

(Felgenträger A, Regensburger J, Maisch T, Bäumler W)

"Generation of Singlet Oxygen by UVB-irradiation of endogenous molecules"

(Knak A, Regensburger J, Felgenträger A, Bäumler W)

"Comparison of photodynamic inactivation of *Candida albicans*"

(Gonzales F, Felgenträger A, Maisch T)

"Novel cationic-charged methylene blue derivatives for antimicrobial PDT"

(Späth A, Felgenträger A, Maisch T, Bäumler W)

8th International Symposium on Photodynamic Therapy and Photodiagnosis in Clinical Practice, Bressanone / Italy. October 2010.

POSTER PRESENTATION **"Photodynamic inactivation of *Candida albicans* biofilm: Detection of singlet oxygen luminescence and phototoxic efficacy"**

(Felgenträger A, Gonzales F, Bäumler W, Maisch T)

"Susceptibility of *Candida albicans* biofilm to photodynamic therapy with a porphyrin-derivative and visible light"

(Gonzales F, Felgenträger A, Maisch T)

"Improvement of time-resolved singlet oxygen detection for measurement in bacteria suspensions"

(Regensburger J, Knak A, Felgenträger A, Maisch T, Santarelli F, Bäumler W)

"Novel multiple-cationic methylene blue derivatives for antimicrobial PDT"

(Späth A, Felgenträger A, Maisch T, Bäumler W)

American Society for Photobiology (ASP) - Conference, Providence / USA. June 2010.

POSTER PRESENTATION **"Photodynamic inactivation of *Candida albicans* biofilm: Detection of singlet oxygen luminescence and phototoxic efficacy"**

(Felgenträger A, Gonzales F, Bäumler W, Maisch T)

"Photodynamic inactivation of *Candida albicans* in Planktonic and Biofilm-Grown Celly by a Two-Fold Positive Charged Porphyrin-Derivative and Visible Light"

(Gonzales F, Felgenträger A, Maisch T)

SELBSTSTÄNDIGKEITSERKLÄRUNG

ICH, ARIANE FELGENTRÄGER, GEBOREN AM 8.9.1983 IN KÖTHEN ERKLÄRE HIERMIT, DASS ICH DIE VORLIEGENDE ARBEIT OHNE UNZULÄSSIGE HILFE DRITTER UND OHNE BENUTZUNG ANDERER ALS DER ANGEGEBENEN HILFSMITTEL ANGEFERTIGT HABE.

DIE AUS ANDEREN QUELLEN DIREKT ODER INDIREKT ÜBERNOMMENEN DATEN UND KONZEPTE SIND UNTER ANGABE DER QUELLE GEKENNZEICHNET. INSBESONDERE HABE ICH NICHT DIE ENTGELTLICHE HILFE VON VERMITTLUNGS- BZW. BERATUNGSDIENSTEN (PROMOTIONSBERATER ODER ANDERE PERSONEN) IN ANSPRUCH GENOMMEN.

DIE ARBEIT WURDE BISHER WEDER IM IN- NOCH IM AUSLAND IN GLEICHER ODER ÄHNLICHER FORM EINER ANDEREN PRÜFUNGSBEHÖRDE VORGELEGT.

THIS IS MY OWN ORIGINAL WORK.

REGENSBURG, 28.3.2013